Enhancing the Antitumor Activity of Oncolytic Adenoviruses by Combining Tumor Targeting with Hyaluronidase Expression or by Increasing the Immunogenicity of Exogenous Epitopes

Alba Rodríguez García

UNIVERSITAT DE BARCELONA

FACULTAT DE FARMÀCIA

DEPARTAMENT DE BIOQUÍMICA I BIOLOGIA MOLECULAR

PROGRAMA DE DOCTORAT EN BIOMEDICINA

ENHANCING THE ANTITUMOR ACTIVITY OF ONCOLYTIC ADENOVIRUSES BY COMBINING TUMOR TARGETING WITH HYALURONIDASE EXPRESSION OR BY INCREASING THE IMMUNOGENICITY OF EXOGENOUS EPITOPES

ALBA RODRÍGUEZ GARCÍA

FEBRER 2015

UNIVERSITAT DE BARCELONA

FACULTAT DE FARMÀCIA

DEPARTAMENT DE BIOQUÍMICA I BIOLOGIA MOLECULAR

PROGRAMA DE DOCTORAT EN BIOMEDICINA

ENHANCING THE ANTITUMOR ACTIVITY OF ONCOLYTIC ADENOVIRUSES BY COMBINING TUMOR TARGETING WITH HYALURONIDASE EXPRESSION OR BY INCREASING THE IMMUNOGENICITY OF EXOGENOUS EPITOPES

ALBA RODRÍGUEZ GARCÍA

2015

Memòria presentada per Alba Rodríguez García per optar al grau de Doctor per la Universitat de Barcelona

Dr. Ramon Alemany Bonastre
Director

Dr. Manel Cascalló Piqueras
Director

Alba Rodríguez García
Autora

A mis padres

A mi hermana

ACKNOWLEDGEMENTS

Llegado este momento, en el que toca hacer balance, puedo decir bien orgullosa que esta etapa que ahora se acaba ha sido, sin ninguna duda, la mejor de mi vida hasta el momento en todos los aspectos. Obviamente, esto no sería así de no ser por la gente que me ha acompañado a lo largo de este camino, que me ha ayudado a crecer tanto personal como científicamente, y a la que debo mi más sincero agradecimiento.

El meu primer agraïment és per tu, **Ramon**. Mil gràcies per haver-me donat la oportunitat de realitzar la tesi al teu grup, realment em considero molt afortunada! Gràcies per haver confiat sempre en mi, per haver-me deixat llibertat a l'hora de desenvolupar els projectes, però a la vegada, per haver estat ben a prop per guiar-me i ajudar-me quan les coses no sortien com haurien... Gràcies per transmetre'ns i compartir amb tots nosaltres la teva forma d'entendre la ciència, sense perdre mai de vista l'objectiu de la nostra recerca, per ser un científic brillant però alhora honest i humil en un món en el que de vegades és difícil mantenir els peus a terra. Per mi ets un exemple a seguir i t'admiro profundament com a científic. Però també et vull donar les gràcies per haver estat un jefe tan proper en la part personal, per interessar-te pels meus concerts amb la banda, per tants cops que ens has fet riure a l'hora de dinar amb les teves historietes i anècdotes, i per acompanyar-nos de tant en quant en alguna festa al Salamandra. GRÀCIES!!

També vull donar-li les gràcies al **Manel**. Tot i que ja fa un temps que t'hem "perdut" completament al laboratori, la teva presència va ser clau en els meus inicis. Gràcies per haver-me ensenyat a treballar al laboratori, a cultius, a virus, a l'estabulari... Per estar sempre disposat a ajudar tothom, per tenir solucions per tot i per haver estat una peça fonamental al grup. De fet, encara ara et trobem a faltar! Tot i que som conscients que el que fas ara a VCN també és molt important pel grup i té molt de mèrit tirar-ho endavant.

Y como no, gracias a todos los RATgitos, habidos y por haber!!!! De verdad que, aunque a veces me queje de vosotros (especialmente de los chicos), no hubiera podido tener mejores compañeros de grupo! **Marta**, a tu et vull donar les gràcies per haver-me acompanyat al llarg de tot aquest camí, fent-me costat des del primer dia fins a l'últim. Per tots els moments que hem compartit, tant dins com fora del laboratori i, en definitiva, per la teva amistat i suport incondicional, que per mi ha estat molt important en aquests anys. Estic segura que el nostre recorregut no acaba aquí i espero que em continuïs acompanyant durant mooooolt de temps. **Raulito**, a ti te doy las gracias porque, a pesar de haber tenido nuestros más y nuestros menos, has sido una pieza clave para mí en esta etapa, tanto por el aspecto personal como por la parte científica, en la que siempre me has ayudado pacientemente (a veces, incluso demasiado pacientemente ;)). Te echaré de menos, aunque a lo mejor nos veremos al otro lado del charco (tranquilo, por ahora no entra en mis planes ir a Washington). **Luisito**!!! A ti no sé ni por dónde empezar a agradecerte… Gracias por haber sido el mejor compañero que se podría tener, por haberme ayudado en absolutamente todo, por haberme "criticado" figuras, colores de gráficos, presentaciones, y hasta la

pronunciation. Que voy a hacer sin tus correcciones de palabras mal dichas? Aunque sin duda, lo que más echaré de menos son nuestros habituales piques cuál matrimonio. Por este tipo de cosas dicen que la confianza da asco, pero oye, que todo sea eso! Y ya sé que te va a costar (;P), pero espero que mantengamos esta amistad por mucho tiempo! **Betito**, a ti te tengo que dar las gracias por saberlo todo de todo! Porque contigo he aprendido de ciencia (que de eso se trataba…), pero también de fútbol, de salsa, de series, de música, y como no, de brebajes colombianos (gracias por descubrirnos el guaro!). En serio, te admiro y aprecio muchísimo. Ah, y gracias por aguantar mis bromas pesadas (sorry por lo de los churros). **Marcel**, aunque a ti te conocía mucho antes que al resto, me da la sensación que no había descubierto todo tu potencial hasta que hemos empezado a compartir grupo! Pero bueno, tirando de refranes, más vale tarde que nunca, así que gracias por haber ocupado un lugar destacado en la última mitad de esta tesis y también en las fiestas que su realización ha conllevado. Gracias por tu sentido del humor y por formar un dúo cómico perfecto con Luis, que nos ha amenizado comidas y cafés con bromas de dudosa calidad. **Ahmed**, gracias por estar siempre dispuesto a ayudar a todo el mundo, y por sacarnos una sonrisa con tus "ocurrentes" bromas (tu cabeza, tu cabeza!). Y aunque tu papel como *paparazzi* en fiestas y celebraciones crea un poco de controversia, gracias por reconstruirnos las noches a los que nos despertamos con lagunas! Y si antes ha habido "palito" para los chicos, ahora les agradezco encarecidamente el haberme corregido esta tesis con tanta dedicación, sin duda ha mejorado considerablemente con vuestras aportaciones! **Rafa**, gracias por tu inestimable ayuda en el laboratorio y por desempeñar una función tan difícil en un grupo como este… Perdón por las veces que no he repuesto el material o me he escaqueado de los turnos de limpieza. Pero sobretodo, gracias por haber instaurado la ya tradicional ruta de bares navideña con su por todos conocido himno "Comando Papá Noel". Larga vida a la caminata! **Arianne**, el último gran fichaje! Lo nuestro ha sido corto pero intenso, gracias por ser una tía tan vital y divertida, has aportado mucha alegría y aire fresco al grupo. Y como no, también por hacer las mejores tortillas del mundo! Eskerrik asko!! Gracias también a las chicas de VCN: **Miriam**, por los experimentos fallidos con el maldito WT1 que hemos compartido, **Emma**, por haber formado un buen equipo haciendo reports en su momento y a **Sara**, la recién llegada, bienvenida!

Tampoco quisiera olvidarme de los que ya no están pero que en algún momento han compartido poyata conmigo. En esta tesis hay reflejado algo de cada uno de vosotros. **Juanji**, aunque al principio no me hicieras mucho caso por culpa de un tapón de cera (menuda excusa más mala, se que en realidad me odiabas por llevar gafas rosas), aprendí mucho de tus enseñanzas. Gracias **Jordi**, por tus consejos siempre tan prácticos. A mi particular princess, **Daniela**, por los experimentos, risas y confidencias compartidas, es súper chimbo tenerte tan lejos! **Miguel**, prácticamente te has convertido en una leyenda en el laboratorio, así que estoy muy contenta de haberte conocido personalmente, aunque eso haya implicado algún que otro "encierro" en la sala de virus. Gracias por habernos regalado temazos como "Sigue en pie", ayuda escucharlo de vez en cuando. **Edu**, quién lo iba a decir, pero echo de menos tus borderías! Incluso a tus AAVs, con los dolores de cabeza que me han dado! I especialment, moltes gràcies a tu, **Cris**, per haver-me ajudat sempre en tot al laboratori, realment he après moltíssim de tu. Ets una gran científica! Però també

gràcies per haver compartit amb mi moltes estones fora del lab. Trobo molt a faltar els mítics sopars de nenes junt amb la Marta i la Dani! Ah, i gràcies per intentar trobar-me feina a LA!

I com no! Als que van marxar però… han tornat! No m'oblidava de tu, **Sònia**, gràcies per haver sigut la meva *coach* a l'ESGCT. Per les converses sobre postdocs i pels consells de futur. Espero que puguem (o puguin, més aviat) gaudir-te al grup, que fa molta falta algú com tu que foti canya! Welcome back!

Y cuando digo que me siento afortunada lo digo con razón! Porque también he tenido el placer de compartir laboratorio con una generación de personas excepcional e irrepetible! Gente con la que, además de lugar de trabajo, he compartido innumerables momentos en lugares tan emblemáticos como la "Flama" o "Salamandra" (aprovecho aquí para mencionar a Juan y a Dj Txarnegö, por alegrarnos esos momentos ya sea con medianas o maradonas), así como escapadas de fin de semana (o fin de año), o fiestas tan míticas como las de Sants. De todos y cada uno de esos momentos guardo recuerdos y anécdotas que me acompañaran para siempre. **Currito**, gracias por todas las veces que me has hecho reír con tus parecidos razonables, imitaciones poco fieles a la realidad, bajadas de pantalones, o ideas de bombero, por haber compartido con nosotros tus "hits" y convertirlos en himnos (bum bum!), y por ser el alma del laboratorio. Pero no todo ha sido cachondeo contigo, en este tiempo te has convertido en un gran amigo al que aprecio muchísimo, así que gracias por ello. Moltes gràcies també a les meves tres floretes, per cuidar-me i mimar-me tant!! Perquè sens dubte, aquesta última fase de la tesi no hagués estat el mateix sense vosaltres. Gràcies **Elisenda**, perquè tot i que la nostra relació no va tenir un inici idíl·lic (;P) el final ha estat immillorable! De fet estic ben segura que això no és ni molt menys el final, i que a la nostra amistat encara li queda un llarg camí per recórrer. Gràcies també per haver-me tirat un cable amb les extraccions de RNA i les real-time. **Mariona**, gràcies per totes les vegades que hem cantat (o més ben dit, cridat com boges) i ballat juntes "Limbo", i per les que queden... També per la teva ajuda amb les immunohistoquímiques. I a tu, **Roser**, gràcies per ser encara més dolça que els cupcakes que ens prepares (boníssims, per cert). No voldria passar per alt la nova incorporació al grup, **Ali**, que ja apunta maneres... Benvinguda crack! **Samuelinho**, en mi memoria quedará aquella caipirinha 10X en el parque de Bellvitge. Obrigado! **Jack**, gracias por tener siempre una sonrisa para todo y para todos, se agradece y se echa de menos. **Natalia**, por ser tan maja y no dejarte contagiar por el ambiente de maldad que te rodea en la sala de becarios, jeje. Y **Sarita**, porque aunque ya no coincidamos tantas veces siempre recordaré lo bien que nos lo hemos pasado juntas. Y de este grupo tan variopinto que es Borja también forman parte personas con las que quizás no he compartido poyata ni laboratorio pero no por ello son menos merecedoras de mis agradecimientos. Molt especialment gràcies a tu, **Joan**, per tots els moments que hem viscut junts, per ser un immillorable company de viatges (mai oblidaré la nostra aventura al Marroc: shukran!! que no "sakran"…), birres, cines, festes... , per estar tan boig i fer-me riure tant! Però sobretot, gràcies per la teva amistat, sens dubte és una de les millors coses que m'enduc d'aquesta tesi i que espero conservar per sempre. Encara ens queden moltes coses pendents per fer junts (i em refereixo a viatges, malpensat!). **Eric**, gracias por haberme instruido en el arte del *maradoning*, por los siempre interesantes debates científicos y chapas mutuas sobre temas varios y por aguantar (aunque con alguna que otra queja) mis

frituras y rayadas relacionadas con la escritura de esta tesis. Menos reírse de mis desviaciones! **Iris**, gracias por ser una persona tan especial, clara y transparente, y por habernos acogido en tu casa como si fuéramos de la familia. Esa bajada en trineo está, sin duda, en el *top ten* de recuerdos de estos años… Pero la lista es mucho más larga todavía y aún me dejo a gente, ya sean del LRT1, LRT2, de genética, del COM… , estén todavía aquí o no …: **Gorka**, **Lara**, **María**, **Clara**, **Nick**, **Paco**, **Vane**, **Dæh**, **Karinna**, **Silvia**, **Kira**, **Eva**, **Miguel**, **Helena** … Gracias a todos!!

Y gracias también a toda la gente del LRT1 que en algún momento u otro de esta tesis me ha ayudado, ya sea prestándome algún reactivo, echándome una mano con alguna técnica o simplemente con alguna palabra de ánimo. Gracias a **Natalia Casado**, **Laura**, **Mar**, **Agnés**, **Gabi**, **Susana**, **Lidia**, **Alba**, **Helena Aguilar**, **Mónica**, **Nadia**, **Alberto**, **Francesc**, **Cristina Santos** … Especialmente quiero darle las gracias a **Olga**, por ser tan eficiente y hacernos la vida mucho más fácil en el laboratorio, pero también por ser un ejemplo de superación a nivel personal y por ser como una mami para todos.

Y aunque durante estos años pudiera parecer que sí, la vida no se acaba en el ICO! Fuera de este "micromundo" también hay muchas personas que, en mayor o menor medida, han estado implicadas en esta tesis y por ello merecen mi reconocimiento.

Gracias a mis colegas biotecs: **Dani**, **Estela**, **Laura**, **Meri**, **Marta**, **Agrin**, **Jessi**, **Gemma**, **Olívia** … porque aunque los encuentros sean cada vez un poco más espaciados en el tiempo, siempre ayuda saber que no estamos solos en esto! Muy especialmente quiero darle las gracias a **Anna**, por ser alguien con quien poder compartir absolutamente todo (a pesar de los kilómetros que nos separan), y por ser mi mejor amiga, en definitiva. También un agradecimiento muy especial a ti, **Sarai**, porque eres la que ha vivido más de cerca la culminación de esta tesis, con todo lo que ello conlleva. Aunque se puede decir que lo hemos llevado bastante bien, no? Muchas gracias por estar siempre ahí!

Aunque seguro que ellos no son muy conscientes de su contribución, gracias también a todos mis compañeros y amigos de la **UFP** por haberme hecho desconectar del laboratorio durante todos estos años al menos 4 horas a la semana haciendo lo que más nos gusta, música (o como mínimo, intentándolo)! Gràcies al **Xavi**, per ser en gran part responsable d'això i per haver intentat entendre que era allò de fer una tesi amb virus. Y a mis amigas **Marta** y **Eva**, gracias por las birras post-ensayo y por haberme apoyado y animado en la recta final de esta tesis. Formamos un buen equipo, limonas!

Y como dicen que lo mejor siempre se deja para el final, reservo estas líneas para darle las gracias a mi familia, por ser mi principal fuente de motivación. Gracias a **mis padres,** por la educación que me han dado y por haberme convertido en la persona que soy ahora. Por haber respetado siempre mis decisiones, por haberme apoyado en todo y por haber confiado en mí incondicionalmente. Este logro es, sin duda, mérito vuestro. Y a ti **Lidia**, gracias por ser la mejor hermana y amiga que podría tener, por estar siempre ahí y por enseñarme tantas cosas. Aunque seas la pequeña, para mi eres todo un ejemplo de valentía y te admiro muchísimo. Ah, y gracias a mi prima **Marta** por ayudarme con la portada!

INDEX

FIGURE INDEX

TABLE INDEX

ABBREVIATIONS

%	Percentage
°C	Centigrade degrees
Δ24	*delta*24 mutation, deletion of 24 bp in E1A protein
β_2m	β_2-microglobulin
µF	microfarad
µg	microgram
µL	microliter
µm	micrometer
Ω	Ohm
5-FC	5-fluorocytosine
5-FU	5-fluorouracil
AAALAC	Association for Assessment and Accreditation of Laboratory Animal Care
ABC	ATP-Binding Cassette
ACK	Ammonium-chloride-potassium
ACT	Adoptive T cell therapy
Ad	Adenovirus
ADP	Adenovirus Death Protein
AFP	Alpha-Fetoprotein Promoter
$AgNO_3$	Silver nitrate
ALL	Acute Lymphocytic Leukemia
ALT	Alanine Transaminase
APC	Antigen-Presenting Cell
APS	Ammonium persulfate
ARS	Autonomous Recombination Sequence
AST	Aspartate Transaminase
ATCC	American Type Cell Culture
BAC	Bacterial Artificial Chromosome
Bak	Bcl-2 homologous antagonist/killer
Bax	Bcl-2-associated X protein
BCA	Bicinchoninic Acid Assay
BFA	Brefeldin A
bp	base pairs
BSA	Bovine Serum Albumin
C4BP	Complement Binding Protein-4
$CaCl_2$	Calcium chloride
CAF	Cancer-Associated Fibroblast
CAR	Coxsackievirus B and Adenovirus Receptor or Chimeric Antigen Receptor
CCE	Clarified Cell Extract
CD4 and 8	Cluster of differentiation 4 and 8
cDNA	complementary DNA
CE	Cell Extract
Cm	Chloramphenicol
cm	centimeter
CMV	Cytomegalovirus
CO_2	Carbon dioxide
CPA	Cyclophosphamide
CPE	Cytopathic effect
CRAd	Conditionally Replicative Adenovirus

CRC	Colorectal cancer
CRT	Calreticulin
CsCl	Cesium chloride
CTL	Cytotoxic T Lymphocyte
CTLA-4	Cytotoxic T-Lymphocyte-Associated Protein 4
DAB	3,3'-Diaminobenzidine
DAMP	Damage-Associated Molecular Pattern
DAPI	4',6-Diamidino-2-phenylindole dihydrochloride
DC	Dendritic cell
ddH_2O	bi-distilled water
ddDNTP	2',3' dideoxynucleotides
DMEM	Dulbecco's Modified Eagle's Medium
DMSO	Dimethyl sulfoxide
DNA	Deoxyribonucleic Acid
dNTP	Nucleoside triphosphate
DTT	Dithiothreitol
Dox	Doxorubicin
ECM	Extracellular Matrix
EDTA	Ethylenediaminetetraacetic acid
ELISPot	Enzyme-Linked Immunospot Assay
ER	Endoplasmic Reticulum
FACS	Fluorescence Activated Cell Sorting
FasL	Fas Ligand
FBS	Fetal Bovine Serum
FDA	Food and Drug Administration
FIX	Coagulation factor IX
FX	Coagulation factor X
FR	Furin-Resistant
G	Gauge
g	acceleration of gravity
g	gram
GALV	Gibbon Ape Leukaemia Virus
GCV	Ganciclovir
GE	Gemcitabine
GLP	Good Laboratory Practices
GM-CSF	Granulocyte Macrophage-Colony Stimulating Factor
h	hour
H_2O_2	Hydrogen peroxide
HA	Hyaluronic acid or Hemagglutinin
HBsAg	Hepatitis B surface Antigen
HCC	Hepatocellular carcinoma
HCl	Chloridric acid
HDAC	Histone deacetylases
HEPES	4-(2-hydroxyethyl)-1-piperazineethanesulfonic acid
HIV	Human Immunodeficiency Virus
HLA	Human Leukocyte Antigen
HMGB1	High Mobility Group Box 1 Protein
HRP	Horseradish peroxidase
HSG	Heparan-Sulphate-Glycosaminoglicans
HSP	Heat Shock Protein
HSV	Herpes Simplex Virus

Hyal	Hyaluronidase
ICD	Immunogenic Cell Death
IC_{50}	Inhibitory Concentration 50
IDD	Immunodominant Determinants
IDO	Indoleamine 2,3-dioxigenase
IFN	Interferon
IFP	Interstitial Fluid Pressure
Ig	Immunoglobulin
IL	Interleukin
IP	Intraperitoneal
IT	Intratumoral
ITR	Inverted Terminal Repeats
IV	Intravenous
Kan	Kanamycin
Kbp	kilobase pair
KC	Kupffer Cell
L	Litre
LC	Lactacystin
LMP	Low Molecular Weight Protein
LRP	Lipoprotein Receptor-related Protein
mA	milliampere
MCA	Methylcholanthrene
MDSC	Myeloid-derived Suppressor Cell
Mets	Metastasis
mg	milligram
MHC	Major Histocompatibility Complex
min	minute
MIP	Macrophage Inflammatory Protein
mL	milliliter
MLP	Major Late Promoter
MLU	Major Late transcription Unit
mm	millimeter
mm^3	cubic millimeter
mM	millimolar
MMP	Matrix Metalloprotease
MOI	Multiplicity of Infection
mRNA	Messenger Ribonucleic Acid
MSC	Mesenchymal Stem Cell
MTT	3-(4,5-Dimethylthiazol-2-yl)-2,5-Diphenyltetrazolium Bromide
NAbs	Neutralizing antibodies
NaCl	Sodium chloride
NaH_2PO_4	Monosodium phosphate
NaF	Sodium fluoride
NaOH	Sodium hydroxide
$Na_2S_2O_3$	Sodium thiosulfate
NDV	Newcastle Disease Virus
NF-κβ	Nuclear factor Kappa-light-chain-enhancer of activated B cells
ng	nanogram
NK	Natural Killer
nm	nanometer

NPC	Nuclear Pore Complex
NSCLC	Non-Small Cell Lung Carcinoma
OCT	Optimum Cutting Temperature compound
OD	Optical Density
OG	OVA_{257}-$gp100_{25}$
PAMP	Pathogen-Associated Molecular Pattern
PanCa	Pancreatic cancer
PAGE	Polyacrylamide Gel Electrophoresis
PBS	Phosphate Buffered Saline
PCR	Polymerase Chain Reaction
PD-1	Death Protein-1
PD-L1	Death Protein Ligand-1
PE	R-phycoerythrin
PEG	Polyethylene Glycol
p.i.	Post-infection or post-injection
pg	picogram
pmol	picomol
PRR	Pattern Recognition Receptor
PS	Penicillin-Streptomycin
PSA	Prostate-Specific Antigen
Rb	Retinoblastoma
RCC	Renal carcinoma
RGD	Arginine-glycine-aspartic acid
RID	Receptor Internalization and Degradation
RNA	Ribonucleic Acid
rpm	revolutions per minute
RPMI	Roswell Park Memorial Institute
RT	Radiation Therapy or Room Temperature
RT-PCR	Real-Time PCR
SCCHN	Squamous Cell Carcinoma of the Head and Neck
SD	Standard Deviation
SDD	Subdominant determinants
SDS	Sodium dodecyl sulfate
SEM	Standard Error of the Mean
SFC	Spot forming colony
SPARC	Secreted Protein Acidic and Rich in Cysteine
SSdel	Signal Sequence deletion
Strep	Streptomycin
TAA	Tumor-Associated Antigen
TAE	Tris-Acetate-EDTA
TBE	Tris-Borate-EDTA
TBS	Tris-Buffered Saline
TAP	Transporter Associated to Antigen Processing
TCR	T Cell Receptor
TE	Tris-EDTA
TEMED	Tetramethylethylenediamine
TERT	Telomerase Reverse Transcriptase
TGF-β	Transforming Growth Factor-β
TGN	Trans Golgi Network
TIL	Tumor-Infiltrating Lymphocyte
TK	Thymidine Kinase

TL	Track-Luc cassette (eGFP-Luciferase)
TLP	Tripartite Leader
TNF	Tumor Necrosis Factor
TLR	Toll-Like Receptor
TP	Terminal Protein
TRAIL	TNF-related apoptosis-inducing ligand
T_{reg}	Regulatory T cell
Tris	Tris(hydroxymethyl)aminomethane
TU	Transducing Unit
V	Volt
V	Volume
VA	Virus-Associated
VEGF	Vascular Endothelial Growth Factor
vp	viral particle
VSV	Vesicular Stomatitis Virus
VV	Vaccinia Virus
WHO	World Health Organization

Amino acids

F Phe, phenylalanine	**S** Ser, serine	**Y** Tyr, tyrosine	**K** Lys, lysine	**W** Trp tryptophan
L Leu, leucine	**P** Pro, proline	**H** his, histidine	**D** Asp, aspartic acid	**R** Arg, arginine
I Ile, isoleucine	**T** Thr, threonine	**Q** Gln, glutamine	**E** Glu, glutamic acid	**G** Gly, glycine
M Met, methionine	**A** Ala, alanine	**N** Asn, asparragina	**C** Cys, cysteine	**V** Val, valine

Nucleotides

A adenine T thymine **G** guanine **C** cytosine **U** uracil

RESUM

La viroteràpia del càncer amb adenovirus oncolítics es basa en l'habilitat d'aquests agents en replicar selectivament en cèl·lules tumorals, produint la seva mort sense afectar cèl·lules normals. Les principals limitacions d'aquesta teràpia són la dificultat dels adenovirus per arribar als tumors després de ser administrats sistèmicament i també la seva incapacitat per dispersar-se de manera homogènia dins dels tumors. En aquest treball s'ha generat un adenovirus oncolític que combina dues mutacions descrites amb anterioritat pel nostre grup. Per una banda, la substitució del motiu d'unió a heparan-sulfats glicosaminoglicans situat al domini *shaft* de la fibra pel motiu d'unió a integrines RGD (mutació RGDK) per tal de millorar la ratio de transducció tumor/fetge i d'augmentar la persistència en sang de l'adenovirus. Per altra banda, l'expressió de hialuronidasa amb l'objectiu de degradar l'àcid hialurònic de la matriu extracel·lular del tumor i millorar la dispersió intratumoral de l'adenovirus. Aquest nou virus, l'ICOVIR-17K, va mostrar una potent eficàcia antitumoral en models de ratolí i hàmster que va ser fins i tot incrementada mitjançant la combinació amb gemcitabina, tot mantenint el perfil de toxicitat dels adenovirus oncolítics parentals.

Per altra banda, a més de matar directament les cèl·lules tumorals, els adenovirus oncolítics poden contribuir a la generació de respostes immunes contra el tumor. El tipus de mort cel·lular que generen és altament immunogènic i ajuda al reclutament de cèl·lules del sistema immune que generen respostes contra els antígens tumorals alliberats en aquest procés. Una de les principals limitacions de la immunoteràpia amb virus oncolítics és la resposta esbiaixada cap als antígens virals, que són immunodominants, en lloc de cap als antígens tumorals, que són poc immunogènics. Per tal d'afavorir la generació de respostes immunes antitumorals, en aquest treball s'han incorporat epítops tumorals en la proteïna E3-19K de l'adenovirus, que conté una seqüència senyal que la dirigeix directament al reticle endoplasmàtic, de manera que evadeix els passos previs de processament antigènic per la via del MHC de classe I, comunament afectada en cèl·lules tumorals. Aquesta estratègia va permetre la generació de respostes immunes antitumorals més potents que quan els mateixos epítops eren incorporats a la càpside de l'adenovirus, i a més, van ser traduïdes en una millor eficàcia antitumoral en un model murí de melanoma.

En resum, en aquest treball s'han abordat les principals limitacions dels adenovirus oncolítics des de diferents punts de vista que, eventualment, poden ser combinats per tal d'aconseguir un millor candidat per ser testat exitosament a la clínica.

SUMMARY

Oncolytic adenoviruses represent an appealing therapeutic approach to treat cancer given their capability to infect and kill selectively tumor cells without damaging normal tissues. Tumor targeting upon intravenous administration and subsequent intratumoral virus dissemination are key features to improve oncolytic adenovirus therapy. To address these hurdles, in this work two different genetic modifications previously described by our group were combined in an oncolytic adenovirus backbone with selective replication conditional to pRB pathway deregulation. First, the replacement of the heparan sulfate glycosaminoglycan-binding site KKTK of the fiber shaft with an integrin-binding motif RGDK for tumor targeting that has shown to prolong blood persistence and significantly enhance the therapeutic index compared with a non-RGDK-modified virus. Second, the expression of hyaluronidase to degrade the extracellular matrix and improve the intratumoral spread of the virus. Preclinical toxicology and biodistribution studies conducted in non-permissive mouse and semi-permissive Syrian hamster models supported the selectivity and safety of this novel virus, ICOVIR-17K. Antitumor efficacy was also demonstrated in different tumor models in immunodeficient mice and immunocompetent hamsters upon different routes of administration. Moreover, the combination of ICOVIR-17K with the chemotherapeutic drug gemcitabine further increased the antitumor activity of the virus. The data presented in this thesis strongly supports ICOVIR-17K as a promising clinical candidate which is currently being tested in phase I clinical trials.

Besides direct killing of cancer cells, oncolytic viruses may induce antitumor immune responses. Local inflammation of tumor tissue during an infection by an oncolytic virus provides suitable conditions to trigger antitumor immune responses against the tumor-associated antigens that are released in the immunogenic cell death process caused by these viruses. Oncolytic adenoviruses can be used to promote immune responses against tumors by expressing and/or displaying tumor-associated antigens. However, a key limitation of this immunotherapeutic approach is the bias of the response towards the immunodominant viral antigens instead of the less immunogenic tumor antigens. In addition, defects in MHC class I antigen presentation pathway such as the downregulation of the transporter associated with antigen processing (TAP) are frequently associated with immune evasion of tumor cells and further impair the generation of specific immune responses against tumor antigens carried by oncolytic viruses. In this work we present a novel strategy that benefits from the TAP deficiency on tumor cells to enhance the response against tumor epitopes attached to the viral protein E3-19K. This protein has a signal sequence that targets it to the endoplasmic reticulum, bypassing the need of TAP to transport the epitopes to that compartment. Compared to the display of the epitopes at the adenoviral capsid, this strategy enhanced the immunogenicity of the epitopes

and resulted in more potent antitumor immune responses, tackling a crucial aspect of virotherapy that is often overlooked.

In summary, the two different projects involved in this thesis addressed the main limitations of oncolytic adenoviruses from distinct points of view that may eventually be combined in order to maximize the opportunities of success of oncolytic adenoviruses in the clinics.

INTRODUCTION

1. CANCER

Cancer stands among the leading causes of death worldwide, accounting for 8.2 million deaths in 2012 that corresponded to the 14.6% of all human deaths, according to the World Health Organization (WHO). Nowadays, cancer mortality can be reduced dramatically if detected and treated at early stages. However, there are still some types of cancer, such as pancreatic cancer, in which mortality is almost equal to incidence, and the 5-years survival rate is less than 5% in the European Union.

Mechanisms of cellular division and DNA replication machinery inevitably make mistakes that could compromise the integrity of the genome and potentially result in cancer formation. Cancer is a genetic disease that arises by an evolutionary process where somatic cells acquire several mutations that overcome mechanisms by which uncontrolled expansion of cells is normally restricted. This abnormal proliferation of cancer cells leads to the formation of a primary tumor that can invade surrounding tissues and eventually spread from its original site by the lymphatic system to regional lymph nodes or by blood vessels to distant sites in a process which is known as metastasis.

To become malignant neoplastic cells, normal cells acquire several traits or hallmarks. The most fundamental characteristics of cancer cells are the ability to sustain chronic proliferation, the insensitivity to growth inhibitory signals, the evasion to programmed cell death, the limitless replicative potential, the capability to induce angiogenesis, the capability to produce invasion and metastasis, or the evasion of immune destruction (Hanahan and Weinberg, 2011).

Conventional treatments of cancer include surgery, chemotherapy, and radiation therapy, with successful therapeutic results in localized tumors and initial stages of the disease. However, many tumors are refractory to those therapies and, on the other hand, such therapies induce strong toxic side effects. Therefore, there is a huge necessity to develop new treatment strategies with higher specificity and lower toxicity profiles, such as virotherapy and immunotherapy.

2. VIROTHERAPY OF CANCER

Virotherapy of cancer is the treatment of this disease with oncolytic or replication-competent viruses. These viruses have the capability to infect and kill selectively neoplastic cells without damaging normal tissues (Hedley *et al.*, 2006; Russell *et al.*, 2012). Viral progeny produced after

the initial infection of tumor cells is released to the extracellular media in order to infect neighboring cells, thus amplifying the initial dose and, ideally, ending the process with the complete eradication of the tumor (**Figure 1**).

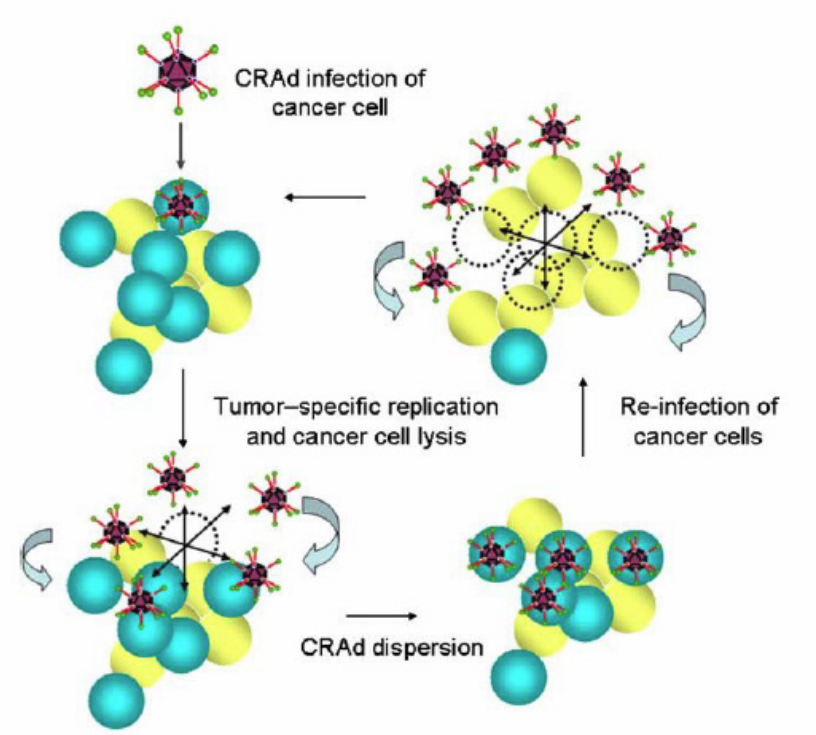

Figure 1. Oncolytic viral spread. Oncolytic viruses replicate in and kill selectively tumor cells. The self-amplification of the virus allows lateral spread in the tumor and greater tumor cell death from an initial infection of only few cells (adapted from (Hedley *et al.*, 2006)). CRAd, conditionally replicative adenovirus.

In addition to the direct killing of infected cells, oncolytic viruses can mediate the killing of uninfected cancer cells by indirect mechanisms, such as destruction of tumor blood vessels, amplification of specific anticancer immune responses, or through specific activities of transgene-encoded proteins expressed from engineered viruses (Russell *et al.*, 2012).

The use of viruses to treat cancer is an old concept that has been revisited during the last two decades with viruses genetically modified to acquire selectivity and potency. Soon after the discovery of viruses, in the turn of nineteenth century, emerged the idea to use them as possible anticancer agents. This concept came from the observation of spontaneous tumor regressions in patients that had undergone natural virus infections or which had been vaccinated (Sinkovics and Horvath, 1993; Kelly and Russell, 2007). Dock described in 1904 a leukemia case that went into remission after a presumed influenza infection (Dock, 1904). However, it was not until 1912

when DePace associated for the first time the regression of a cervix tumor after the administration of rabies vaccine to a patient with viral-related oncolysis (DePace, 1912).

In 1950s an 1960s, the advent of cell and tissue culture systems allowed *ex vivo* virus propagation, leading to the evaluation in human patients of the oncolytic properties of different viruses which had been previously tested in rodents (Southam and Moore, 1952; Huebner *et al.*, 1956; Hunter-Craig *et al.*, 1970; Yamanishi *et al.*, 1970). However, poor efficacy results together with the pathogenicity of some viruses lead to the abandonment of the field.

Nevertheless, a modern era of virotherapy started in the 1990s, thanks to the development of genetic engineering techniques that allowed the rational design of oncolytic viruses. Pioneers in this goal were Martuza and colleagues, who in 1991 published a thymidine kinase-negative HSV that replicated in dividing cells but crippled in non-dividing cells. This virus showed to be active in murine glioblastoma models (Martuza *et al.*, 1991). In 1996, McCormick improved the prospects of selectivity and efficacy by targeting defects that cause cancer with virus modifications (Bischoff *et al.*, 1996). From that moment on, several engineered oncolytic viruses from at least 10 different families have been tested in Phase I-III clinical trials, demonstrating excellent tolerability profile. Until now, evidences of antitumor activity after single-agent treatment have been observed in clinical trials with two different oncolytic viruses. The first of them was talimogene laherparepvec or simply known as T-Vec (or OncoVEX until BioVex was acquired by Amgen), which is an oncolytic Herpes Simplex Virus (HSV) encoding the granulocyte macrophage-colony stimulating factor (GM-CSF). Intratumoral administration of this virus led to complete regressions in 8 of 50 treated patients with metastatic malignant melanoma in a phase II clinical trial (Senzer *et al.*, 2009). More recently, a phase III clinical trial in patients with unresectable stage IIIB-IV melanoma showed an overall objective response rate of 26.4% including 10.8% of complete responses (Bartlett *et al.*, 2013). Importantly, T-Vec is likely to be approved next year for the treatment of melanoma. The second virus is a Vaccinia Virus (VV) which also expresses GM-CSF, named pexastimogene devacirepvec or Pexa-Vec (also known as JX-594). Intratumoral administration of this virus induced objective responses in 3 out of 10 evaluable patients with nonreseactable hepatocellular carcinoma (Park *et al.*, 2008). Later, a phase I clinical trial with Pexa-Vec demonstrated for the first time virus presence and selective replication in tumors after intravenous administration, besides dose-dependent antitumor activity (Breitbach *et al.*, 2011). Recently, a significant survival increase from 6.7 to 14.1 months was achieved in a phase I/II clinical trial in hepatocellular carcinoma patients (Heo *et al.*, 2013).

2.1. ONCOLYTIC ADENOVIRUSES

Adenoviruses have several features that make them attractive to be used as a platform for oncolytic viruses: they are not associated to any serious disease, they have a lytic cycle, their genome can be easily genetically modified to improve selectivity and potency traits, and they can be grown at high titers for its use in the clinical setting (Cody and Douglas, 2009).

2.1.1. General classification of adenoviruses

Adenovirus was firstly isolated from human adenoid cells in 1953 (Rowe *et al.*, 1953). Since then, more than 100 species have been characterized, including 57 different human serotypes, which are classified into 7 subgroups (A-G). The serotype that is more widely used in virotherapy is serotype 5 (Ad5), belonging to subgroup C (Rux and Burnett, 2004). The members of this group infect epithelial tissue from respiratory tract, causing mild respiratory affections.

2.1.2. Adenovirus structure

Adenovirus is a nonenveloped, double-stranded DNA virus. Viral DNA and associated core proteins such as pV, pVII, Mu (pX), and terminal protein (TP), are encased in an icosahedral capsid with 20 triangular faces and 60-90 nm of diameter. Each of the triangular faces is formed by 12 copies of hexon trimer (polypeptide II). Complexes formed by the pentameric penton base (polypeptide III) and trimeric fiber (polypeptide IV) form the vertices. Fiber protein, which radiates from the 12 vertices of the virion is structured in 3 domains: the N-terminal tail, that attach to the penton base, a central *shaft*, and a C-terminal globular *knob* domain that function as the cellular attachment site. Moreover, other minoritary proteins such as protein IIIa, VI, VIII, and IX make up the capsid, acting as cement between hexons (**Figure 2**).

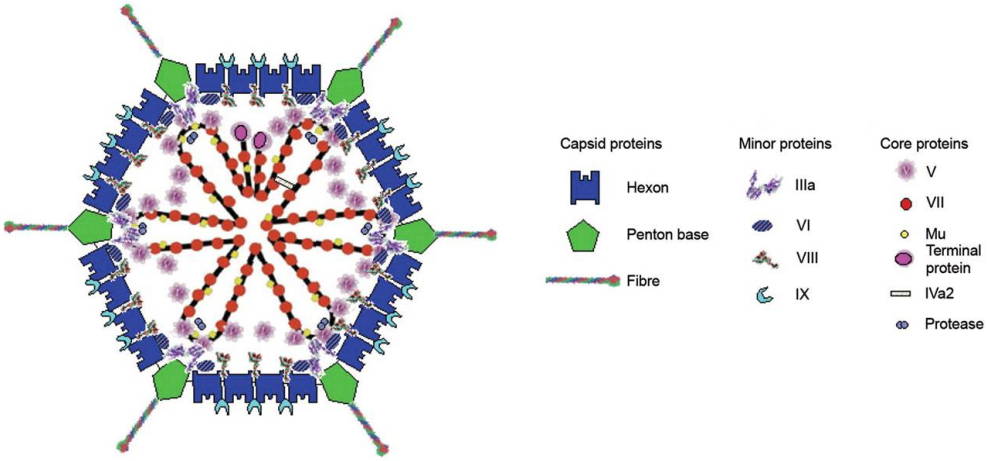

Figure 2. Adenovirus virion structure. Schematic representation of the capsid and core proteins of an adenovirus (adapted from (Russell, 2009)).

2.1.3. Genome structure

The genome of Ad5 consists in a 36 Kb lineal molecule of double-stranded DNA. Genetic information is organized in overlapping transcription units on both strands. Extensive splicing leads to the translation of over 50 proteins, from which 11 are structural virion proteins (Verma and Weitzman, 2005). Adenovirus genes are classified in 3 groups, according to the time course of their expression during viral cycle: early (E1A, E1B, E2, E3, and E4), delayed (IX and Iva2), and the major late transcription unit (MLU). The later is processed into 5 mRNA (L1-L5) that produce all the structural proteins. Moreover, adenovirus genome also contains the viral-associated (VA) genes that codify for two untranslated RNAs. At both sides of the genome there are two inverted terminal repeats (ITR) which contain the viral DNA replication origins. The packaging signal is located at 100 bp of the left ITR, it is rich in adenine and timidine and has an important role on the encapsidation of the virus. **Figure 3** depicts a schematic representation of the Ad5 genome.

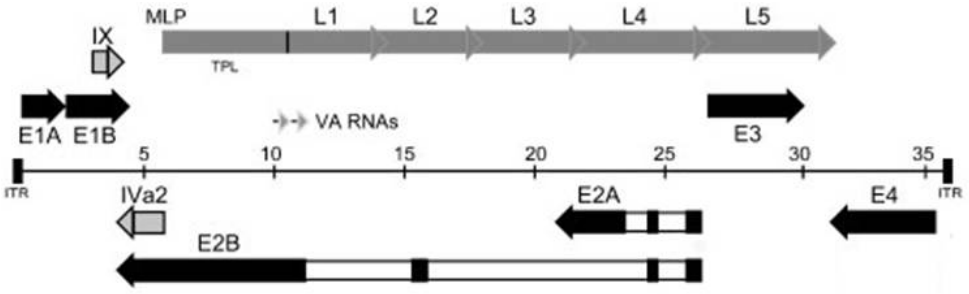

Figure 3. Adenovirus genome structure. The linear double-stranded genome is depicted in the center as a thin line, with the inverted terminal repeats (ITR) at each end: lengths are marked in kbp. Early transcription units are shown relative to their position and orientation in the Ad5 genome. Early genes are indicated by black bars and genes expressed at intermediate and late times of infection are indicated by gray bars (modified from (Tauber and Dobner, 2001)). MLP, Major Late Promoter; TLP, Tripartite leader; VA, virus-associated.

2.1.4. Biology of the infectious cycle

2.1.4.1. Binding and entry

Initial attachment of adenovirus type 5 (Ad5) particles to cell surface occurs through primary interaction between the fiber *knob* and the coxsackievirus B and adenovirus receptor (CAR). Since this binding is not sufficient for the internalization of the virus, a secondary interaction between an exposed RGD (Arg-Gly-Asp) motif located on the penton base protein and $\alpha_V\beta_3$ and $\alpha_V\beta_5$ integrins is needed (Wickham *et al.*, 1993; Wickham *et al.*, 1994). Interestingly, genetically

engineered Ad5 that lack CAR binding showed identical liver transduction than wild-type Ad5 after intravenous administration in rodents and primates, evidencing alternative mechanisms of virus transduction (Alemany and Curiel, 2001; Smith *et al.*, 2003a). Low affinity interactions with heparan-sulphate-glycosaminoglicans (HSG) are described to contribute to adenovirus internalization, and could mediate Ad2 and Ad5 transduction in the absence of CAR (Dechecchi *et al.*, 2001; Bayo-Puxan *et al.*, 2006). The conserved aminoacidic sequence $KKTK^{91-94}$ within the fiber *shaft* domain has been postulated as the putative HSG-binding motif (Zhang and Bergelson, 2005).

Moreover, liver transduction after intravenous administration occur by different mechanisms involving plasma proteins such as coagulation factor IX (FIX) and complement binding protein-4 (C4BP), which binds to fiber *knob*, and coagulation factor X (FX), which binds to hexon. Both interactions act as a bridge between adenovirus particle and alternative receptors such as HSGs and lipoprotein receptor-related proteins (LRPs) in the hepatocytes (Shayakhmetov *et al.*, 2005; Kalyuzhniy *et al.*, 2008; Waddington *et al.*, 2008). Alternatively, it has been recently shown that enhanced liver transduction of Ad5 vectors promoted by FX is due to its ability to protect the virus from the attack by classical complement pathway (Xu *et al.*, 2013).

The binding of adenovirus particles to its cellular receptors triggers virus internalization by clathrin-dependent, receptor-mediated endocytosis (Stewart *et al.*, 1997; Meier *et al.*, 2002). The acidic environment of endosomes induces escape of virions into the cytoplasm, where they traffic along microtubules toward the nucleous. After the dissembling of the capsid at the nuclear pore complex (NPC), viral transcriptional program starts (**Figure 4**).

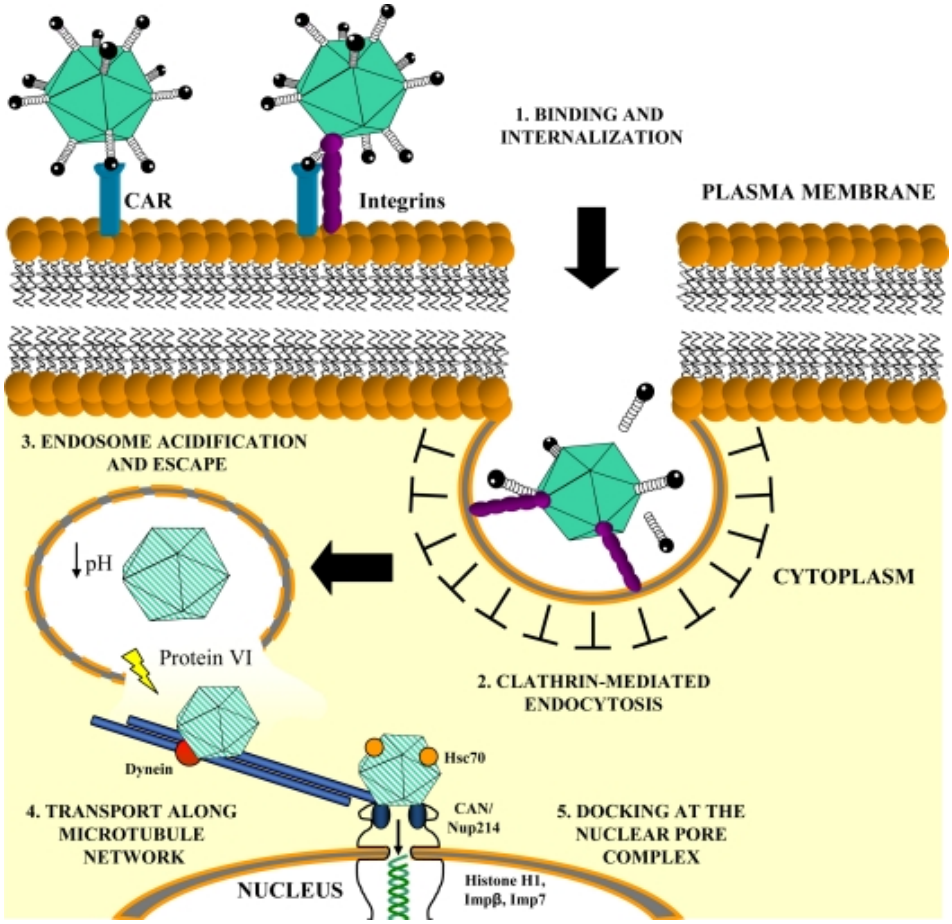

Figure 4. *In vitro* entry pathway of Ad5. Schematic representation of the different steps involved in the entry pathway of Ad5 *in vitro* (adapted from (Coughlan *et al.*, 2010)).

2.1.4.2. Early gene expression and DNA replication

E1A is the first viral transcription unit expressed, producing multiple mRNA and protein products by differential splicing or mRNA processing. During early infection, two transcripts are produced: 13S mRNA, encoding 289R protein, and 12S mRNA that encodes 243R protein. The main functions of E1A proteins are to induce the cell to enter in phase S in order to create an optimal environment for virus replication and the *trans*-activation of other adenovirus early transcription units (E1B, E2, E3, and E4) (Berk, 1986). The mechanism by which E1A activates cell cycle is the interaction of its products with Retinoblastoma (Rb) protein, which is a tumor suppressor that inhibits cell cycle via binding to E2F transcription factor. Conserved regions CR1, CR2, and CR3 of 289R and 243R proteins are able to sequester pRb and other members of its family such as p107 and p130 releasing free E2F, thus promoting DNA replication (Parreno *et al.*, 2001).

Cell cycle deregulation by E1A results in the accumulation of the tumor suppressor p53, which can turn out in apoptosis. In order to avoid premature death of infected cells and maximize viral yields, adenovirus protein E1B-55K acts to block p53-dependent apoptosis by directly binding p53 and preventing its ability to promote the expression of pro-apoptotic genes. In this sense, E1B-19K protein also contributes to this purpose by directly binding to proapoptotic proteins such as Bak and Bax.

E2 region encodes for proteins necessary to carry out viral genome replication, including DNA polymerase, preterminal protein and the single-stranded DNA-binding protein.

Products of E3 region function to subvert the host immune response, and allow persistence of infected cells. E3-gp19K (E3-19K) is a transmembrane glycoprotein targeted for membrane insertion via a cleavable N-terminal signal peptide (Wold *et al.*, 1985) and anchored in the membrane by an hydrophobic transmembrane domain near the C-terminus. Moreover, its cytoplasmatic tail contains a linear dilysine and a conformational endoplasmic reticulum (ER) retrieval motif that account for the protein's predominant localization in the ER (Paabo *et al.*, 1987; Nilsson *et al.*, 1989). E3-19K acts in two ways to prevent the presentation of viral antigens by the major histocompatibility complex (MHC) class I pathway, thereby avoiding the recognition and lysis of infected cells by cytotoxic T cells. First of all, its luminal domain is able to sequester MHC class I molecules in the ER, preventing its transport to the cellular surface. Moreover, it has been described that E3-19K can also bind the transporter associated to antigen processing (TAP), which is the responsible to translocate processed peptides generated by the proteasome in the cytoplasm to the ER, and interfering with the loading of peptides onto MHC class I molecules. Indeed, E3-19K binding to TAP blocks tapasin-mediated interaction with MHC class I molecules and TAP, thus accounting for delay in class I antigen maturation and cell surface antigen presentation even in the presence of MHC class I alleles that bind poorly to E3-19K (Cox *et al.*, 1991; Bennett *et al.*, 1999).

Other proteins of this transcription unit have been shown to inhibit induction of apoptosis by TNF-α, Fas ligand (FasL), and TRAIL. 10.4K and 14.5K proteins form a complex named receptor internalization and degradation (RID) that induce the clearance of chemokine receptors from the cell surface. This complex together with 14.7K protein also inhibits TNF-α induced secretion of arachidonic acid, which is an inflammatory mediator (McConnell and Imperiale, 2004).

E4 transduction unit encodes for proteins that play a role in cell cycle control and transformation. Moreover, other functions of these proteins include viral replication, stability and transport of viral mRNA, and induction of late gene expression.

2.1.4.3. Late gene expression and viral assembly

After the onset of DNA replication, transcription from major late promoter (MLP) is intensified to ensure the production of adequate amounts of structural proteins. The MLP regulates the expression of genes from major late transcription unit (MLU), which encodes for 15 to 20 different mRNAs derived from a single pre-mRNA by differential splicing and polyadenylation. Most adenovirus late genes are expressed from five regions, L1-L5, and correspond mostly to structural proteins and other proteins involved in virion assembly (McConnell and Imperiale, 2004). Transcription of these genes begins thanks to a conformational change in the adenoviral genome structure and to the activation by IVa2 protein (Chen *et al.*, 1994). Late mRNA are accumulated in the cytoplasm and specifically translated thanks to the tripartite leader sequence (TLP) that is shared by all the mRNA produced from MLP and allows the helicase-independent transcription of these genes (Huang and Schneider, 1991). Then, translated proteins are transported to the nucleus, where virions are assembled. Finally, adenoviral DNA is packaged in the capsid thanks to the binding of IVa2 protein to the packaging signal (Zhang and Imperiale, 2000).

Cell lysis and release of progeny virions occurs approximately 30 hours after the infection. Capsids are accumulated in the nucleus and intermediate filaments are disaggregated giving to the cells a round aspect which is characteristic of cytopathic effect (CPE). This process also involves E3-11.6K protein or adenovirus death protein (ADP), which unlike other products of E3 region, is only produced during the late phase of infection and is transcribed from MLP rather than E3 promoter (Tollefson *et al.*, 1996a; Tollefson *et al.*, 1996b).

2.1.5. Design of tumor selective oncolytic adenoviruses

Unlike other viruses such as reovirus, Newcastle disease viruses (NDV) or vesicular stomatitis virus (VSV), adenoviruses are not naturally selective for tumor cells. For this reason, genetic manipulation of adenovirus genome is needed to achieve tumor replication selectivity. Several strategies have been used with this purpose, including the deletion of viral genes that are essential for virus propagation in normal cells but complemented in tumor cells, the insertion of tumor-specific promoters controlling the expression of essential viral genes (transcriptional or translational targeting) or the modification of capsid proteins to achieve specific and efficient

infection of tumor cells (transductional targeting). The combination of these strategies has allowed the rational design of oncolytic adenoviruses.

2.1.5.1. Deletion of viral genes that confer tumor selectivity

It is known that adenovirus infection and oncogenic transformation induce similar signaling cascades in eukaryotic cells. Consequently, some mutant adenoviruses which showed impaired replication in normal cells are complemented for productive replication in tumor cells with deregulation on p53 and pRb pathways. Deletion of viral genes involved in these processes generates conditionally replicative adenoviruses. In fact, the first CRAd, proposed by Frank McCormick on 1996, was based on this concept. *dl1520* virus, also called ONYX-15, contained the deletion of E1B-55K gene, which function is to inactivate p53 protein and avoid death of infected cells by apoptosis (Bischoff *et al.*, 1996). Most tumor cells present natural inactivation of p53, being the function of E1B-55K dispensable in this type of cells whereas essential in normal cells. However, E1B-55K has other functions that are not complemented in tumor cells, attenuating viral replication.

Other examples of the use of this strategy to create tumor-selective replicating adenoviruses are Δ24 and *dl922-927* mutations. These viruses contain the deletion of the conserved region CR2 of E1A, which is responsible to bind and inactivate Rb. This function is necessary to induce S phase of cell cycle in normal cells but redundant in tumor cells, which have defects in Rb pathway. Viruses containing this mutation are not able to break the union between Rb and E2F in normal cells, presenting attenuated replication in these cells while preserving oncolytic potency in tumor cells (**Figure 5**). However, the selectivity of these viruses is limited since other regions of E1A can also interact with pRB (Fueyo *et al.*, 2000; Heise *et al.*, 2000).

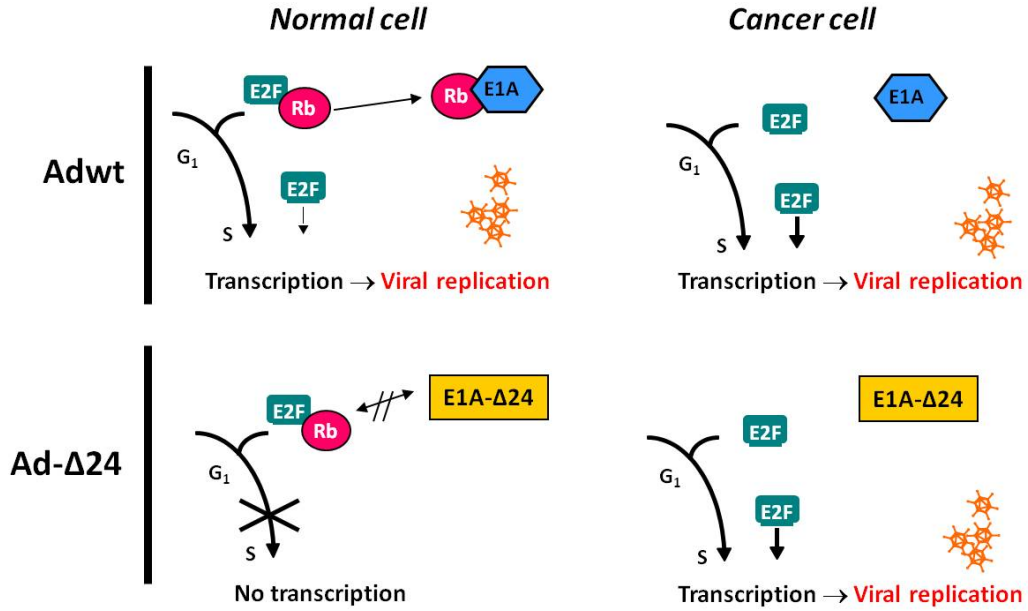

Figure 5. Δ24 selectivity mechanism. E1A protein binds and inactivates Rb to induce S phase of cell cycle and viral replication. In tumor cells this function is redundant, since Rb pathway is truncated and E2F is already free. In normal cells, Δ24 deletion avoids the dissociation of Rb and E2F and no viral replication occurs.

The deletion of the VA-RNAs genes is also described as a mechanism to confer selectivity for tumor cells with activated Ras pathway or truncated interferon (IFN) pathway, which are very common defects in tumors (Cascallo *et al.*, 2003; Cascallo *et al.*, 2006).

2.1.5.2. Transcriptional and translational targeting

The second strategy to confer tumor selectivity to oncolytic adenoviruses consists in the insertion of tissue-specific or tumor-specific promoters in their genome to regulate viral gene expression, especially E1A, since it is the first viral gene expressed, but also other early genes such as E1B, E2 or E4. Transcriptional targeting of adenoviruses was firstly introduced by Rodriguez and colleagues in 1997, when they used the prostate-specific antigen promoter (PSA) to drive the expression of E1A in the adenovirus CV706 (CN706) (Rodriguez *et al.*, 1997). Other specific promoters that have been used to target other type of tumors are the α-fetoprotein promoter (AFP) for hepatic carcinoma (Hallenbeck *et al.*, 1999), the osteocalcin promoter for osteosarcoma (Hsieh *et al.*, 2002), the melanoma-specific tyrosinase promoter (Nettelbeck *et al.*, 2002) or promoters that respond to hypoxia and estrogens to treat breast cancer (Hernandez-Alcoceba *et al.*, 2002).

Since this strategy is restricted to certain types of tumors that express the corresponding tumor-specific antigens, promoters which exploit common and general characteristics of tumor cells have also been used to allow for a wide applicability in different tumor types. In this regard,

the promoter of telomerase reverse transcriptase (TERT) has been used to drive E1A expression in oncolytic adenoviruses, since high telomerase activity in tumor cells is one of the hallmarks of their immortality and it is active in most human malignancies including lung, liver, gastric, breast, bladder, and prostate cancers (Huang *et al.*, 2002). Another exploitable characteristic is the deregulation of Rb pathway in almost all tumors. Taking this into account, promoters that respond to E2F transcription factor are suitable to achieve restricted replication in a broad range of tumor cells. Among others, regulation of E1A expression under E2F-1 promoter confers high potency of transcription (Johnson *et al.*, 2002; Tsukuda *et al.*, 2002; Cascallo *et al.*, 2007; Rojas *et al.*, 2009). Oncolytic adenoviruses that regulate the expression of E1A under the control of E2F-1 promoter inhibit its transcription by binding pRb-E2F-HDAC complexes in normal cells. Since pRb pathway is deregulated in tumor cells, E2F is free and can induce E1A expression, initiating viral cycle and promoting the transcription of other adenoviral proteins.

In this sense, an alternative strategy that has been used by our group for the generation of ICOVIR-15 is the modification of the endogenous E1A promoter by inserting E2F-binding sites to redirect E1A expression toward pRb deregulation (Rojas *et al.*, 2010). Moreover, this promoter also includes a Sp-1-binding site, since it has been described that both, E2F and Sp-1 transcription factors work together to activate transcription (Karlseder *et al.*, 1996).

2.1.5.3. Transductional targeting

The concept of transductional targeting refers to the modification of capsid proteins in order to achieve preferential infection of tumor cells rather than normal cells. Virus attachment proteins can be adapted to use receptors that are expressed preferentially or exclusively on the surface of tumor cells. Upon intravascular administration, adenovirus accumulates mostly in the liver, causing toxicity and limiting the amount of virus available to reach tumor nodes. Therefore, transductional strategies include both, the ablation of the interaction of adenoviruses with its normal receptors, especially those implicated in hepatic transduction (detargeting), and the redirection of virion binding to tumor-associated receptors (retargeting).

In this sense, as it has been described the importance of coagulation factors in hepatic tropism, the abrogation of the interaction between adenovirus capsid and these factors has shown to greatly reduce liver transduction (Bayo-Puxan *et al.*, 2006; Waddington *et al.*, 2008). Unfortunately, these modifications also reduced tumor transduction, evidencing the important role of coagulation factors in this process *in vivo* (Gimenez-Alejandre *et al.*, 2008). Alternatively, the mutation of the putative HSG-binding domain KKTK, located in the fiber *shaft*, abrogates liver

transduction in mice, rats, and non-human primates (Smith *et al.*, 2003a; Smith *et al.*, 2003b; Nicol *et al.*, 2004). However, this mutation also causes a significant reduction of tumor cells infectivity (Bayo-Puxan *et al.*, 2006).

With regard to tumor targeting, adenoviruses exposing different ligands in fiber (C-terminal or HI-loop) (Dmitriev *et al.*, 1998; Krasnykh *et al.*, 1998; Belousova *et al.*, 2002; Kurachi *et al.*, 2007), hexon (Wu *et al.*, 2005), penton base (Wickham *et al.*, 1996; Einfeld *et al.*, 1999), or pIX (Campos *et al.*, 2004; Le *et al.*, 2004; Meulenbroek *et al.*, 2004; Le *et al.*, 2005) capsid proteins have been described. Among all of them, the HI-loop in the *knob* domain of the fiber is one of the most explored locations, allowing the incorporation of large polypeptides (up to 83 amino acids) that exceed almost 50% in size the *knob* domain with only marginal negative consequences in viral replication (Belousova *et al.*, 2002).

A widely used ligand to achieve tumor tropism is the RGD-4C motif (CDCRGDCFC) which targets RGD-binding integrins that are overexpressed in tumor cells (Dmitriev *et al.*, 1998; Cripe *et al.*, 2001; Grill *et al.*, 2001; Wesseling *et al.*, 2001; Nagel *et al.*, 2003). The insertion of this ligand in the HI-loop allows the use of integrins as primary receptors instead of CAR, which is not highly expressed in tumor cells (Bauerschmitz *et al.*, 2002).

The combination of hepatic tropism ablation by mutation of the KKTK domain and the insertion of targeting peptides in the HI-loop such as RGD has not been successful, presumably due to a negative effect on the bending or structure of the fiber (Bayo-Puxan *et al.*, 2006; Kritz *et al.*, 2007; Rittner *et al.*, 2007). However, the replacement of the KKTK domain with an RGD motif described by our group (RGDK modification), significantly increased tumor cell transduction and improved the tumor-to-liver ratio *in vivo* in the context of a non-replicative adenovirus (Bayo-Puxan *et al.*, 2009).

2.1.6. ICOVIR-15K

ICOVIR-15K is an oncolytic adenovirus that has been developed by our group and that we currently use as a platform to incorporate novel modifications and improvements (Rojas *et al.*, 2011). This virus derives from ICOVIR-15 (Rojas *et al.*, 2010), and combines modifications corresponding to the three previously described strategies to achieve tumor selectivity. First of all, the endogenous promoter of E1A has been modified by incorporating eight extra E2F-responsive sites organized in four palindromes and one extra Sp-1-binding site. Second, it contains the Δ24 deletion in E1A that abrogates the interaction of this protein with pRb, so in case that leaky expression of E1A occurs, E1A-Δ24 won't be able to release E2F from pRb. Both of

these modifications confer replication dependency on Rb pathway deregulation. As a third modification, distinct from ICOVIR-15 that contains the RGD ligand in the HI-loop of the fiber, ICOVIR-15K incorporates the transductional targeting mutation RGDK. As described in the section above, RGDK consists in the replacement of the KKTK HSG-binding domain by an RGD motif in order to reduce hepatic tropism and increase tumor transduction (Bayo-Puxan *et al.*, 2009). Moreover, ICOVIR-15K has shown increased bioavailability of the virus after systemic administration and greater antitumor activity *in vivo* compared to ICOVIR-15 (Rojas *et al.*, 2011) (**Figure 6**).

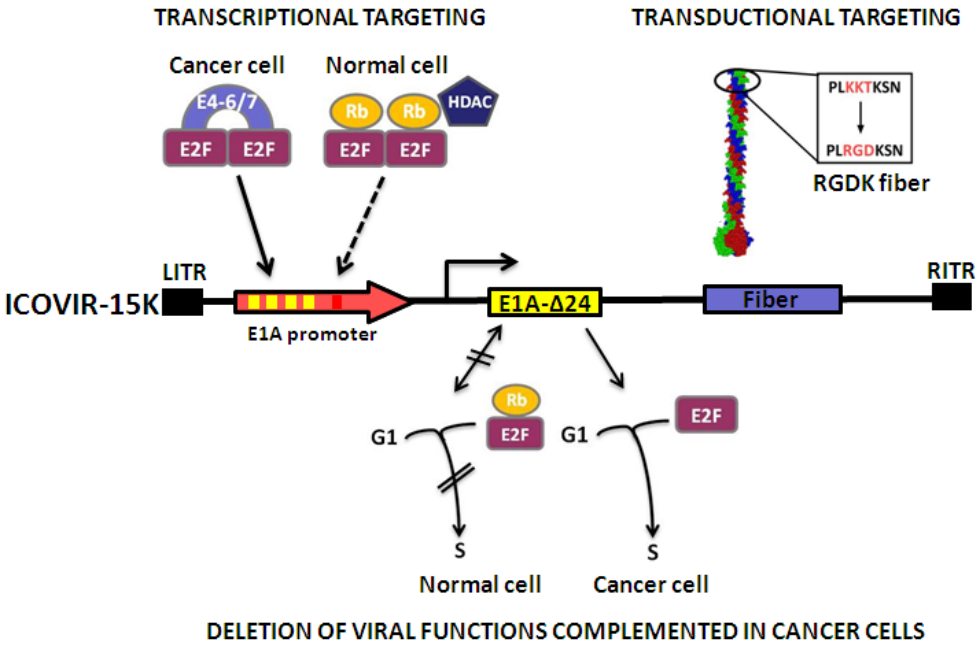

Figure 6. Schematic representation of the modifications in ICOVIR-15K genome. ICOVIR-15K contains the modified E1A promoter (including four E2F boxes and one Sp1 box) and the truncated E1A protein to confer selectivity for tumor cells. It also has the RGD motif replacing the KKTK domain in the shaft of the fiber.

2.1.7. Clinical experience with oncolytic adenoviruses

So far, several oncolytic adenoviruses have been tested in the clinic involving different types of tumors and routes of administration. *dl1520* or ONYX-015, developed by Onyx Pharmaceuticals, was the first engineered replication selective virus to be used in humans (Bischoff *et al.*, 1996). Up to eighteen phase I and II clinical trials have been performed with this virus. Initial trials included head and neck tumors that were treated by intratumoral administration. Virus administration was well tolerated with only mild flu-like symptoms, but no objective clinical responses were observed (Ganly *et al.*, 2000a). Later, encouraging results were obtained with the combination of ONYX-015 and chemotherapy in a phase II trial in the same type of tumors, where 19 out of 30 injected tumors decreased 50% or more in size and 8 complete responses were reported (Khuri *et al.*, 2000b; Lamont *et al.*, 2000). However, long-term survival was not

improved. Other bad prognosis tumor types such as pancreatic carcinoma or glioblastoma were treated with intratumoral injections of ONYX-015, without observing toxicity or objective responses (Mulvihill *et al.*, 2001; Hecht *et al.*, 2003; Chiocca *et al.*, 2004). After intratumoral administration, intraperitoneal injection was also tried for metastatic ovarian carcinoma (Vasey *et al.*, 2002). The lack of toxicity in these studies encouraged intravascular administration in patients with hepatic metastasis of colorectal carcinoma or lung metastasis (Nemunaitis *et al.*, 2001a; Reid *et al.*, 2002a). The highest dose administered to a patient was of $2x10^{13}$ viral particles (vp) on day 1, followed by 11 weekly doses of $2x10^{12}$ vp, resulting in an accumulated dose of $4.2x10^{13}$ vp. Although some dose-dependent toxicity corresponding to fever, vomits, nauseas, and chills was observed, maximum tolerated dose was not reached. Unfortunately, no responses were seen. Despite the poor efficacy of this virus, the Chinese company Sunway Biotech is commercializing H101 in China for the treatment of head and neck cancer via intratumoral injection. This virus is a derivative of ONYX-015 which, besides E1B-55K, it also lacks E3 proteins, resulting less potent and more immunogenic (Garber, 2006). The next oncolytic adenovirus to be tested upon systemic administration was CV787, named CG7870 after the acquisition of Calydon by Cell Genesys. This virus expresses E1A under the control of probasin promoter and E1B under the control of PSA promoter, making it specific for prostatic cancer. Flu-like toxicity was also observed for this virus in phase I clinical trial, and despite a drop in PSA levels in 3 out of 8 patients treated with the highest dose, no longer efficacy was observed (Small *et al.*, 2006). Lately, other phase I clinical trials involving intratumoral or intracavity routes of administration of oncolytic adenoviruses such as Telomelysin, Ad5-CDTKrep or Ad5-Δ24-RGD have been completed with good safety profiles but discrete clinical responses. Most notable in this regard are the results with intraperitoneal Ad5-Δ24-RGD, which is a parental virus of ICOVIR-15 that has obtained 71% stable disease (Bauerschmitz *et al.*, 2002; Kimball *et al.*, 2010). Regardless these modest clinical results in terms of antitumor efficacy, more encouraging results were exhibited by oncolytic adenoviruses that also induce or modulate immune responses, as it will be reviewed in *section 2.6.1*.

With regard to intravenous administration, the oncolytic adenovirus ColoAd1 (Enadenotucirev), a chimeric Ad11 with a nearly complete E3 region deletion, a smaller deletion in the E4 region, and a chimeric Ad3/Ad11p E2B region, is currently being tested in phase I/II clinical trials. Moreover, phase I clinical trials have started recently to evaluate the safety and efficacy of two oncolytic adenoviruses developed by our group: ICOVIR-5 and VCN-01 (ICOVIR-17K, described in this thesis). Parallel clinical trials with both viruses are currently ongoing upon intratumoral and intravenous administration.

Virus	Modifications	Phase	Tumor	Route	Combination	Site	Status	Reference
Oncorine (H101)	E1B-55K$^-$, E3$^-$	2	SCCHN	IT	Cisplatin	Multicenter	Completed	(Xu *et al.*, 2003)
		3	SCCHN	IT	Cisplatin	Multicenter	Completed	(Xia *et al.*, 2004)
Onyx-015	E1B-55K$^-$, E3$^-$	1	Lung Mets	IV	-	Multicenter	Completed	(Nemunaitis *et al.*, 2001a)
		1	Glioma	Intracavity	-	Multicenter	Completed	(Chiocca *et al.*, 2004)
		1	Ovarian cancer	IP	-	Multicenter	Completed	(Vasey *et al.*, 2002)
		1	SCCHN	IT	-	Multicenter	Completed	(Ganly *et al.*, 2000a)
		1	Solid tumors	IV	Enbrel	Mary Crowley	Completed	(Nemunaitis *et al.*, 2007)
		1	Sarcoma	IT	Mitomycin-C, Dox, Cisplatin	Mayo Clinic	Completed	(Galanis *et al.*, 2005)
		1/2	PanCa	IT	Gemcitabine	UCLA	Completed	(Hecht *et al.*, 2003)
		2	CRC	IV	-	Multicenter	Completed	(Hamid *et al.*, 2003)
		2	Hepatobiliary	IT	-	Montefiore	Completed	(Makower *et al.*, 2003)
		2	CRC, PanCa	IA	-	Multicenter	Completed	(Reid *et al.*, 2002a)
		2	SCCHN	IT	-	Multicenter	Completed	(Nemunaitis *et al.*, 2001b)
		2	SCCHN	IT	Cisplatin, 5-FU	Multicenter	Completed	(Khuri *et al.*, 2000a)
		2	CRC	IV	5-FU/leucovorin	Stanford	Completed	(Reid *et al.*, 2005)
CG7060	PSA control	1	Prostate cancer	IT	RT	John Hopkins	Completed	(DeWeese *et al.*, 2001)
CG7870/CV787	Rat probasin-E1A, hPSA-E1B, E3$^+$	1/2	Prostate cancer	IV	-	Multicenter	Completed	(Small *et al.*, 2006)
		1/2	Prostate cancer	IV	Docetaxel	Mary Crowley	Terminated	-
CG0070	E2F-1, GM-CSF	2/3	Bladder cancer	Intracavity	-	UCSF	Not open	(Ramesh *et al.*, 2006)
Telomelysin	hTERT	1	Solid tumors	IT	-	Mary Crowley	Completed	(Nemunaitis *et al.*, 2010)
Ad5-CD/TKrep	CD/TK	1	Prostate cancer	IT	5-FC and GCV	Henry Ford	Completed	(Freytag *et al.*, 2002)
		1	Prostate cancer	IT	5-FC, GCV, and RT	Henry Ford	Completed	(Freytag *et al.*, 2003)
H103	Ad2, HSP70	1	Solid tumors	IT	-	Cancer Hospital, Chinese Academy of Medical Sciences	Completed	(Li *et al.*, 2009b)

Virus	Modifications	Phase	Tumor	Route	Combination	Site	Status	Reference
Ad5-D24-RGD	RGD, Delta-24	1	Ovarian Cancer	IP	-	UAB	Completed	(Kimball *et al.*, 2010)
		1	Glioma	IT	-	MD Andersen	Recruiting	-
		1/2	Glioma	IT	-	Erasmus Medical	Recruiting	-
Ad5-SSTR/TK-RGD	SSTR, TK, RGD	1	Ovarian cancer	IP	GCV	UAB	Active	-
CGTG-102	Ad5/3, GM-CSF, Delta-24	1/2	Solid tumors	IT	-	Baylor	Not open	(Koski *et al.*, 2010)
		1	Solid tumors	IT/IV	Metronomic CPA	Docrates Hospital Helsinki	Recruiting	-
INGN-007 (VRX-007)	wtE1a, ADP	1	Solid tumors	IT	-	Mary Crowley	Not open	(Lichtenstein *et al.*, 2009)
ColoAd1	Ad3/11p	1/2	CRC, HCC	IP	-	Multicenter	Recruiting	(Kuhn *et al.*, 2008)
		1/2	CRC, Bladder cancer, NSCLC, RCC	IT/IV	-	Multicenter	Recruiting	-
		1/2	Solid tumors, Bladder cancer, CRC	IV	-	Multicenter	Recruiting	-
ICOVIR5	E2F-1 promoter, Delta-24, Kozak sequence, DM, RGD	1	Melanoma	IV	-	ICO	Recruiting	-
		1/2	Solid tumors	IP (via MSCs)	-	Hospital Infantil Universitario Niño Jesús	Recruiting	-
VCN-01 (ICOVIR-17K)	Modified E1A promoter, delta-24, RGDK, HYAL	1	PanCa	IT	Gemcitabine	Multicenter	Recruiting	-
		1	Solid tumors	IV	Gemcitabine	Multicenter	Recruiting	-

Table 1. Completed and ongoing clinical trials with oncolytic adenoviruses. Adapted from (Russell et al., 2012). 5-FC, 5 fluorocytosine; 5-FU, 5-fluorouracil; CPA, cyclophosphamide; CRC, colorectal cancer; Dox, doxorubicin; GCV, ganciclovir; HCC, hepatocellular carcinoma; IV, intravenous; IT, intratumoral; IP, intraperitoneal; Mets, metastasis; MSC, mesenchymal stem cells; NSCLC, non-small cell lung carcinoma; PanCa, pancreatic cancer; RCC, renal carcinoma; RT; radiation therapy; SCCHN, squamous cell carcinoma of the head and neck.

2.1.8. Limitations of oncolytic adenoviruses

Overall, clinical data on oncolytic adenoviruses, especially after intravenous administration, point out the need of more potent and selective viruses. Beyond the difficulties of this route of administration, other barriers to virotherapy success imposed by the tumor microenvironment need to be addressed (**Figure 7**).

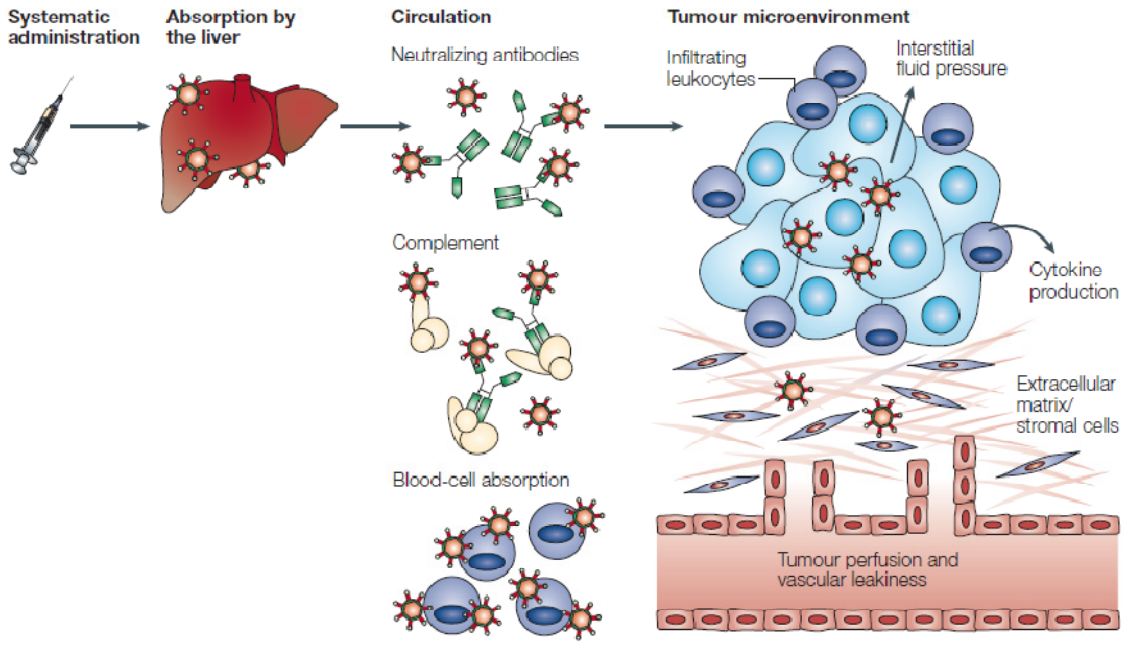

Figure 7. Barriers to intravenous delivery of oncolytic viruses *in vivo*. Within minutes after systemic administration of an oncolytic virus, most of the initial dose is retained by the liver. Moreover, oncolytic viruses can be neutralized by the interaction with blood cells, the complement or neutralizing antibodies. Finally, to enter into the tumor mass, the virus must cross the vascular endothelium against a gradient of interstitial fluid pressure. In addition, tumor stroma and infiltrating leukocytes limit the intratumoral spread of the virus (adapted from (Parato *et al.*, 2005)).

2.1.8.1. Tumor targeting upon systemic administration

Although many ongoing clinical trials are using intratumoral administration, systemic delivery will likely be required for metastatic disease treatment. In this sense, current research on the field is focused basically on avoiding neutralization of the virus by serum factors, minimizing sequestration of the virus in the liver and spleen and enhancing tumor vessels permeability.

Since adenoviruses are not blood-borne viruses, they are rapidly cleared from the circulation resulting in a half-life of less than 2 minutes in mice (Alemany *et al.*, 2000) and 10 minutes in humans (Reid *et al.*, 2002b). Intravascular delivery of adenoviruses leads to a complex series of

interactions with blood components such as coagulation factors, complement, blood cells, and neutralizing antibodies. Moreover, the loss of virus through vascular fenestrations of spleen and liver and subsequent uptake of adenovirus particles by Kupffer cells (KC) in the liver contribute to clearance. Opsonization of viral particles with natural antibodies and complement, together with unspecific interaction with scavenger receptors are responsible of the uptake by KCs (Smith *et al.*, 2008; Xu *et al.*, 2008).

Some strategies involving genetic modifications of capsid proteins to improve tumor targeting and reduce liver transduction have been discussed in *section 2.1.5.3* (transductional targeting). Moreover, chemical modification of the capsid by coating it with polymers such as polyethylene glycol (PEG) is utilized in order to mask the virion, thus shielding it from undesirable interaction with blood factors or native receptors (Coughlan *et al.*, 2010).

Leaky vasculature of tumors could be exploited to enhance delivery of therapeutic macromolecules into tumor tissues (Fang *et al.*, 2011). However, tumors are heterogenic organs composed by a dense stroma containing extracellular matrix proteins (collagen, fibronectin, laminin, fibrin, and sparc/osteonectin), polysaccharides (proteoglycan glycosaminoglycans such as protein-attached heparin, condroitin and keratin-sulfates, and non-proteoglycan glycosaminoglycans such as hyaluronan), and cells such as fibroblasts or inflammatory cells. This stromal tissue, together with poor lymphatic drainage, increases the interstitial fluid pressure in tumors, hampering virus extravasation and diffusion (Baumgartner *et al.*, 1998).

2.1.8.2. Intratumoral spread of oncolytic adenoviruses

Replication, amplification, and dissemination of oncolytic adenoviruses within tumors is one of the advantages of virotherapy compared to conventional therapies, since the initial dose is amplified until the complete lysis of the tumor mass is produced. However, besides precluding virus arrival to the tumors via vasculature, the tumor stroma also halts intratumoral virus spread, since adenoviruses neither cross barriers imposed by extracellular matrix nor replicate in non-tumor cells such as fibroblasts.

Several strategies to improve intratumoral spreading of oncolytic adenoviruses are currently being explored. Arming oncolytic viruses with ECM-degrading enzymes is a commonly exploited strategy to enhance viral penetration of solid tumors (Smith *et al.*, 2011). Different proteins that modulate the configuration of ECM have been used to increase viral spread and antitumor efficacy in different tumor models. For instance, small molecules such as relaxin and decorin have been expressed from oncolytic adenoviruses, aiming at inhibit collagen production and

upregulate the expression of matrix metalloproteases (MMP) that participate in the degradation of this connective tissue protein (Kim *et al.*, 2006; Ganesh *et al.*, 2007; Choi *et al.*). Our group has previously explored the expression of hyaluronidase from an oncolytic adenovirus, which demonstrated to improve intratumoral virus spread in addition to increase antitumor activity compared to its parental oncolytic adenovirus (Guedan *et al.*, 2010). This effect is associated to the digestion of hyaluronic acid (HA) that is one of the main components of the extracellular matrix of tumors. Depletion of HA by hyaluronidase decreases the interstitial fluid pressure inside the tumors, decompressing blood vessels and increasing vascular permeability, thereby favouring the penetration of the virus to the tumor core (Beckenlehner *et al.*, 1992; Spruss *et al.*, 1995; Smith *et al.*, 1997; Pillwein *et al.*, 1998; Eikenes *et al.*, 2005; Provenzano *et al.* 2012). One of the objectives of this thesis was to combine the expression of hyaluronidase with the retargeting modification RGDK, described in the previous *section 2.1.5.3.*, in a single oncolytic adenovirus named ICOVIR-17K.

Strategies to improve virus replication in stromal non-tumor cells such as fibroblasts are also under investigation. For example, one approach is the use of specific promoters, such as the SPARC promoter, that allow for virus replication in tumor and stromal cells (Lopez *et al.*, 2012). Alternatively, our group recently described that the truncation of the i-leader adenoviral protein enhanced the release and cytotoxicity of the virus in cancer-associated fibroblasts (CAFs) *in vitro* and increased its antitumor activity *in vivo* (Puig-Saus *et al.*, 2012; Puig-Saus *et al.*, 2014).

2.1.8.3. Immune responses

Intravenous administration of adenoviruses leads to a strong activation of the innate immune system, mediated by neutrophils, macrophages, natural killer (NK) cells, and soluble factors such as complement and inflammatory cytokines.

Interaction of adenoviruses with preexisting specific anti-adenovirus antibodies in the bloodstream, and the activation of the classical arm of the complement pathway with the consequent opsonization of viral particles, neutralize the virus and facilitate its rapid clearance from blood by cellular elements of the innate immune response, including KCs and other cells of the reticulo-endothelial system.

Once captured by innate immune cells such as macrophages, dendritic cells (DCs), and epithelial cells, response against adenoviruses starts with the recognition of pathogen-associated molecular patterns (PAMPs) mediated by pattern recognition receptors (PRRs) such as Toll-like receptors (TLRs). This effect is strongly associated with the induction of inflammatory cytokines

or chemokines such as IL-6, TNF-α, MIP-2, MIP-1α, and type I IFNs (Hartman *et al.*, 2008). All these cytokines act recruiting neutrophils and NK cells to the site of infection, and later monocytes and T cells. Moreover, induced cytokines also activate trafficking of DCs to draining lymph nodes and their maturation to engage adaptive and memory immune responses that rapidly eliminate infected cells (Alemany and Cascallo, 2009).

The immune system can be seen as an ally or as an enemy for virotherapy. From the "virocentric" point of view, the immunosuppression of the tumor is beneficial for the treatment with oncolytic viruses, since it might be more permissive to viral replication. Although adenoviruses possess several mechanisms to counteract the effect of the immune system such as the retention of MHC class I molecules by E3-19K protein (that prevents its surface presentation and subsequent recognition by NK cells -that attack cells with low surface MHC class I levels- and presentation of viral epitopes in the cell surface), they are not enough to evade immune responses.

Supporting the "virocentric" hypothesis, studies combining oncolytic adenoviruses with the immunosuppressive agent cyclophosphamide (CPA) demonstrated sustained replication of the virus and increased antitumor activity in a relevant immunocompetent model as it is the Syrian hamster (Thomas *et al.*, 2008a). Moreover, data from clinical trials supports this notion since best responses have been obtained in immunosuppressed patients (Kelly and Russell, 2007).

In addition to a combined treatment with immunosuppressive agents, other strategies have been explored to evade the immune system. Preimmunity against adenovirus 5 in humans can be counteracted by the genetic engineering or chemical modification of the adenoviral capsid to abrogate the interaction with neutralizing antibodies. Some approaches are the switch of capsid proteins from high-prevalent serotypes such as Ad5 to other uncommon serotypes such as Ad48, or the coating of the viral particle with polymers such as PEG. A different approach consists in the use of cell carriers to hide adenoviruses from antiviral immune responses. With this aim, autologous mesenchymal stem cells (MSCs) or monocytes have been used to bring oncolytic adenoviruses to tumors without being eliminated by the immune system, thanks to their intrinsic tumor homing properties (Garcia-Castro *et al.*, 2010; Nakashima *et al.*, 2010; Bunuales *et al.*, 2012). Finally, the genetic engineering of oncolytic viruses to express genes with immunosuppressive functions has been explored to achieve enhanced antitumor activity (Haralambieva *et al.*, 2007; Altomonte *et al.*, 2009).

On the other hand, for “immunocentrics”, the immunogenicity of oncolytic viruses might break the local immunosuppressive state of tumors, thus favoring the generation and amplification of specific antitumor immune responses and improving the outcome of virotherapy. However, an important hurdle of this strategy is that the strong immune response generated against viruses might mask specific responses against tumor antigens, limiting the efficacy of this approach (Alemany and Cascallo, 2009). This issue will be further discussed below.

2.1.9. Combination of oncolytic adenoviruses and chemotherapy

Besides improvement of the oncolytic adenovirus by itself, other strategies such as the combination with drugs have been used to further enhance antitumor efficacy in the clinical setting.

Preclinical studies *in vitro* and in animal models have shown synergistic and/or additive effects between oncolytic adenoviruses and chemotherapeutic drugs including gemcitabine, cisplatin, doxorubicin, irinotecan, 5-fluororacil, taxanes, etoposide, or mitoxantrone (You *et al.*, 2000; Yu *et al.*, 2001; Raki *et al.*, 2005; Fujiwara *et al.*, 2006; Bhattacharyya *et al.*, 2011; Siurala *et al.*, 2014). Furthermore, superior antitumor activity has been observed with the virus and chemotherapy combination than with single-agent treatments in several clinical trials (Khuri *et al.*, 2000a; Hecht *et al.*, 2003; Xia *et al.*, 2004).

Mechanisms involved in this synergistic effect are not well-known so far, but might vary regarding the kind of chemotherapeutic drug and its mechanism of action, as well as the genetic modifications possessed by each particular oncolytic adenovirus. Some possibilities include chemosensitization induced by E1A, drop of intratumoral interstitial fluid pressure (IFP) leading to increased penetration of the drugs, and induction of abnormal mitosis causing apoptosis (Bressy and Benihoud, 2014). In addition, it has been reported that metronomic administration of chemotherapeutic drugs such as gemcitabine, docetaxel, temozolomide, paclitaxel, CPA, or vinorelbine may activate antitumor immunity by several mechanisms (Chen *et al.*, 2014).

In this work we have combined the novel oncolytic adenovirus containing the RGDK retargeting modification and expressing hyaluronidase with the chemotherapeutic drug gemcitabine. In this regard, early clinical trials have demonstrated that hyaluronidase enhances chemotherapy efficacy in cancer patients (Baumgartner *et al.*, 1998). Preclinical studies by Provenzano and coworkers have attributed the beneficial effect of hyaluronidase to lower interstitial pressure in HA-depleted tumors, leading to blood vessel decompression and

increasing the vascular permeability, thereby favoring the penetration of drugs to the tumor core (Provenzano *et al.*, 2012) (**Figure 8**).

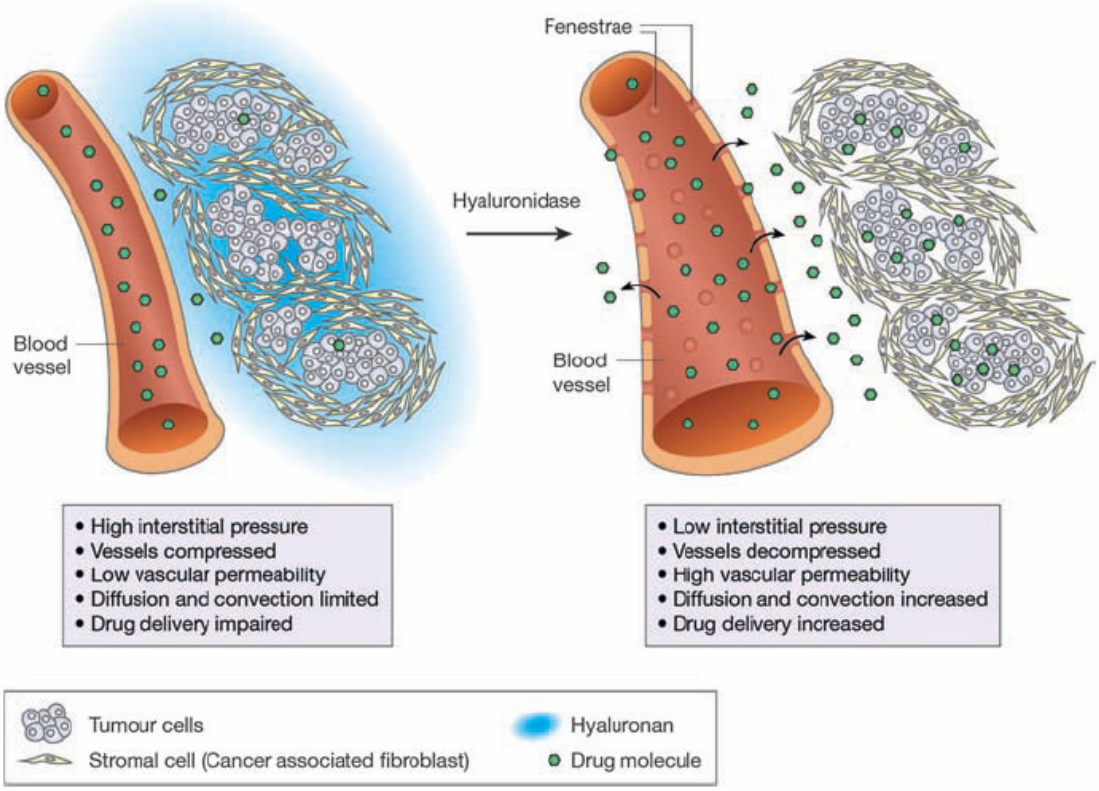

Figure 8. **Effects of hyaluronidase on the tumor vasculature and interstitial fluid pressure in tumors.** Adapted from (Michl and Gress, 2012).

3. IMMUNOLOGY OF CANCER

The idea that the immune system can control cancer has been discussed for over a century. In the early 1900s, Paul Ehrlich was the first author to suggest that tumor development can be suppressed by the immune system. An enhanced understanding of the immune system and the evidence of the existence of tumor antigens resurfaced this idea 50 years later. These advances led to the proposal of the immunosurveillance hypothesis by Burnet and Thomas, which postulates that adaptive immunity is responsible for preventing cancer development in immunocompetent hosts (Burnet, 1957). This hypothesis was supported by the discovery of the role of IFN-γ in promoting immunological induced rejection of transplanted tumor cells (Dighe *et al.*, 1994). Moreover, it was observed that immunodeficient mice lacking IFN-γ responsiveness (gene-targeted mice lacking either the IFN-γ receptor or the STAT1 transcription factor required for IFN receptor signaling) or adaptive immunity ($RAG2^{-/-}$ mice, lacking T, B, and NKT cells) were more susceptible to carcinogen-induced and spontaneous neoplasia than immunocompetent mice (Kaplan *et al.*, 1998; Shankaran *et al.*, 2001). Furthermore, a relatively high percentage of tumors (40%) of methylcholanthrene (MCA) carcinogen-induced sarcomas derived from immunodeficient $RAG2^{-/-}$ mice were spontaneously rejected when transplanted into wild-type mice. In contrast, tumors derived in immunocompetent mice grew normally after its transplantation into wild-type syngenic mice (Shankaran *et al.*, 2001). These evidences strongly suggested that tumors formed in immunocompetent recipients are less immunogenic than those developed in the absence of an intact immune system, being the former more aggressive since they have been “edited” in order to eliminate those cells which were more susceptible to be attacked by the immune system (Schreiber *et al.*, 2011).

This process of immunoediting of tumors occurs through three distinct phases known as “elimination”, “equilibrium”, and “escape” represented in **Figure 9** (Dunn *et al.*, 2002). The elimination phase is an updated version of cancer immunosurveillance, in which innate and adaptive immune systems work together to detect the presence of a developing tumor and destroy it before it becomes clinically apparent. Classical “danger signals” such as type I IFN (Matzinger, 1994) may be involved in this process, activating dendritic cells (DCs) and promoting the induction of adaptive antitumor immune responses. Moreover, damage-associated molecular pattern molecules (DAMPs) that are released from dying tumor cells or damaged tissues may also play a key role. Finally, a third mechanism involve stress ligands such as RAE-I or H60 (mouse) or MICA/B (human) that are frequently expressed on tumor cells surface. Binding of these ligands to activating receptors leads to a release of pro-inflammatory and immunomodulatory cytokines

that facilitates development of a tumor-specific adaptive immune response (Guerra *et al.*, 2008). Additionally, expression of tumor antigens is needed to propagate $CD4^+$ and $CD8^+$ T cells. Sometimes, tumor cell variants may survive to the elimination phase and enter into the equilibrium phase, in which the adaptive immune system prevents tumor growth and tumor cells remain functionally dormant and clinically unapparent (Koebel *et al.*, 2007). This latency state could be broken by several mechanisms and tumors enter in the escape phase, in which tumor cells that have acquired the ability to circumvent immune recognition emerge as progressively growing clinically visible tumors. Mechanisms of tumor escape will be discussed in *section 3.3*. In this case, the immune system contributes to tumor progression by selecting more aggressive tumor variants, suppressing the antitumor immune response, or promoting tumor cell proliferation (Vesely *et al.*, 2011).

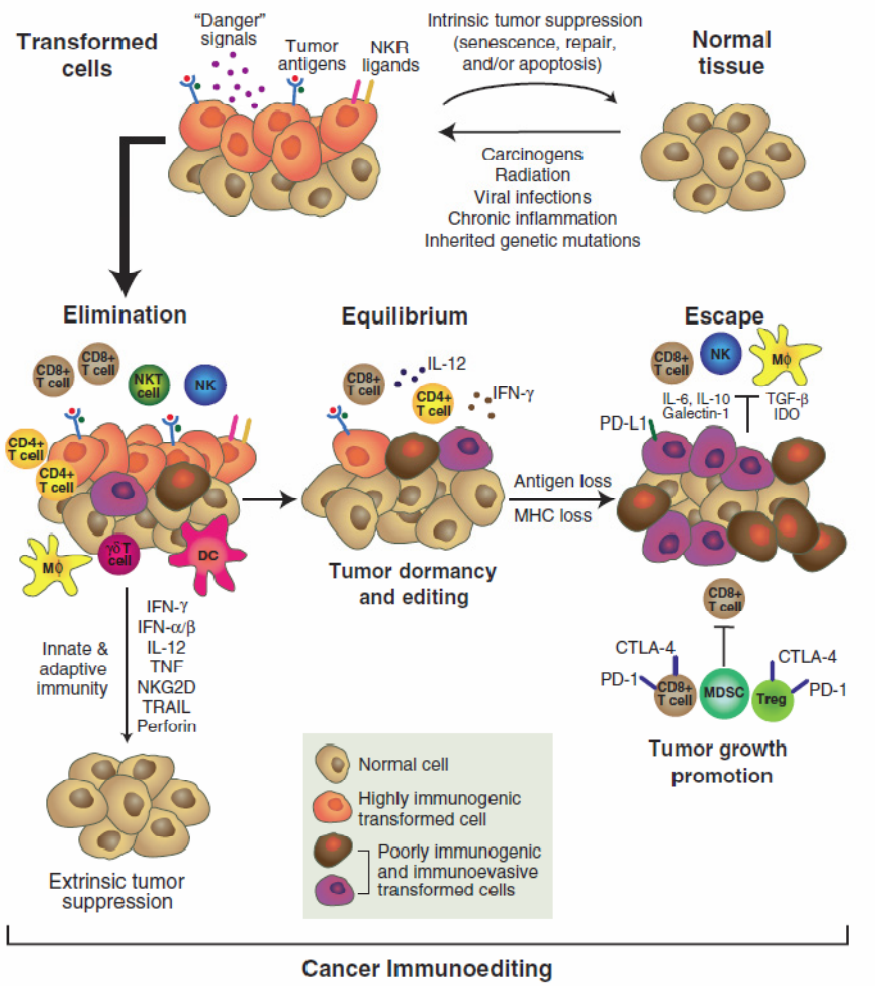

Figure 9. Cancer immunoediting concept. Cancer immunoediting consists of three sequential phases: elimination, equilibrium, and escape. In the elimination phase, innate and adaptive immunity destroy developing tumors before they become clinically apparent. If a rare cancer cell variant is not destroyed in the elimination phase, it may then enter the equilibrium phase, in which its outgrowth is prevented by immunologic mechanisms. Editing of tumor immunogenicity occurs in the equilibrium phase. Tumor cell variants may enter the escape phase, in which their outgrowth is no longer blocked by immunity. These tumor cells emerge to cause clinically apparent disease ((Schreiber *et al.*, 2011)).

3.1. ANTITUMOR IMMUNE RESPONSE

Analysis of the tumor microenvironment in patients with a variety of cancer types including colorectal cancer, breast cancer, renal cell carcinoma, ovarian cancer, melanoma, and gastrointestinal stromal tumors, has revealed that the presence of tumor-infiltrating lymphocytes (TILs) is strongly associated with a positive prognostic and a favorable clinical outcome (Pages *et al.*, 2005; Galon *et al.*, 2006).

Innate immune activation triggered by stress-associated signals or DAMPs may act as a bridge toward adaptive immunity that can allow that some patients spontaneously develop specific antitumor $CD8^+$ T cell responses. Type I IFN production by host DCs in tumors might participate in innate recognition of tumors, although the mechanism is not still well-known (Gajewski *et al.*, 2013).

The initiation of antitumor immunity begins with the capture of antigens derived from tumors by DCs, which process them for presentation or cross-presentation on MHC class I and II molecules. Tumor-antigen-loaded DCs migrate to draining lymph nodes where, under stimulating signaling conditions, will elicit antitumor effector T-cell responses. T cells interact with the complex formed by the presented peptide and the MHC molecules in DCs by specific T cell receptors (TCR), initiating a signaling cascade that leads to its activation. In addition, costimulatory signals are needed, and on its nature depends the kind of response that will be triggered. In the absence of immunogenic stimulus, DCs will instead induce tolerance, anergy, or the production of regulatory T cells (T_{regs}). DCs also trigger B cell and NK cell responses, which may contribute to antitumor immunity. Finally, cancer-specific T cells might enter the tumors, where they will recognize specifically tumor cells that present the tumor antigen associated to MHC class I molecules on its surface (Mellman *et al.*, 2011) (**Figure 10**). Production of cytokines and activation of $CD4^+$ T cells are also required to generate a potent and sustained response.

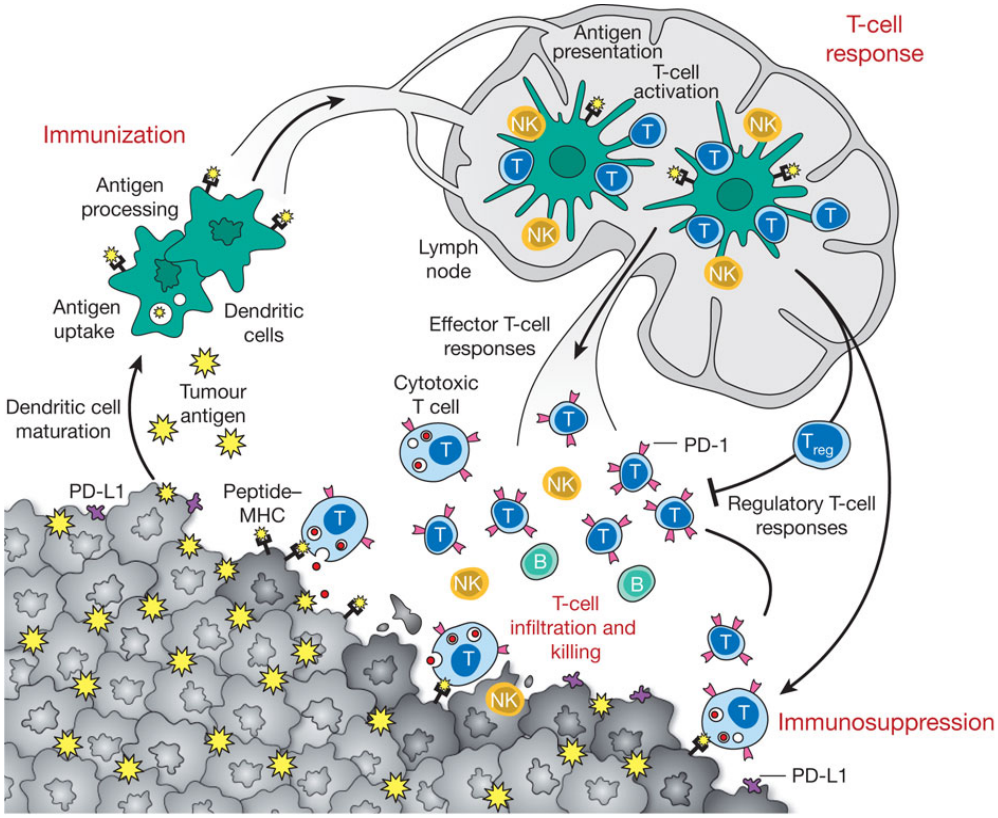

Figure 10. Generation and regulation of antitumor immunity. Antitumor immune responses start with the capture and processing of tumor-associated antigens by DCs for presentation on MHC class II or cross-presentation on class I molecules. Then, DCs migrate to draining lymph nodes where, in the presence of an immunogenic stimulus, will elicit anticancer effector T-cell responses in the lymph node. On the contrary, without such stimulus, dendritic cells will induce tolerance. In the lymph node, antigen presentation to T cells will elicit a response depending on the type of dendritic cell maturation stimulus received and on the interaction of T-cell co-stimulatory molecules with their surface receptors on dendritic cells. Antigen-educated T cells will exit the lymph node and enter the tumor bed, where immunosuppressive defense mechanisms produced by tumors oppose effector T-cell function (obtained from (Mellman *et al.*, 2011)).

3.2. MHC CLASS I ANTIGEN PRESENTATION PATHWAY

The T cell arm of the adaptive immune response has evolved to recognize products of intracellular proteolysis. Peptides coming from the ubiquitine-proteosome pathway, which is mainly involved in the degradation of cytosolic proteins, including misfolded proteins, regulatory proteins, defective ribosomal products, mutated proteins in cancer cells, or viral proteins produced in infected cells, are presented by MHC class I molecules to $CD8^+$ T cells. In contrast, $CD4^+$ T cells recognize peptides coming from the lysosomal pathway, which degrades proteins taken up by endocytosis and bound to MHC class II molecules. The cross-presentation process constitutes a major exception of this rule and consists in the presentation of peptides derived from proteins that have entered the lysosomal pathway by MHC class I molecules in professional

antigen-presenting cells (APCs) (Joffre *et al.*, 2012). Since this work is focused in the presentation of antigens by MHC class I, only the ubiquitine-proteasome pathway is going to be detailed.

In vertebrates, MHC genes are encoded from a large multigenic region. In mice, there are two or three genes (depending on the strain) encoding MHC class I molecules, called H-2D, -K, and -L, within the H2 complex, and two MHC class II, called I-A and I-E. In humans, there are three main (and several minor) genes encoding classical MHC class I molecules within the human leukocyte antigen (HLA) complex, named HLA-A, -B, and -C, and three MHC class II molecules called HLA-DR, -DQ, and -DP.

MHC genes show enormous allelic polymorphism, and the amino acid sequence variation is concentrated in the parts interacting with peptides in order to allow different alleles to bind a broad range of peptides. The peptide-binding structure consists of a membrane-distal groove formed by two antiparallel α-helices overlaying an eight-strand β-sheet. Membrane-proximal regions consist of two conserved domains that are homologous to immunoglobulin (Ig) constant region domains: one is provided by the heavy chain and the other is a separate protein called β_2-microglobulin (β_2m), which is product of a non-MHC-linked gene.

The proteasome is a multimeric protein complex located in the cytosol and the nucleus. It has a cylindrical shape and contains a catalytic core and regulatory particles. The core is a barrel-shaped structure called 20S and consists of four stacked rings of seven subunits each. The two outer rings are composed by α-subunits (α1-α7) and interact with regulatory particles (such as 19S or PA28) creating a physical barrier that regulates the access to the gate. The cleavage of the N-terminal of subunit α3 causes the opening of the gate and activates the proteasome. The two inner rings are composed by β-subunits (β1- β7), three of which (β1, β2, and β5) constitute the active proteolytic components with different specificities. Upon the exposition to IFN-γ, variants of the active β-subunits are produced and replace the constitutive versions. These subunits are called low molecular weight protein (LMP) 2 (β1i), LMP7 (β5i) and LMP10 (β2i), and the proteasomes incorporating them in the context of an inflammatory process are called immunoproteasomes. Cleavage specificities of the immunoproteosome are different to that of the proteasome, cleaving peptides after basic and hydrophobic residues instead of acidic residues, and length and quantity of the generated peptide repertoire also varies. Generated peptides can be further cleaved by cytosolic proteases such as tripeptidyl peptidase II (TPPII). Afterwards, peptides generated in the cytosol are translocated into the endoplasmic reticulum (ER) by the transporter associated with antigen processing (TAP). TAP is a member of the ATP-binding cassette (ABC) family of transporters, and is formed by TAP1 and TAP2 subunits, which

contain a hydrophobic transmembrane domain and a cytosolic nucleotide-binding domain each. TAP forms a transmembrane pore in the ER membrane whose opening and closing depends on ATP binding and hydrolysis, respectively. Peptides transported by TAP are mainly of 8-12 residues of length and with hydrophobic or basic C-terminal that are the ones that have more affinity to MHC class I molecules. Once in the ER, peptides can be further trimmed by enzymes such as the ER aminopeptidase ERAP1. Next, transported peptides are loaded onto empty MHC class I molecules with the assistance of chaperones calnexin, thiol oxidoreductase (ERp57), calreticulin, and tapasin. The latter is the responsible of bridging MHC class I molecules and TAP, allowing peptides to gain access to the ER for class I binding and also stabilizing the heterodimers formed by the heavy chain and β_2m. Finally, the complexes formed by MHC class I molecules and the bound peptides, leave the ER within vesicles that traverse Golgi apparatus and migrate to the cell membrane. The peptide is exposed to be recognized and interact with the TCR on $CD8^+$ T cells (Blum *et al.*, 2013). **Figure 11** shows a schematic representation of the MHC class I antigen processing pathway.

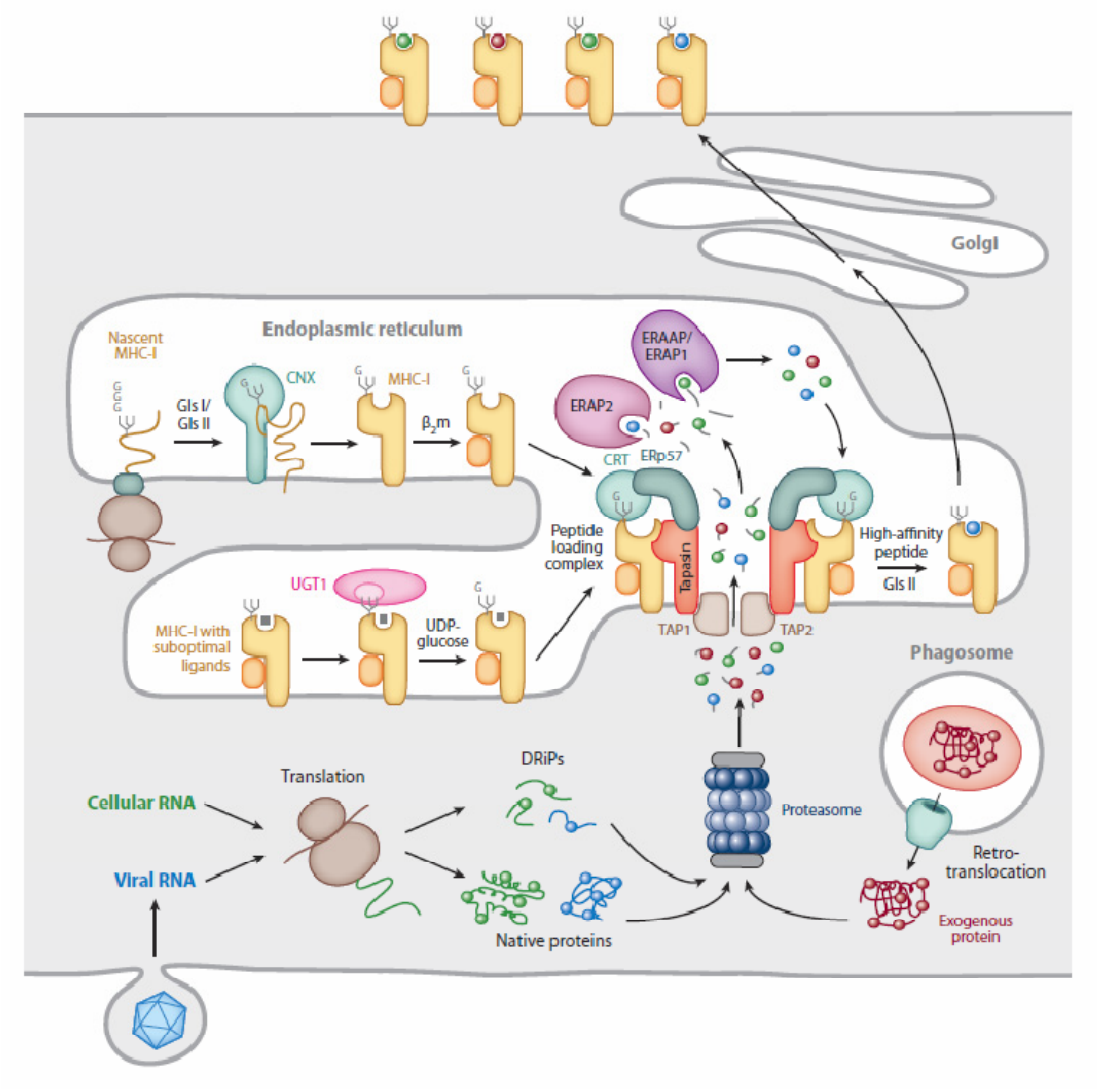

Figure 11. MHC class I antigen presentation pathway. Peptides translocated into the ER by TAP originate primarily from the proteasomal degradation of endogenous proteins either self or foreign (i.e., viral) or, in the case of cross-presentation, by translocation into the cytosol from endosomes or phagosomes. Many of the peptides that are delivered into the ER are trimmed by ER aminopeptidases and finally high-affinity peptides bind to MHC-I molecules by a tapasin-mediated process. MHC-I/peptide complexes transit to the cell surface for T cell recognition by CD8+ T cells (adapted from (Blum *et al.*, 2013)).

3.2.1. TAP-independent presentation pathway

The vast majority of peptides presented by MHC class I molecules are originated in the cytosol by proteasome-mediated degradation. TAP seems to play an important role in the generation of specific $CD8^+$ T cell responses. The observations of that tumor cells lose TAP expression (Pettit *et al.*, 2000) and that many viral functions target this transporter complex (Momburg and Hengel, 2002) support this statement. However, it has been reported that TAP-deficient human beings are not especially susceptible to viral infections, and also possess virus-specific $CD8^+$ T cells (Gadola *et al.*, 2000; de la Salle *et al.*, 2002). Indeed, different reports have shown the existence

of an alternative antigen processing pathway within the secretory route. It has been observed that some ligands can also be generated in TAP-deficient cells. Initial studies lead to the observation that hydrophobic peptides derived from signal sequences, which are targeted directly to the ER membrane and cleaved by signal peptidase (SP), may become TAP-independent class I antigens (Henderson *et al.*, 1992; Wei and Cresswell, 1992). Later studies using large-scale mass spectrometry have identified a large number of peptides that are presented independently of TAP. Many studies relate the source protein of epitopes that do not require TAP to be presented by MHC class I molecules to proteins or constructs that contain membrane-translocating ER-targeting signal sequences or that are based on natural membrane proteins. However, other putative mechanisms by which cytosolic proteins or peptides may gain access to the ER have been postulated, including diffusion through membrane, transport through an altered ER translocon or an unidentified ER transporter, transport through an unidentified lysosomal transporter, and autophagy (Del Val *et al.*, 2011). Once in the ER, these proteins need to be processed in the secretory pathway by proteases such as the ER signal peptidase (Henderson *et al.*, 1992; Wei and Cresswell, 1992), the proprotein convertase 7 (PC7) located in the trans Golgi network and in the endocytic vesicles (Leonhardt *et al.*, 2010), endolysosomal cathepsins (Tiwari *et al.*, 2007), and the trans Golgi network protease furin (Gil-Torregrosa *et al.*, 1998; Gil-Torregrosa *et al.*, 2000; Tiwari *et al.*, 2007). Furin belongs to the maturing proteases category, which are involved in performing selective cleavages on selected substrates, often involving their maturation or activation. This protease has restricted cleavage specificity at polybasic sites on protein substrates, and turns fully active in the trans Golgi network (TGN), so it cannot efficiently cleave substrates in the ER. This means that peptides would be generated where furin enzyme is active and then travel back through retrograde vesicular transport to the ER in order to be bound by MHC class I molecules.

3.3. MECHANISMS OF TUMOR ESCAPE

Tumor escape can occur through many different mechanisms that can be classified as cell-autonomous modifications or changes in tumor microenvironment. At tumor cell level, alterations leading to reduced immune recognition or to induction of central or peripheral tolerance can prevent tumor cell detection by the immune system. Central tolerance refers to the process by which self-reactive T cells are eliminated in the thymus, while peripheral tolerance is the process by which T cells reactive to self-antigens that are not expressed in the thymus are deleted in the periphery.

3.3.1. Defects in antigen processing machinery and reduced immune recognition

Tumor cells can acquire defects in antigen processing and presentation pathways, leading to evasion from adaptive immune recognition. Loss of different components of MHC class I pathway such as TAP, MHC class I molecules, β2m, immunoproteasome subunits (LMP2, LMP7, and LMP10), or chaperones have been detected in many different tumor types (Jager *et al.*, 1996; Restifo *et al.*, 1996; Khong *et al.*, 2004; Dunn *et al.*, 2006; Leone *et al.*, 2013).

Among this defects, one of the most common is the deficiency of TAP. Low to undetectable levels of TAP1 and/or TAP2 mRNA and/or protein have been reported in primary cell cultures from tumor types including carcinomas of head and neck, esophagus, stomach, pancreas, colorectal, breast, and cervix; renal cell, prostate, and bladder cancer; and melanoma, astrocytoma, medulloblastoma, neuroblastoma, acute myeloid leukemia, and multiple myeloma (Leone *et al.*, 2013). These deficiencies may be due to downregulation, which is normally restored by IFN-γ treatment in several tumor cell lines (Traversari *et al.*, 1997; Tao *et al.*, 2008). However, mutations at the genetic level in TAP genes that resulted in loss of expression or in expression of a nonfunctional protein have also been observed, as well as epigenetic alterations or post-translational downregulation (Kaklamanis *et al.*, 1994; Chen *et al.*, 1996; Fowler and Frazer, 2004). Moreover, some tumors could lose the ability to respond to IFN-γ by mutating or silencing genes encoding for receptor signaling components, failing in the upregulation of MHC class I molecules and being unable to produce the intracellular machinery of antigen processing (TAP1, TAP2, or immunoproteasome components) (Respa *et al.*, 2011).

Abnormalities in the expression of antigen processing machinery components, especially TAP and MHC class I, are strictly linked with disease aggressiveness and clinicopathological outcome. APM dysfunction is related with numerous possible defects that may negatively affect immune recognition of tumor cells. Downregulation of proteasome subunits inhibits the processing of antigens in the cytoplasm, decreasing the efficiency of epitope generation; TAP abnormalities reduce the capacity to transport peptides from the cytosol to the ER, preventing formation of peptide/MHC class I complexes; and a change in chaperone levels may hamper proper loading of peptides into MHC class I, altering their maturation and stability. Only mature peptide-bound MHC class I molecules are able to be recognized by $CD8^+$ T cells, in order to activate T cell adaptive response.

In this regard, linking tumor-specific epitopes to membrane-translocating peptides that allow their targeting to the ER is a previously reported strategy that has been used to bypass antigen

processing steps and promote the presentation of the epitopes by TAP-independent pathways (*section 3.2.1*) (Lu *et al.*, 2004; Raafat *et al.*, 2012).

Inherent genetic instability of tumor cells also could result in the loss of tumor antigens, becoming no longer detectable by antigen-specific $CD8^+$ T cells. Similarly, tumor cells can avoid recognition by innate immune system by the loss of expression of ligands for the NK cell effectors molecule NKG2D (Stern-Ginossar *et al.*, 2008) or by the suppression of proinflammatory danger signals to impair DC maturation (Wang *et al.*, 2004).

3.3.2. Increased resistance to apoptosis

Another mechanism to avoid immune cell detection is to increase resistance to the cytotoxic effects of immunity, for example through induction of anti-apoptotic molecules such as FLIP and BCL-XL (Kataoka *et al.*, 1998; Hinz *et al.*, 2000) or through the expression of inactive forms of death receptors including TRAIL, DR5, and Fas (Shin *et al.*, 2001; Takahashi *et al.*, 2006). Finally, tumor cells can express on its surface immune-inhibitory ligands that even recognized by immune cells inhibit its cytotoxic actions in a cell-contact mediated manner. Some examples are PD-1, PD-L1 (B7-H1), PD-L2 (B7-DC), whose receptors are highly expressed in TILs (Dong *et al.*, 2002).

3.3.3. Immunosuppression in tumor microenvironment

Alternatively, escape may result from the establishment of immunosuppressive status within the tumor microenvironment. Tumor cells can promote such state by the production of immunosuppressive cytokines that inhibits DCs function such as vascular endothelial growth factor (VEGF) (Gabrilovich *et al.*, 1999), transforming growth factor-β (TGF-β) which also inhibits T and NK cell function (Wrzesinski *et al.*, 2007) or IL-10 that can also skew T cell responses toward a type 2 immune response (T_H2) that favor tumor progression (Aruga *et al.*, 1997). Galectin production impedes T cell activity and survival (Rubinstein *et al.*, 2004). Expression of indoleamine 2,3-dioxigenase (IDO) enzyme by tumor cells metabolizes tryptophan to generate kynurenines and inhibits $CD8^+$ T cell proliferation and promotes $CD4^+$ T cell apoptosis (Uyttenhove *et al.*, 2003). Recruiting of regulatory immune cells such as regulatory T cells (T_{reg} cells) and myeloid-derived suppressor cells (MDSCs) also can suppress immune function. Both of these cell types are leukocyte populations that play key roles in inhibiting host-protective antitumor responses. T_{reg} cells inhibit tumor-specific T lymphocytes function by producing IL-10 and TGF-β cytokines, by expressing the negative co-stimulatory molecules CTLA-4, PD-1, and PD-L1, and by consuming IL-2, a cytokine that is critical for cytotoxic T lymphocytes (CTLs) function (Terabe and Berzofsky, 2004). MDSCs inhibit lymphocyte function by inducing T_{reg} cells (Huang *et*

al., 2006), producing TGF-β (Li *et al.*, 2009a), depleting amino acids arginine, tryptophan, or cysteine, required for T cell function (Srivastava *et al.*, 2010), or by nitrosilation of T cell receptors (TCR) or chemokine receptors on tumor-specific T cells (Nagaraj *et al.*, 2007).

3.4. IMMUNOTHERAPY OF CANCER

Taking into account the different mechanisms of tumor escape to the immune system and thanks to recent advances in molecular and cellular immunology, several immunotherapeutic treatments have been proposed to overcome this acquired resistance. Different approaches involve the use of antitumor antibodies, adoptive T cell therapy, immune checkpoint blockade, and therapeutic cancer vaccines.

3.4.1. Monoclonal antibodies

So far, monoclonal antibodies constitute one of the most successful forms of immunotherapy. Nine monoclonal antibodies targeting six cancer-associated proteins (Her2/neu, EGFR, VEGF, CD20, CD52, and CD33) are clinically approved for the treatment of cancer. By binding to their targets, antibodies exercise their functions through several effector mechanisms, including steric inhibition and neutralization, complement activation, and activation of cell-mediated cytotoxicity.

3.4.2. Adoptive T-cell therapy

Adoptive T cell therapy (ACT) is one of the most promising immunotherapy approaches, and involves the infusion of externally manipulated T cells. These includes expanded and activated tumor infiltrating lymphocytes (TILs) (Dudley *et al.*, 2002; Rosenberg *et al.*, 2008), T cells modified *ex vivo* to express a specific TCR, and T cells engineered to express a receptor that is a fusion between an antibody and the T cell receptor's intracellular machinery, called chimeric antigen receptor (CAR) (June, 2007). Adoptive T cell therapy with TILs has reported a 70% of overall objective response rate and 20% of complete responses in melanoma patients (Rosenberg *et al.*, 2011) whereas the use of CARs against acute lymphocytic leukemia (ALL) has achieved 80% of complete response rate (Maus *et al.*, 2014). However, serious adverse effects have been reported.

3.4.3. Immune checkpoint blockade

Among the most promising approaches to activate therapeutic antitumor immunity is the blockade of immune checkpoints that are crucial for maintaining immune resistance against T

cells that are specific for tumor antigens. Since immune checkpoints are initiated by ligand-receptor interactions, its blockade could be easily achieved by antibodies or recombinant forms of ligands or receptors. Some examples are the use of CTLA4 antibodies, Ipilimumab, which was the first of this class of immunotherapeutic treatments to be approved by the Food and Drug Administration (FDA), or blockers of the PD1 pathway.

3.4.4. Therapeutic cancer vaccines

The discovery of the expression of several immunogenic tumor antigens by tumor cells and the detection of tumor-specific CTLs against these antigens in cancer patients supports the interest of using vaccines as antitumor treatment. There are a large number of different cancer vaccine platforms. These includes synthetic TAAs as short peptides or full-length proteins in combination with adjuvants, delivery of whole tumor lysates, *ex vivo* peptide-activated DCs or TAA-encoding vectors, in the form of naked DNA or RNA or in viral vectors. However, the weakly immunogenic nature of TAAs often limits the successful of this kind of therapies.

3.5. ONCOLYTIC VIRUSES FOR CANCER IMMUNOTHERAPY

One of the main problems of immunotherapeutic treatments is the negative influence of the immunosuppressive tumor microenvironment. Oncolytic viruses constitute a feasible solution to this problem and might overcome this cancer-associated immunosuppression.

Oncolytic viruses have the ability to selectively replicate in and kill tumor cells while sparing normal tissues. In contrast to the vision that host's immune system can limit the efficacy of virotherapy by rapid clearance of the infection, evidence supporting that the virus-induced immune activation can generate innate and adaptive immune responses critical to achieve antitumor activity has accumulated during the last years (Alemany and Cascallo, 2009; Woller *et al.*, 2014).

Local inflammation of tumor tissue during an infection by an oncolytic virus provides suitable conditions to trigger antitumor immune responses. Cancer cell death induced by oncolytic viruses can be classified as a immunogenic cell death (ICD) (**Figure 12**). This kind of cell death involves changes in the composition of cell surface and also the release of soluble mediators known as danger signals that are basically pathogen-associated molecular patterns (PAMP) or damage-associated molecular patterns (DAMP). Classical PAMPs are DNA with unmethylated CpG or defective viral genomes, and are recognized by pattern recognition receptors (PRRs) present on innate immune cells like antigen-presenting cells (APCs). Surface exposition of calreticulin (CRT)

and heat shock proteins such as HSP60 and HSP90, and secretion of ATP, high mobility group box 1 protein (HMGB1), hyaluronan fragments, or uric acid by dying cells are crucial DAMPs that lead to the expression of genes with inflammatory properties that activate DCs to provide for the stimulation needed to activate antigen-specific T-cells.

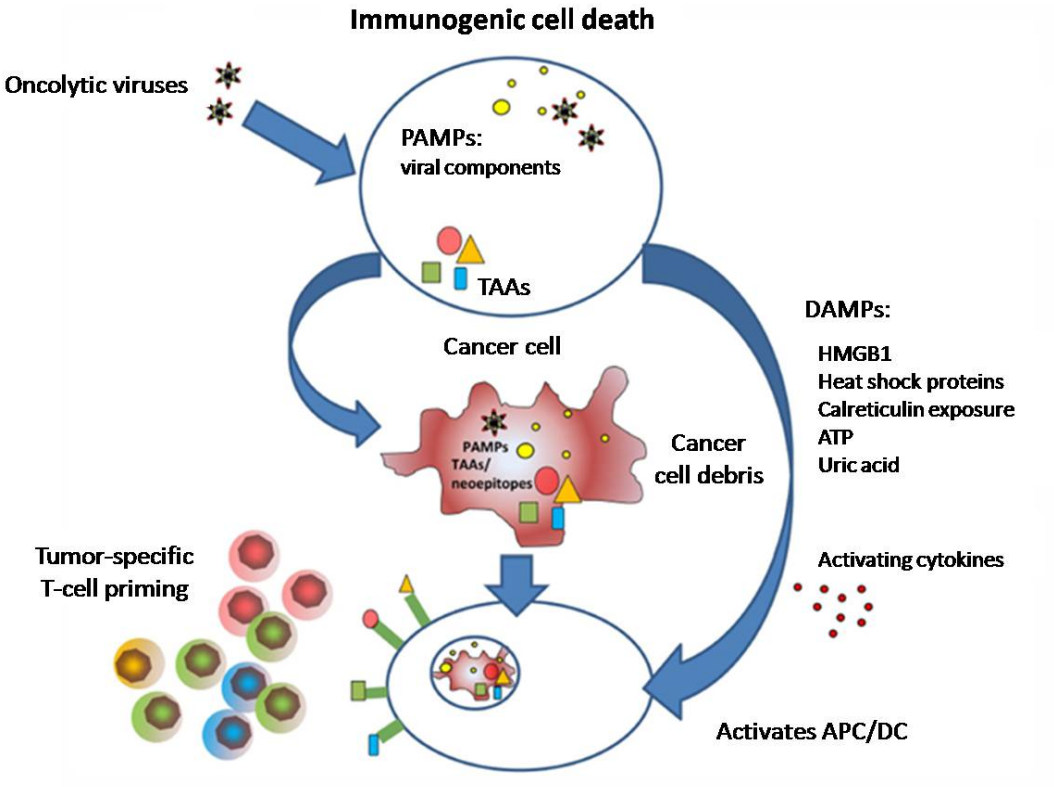

Figure 12. Oncolytic viruses for cancer immunotherapy. Viral oncolysis of tumor cell induces immunogenic cell death by accumulation of PAMPs and the release of DAMPs. All these danger signals activate antigen-presenting dendritic cells that can induce cytotoxic T cell responses against tumor-associated antigens. PAMPs, pathogen-associated molecular patterns; DAMPs, damage-associated molecular patterns; TAAs, tumor-associated antigens (adapted from (Woller *et al.*, 2014)).

Besides these danger signals, tumor cell death by oncolytic viruses promotes the release of a natural repertoire of TAAs, that are uptaken and cross-presented by DCs, activating specific antitumor $CD8^+$ T cells against numerous epitopes. In particular, oncolytic adenoviruses were also shown to induce autophagy, which further facilitates cross-presentation by DCs (Jiang *et al.*, 2011; Rodriguez-Rocha *et al.*, 2011). All these findings provide a rationale for combining virotherapy with immunotherapy. In addition, several strategies have been suggested to further exploit the inherent capability of oncolytic viruses of breaking immunosuppression by arming them with several kinds of genes.

3.5.1. Oncolytic adenoviruses and immunotherapy

Among others, adenoviruses are appealing to be used as vaccine platforms, since they are able to induce potent humoral responses and cellular immunity in mice, primates and humans compared to other vectors (Shiver *et al.*, 2002; Bett *et al.*, 2010). Several adenovirus-based vaccines expressing different TAAs (i.e Her2, Trp-2, gp100, MART-1, PSA, CEA or WT1) (Rosenberg *et al.*, 1998; Hartman *et al.*, 2008; Gabitzsch *et al.*, 2010; Karan *et al.*, 2011) or immunomodulatory molecules (i.e. IL-12, IFN-α, GM-CSF, CD40L, anti-CTLA-4, CCL21, or MyD88) (Gambotto *et al.*, 1999; Sangro *et al.*, 2004; Gao *et al.*, 2008) have been evaluated mostly preclinically and with suboptimal results in the clinic. This lack of success could be attributable to the poor immunogenicity and self tolerance of TAAs compared to viral antigens (phenomenon that will be described in the section below, *3.5.1.1.*) together with the immunosuppressive tumor microenvironment.

Alternatively, as mentioned before, oncolytic viruses could shift the tumor microenvironment from immune suppression to immune activation. The detection of activated antiviral as well as antitumor specific $CD8^+$ T cells in patients treated with oncolytic adenoviruses supports the usefulness of adenoviruses as immunovirotherapeutic platforms (Cerullo *et al.*, 2010; Koski *et al.*, 2010; Nokisalmi *et al.*, 2010; Pesonen *et al.*, 2011).

Oncolytic adenoviruses have been modified in several ways in order to improve antitumor activity through modulation of immune system. Toll-like receptors (TLRs) are a family of PRRs that recognize PAMPs and DAMPs and trigger the activation and maturation of DCs. As an example, TLR9 responds to viral dsDNA by recognizing unmethylated CpG sequences. An oncolytic adenovirus with enriched CpG motifs in its genome has shown to increase antitumor activity and tumor antigen-specific T cells in animal models (Cerullo *et al.*, 2012). However, arming oncolytic adenoviruses with immunomodulatory transgenes is the most exploited strategy in the field of immunovirotherapy. Several cytokines such as IL-15 (Gaston *et al.*, 2013), IL-23 (Choi *et al.*, 2013), IFN-α (Shashkova *et al.*, 2007), or IFN-γ (Su *et al.*, 2006), and chemokynes such as CCL5/RANTES (Lapteva *et al.*, 2009) have been used with this aim. Among many others, the ones armed with interleukin-12 (IL-12) or the granulocyte-macrophage colony-stimulating factor (GM-CSF) have been the most successful so far. IL-12 is a pro-inflammatory cytokine that leads to the activation of NK cells, cytotoxic T cells, as well as the development of T_H1 immune responses, that are related to antitumor immune responses. Oncolytic adenoviruses carrying the IL-12 gene have shown enhanced antitumor efficacy (Lee *et al.*, 2006; Bortolanza *et al.*, 2009). GM-CSF mediates antitumor immunity by recruiting NK cells and by activating DCs. Oncolytic

adenoviruses encoding this cytokine can induce potent antitumor responses in preclinical models (Bristol *et al.*, 2003; Ramesh *et al.*, 2006). Importantly, one of them (Ad5-D24-GMCSF) has been able to induce antitumor immunity in cancer patients: from 16 evaluable patients, 2 had complete responses and 5 stable disease (Cerullo *et al.*, 2010). A version of this GM-CSF-expressing adenovirus containing the 5/3 chimeric capsid (Ad5/3-D24-GMCSF) was tested in patients with advanced refractory solid tumors upon intratumoral or intravenous administration in combination with low-dose metronomic cyclophosphamide. Similar clinical results to that of its parental oncolytic adenovirus were obtained, with 8 among 12 patients showing objective clinical benefit. Both, antiadenoviral and antitumoral immune responses were detected in those patients (Koski *et al.*, 2010). More recently, another GM-CSF-armed oncolytic adenovirus, CG0070, showed 48.6% of complete responses in bladder cancer patients (Burke *et al.*, 2012). It is important to highlight, that two of the most advanced oncolytic viruses in the clinical setting until the date are a vaccinia virus (VV) (JX-594, or Pexa-Vec) and a herpes simplex virus (HSV) (T-Vec, or talimogene laherparepvec) that also express GM-CSF and had obtained very promising results (Senzer *et al.*, 2009; Kaufman and Bines, 2010; Heo *et al.*, 2013) (see *section 2* above). Importantly, intratumoral injection of these viruses led to the response of uninjected lesions, demonstrating a systemic immunological effect.

Given the encouraging results of oncolytic adenoviruses armed with these two cytokines, an oncolytic adenovirus expressing IL-12 and GM-CSF simultaneously in the E1 and E3 regions has been constructed. Coexpression of both cytokines significantly enhanced antitumor activity in an immunocompetent murine melanoma model (Zhang *et al.*, 2011). This oncolytic adenovirus was able to inhibit immune suppression in the tumor microenvironment and, moreover, enhance the efficacy of subsequently administered DC vaccine. However, it has not yet been tested in the clinical setting.

Despite the fact that PAMPs, DAMPs, and TAAs released from tumor cells is supposed to induce DC activation and maturation, there is evidence demonstrating that even though human DCs efficiently phagocytose adenoviral oncolysates, they require additional stimulation to mature (Schierer *et al.*, 2012). To overcome this hurdle, oncolytic adenoviruses have also been engineered to express costimulatory molecules such as a soluble form of the CD40 ligand that interacts to the CD40 receptor in APCs, thereby triggering antigen presentation and T-cell activation (Diaconu *et al.*, 2012). Besides proving its efficacy and increased immunogenicity in preclinical models, the treatment of 9 patients with advanced solid tumors with the oncolytic adenovirus Ad5/3-hTERT-CD40L resulted in controled disease in 83% of them (Pesonen *et al.*,

2011). Importantly, high levels of virus, CD40L, RANTES and tumor-specific CD8+ T-cells were detected in tumor biopsies.

Other costimulatory molecules whose expression has been combined with IL-12 or GM-CSF is the B-lymphocyte activation antigen (B7-1, or CD80), that provides a secondary costimulatory signal by its interaction with the CD28 molecule in the surface of T cells leading to its activation. Both viruses showed improved antitumor activity in immunocompetent mice bearing melanoma tumors and CD4+ and CD8+ T cell infiltration at the tumor site (Lee *et al.*, 2006; Choi *et al.*, 2013).

Another strategy to revert tumor immunosuppression that has not been yet tested in human cancer patients is the combination of oncolytic virotherapy with immune checkpoint blockade. In addition to costimulatory signals required for T-cell stimulation, the immune system has developed inhibitory strategies to regulate T-cell activation. The cytotoxic T-lymphocyte-associated antigen 4 (CTLA-4) is a receptor which is expressed on T cells and whose activity counteracts that of the CD28 co-stimulatory receptor (Pardoll, 2012). Importantly, T_{reg} cells inhibit CTLs via CTLA-4 (Terabe and Berzofsky, 2004). An oncolytic adenovirus encoding an antibody against CTLA-4 has been tested in the preclinical setting with promising results (Dias *et al.*, 2012).

Altogether, these results underscore the significance of combining immumodulatory genes with oncolysis of tumor cells by oncolytic adenoviruses to enhance antitumor activity.

Different approaches aim at directly enhancing antitumor-specific T-cell responses. One possibility is to arm oncolytic viruses with transgenes that enhance the cross-presentation and priming of TAAs such as heat shock proteins (HSPs) that can induce an MHC restricted tumor antigen-specific CD8+ T cell responses in different cancer models in immunocompetent mice. Indeed, an oncolytic adenovirus overexpressing HSP70 has been tested in a phase I clinical trial upon intratumoral administration, resulting in clinical benefit in 48.1% of the treated patients (Li *et al.*, 2009b). Interestingly, transient and partial regression of untreated tumors was observed in three patients, thus suggesting systemic effect.

Finally, in the line of the previous approach, another possibility to enhance immune response against an antigen could be its display or expression by oncolytic adenoviruses. Regarding the first option, the incorporation of antigens into the capsid has been further explored in the field of adenovirus-based vaccines, especially in the case of infectious diseases. This approach presents some advantages with respect to its expression as transgenes. Preexisting immunity to adenoviruses present in 50 up to 90% of the population can preclude transgene expression.

Moreover, incorporating immunogenic antigens to the capsid could result in a strong humoral response similar to the response generated by native adenovirus capsid proteins, and may have benefits in promoting immune cross-priming and activation of $CD8^+$ T cells. There are four different proteins that allow the introduction of heterologous peptides in adenovirus capsid: fiber, hexon, penton base, and pIX. Krause et al. performed a study in which they compared the anti-epitope immunity after incorporating the hemagglutinin (HA) protein from the influenza A virus in the different proteins of the adenoviral capsid. Results demonstrated that higher humoral and cellular responses against HA were detected when the antigen was incorporated into the fiber *knob*, despite fiber is 60 times less abundant than hexon (Krause *et al.*, 2006). However, other issues such as the size of the fragments that can be incorporated in each location or if the epitope is conformational or not must be taken into account. Nevertheless, no experience exists with the incorporation of tumor epitopes in oncolytic adenoviruses capsid. The second option was the expression of TAAs by oncolytic viruses, that has shown to increase the levels of activation of naïve T cells against the antigen, which is translated into increased antitumor therapy in different kind of viruses such as vesicular stomatitis virus (VSV) or HSV (Diaz *et al.*, 2007; Castelo-Branco *et al.*, 2010; Kottke *et al.*, 2011). However, again in the case of adenovirus, only non-replicative vectors have been armed with TAAs, while no experience with oncolytic adenoviruses has been published.

3.5.1.1. Immunodominance

From the experience in the field of adenovirus-based vaccines against infectious diseases, especially for HIV and malaria, a potential limitation of the use of adenovirus as cancer vaccines is that the immunodominance of adenoviral epitopes can mask immune responses to exogenous epitopes.

Immunodominance and immunodomination terms were originally used to describe prominent humoral responses to various antigens in the late 1960s and early 1970s (Johnston and Simmons, 1968; Curtiss and Krueger, 1975). Soon after, it was noticed that CTL immune response to antigens in mouse were restricted by a single or just a few H-2 haplotypes (Zinkernagel and Doherty, 1975; Doherty *et al.*, 1978). It is now well-established that antigen-specific immunodominant responses are linked to particular MHC alleles. Moreover, it was found that cellular immunity was highly toward one, or just a few, antigenic determinants, even during immune responses to complex microorganisms or antigens (Bennink and Yewdell, 1988). This phenomenon is known as immunodominance, and determinants involved in detectable responses were classified as either immunodominant determinants (IDDs) or subdominant

determinants (SDDs) depending on their reproducibility and magnitude (Sercarz *et al.*, 1993). Immunodominance has been mostly observed in antiviral and antibacterial immune responses, both in mouse models and in human diseases. Tumor-specific immunodominance has not been well characterized for nonviral self-antigens differentially expressed by tumors and normal tissues. In this case, $CD8^+$ T cell response hierarchy behaves differently to that of antiviral immune responses since self-tolerance mechanisms may also affect the $CD8^+$ T cell repertoire.

Factors that might lead to an immunodominant $CD8^+$ T cell response include the efficient generation of the determinant by the immunoproteasome, the transport of precursors to the ER by TAP, the suitable binding affinity of the peptide for the MHC class I, and the recognition of these complexes by $CD8^+$ T cells bearing the correct antigen-specific TCR. Other factors such as the route of infection also contribute to immunodominance complexity *in vivo*.

Immunodomination is another related concept referred to the circumstances by which the T cell response to a given antigenic determinant is inhibited or suppressed either directly or indirectly by T cells specific to other determinant antigens from the same antigen or the same pathogen (Kedl *et al.*, 2003). This is related to the interplay between T cells of different specificities and the interaction between T cells and the APCs more than the processing or presentation of antigens that have a more important role in immunodominance (Chen and McCluskey, 2006).

3.5.1.1.1. Immunodominance in adenoviral vectors

The main limitation of the use of viral vectors as vaccines, both for cancer or infectious diseases, is that vector-specific $CD8^+$ T cell immune responses may become immunodominant over immune responses against exogenous antigens (Sharpe *et al.*, 2001; Harrington *et al.*, 2002).

Regarding adenovirus-based vaccines, the immunodominance of specific responses against protein antigens of the vector was clearly demonstrated by Schirmbeck and colleagues in a study with an adenoviral vector encoding for the hepatitis B surface antigen (HBsAg) (Schirmbeck *et al.*, 2008). The response against the subdominant D^d-restricted epitope $HBsAg_{201\text{-}209}$ was analyzed in BALB/c ($H\text{-}2^d$) mice after its immunization with an E1-deleted adenoviral vector or a plasmid expressing HBsAg. Specific $CD8^+$ T cell response was efficiently induced by both, the plasmid and the adenoviral vector. However, the $D^d/HBsAg_{201\text{-}209}$-specific $CD8^+$ T cells in animals vaccinated with the adenovirus were two- to threefold lower than those in mice vaccinated with the plasmid, thereby suggesting that adenovirus-specific immune responses may downmodulate the response to HBsAg. Furthermore, when F1 (BALB/c x B6) mice ($H\text{-}2^d$ and $H\text{-}2^b$) were immunized in

the same way, no detectable responses against the HBsAg epitope were seen after the immunization with the adenoviral vector whereas similar levels of D^d/ $HBsAg_{201-209}$-specific $CD8^+$ T cells were elicited by vaccination with the plasmid in BALB/c and F1 mice. This observation could be related to the specific response against the 2^b-restricted viral epitope, dbp43, detected in F1 mice vaccinated with the adenoviral vaccine. It seems that even presented by different haplotypes, the viral epitope is immunodominant compared with the exogenous epitope, $HBsAg_{201-209}$.

Another study that evidences the problem of the immunodominance of viral epitopes over exogenous antigens was the one performed by Frahm and colleagues. They analyzed adenovirus-specific responses and HIV-specific responses in 35 patients receiving MRKAd5/HIV-1 vaccine one year after the first vaccination. A higher magnitude of baseline Ad-specific $CD4^+$ T cell responses were associated with a reduced magnitude of HIV-specific memory $CD4^+$ T cell responses (Frahm *et al.*, 2012).

To overcome this hurdle several strategies have been proposed. One of the most successful by the moment is the use of heterologous prime-boost regimens that consist in immunizing with two different vectors expressing the same antigen. This has been shown in a work performed by Bridle *et al*. in which the immunization with an adenoviral vaccine encoding for a TAA prior to the treatment with an oncolytic VSV virus expressing the same antigen enhanced antitumor activity. More importantly, this approach also shifted the immune response from viral antigens to tumor antigens (Bridle *et al.*, 2010). Moreover, heterologous prime and boost regimens may also avoid the formation of neutralizing antibodies.

As mentioned before, one of the factors that contribute to the immunodominance of some epitopes among others is their efficient transport from the cytosol to the ER by TAP. As it has been discussed previously (*section 3.3.1*), deficiencies in TAP expression constitute a common feature of many tumors to avoid its recognition by the immune system. In order to address this problem, we propose in this thesis to circumvent the need of TAP by linking the tumor-associated epitopes to the natural ER-targeting signal sequence that contains the adenoviral protein E3-19K. Importantly, this strategy attempts to shift the immune response from viral antigens to tumor antigens.

OBJECTIVES

Oncolytic adenoviruses can kill infected tumor cells directly by intracellular replication but also they can promote the death of uninfected cells by indirect immune-mediated mechanisms. The main obstacles that limit the efficacy of oncolytic adenoviruses are the poor tumor targeting after systemic administration, the deficient intratumoral spread, and the dominant immunogenicity of viral antigens.

The general objective of this work has been to improve the antitumor efficacy of oncolytic adenoviruses by using different strategies, and it has been carried out within the context of two independent projects. The first project consisted on the combination of a tumor-targeting capsid modification with the expression of an extracellular matrix-degrading enzyme, whereas the second one was focused on increasing the immunogenicity of exogenous epitopes expressed by oncolytic adenoviruses.

Several specific objectives have been addressed:

Chapter 1

- To generate an oncolytic adenovirus that combines two modifications previously described by our group: the RGDK mutation and the hyaluronidase expression, and validate its *in vitro* properties in terms of viral fitness.
- To characterize the toxicology and efficacy profile of the RGDK and hyaluronidase-modified oncolytic adenovirus in immunodeficient and immunocompetent animal models.
- To combine the RGDK and hyaluronidase-modified oncolytic adenovirus with the chemotherapeutic drug gemcitabine in order to improve its antitumor activity.

Chapter 2

- To incorporate immunogenic epitopes from tumor-associated antigens in the adenoviral protein E3-19K of an oncolytic adenovirus to promote their TAP-independent processing and evaluate the presentation of the epitopes in infected cells *in vitro*, comparing this strategy to the display of the same epitopes on the viral capsid.
- To determine the immune responses against tumor epitopes upon immunization of mice with oncolytic adenoviruses containing such epitopes and evaluate the antitumor activity of the elicited immune responses.

MATERIALS AND METHODS

1. HANDLING OF BACTERIA

In order to obtain enough amounts of plasmidic DNA to be easily manipulated, its amplification in bacteria was required. For this reason, the plasmid should have a replication origin that allows its replication on the desired strain and a gene that confers resistance to an antibiotic in order to select the bacteria and avoid contaminations. In this work, the *Escherichia coli* strains DH5α and DH10B have been used with this purpose. Moreover, SW102 strain has been used to perform homologous recombination.

1.1. PREPARATION OF COMPETENT BACTERIA

The bacteria stock was conserved at -80°C with 15% glycerol. In order to induce competence, the glycerinate was scratched with a sterile pipette tip into 10 mL of LB (1% Tryptone, 0.5% Yeast Extract, 0.5% NaCl) and it was grown overnight at 37°C in agitation in a 50 mL Falcon tube. Next day, the 10 mL preculture was grown in 1 L of LB at 37°C in agitation until the culture reached an OD of 0.6-0.7 at 600 nm of wave length. The bacterial solution was distributed in 250 mL bottles (suitable for centrifugation in SORVALL centrifuge) and kept 40 minutes on ice in order to stop bacterial growth. Further manipulation of bacteria was carried on at 4°C. Next, bacteria were centrifuged 15 minutes at 4000 *g* and 4°C in a SORVALL centrifuge, supernatant was discarded and the pellet was washed with cold bi-distilled (dd)H_2O water (4°C). This centrifugation/washing process was repeated 3 times and in the last wash the pellet was resuspended in 45 mL of water with 10% glycerol. Bacteria were centrifuged one more time and, finally, resuspended in 3 mL of water containing 10% glycerol. Next, OD at 600 nm was measured from a 1:100 dilution of the suspension. OD value should be close to 1 (which is equivalent to $2.5x10^8$ bacteria/mL). Finally, the bacterial suspension was distributed in 50 µL aliquots that were immediately frozen in carbon dioxide and stored at -80°C.

1.2. TRANSFORMATION OF COMPETENT BACTERIA BY ELECTROPORATION

Bacteria aliquots stored at -80°C were thawed on ice and an amount of plasmidic DNA between 10 pg and 25 ng in a final volume of 2 µL was added. The mixture was incubated 5 minutes on ice and added to electroporation cuvettes that were previously cooled. Then, bacteria were electroporated with the electroporator machine Electro Cell Manipulator™ ECM 630 at the following conditions: 50 µF, 1500 V and 125 Ω. Pulses lower than 5 miliseconds were considered correct. Immediately, bacteria were resuspended in 300 µL of LB and incubated for 1

hour in agitation at 37°C. The suspension was plated on LB plates including the corresponding selection antibiotic for each plasmid.

1.3. OBTAINING PLASMIDIC DNA FROM BACTERIAN CULTURES

In this work, plasmidic DNA was obtained from saturated *E.coli* cultures which grew in LB with antibiotic according to protocols based on an alkaline lysis with SDS. DNA was prepared at small and large scale.

1.3.1. Small scale DNA preparations

DNA minipreparations were performed following an adapted protocol described by Birnboim y Doly (Birnboim and Doly, 1979), which allows the obtaining of 20-50 µg DNA preparations. The procedure is detailed below.

First of all, a colony grown in a LB-antibiotic dish was inoculated in 2 mL of LB+antibiotic and incubated over night. Then an aliquot of 1.5 mL was taken and centrifuged at 13000 rpm 1 minute. Then the pellet was resuspended in 200 µL of pre-cooled solution 1 (25 mM Tris-HCl pH 8, 10 mM EDTA, 50 mM glucose). 200 µL of freshly prepared solution 2 (SDS 1%, NaOH 0.2 M) were added and the mixture was blended by inversion. Finally, 200 µL of pre-cooled solution 3 (3 M potassium acetate, 11.5% acetic acid) were added and the mixture was blended again by inversion until a white precipitate appears. The mixture was incubated 5 minutes on ice and centrifuged 15 minutes at 15000 *g*. Next, the clear supernatant was collected without taking the white pellet that corresponds to cellular DNA, proteins and SDS, and 2 volumes of ethanol were added. The mixture was incubated 15 minutes at room temperature (RT) and plasmidic DNA was precipitated by centrifugation during 10 minutes at 15000 *g*, supernatant was discarded and the pellet was washed with 70% ethanol. It was centrifuged again 5 minutes at 15000 *g*, supernatant was discarded and the pellet was dried. Finally, plasmidic DNA was resuspended in 50 µL of TE with RNAse (10 mM Tris-HCl, 1 mM EDTA, 0.1 mg/mL RNAse).

1.3.2. Large scale DNA preparations

DNA maxipreparations allow obtaining large amounts of high purity plasmidic DNA (≥100 µg). Maxipreps were prepared from 200 mL of saturated bacteria culture using the Invitrogen commercial kit "PureLink™ HiPure Plasmid Filter Purification Kits", following manufacturer's instructions.

1.4. POSITIVE-NEGATIVE SELECTION HOMOLOGOUS RECOMBINATION IN BACTERIA

Most of the homologous recombinations performed in this work have been conducted in bacteria because of the high efficiency of the system developed by Richard Stanton (Stanton *et al.*, 2008), who kindly gave us the plasmid pAdZ5-CV5-E3^{+} in SW102 strain of *E.coli*, which has the adenovirus genome type 5 (E1^{-}) as a bacterial artificial chromosome (BAC) and with chloramphenicol (Cm) resistance. This system works using phage *λ* genes Red*γβα* under the control of a temperature-sensitive promoter which is repressed at 32°C and activated by incubating bacteria at 42°C.

Resistance genes SacB and Ampicilline (Amp) were replaced by the more efficient system rpsL-neo in the original plasmid. The modification was done in two phases, and for each of them a fragment of DNA or insert was constructed. In the first phase or positive selection, we selected bacteria cells that have incorporated the inserted DNA. This first fragment had homology regions (about 40 bp) with the site we wanted to modify on each end. Moreover, this fragment includes rpsL-neo genes, so after the first transformation recombinant clones with Kanamycin (Kan) resistance provided by neo gene were selected. In the second phase or negative selection, susceptibility to Streptomycin (Strep) provided by rpsL gene (since SW102 strain is naturally resistant to Strep) was lost. The second fragment had the same homology arms but in this case it included the modification that we wanted to insert. After the second transformation, recombinant clones were those that had incorporated the inserted DNA and had lost rpsL-neo fragment.

Plasmid pAdZ5-CV5-E3^{+} was modified in order to obtain pAdZ-ICOVIR-15K plasmid, backbone that has been used to introduce most of the modifications described in this thesis.

The procedure that has been followed to perform recombinations is described next. First of all, glycerinates of the bacteria that contain the plasmid to be modified were scratched with a sterile pipette tip, inoculated in 5 mL of LB media including Cm + Strep antibiotics (12.5 µg/mL, and 1 mg/mL, respectively) and incubated overnight at 32°C and constant agitation. Then 25 mL of LB Cm + Strep were inoculated with 0.5 mL of the previous culture and incubated 32°C with agitation until it reached an OD measure of 0.5-0.6 at 600 nm. At this moment, culture was divided in two Falcon tubes with equal volumes. One of them was induced by incubating it during 15 minutes at 42°C and then cultures were incubated on ice 15 minutes more. From that moment, manipulation was done at 4°C in order to ensure transformation efficiency. Both cultures (induced and non-induced) were centrifuged 5 minutes at 4000 *g* at 4°C and supernatant

was discarded. Bacteria pellet was resuspended in 12 mL of cold ddH_2O water and centrifugation was repeated. In the same way, two more washes were performed and in the last one the pellet was resuspended in the remaining water (≤300 µL). Afterwards, 50 µL aliquots of bacteria (both, from the induced and non-induced cultures) were transformed with 100-200 ng of DNA (the fragment which contains rpsL-neo). Bacteria were recoverd in 1 mL of LB and incubated 70 minutes at 32°C. Finally, they were plated into LB plates containing Cm and Kan (12.5 µg/mL, and 15 µg/mL, respectively) and incubated overnight at 32°C. About 20-24 hours later, colonies should be grown and the ratio between the colonies obtained in the induced culture (recombinant) and the non-induced one (control) were compared in order to assess recombination efficiency. Then, colonies were picked, minipreparations of DNA were made and restriction patterns of different clones were checked. Finally, the correct clone was frozen as a glycerinate.

A similar procedure was followed for the second phase, in which the clones obtained in the previous step were inoculated in 5 mL of LB Cm+Kan and cultured overnight at 32°C. Next day, the bacteria were made competent for its transformation by electroporation in the same way described previously. Again, 100-200 ng of DNA (insert) containing the desired modification were transformed. After the recovery incubation 100 µL from a 1:25 dilution were plated in LB agar Cm+Strep and plates were incubated overnight at 32°C. 24 hours later, colonies were picked, minipreparations of DNA were performed and clones were checked by the analysis of restriction pattern and/or sequentiation of the recombinant region.

2. HANDLING OF YEAST

In the same way than in bacteria, elements necessary for replication and a selection trait which is mutated or deleted in the strain of yeast to be used must be introduced in order to amplify plasmids in yeast. In this work, plasmids used for recombination in yeast contained CAL sequence (Sikorski and Hieter, 1989). CAL sequence has a centromere, a yeast replication origin or autonomous recombination sequence (ARS) and leucine gene. Plasmids obtained by homologous recombination are low copy (1-3 copies per cell) and must be amplified in bacteria. Therefore, it is necessary that these plasmids contained also the necessary elements to replicate in bacteria and a gene that confers resistance to antibiotics.

Yeast used in this work belongs to *Saccharomyces cerevisiae* YPH857 strain. This strain has been genetically modified to present mutations or deletions in genes involved in the synthesis of different molecules (ura3-53, lys2-801, ade2-101, his3-Δ200, trp1-Δ63, leu2-Δ1cyh2R). These

mutations are responsible for that this strain is not able to grow in media without uracile, lysine, adenine, hystidine, tryptophan or leucine. In this case, the selection of yeast containing recombinant plasmids was performed with media containing all these amino acids with the exception of leucine.

Homologous recombinations were performed by means of the transformation of the two linearized DNA fragments of interest in yeast to which competence has been previously induced. Homology regions needed for efficient recombination are of 40 bp length at each end.

2.1. PREPARATION OF COMPETENT YEAST

YPH857 strain stock was conserved as a glycerinate at -80°C. This glycerinate was scratched with a sterile pipette tip and striked in an agar plate containing rich media appropriate for yeast growth ($YPDA^{++}$). They were incubated during 3 days at 30°C and then the plate was stored at 4°C for a maximum period of 2 weeks.

In order to induce competence to the yeast, a colony was picked from the plate and was grown overnight in 5 mL of liquid $YPDA^{++}$ at 30°C and agitation of 200 rpm. Next day, OD was measured from a 1:10 dilution (OD_{600} = 1 is equivalent to $1.5x10^7$ cells/mL) and a yeast suspension of OD_{600} = 0.15 was prepared in a finale volume of 50 mL. This suspension was incubated at 30°C and 200 rpm agitation until it reached OD_{600} = 0.4-0.9 (5 hours approximately). Then, the suspension was passed to a 50 mL falcon tube and centrifuged 5 minutes at 3000 *g* and RT. Supernatant was discarded and washed with 25 mL of ddH_2O water and the suspension was pelleted again and resuspended in 1 mL of water. The suspension was transferred to an eppendorf tube and centrifuged 30 seconds at 6500 *g* in a microcentrifuge. The supernatant was discarded again and water was added to a final volume of 1 mL and distributed in 100 µL aliquots (10^8 cells), which were centrifuged during 30 seconds at 6500 *g* in a microcentrifuge. The supernatant was removed and the yeast pellet was ready to be transformed with DNA. This process must be performed the same day of utilization since competent yeast must be fresh.

2.2. TRANSFORMATION OF YEAST BY THE LIAC/SS-CARRIER DNA/PEG METHOD

Protocol for yeast transformation has been adapted from Gietz and Woods (Gietz and Woods, 2002). It is based on the desestabilization of yeast membranes by lithium acetate and the use of single chain DNA (SS-carrier DNA) to block repeated sequences where DNA to be transformed could bind unspecifically. The DNA is transformed by thermal shock.

First of all, SS-carrier DNA (salmon sperm DNA) was boiled in a boiling water bath for 5 minutes. For each transformation, a mix containing the following components was made up: 240 µL PEG (50%, w/v), 36 µL 1 M lithium acetate, 10 µL boiled SS-Carrier DNA at 10 mg/mL and 74 µL of plasmid DNA and insert plus ddH_2O. The amount of DNA for each recombination was 100 ng of insert and 10-fold less moles of the vector to which the insert was going to be incorporated. The 360 µL of the transformation mix was added to the yeast pellet and the cells were resuspended by vigorous mixing with a vortex. The tubes were then incubated in a 42°C water bath for 40 minutes. Then, tubes were microcentrifuged at 6500 *g* at RT for 30 seconds and the supernatant was removed with a micropipette. The pellet was resuspended in 100 µL of H_2O and spread gently onto SC Leu-agar plates. Plates were then incubated at 30°C for 2-3 days until recombinant yeast colonies appeared.

2.3. OBTAINING PLASMIDIC DNA FROM YEAST CULTURES

2 mL of liquid SC Leu- was seeded overnight at 30°C with the desired colony. 1.5 mL was transferred to an eppendorf tube and centrifuged at maximum speed 5 seconds in a microcentrifuge. The supernatant was discarded and the pellet resuspended in residual liquid. 400 µL of yeast miniprep mix containing: 2% Triton X-100, 1% SDS, 0.1 M NaCl, 10 mM Tris-HCl, pH 8.0, 1 mM EDTA, was added and mixed. Then 400 µL of phenol:chloroform:isoamyl (25:24:1) and 0.3 g of glass beads were added. The mixture was vortexed during 2 minutes at 4°C and centrifuged for 5 minutes at maximum speed. Supernatant was transferred to a new tube and plasmidic DNA was precipitated with 2 volumes of ethanol containing 2% sodium acetate during 30 minutes at -20°C. Then, the solution was centrifuged for 20 minutes at maximum speed and RT and the DNA pellet was resuspended in 25 µL of ddH_2O. 2 µL of the minipreparation of DNA were transformed by electroporation to electrocompetent bacteria (e.g. DH5α strain).

3. CELL CULTURE

3.1. HEK293

Human Embryonic Kidney 293 (HEK293) cells derive from human primary embryonic kidney cells. This cell line has been transformed with a fragment of the Ad5 genome including the E1A gene. 293 cells are highly permissive for the generation and replication of adenoviruses and are easily transfectable by the calcium phosphate method. This cell line has been used for the generation and functional titration of the oncolytic adenoviruses.

3.2. TUMOR CELL LINES

Tumor cell lines used in the *in vitro* and *in vivo* experiments and their origins are summarized in the following table:

Cell line	Tumor type	Origin specie
A549	Lung adenocarcinoma	Human
Skmel-28	Melanoma	
NP-9 NP-18 NP-29 NP-31 BxPC-3 Rwp-1 MiaPaca2 Panc-1	Pancreatic adenocarcinoma	
SCC-25 SCC-29 FaDu	Head and neck adenocarcinoma	
HP-1	Pancreatic adenocarcinoma	Syrian Hamster
B16 B16CAR B16-OVA B16CAR-OVA	Melanoma	Mouse
TRAMPC2	Prostate carcinoma	
P815K^{b}	Mastocytoma	

Table 2. Tumor cell lines used in this work.

A549 cell line has been used to amplify the different oncolytic adenoviruses due to its high efficiency to produce virus. NP-9, NP-18, NP-31, and NP-29 pancreatic tumor cell lines were established by the *Servei de Digestiu de l'Hospital de la Santa Creu i Sant Pau* from Barcelona and provided by the *Laboratori d'Investigació Gastrointestinal* from the same Hospital (Villanueva *et al.*, 1998). The hamster cell line HP-1 was provided by Dr. Rubén Hernández-Alcoceba (CIMA, Pamplona). The murine TRAMPC2 cell line was obtained from Dr. NM Greenberg (Baylor College of Medicine, Houston, TX). B16CAR murine cell line was obtained from Dr. Philippe Erbs (Transgene, France). B16 and B16-OVA cell lines were obtained from Dr. Pablo Sarobe (CIMA, Pamplona). B16CAR-OVA cell line was generated by the stable transfection of B16CAR with the plasmid pAcNeoOVA (Addgene plasmid 22533, Cambridge, UK) (Moore *et al.*, 1988). P815K^{b} (H-2^{d}

haplotype transfected with H-2K^b) cell line was provided by Dr. Daniel López (Instituto de Salud Carlos III, Madrid, Spain). The rest of the cell lines had been obtained at the American Type Cell Culture (ATCC). All cell lines were maintained in Dulbecco's modified Eagle's medium (DMEM) supplemented with 5% fetal bovine serum (FBS, Invitrogen Carlsbad, CA, USA) previously inactivated by heating at 56°C for 30 minutes and penicillin-streptomycin (PS, Gibco-BRL, Barcelona, Spain) (100 U/mL and 100 µg/mL, respectively) at 37°C and 5% CO_2. B16CAR were maintained with 0.5 mg/mL hygromycin (Invivogene, San Diego, CA) and B16CAR-OVA also with 0.5 mg/mL G418 (Invivogene, San Diego, CA).

3.3. PRIMARY BIOPSIES OF NORMAL CELLS

Pancreatic islets were kindly provided by Dr. Montanya (Endocrinology Service of the Hospital de Bellvitge, Barcelona, Spain). Isolated islets were cultured in CMRL-1066 medium supplemented with 0.5% of albumin and maintained at 37°C and 5% CO_2.

3.4. CELL COUNTING

To determine cell numbers manual or automatic methods were performed, using in both cases trypan blue dying exclusion test. Adherent cells were detached by incubating them with Trypsin-EDTA 0.05% (GIBCO RBL) and were resuspended in fresh medium supplemented with FBS. For the manual counting, a dilution in which 10 to 100 cells could be counted in each quadrant of the Neubauer chamber was made. Viable cells in each quadrant were counted and the mean was calculated. The number of cells per mL was calculated according to the following formula:

$$Number\ of\ \frac{cells}{mL} = Mean\ number\ of\ viable\ cells\ per\ quadrant \times Dilution\ factor \times 10^4$$

The automatic counting was performed with a cell counter TC20^{TM} (Bio-Rad) according to the manufacturer's instructions.

3.5. CELL FREEZING AND CRYOPRESERVATION

Cells were counted as explained above and resuspended in cold freezing medium (90% FBS 10% DMSO) at a final concentration of 5-10x10^6 cells/mL depending on the cell line. Cell suspension was distributed in cryotubes at 1 mL/tube and placed in a container filled with 2-propanol for its freezing at -80°C during 24 hours. Then the cryotubes were stored in a liquid nitrogen tank. For cell thawing, the cells were rapidly moved from the liquid nitrogen to a water bath at 37°C. Then the cells were diluted in pre-warmed medium and trespassed to a 15 mL

Falcon tube. Soft centrifugation at 1000 *g* was carried out for 5 minutes and the pellet of cells was resuspended in fresh medium and plated at high confluence to optimize the recovery.

3.6. MYCOPLASMA TEST

All cell lines were routinely tested for mycoplasma contamination by PCR using the following oligonucleotides:

Oligonucleotide	Sequence
MICO-1	5'- GGCGAATGGGTGAGTAACACG-3'
MICO-2	5'-CGGATAACGCTTGCGACTATG-3'

Table 3. Oligonucleotides used for the detection of mycoplasma contamination.

As a template for the PCR, medium from cells that had been in overconfluence and absence of antibiotics for at least 5 days was used. If the result was positive, cells were treated with Plasmocin™ at 25 µg/mL for 2 weeks, and then the cells were tested again.

4. CONSTRUCTION OF RECOMBINANT ADENOVIRUSES

Human adenovirus serotype 5 (Adwt) was obtained from ATCC, and AdwtRGDK, AdTL, AdTLRGDK, ICOVIR-15K, and ICOVIR-17 have been previously described (Bayo-Puxan *et al.*, 2009; Rojas *et al.*, 2009; Guedan *et al.*).

Following, the details of the construction of the recombinant vectors generated in this work are described.

ICOVIR-17K

The genome of ICOVIR-17K was generated by homologous recombination in yeast.

ICOVIR-17K was created by replacing the fiber containing the RGD motif in the HI loop for the RGDK fiber in the ICOVIR-17 genome. To achieve this, an *EcoR*I digestion fragment of the pBSattKKT plasmid15 (Bayo-Puxan *et al.*, 2009) containing the RGDK fiber was recombined in *Saccharomyces cerevisiae* YPH857 with the pICOVIR17CAL plasmid (CAU sequence, which includes the yeast autonomous replication elements and a selectable marker for uracil, was replaced by CAL, analogous to CAU but with a selectable marker for leucine instead of uracil in pICOVIR17CAU plasmid (Guedan *et al.*, 2010)) partially digested with *Nde*I.

ICOVIR-15K-E3OG

From now on, all the modifications were performed using homologous recombination in bacteria. All the oligonucleotides used and their sequences are summarized in **Table 3**.

For the generation of the oncolytic adenovirus containing the OVA_{257} and the $gp100_{25}$ epitopes in the E3-19K protein, the first step was the amplification of the rpsL-neo cassette by PCR from pJetRpsLneo, a plasmid containing the rpsLneo positive-negative selection markers cloned into pJet1.2/blunt (GenScript, Wheelock House, Hong Kong). The specific oligonucleotides used were E319KrpslF and E319KrpslR. The rpsL-neo cassette was then inserted in the E3-19K of pAdZICOVIR15K plasmid, which contained the genome of ICOVIR-15K in the pAdZ backbone (Gil-Hoyos, 2014). The fragments containing the epitopes and the linkers were generated by PCR using the following overlapping oligonucleotides: E319KepF1, E319KepR1, E319KepF2, and E319KepR2. The generated fragment was used to replace the rpsL-neo cassette in the E3-19K.

ICOVIR-15K-HIOG

The same strategy was used for the generation of the vector containing the epitopes in the HI-loop domain of the fiber. In this case, the oligonucleotides used for the amplification of the rpsL-neo cassette to be inserted in the HI-loop were HIlooprpslF and HIlooprpslR. For the generation of the fragment containing the epitopes the following oligonucleotides were used: HIWT1epiF, HIepF1, HIepR1, and HIWT1epiR. The generated fragment was used to replace the rpsL-neo cassette in the HI-loop.

ICOVIR-15K-SSdelE3OG and ICOVIR-15K-SSdelE3OGFR

The plasmid containing the rpsL-neo cassette in the E3-19K was used as a backbone for the generation of mutant adenoviruses of ICOVIR-15K-E3OG. For the deletion of the signal sequence of E3-19K, the oligonucleotide E319KSSdelOVA was used instead of E319KepF1 to generate the fragment containing the epitopes. To generate the fragment with the furin-resistant linkers we used the oligonucleotides E319KepFurResR1, E319KepFurResF2, and E319KepFurResR2. The generated fragments were used to replace the rpsL-neo cassette in E3-19K.

Oligonucleotide	Sequence (5'→3')
E319KrpslF	CATAATCCTAGGTTTACTCACCCTTGCGTCAGCCCACGGTGGCCTGGTGATGATG
E319KrpslR	CATTACAGGCTGGCTCCTTAAAATCCACCTTTTGGGTGGTTCAGAAGAACTCGTCA
E319KepF1	CATAATCCTAGGTTTACTCACCCTTGCGTCAGCCCACGGTACTACC
E319KepR1	CCGCTTCACGCGCAGTTTTTCAAAGTTGATTATACTGGTAGTACCGTGG
E319KepF2	GCGTGAAGCGGAAAGTACCCAGAAACCAGGACTGGCTTAGAGTTAAACGC
E319KepR2	ATTACAGGCTGGCTCCTTAAAATCCACCTTTTGGGTGGTGCGTTTAACTC
HIlooprpslF	CATTACACTAAACGGTACACAGGAAACAGGAGACACAACTGGCCTGGTGATGATG
HIlooprpslR	CAGACCAGTCCCATGAAAATGACATAGAGTATGCACTTGGTCAGAAGAACTCGTCA
HIWT1epiF	CATTACACTAAACGGTACACAGGAAACAGGAGACACAACTGGAAGCGGTTCTCGC
HIepF1	CCGGAAGCAGAAAAGTACCCAGAAACCAGGACTGGCTTGCCGGTTCTGG
HIepR1	CTGCTTCCGGAACCAGCCAGTTTTTCAAAGTTGATTATACTGCGAGAACC
HIWT1epiR	CAGACCAGTCCCATGAAAATGACATAGAGTATGCACTTGGGGAGCCAGAACCGGC
E319KSSdelOVA	AAACGCTGGGGTCGCCACCCAAGATGAGTATAATCAACTTTGAAAAACTG
E319KepFurResR1	CACAACGCGCACCAGTTTTTCAAAGTTGATTATACTGGTAGTACCGTGG
E319KepFurResF2	TGCGCGTTGTGAAAGTACCCAGAAACCAGGACTGGCTTGTTAGAGTGGTA
E319KepFurResR2	AGGCTGGCTCCTTAAAATCCACCTTTTGGGTGGTTACCACTCTAACAAGC

Table 4. Oligonucleotides used for the generation of recombinant adenovirus genomes.

4.1. ADENOVIRUS GENERATION BY CALCIUM PHOSPHATE TRANSFECTION

Once the desired modifications have been incorporated into the viral genome included in a plasmid, this recombinant viral DNA needs to be introduced into packaging cells to generate the adenovirus. With this aim we used HEK293 cells (Graham *et al.*, 1977) which were transfected with the viral DNA by the calcium phosphate-based method. In the case that the recombinant viral DNA had been obtained by recombination in yeast, the viral genome needed to be released from the plasmid by digestion with the restriction enzyme *Pac*I. This step was not necessary for the viral genomes constructed in pAdZ plasmids in bacteria, since they incorporate a self-excising system. Once the plasmid enters the cell, the endonuclease I-*Sce*I is expressed and releases the viral genome. This system increases the efficiency of the transfection, since circular DNA is transfected more efficiently than lineal DNA. After the transfection of the viral genome into the cells, the viral cycle begins, and after several rounds of replication (about 7 days post-transfection), foci of cytopathic effect are clearly seen.

For transfection, monolayers of HEK293 cells seeded in 6-well plates and at a confluence of 60-80% were used. For each plasmid to be transfected the following mixture was prepared in a 1.5 mL tube:

- 19.5 µL of $CaCl_2$ 2 M
- 3 µg of DNA
- ddH_2O up to a final volume of 162 µL

This solution was mixed up softly for 10 seconds, and another 1.5 mL tube containing 162 µL of HBS 2X (NaCl 274 mM, HEPES 50 mM, and NaH_2PO_4 1.5 mM in H_2O, pH adjusted to 6.95 – 7.05 with NaOH) was prepared. Then, the solution containing the DNA was added drop by drop to the tube containing the HBS while air was being bubbled with a pipette. The mixture was incubated for 1 minute at RT and added to the cells while shaking softly the plate to allow a homogenous distribution. 2 hours later the precipitates became visible and 16 hours post-transfection the medium was removed and exchanged by fresh medium.

When the foci of cytophatic effect were visible, the cells were collected together with the supernatant (cell extract, CE) and underwent through 3 rounds of freeze (-80°C) and thaw (37°C) to completely release the viral particles from the cells. In this way, the first viral lysate (passage 0, CEp0) was obtained.

4.2. CLONE ISOLATION BY PLAQUE PURIFICATION ASSAY

In order to have a homogenous stock of each generated recombinant adenovirus, clone isolation by plaque purification assay was performed with the initial viral lysate (CEp0). This assay was performed in A549 cells in order to avoid the possible homologous recombination between the modified E1 region of the adenovirus and the wild-type E1 region of the packaging cells HEK293. Once isolated, the clones were characterized and those which were correct were amplified for its subsequent use in *in vitro* and *in vivo* assays. The plaque formation assay is based on the infection of cell monolayers with a bank of serial dilutions made from the CEp0 of the different adenoviruses. Then, the infected cells are covered with an agarose matrix that allows the nutrient and gases exchange with the medium but does not allow the diffusion of the viral progeny. In this way, the viral particles released from the cells are only able to infect neighboring cells leading to the formation, after several round of replication, of viral plaques within the cellular monolayer.

First, serial dilutions ranging from 10^{-1} to 10^{-7} were prepared from the CEp0 in DMEM 5% FBS. Each well of the 6-well plate, which contains monolayers of A549 at an 80% of confluence, was infected with 100 µL of each viral dilution during 4 hours at 37°C. Then, cells were covered with 3 mL of a 1:1 solution of DMEM 5% FBS and 1% agarose previously prepared at 56°C. Once solidified, 2 mL of fresh medium was added over the agarose matrix. The plates were incubated at 37°C until the plaques appeared at day 5-8 post infection. At that moment, the medium was removed carefully and the plaques were picked through the agarose matrix using a pipette tip. The aspirated agarose/medium was resuspended in 500 µL of DMEM 5% FBS.

4.3. AMPLIFICATION AND PURIFICATION OF ADENOVIRUSES

Amplification and purification processes allowed the obtainment of sufficient amounts of the recombinant adenoviruses and in the appropriated formulation to be used for *in vitro* and *in vivo* assays. The amplification of the adenovirus is based on the propagation of the viral vector through culture plates of larger sizes at each passage and in bigger amounts. The purification of the adenovirus is based on its separation from the cell debris by an ultracentrifugation step in cesium chloride. Both processes are described in the following sections.

4.3.1. Amplification of recombinant adenoviruses

Taking into account that HEK293 cells contained in its genome the wild-type E1 region of the adenoviral genome, and that our conditionally replicative viruses have a modified E1 region, the amplification of all the oncolytic adenoviruses has been carried out in A549 cells to avoid undesirable recombinations.

The starting material for the amplification of the adenoviruses was the plaque obtained from the plaque isolation assay. 250 µL of the medium containing the isolated clone were used to infect a well from a 6-well plate of A549. When the cytopathic effect (CPE) was completed, the cells were harvested together with the supernatant (CE) and submitted to 3 rounds of freeze and thaw to release the viral particles from the cells. With the CE obtained from the 6-well plate (CEp1), 2 plates of 10 cm were infected. Again, when CPE was complete (around 72 hours post-infection) the CE was collected (CEp2). One of these plates was used to obtain viral DNA by Hirt's method (detailed in following sections) and the second one was used to infect 3 plates of 15 cm and continue with the amplification process. The CE from one of these 15 cm plates contains the sufficient amount of virus to perform *in vitro* studies and was kept at -80°C for this use. In order to purify the virus for *in vivo* usages, with the CE from the other 2 plates, 20 more 15 cm plates of A549 were infected. For the final amplification step, the CE was collected when the CPE was

evident in 90-100% of the cells but they were not completely detached from the plate, since the purification process is carried out with cell pellets and the virus present in the supernatant will be lost. At that moment, the cells and the supernatant were collected in 50 mL Falcon tubes and centrifuged 5 minutes at 1000 *g*. The supernatant was discarded (except for 40 mL that were kept at -80°C to be used in the purification process) and the cells from each tube were carefully resuspended in the remaining supernatant and joined into one Falcon tube in an approximate volume of 10 mL. This CE was kept at -80°C until the moment of purification.

4.3.2. Purification of recombinant adenoviruses

The purification of the adenoviruses is performed in order to have a viral stock with the appropriate formulation and concentration to be administered in mice and hamsters by systemic injection.

The method used in this work for the purification of adenovirus is based on using a cesium chloride (CsCl) density gradient combined with ultracentrifugation to separate viral particles from the rest of the CE components (cell debris, empty viral capsids, etc.) and to concentrate them. The buffer-exchange was performed by dialysis.

In order to release the viral particles from the cells, the pellets obtained in the amplification step were submitted to 3 freeze/thaw cycles. The viral extract was centrifuged 5 minutes at 1000 *g* and the supernatant containing the virus, which is called clarified cell extract (CCE), was collected. The pellet was resuspended in 10 mL of the supernatant that was kept from the amplification process and centrifuged again at the same conditions. This step was repeated 3 times until a volume of 42 mL of CCE was obtained. This CCE was then loaded onto the CsCl gradients. The CsCl gradients were prepared in ultracentrifugation tubes (Beckman Coulter) using 3 solutions at different concentrations. First, 0.5 mL of a 1.5 g/mL CsCl solution was layered in the bottom of 6 tubes. The second and third layers consisted in 2.5 mL of CsCl solutions at respective concentrations of 1.35 g/mL and 1.25 g/mL. These layers were added drop by drop in order to not disturb the formed gradient. Finally, 7 mL of the CCE were carefully loaded onto each tube containing the gradients. Then the tubes were ultracentrifuged 2 hours at 10°C and 150000 *g* (35000 rpm, SW40 Ti rotor, Beckman). At these conditions, viral particles are separated from cell debris and appeared as 2 bluish-white bands at the interface between 1.25 and 1.35 g/mL layers. The upper band corresponds to empty viral capsids and was removed by suction. Then, the band of interest was collected carefully and placed on ice in a 50 mL Falcon tube. For further purification, a second centrifugation step using a continuous CsCl gradient was necessary. The

solution containing the virus was brought up to 24 mL with the CsCl solution at 1.35 g/mL and distributed into 2 ultracentrifuge tubes. The second centrifugation was carried out overnight at the same conditions. After this centrifugation, the solution above the white band was discarded by suction and the band corresponding to the virus was collected in the smallest volume possible (in order to keep the virus highly concentrated) and introduced into a dialysis membrane. Three steps of 2 hours dialysis (each at 4°C) were carried out against 1 L of a PBS^{++} buffer (PBS supplemented with calcium chloride and magnesium). At the final dialysis, 5% glycerol was added to the buffer as a cryoprotectant. Other buffer that has been used to dialyze the virus was the Tris buffer (Tris-HCl 20 mM, NaCl 2 mM, and glycerol 2.5%).

4.4. TITRATION OF ADENOVIRUSES

4.4.1. Determination of physical viral particles by spectrophotometry

This method allows the quantification of the viral particles (vp) from a purified adenovirus stock without discrimination between infective or defective particles, and is based on the determination of the absorbance of viral DNA at a weight length of 260 nm.

Three different dilutions (1:5, 1:10, and 1:20) of the purified viral stock were prepared in lysis buffer (Tris 10 mM, EDTA 1 mM, 0.1% SDS, pH 8.0) and incubated for 5 minutes at 56°C. Then, OD was measured at 260 nm and 280 nm with a spectrophotometer. Final concentration of the virus could be calculated by the following formula, taking into account that the extinction coefficient of adenoviruses is $1.1x10^{12}$ per OD unit:

$$vp/mL = OD_{260\,nm} \times sample\ dilution \times 1.1 \times 10^{12}$$

The ratio between the absorbance at 260 nm and 280 nm gives an idea of the integrity of the purified sample, and should be around 1.4.

4.4.2. Determination of functional viral particles by anti-hexon staining

This method is based on the detection of positive cells for the immunodetection of the viral protein hexon in monolayers of infected HEK293 cells. This technique allows the determination of functional infective viral particles (TU) in purified stocks as well as in cell extract samples.

Serial 1:10 dilutions of the viral stock were prepared per triplicate in 96-well plates in a total volume of 100 µL per well of DMEM 5% FBS. Then, a cell suspension at 50000 cells/well was added to the wells and the plates were incubated for 36 hours at 37°C. After this time, the medium was removed by suction and the cells were dried for 5 minutes at RT. 100 µL of cold

methanol were added to each well in order to fix the cells and incubated 10 minutes at -20°C. The methanol was removed and the wells were washed twice with PBS^{++} containing 1% BSA. Next, the cells were incubated with a primary antibody against the hexon protein of the capsid obtained from the hybridoma 2Hx-2 (ATCC, Manasas, VA, USA), diluted 1:5 during 1 hour at 37°C. Afterwards, the cells were washed three times more and incubated with an anti-mouse secondary antibody conjugated with the fluorochrom Alexa-488 (Invitrogen) diluted 1:500 during 1 hour. Finally, the cells were washed thrice again and the viral titer was determined by the counting of stained cells using an inverted fluorescence microscope. To calculate the number of transducing units per mL the following formula was used:

$$TU/mL = \frac{Mean\ of\ positive\ cells}{100\ \mu L} \times Dilution\ factor \times 1000\ \mu L$$

4.5. CHARACTERIZATION OF RECOMBINANT ADENOVIRUSES

4.5.1. Methods for obtaining viral DNA

In this work, viral DNA has been obtained from two different sources: infected cells or purified virus stocks. The methods used in each case are detailed following.

4.5.1.1. Obtaining viral DNA from infected cells (Hirt's)

This method has been used for the analysis and validation of the clones obtained in the plaque formation assay.

The cell extract of infected cells was harvested and centrifuged 5 minutes at 1000 *g*. The supernatant was discarded and the pellet resuspended in 1 mL of PBS. The cell suspension was pelleted again by centrifugation and resuspended in 350 µL of ddH_20. 350 µL of Hirt's solution 2X (10 mM Tris pH 8.0, 20 mM EDTA, 1.2% SDS, and 200 µg/mL of proteinase K) were added to the cell suspension. The sample was mixed up and incubated for 1 hour at 56°C. Next, 200 µL of NaCl 5 M were added drop by drop to the mixture while vortexing and was incubated at 4°C for 8-16 hours until a white precipitate corresponding to the cellular DNA appeared. In order to eliminate this cellular DNA, the suspension was centrifuged for 30 minutes at 15000 *g* and 4°C and the clear supernatant containing the viral DNA was collected. This supernatant was incubated with RNAse at a final concentration of 100 µg/µL for 1 hour at 37°C. Then, a phenol:chloroform DNA

extraction was performed and the DNA was precipitated with ethanol containing 2% of sodium acetate. Finally, the pellet corresponding to the viral DNA was resuspended in 25 µL of ddH_2O or TE pH 8.0.

4.5.1.2. Obtaining viral DNA from purified virus stocks

This method has been used to verify the identity of each generated virus purified stock. Usually, the starting material has been a 50 µL aliquot of purified virus, containing approximately $2x10^{10}$ vp, corresponding to 1 µg of viral DNA.

To this aliquot, we added:

- EDTA pH 8.0 (16 µL 0.5 M)
- SDS (20 µL 10%)
- Proteinase K (8 µL, 10 mg/mL)
- TE pH 8.0 up to 400 µL

The mixture was incubated for 2 hours at 56°C and like in the method above, phenol:chloroform extraction and precipitation of DNA with ethanol 2% sodium acetate were performed. Finally, the pellet corresponding to the viral DNA was resuspended in 25 µL of ddH_2O or TE pH 8.0.

4.5.2. Characterization of the viral genome by enzyme restriction and sequencing

Both techniques had been used to confirm the identity of the generated adenoviruses using DNA from both, infected cells or purified stocks.

4.5.3. Digestion of DNA with restriction enzymes

As starting material for the digestion of viral DNA with restriction enzymes, 500-800 ng of DNA were used. To this amount of DNA, 1 unit of the enzyme, the appropriate buffer to each one (provided by the manufacturer at 10X), and ddH_2O up to the desired final volume were added. The mixture was incubated normally for 2 hours in a water-bath at 37°C and then the samples were resolved in a 1% agarose electrophoresis gel prepared in Tris-Acetate-EDTA (TAE) buffer, together with a molecular weight marker. The restriction enzymes that had been used in this work to assess the integrity of the viral genome were *Sac*II, *Kpn*I, *Hind*III, *Nde*I, *EcoR*I, and *EcoR*V.

4.5.4. Sequencing viral DNA

Sequencing of viral DNA was performed using 100 ng of DNA to which 5 µL of the sequencing mix 3.1 (Applied Biosystems) containing dNTPs and ddDNTPs marked with different fluorochroms, 5 µL of 5X sequencing buffer, 3.2 pmols of the corresponding oligonucleotide, and ddH_2O up to 10 µL. The conditions of the sequencing reaction were 24 cycles consisting on: 30 seconds at 96°C, 15 seconds at 50°C, and 4 minutes at 60°C. The sequencing reactions were analyzed with an automatic sequentiator at the "Servei de Seqüenciació i Genòmica dels Serveis Científics de la Universitat de Barcelona".

5. *IN VITRO* ASSAYS WITH RECOMBINANT ADENOVIRUSES

5.1. ASSAYS FOR THE DETECTION OF HYALURONIDASE EXPRESSION

Two different assays were used for demonstrating that ICOVIR-17K expressed functional soluble hyaluronidase. For both techniques the procedure followed for the obtaining of the samples was the same. Monolayers of A549 cells seeded in 10 cm plates were infected at 20 MOI with each virus. Infection media was removed 4 hours after infection, cells were washed once with PBS and fresh medium (without FBS) was added. 72 hours post infection the supernatant was collected and concentrated with 10K Amicon Ultra centrifugal filters (Millipore, Billerica, MA).

5.1.1. Microanalysis of hyaluronan oligosaccharides by PAGE

The first technique consisted on the analysis of the oligosaccharides generated by the incubation of supernatants of cells infected with adenoviruses expressing hyaluronidase and a high molecular weight hyaluronic acid solution. This method was described by Ikegami-Kawai (Ikegami-Kawai and Takahashi, 2002) and is based on the electrophoresis analysis of the oligosaccharides product of the digestion in polyacrylamide gels and its visualization using combined Alcian blue and silver staining protocol.

Each concentrated sample (15 µL) was incubated overnight at 37°C with 115 µL of a hyaluronic acid (Sigma, St Louis, MO) solution (1.5 mg/mL) in phosphate buffer (pH 6.0) containing 0.1 mol/L NaCl and 0.05% BSA. Hyaluronic acid degradation products from digestion were resolved by Polyacrylamide gel electrophoresis (PAGE). Digested samples were mixed 1:5 with sucrose 2 M in TBE buffer 5X and loaded in a 15% polyacrylamide gel (8.22 ddH_2O, 6 mL 40% acrylamide-bisacrylamide, 1.6 mL TBE 10X 1 M pH 8.3, 160 µL APS, 16 µL TEMED). The gel was run at 4°C at the following conditions: 20 minutes at 250 V, 10 minutes at 580 V, and 15 minutes at 450 V.

Next, the samples were fixed by soaking the gel in 0.05% Alcian blue dissolved in ddH_2O for 30 minutes in the dark. Then, the gel was destained by submerging it in ddH_2O for 30 minutes more and the oligosaccharides were revealed following a silver staining protocol. The gel was incubated for 30 minutes with 100 mL of the pretreatment solution (0.02% $Na_2S_2O_3$, 30% ethanol, 6.8% sodium acetate). Then, it was washed three times with ddH_2O and incubated 20 minutes in the dark at RT with the staining solution (0.2% $AgNO_3$, 0.015 % formaldehyde). Immediately, the gel was washed thrice again with ddH_2O and the gel was developed from 1 to 10 minutes with 100 mL of stopping solution (40 mM EDTA). Finally, the gel was washed 3 times for 5 minutes with ddH_2O and conserved in preserving solution (30% ethanol, 4% glycerol).

5.1.2. Quantitative turbidimetric hyaluronidase activity assay

In contrast to the previous method, the second technique was quantitative and the protocol was modified from the one developed by Dorfman (Dorfman and Ott, 1948). This method is based on an enzymatic reduction in which hyaluronic acid is measured by its ability to form turbidity with serum albumin solution at an acidic pH. Under the assay conditions, turbidity is directly proportional to hyaluronic acid concentration and can hence be related to enzyme activity. Generated turbidimetry is measured spectrophotometrically at 600 nm.

100 µL of supernatant samples containing soluble hyaluronidase were mixed with 100 µL of the hyaluronic acid solution and samples were incubated overnight at 37°C. After the incubation, samples were precipitated with 5 volumes of a solution containing 24 mM sodium acetate, 79 mM acetic acid and 0.1% of BSA (pH 3.75) and the absorbance at 600 nm was read. The units of activity for each sample were determined by comparing the OD_{660nm} of the sample with the OD_{660nm} of a standard curve of hyaluronidase activity, generated from a solution of bovine testicular hyaluronidase (Sigma, St Louis, MO)(Dorfman and Ott, 1948).

5.2. PROTEIN DETECTION BY WESTERN BLOT

Preparation of lysates from cell culture

Cells were seeded in 24-well plates in order to have an 80% of confluence at the moment of the infection. The infection was performed at a MOI of 20 in the case of A549 cells or 100 MOI for B16CAR and TRAMPC2 cells, and incubated during 4 hours at 37°C and 5% CO_2. Then, the cells were washed 3 times with PBS and incubated with fresh medium. 24 hours later, cells were softly trypsinized, resuspended, and centrifuged 5 minutes at 6000 *g*. The pellet was washed with PBS and centrifuged again to freeze dried pellets at -80°C.

Afterwards, cells were resuspended in Shieh's lysis buffer and incubated in agitation during 45 minutes at 4°C. Then, samples were centrifuged and protein extracts were collected and frozen in order to titer them. Shieh's lysis buffer contains:

- Tris-HCl 10 mM pH 7.4 (50 µL from a 1 M pH 7.5 stock)
- NaCl 400 mM (400 µL from a 5 M stock)
- NaF 5 mM (50 µL from a 0.5 M stock)
- Glycerol 10% (500 µL from a 100% stock)
- EDTA 1 mM (10 µL from a 0.5 M stock)
- Orthovanadate 1 mM (10 µL from a 0.5 M stock)
- Nonidet P-40 0.5% (25 µL from a 100% stock)
- Protease inhibitors cocktail 1x (100 µL from a 50X stock Complete Mini, Roche, Switzerland)

Quantification of the protein extracts

In order to quantify protein, a standard curve was done with known concentrations of BSA. 96-well plates were used to perform the serial dilutions of BSA in order to have 0, 1, 2, 3, 4, and 5 µg of protein in each well and per triplicate in a final volume of 160 µL. 1:10 dilutions of the samples of interest were prepared in 160 µL (always handling the samples on ice) and loaded onto other wells. 40 µL of Bradford reagent were added to the wells and mixed carefully without making bubbles. 5 minutes later, absorbance at 595 nm was read and protein concentration was determined taking into account the absorbance of the BSA standard curve.

SDS-PAGE and protein transfer to nitrocellulose membrane

First of all 10% acrylamide-bisacrylamide gel was prepared using 1.5 mm glass plates from Bio-Rad (Hercules, CA, USA). The gel consisted of two parts:

- Stacking gel: 4.4 mL of H_20, 0.75 mL of 40% acrylamide-bisacrylamide, 0.75 mL of Tris-HCl 1.5M pH 6.8, 60 µL of 10% SDS, 60 µL of 10% APS, 60 µL of TEMED.

- Resolving gel: 4.65 mL of H_20, 2.55 mL of 40% acrylamide-bisacrylamide, 2.6 mL of Tris-HCl 1.5M pH 6.8, 100 µL of 10% SDS, 100 µL of 10% APS, 10 µL of TEMED.

In order to reduce and denature the samples, each lysate was boiled in sample buffer (Laemmli buffer: 300 mM Tris-HCl pH 6.8, 600 mM DTT, 12% SDS, 0,6% bromophenol blue, 60% glycerol) at 100°C for 5 minutes. 20-30 µg of protein were loaded into the wells of SDS-PAGE gel

along with molecular weight markers. The gel was submerged into running buffer (25 mM Tris, 192 mM glycine, 0.1% SDS) and was run for 2 hours at 100 V and 20 mA.

Then the proteins were transferred from the gel to the nitrocellulose membrane. The transfer stack was mounted in the following order: sponge, 3 Wattman papers, gel, membrane, 3 Wattman papers, and sponge. The transfer was run for 2 hours at 200 mA and 100 V.

Blocking, hybridation and detection

The membrane was blocked for 1 hour at RT in agitation with TBS-0.05% Tween containing 5% of milk to prevent unspecific binding of the antibody to the membrane. Then, the membrane was incubated with appropriate dilutions of primary antibody in TBS-0.05% Tween 1% milk overnight at 4°C. After the incubation, four washes of TBS-0.05% Tween buffer, 10 minutes each, were performed and the membrane was incubated with the secondary antibody in TBS-0.05% Tween 1% milk during 2 hours at RT. Finally, the membrane is washed 4 times 10 minutes with TBS-0.05% Tween, and developed with ECL Amersham (GE Healthcare, Pisacatawey, NJ, USA) following the manufacturer's indications.

Antibody	Antigen	Specie	Dilution	Manufacturer
4D2	Adenovirus fiber	Mouse monoclonal	1:4000	Fitzgerald
SN Tw1.3	Adenovirus E3-19K	Mouse hybridoma	1:5	ATCC
hVIN-1	Vinculin	Mouse monoclonal	1:2000	Sigma
HRP anti-mouse	Mouse IgG	Goat monoclonal	1:2000	DAKO Cytomation

Table 5. Primary and secondary antibodies used for the Western blot detections.

5.3. VIRAL INFECTIVITY ASSAYS

B16CAR or TRAMPC2 cells were seeded in 24-well plates in order to have 80% of confluence at the moment of the infection. Then, each cell line was infected with different adenoviral vectors expressing GFP and luciferase (Track-Luc cassette) at different MOI (25, 50, 100, and 200 TU/cell) during 4 hours at 37°C. After this time, infection media was removed and replaced by fresh medium. 24 hours later, fluorescence was analyzed by microscopic observation.

On the other hand, cells were trypsinized, resuspended in FACS buffer (PBS 10% FBS, 0.01% sodium azide) and analyzed by flow cytometry for the expression of GFP. Gallios™ (Beckman Coulter) cytometer was used and 10000 events were analyzed for each sample. FlowJo v7.6.5 (Tree Star, Inc.) software was used for the data analysis.

5.4. VIRAL PRODUCTION ASSAYS

To perform viral production assays, a known number of tumor cells were seeded into 24-well plates in order to have an 80% of confluence at the moment of the infection. Then, each cell line was infected per triplicate at a MOI to allow for 80 to 100% of infection. A549 were infected at 25 TU/cell, Skmel-28 and NP-18 at 30 TU/cell, NP-9 and HP-1 at 20 TU/cell, and B16CAR and TRAMPC2 at 100 TU/cell. 4 hours later, infection media was removed, cells were washed 3 times with PBS and incubated with fresh medium. At indicated time points (4, 24, 48, and 72 hours post infection), cells and medium (CE) were harvested and subjected to 3 rounds of freeze-thaw lysis.

Isolated pancreatic islets were distributed in independent tubes (7 islets/tube) in 100 µL of final volume and infected in triplicate at 200 TU/cell with the different adenoviruses (assuming 1000 cells per islet). Infection was performed in suspension and with constant agitation during 2 hours at 37°C. Islets were washed 3 times with PBS and seeded in 96-well plates with fresh virus-free medium. After washing, a small fraction of the SN was collected to determine the input virus (background level). At day 6 after infection, the islets and the medium were harvested and freeze-thawed 3 times to obtain the cell extract.

After the freeze-thaw cycles the cell extracts were centrifuged 5 minutes at 5000 *g* to separate cell debris and viral titers were determined in triplicate according to the anti-hexon staining-based method, described previously.

5.5. CYTOTOXICITY ASSAYS

Cytotoxicity analysis *in vitro* is based on the evaluation of the cell viability after the exposure of tumor cells to the different adenoviruses. Such analysis was performed by the quantification of total protein content by the bicinchoninic acid assay (BCA, Pierce Biotechnology, Rockford, IL, USA). This assay combines the reduction of Cu^{2+} to Cu^{1+} by proteins in an alkaline medium with the highly sensitive and selective colorimetric detection of the cuprous cation (Cu^{1+}) by bicinchoninic acid. The reaction of two molecules of BCA with one Cu^{1+} resulted in an intense purple-colored product that exhibits a strong linear absorbance at 540 nm with increasing protein concentrations.

Cytotoxicity assays were performed by seeding 40000 Skmel-28, NP-18 or NP-31 cells, 30000 A549, FaDu, and Panc-1, 20000 NP-29 or BxPC-3 cells, 15000 NP-9, Rwp-1, MiaPaCa-2, SCC-29 or SCC-25 cells or 10000 HP-1 cells per well in 96-well plates in DMEM with 5% FBS. Cells were infected with serial dilutions starting with 400 TU/cell for SCC-25 and FaDu cells, 300 TU/cell for

Rwp-1, MiaPaCa-2 and SCC-29 cells or 200 TU/cell for A549, Skmel-28, NP-18, NP-9, NP-29, NP-31, BxPC-3, Panc-1 and HP-1 cells. For the cytotoxicity assays including gemcitabine, cells were treated with doses of this drug close to the IC_{50} value for each cell line that was previously calculated (15 nM for FaDu and NP-18, 25 nM for A549 and HP-1, 100 nM for BxPC-3, 250 nM for NP-9, and 1000 nM for SCC-25) 24 hours prior to the infection with the serial dilutions of the adenovirus. At day 5 or 6 post-infection, plates were washed with PBS and incubated with 200 µL of BCA reagent during 30 minutes at 37°C. Absorbance was quantified at 540 nm and the TU/cell required to produce 50% of inhibition (IC_{50} value) was estimated from dose-response curves by standard nonlinear regression (GraphPad Software Inc., CA, USA). In the case of gemcitabine/virus combination, the percentage of cell survival was normalized with that of the cells treated with gemcitabine alone.

5.6. PLAQUE SIZE ASSAYS

Serial dilutions of the adenoviruses were prepared from cell extract (CE) samples ranging from 10^{-4} to 10^{-9}. Monolayers of A549 cells at a confluence of 80-100% that were previously seeded in 6-well plates were infected with 100 µL of each viral dilution during 4 hours at 37°C. Then, cells were covered with 3 mL of a 1:1 solution of DMEM 5% FBS and 1% agarose and once solidified, 2 mL of fresh medium was added over the agarose matrix. The plates were incubated at 37°C until the plaques appeared at day 5-8 post infection. For the correct visualization of the plaques, they were stained by the incubation of the cells during 3 hours at 37°C with 0.1 mL of a 5 mg/mL solution of MTT (Sigma-Aldrich, MO, USA).

6. *IN VIVO* ASSAYS WITH RECOMBINANT ADENOVIRUSES

6.1. ANIMALS AND CONDITIONS

All the animal studies were performed at the IDIBELL facility (AAALAC unit 1155) and approved by the IDIBELL's Ethical Committee for Animal Experimentation.

For the realization of this work, male immunocompetent Balb/C mice were used for the toxicity studies, male immunodeficient Balb/C nu/nu mice were used for the antitumor activity experiments, and female immunocompetent C57BL/6 mice were used for the immunization experiments. In all cases, 6-8 week-old mice with a body weight between 20 and 30 g were used. For the toxicity and antitumor activity experiments involving hamsters, 5 week-old female golden Syrian hamsters (*Mesocricetus auratus*) weighting between 80 and 100 g were used.

Animals were housed at a temperature between 22 and 24°C under an artificial circadian 12 hours light/12 hours dark cycle and received *ad libitum* standard diet and water.

6.2. TUMOR IMPLANTATION AND MONITORING

Tumor cells for the implantation of tumors were maintained in 15 cm plates at standard conditions *in vitro*. At the moment of implantation, cells were trypsinized, resuspended with DMEM 5% FBS, centrifuged during 5 minutes at 1000 *g*, washed with PBS, and counted. Finally, they were resuspended in an appropriate volume of PBS in order to have a final volume of 150 µL for each tumor. The number of cells per tumor varied depending on the cell line and ranged from $3x10^6$ to $1x10^7$ cells/tumor. Mice were anesthetized with isofluorane before the implantation of the tumors and shaved in the case of immunocompetent C57BL/6 mice. For hamster studies, $5x10^5$ cells were implanted in a final volume of 200 µL for each tumor. Hamsters were previously anesthetized with a cocktail of ketamine and xylasine and shaved. The subcutaneous injections were carried out with 29 G hypodermic needles. After tumor implantation, the appearance of the tumors was monitored by palpation, and when they had a measurable volume were measured with a caliper. Tumor volume was calculated according to the following equation:

$$V\ (mm^3) = \frac{\pi}{6} \times L \times W^2$$

where W and L are the width and the length of the tumor, respectively.

The percentage of growth was calculated according to the following formula:

$$\%\ of\ tumor\ growth = \frac{V - V_0}{V_0} \times 100$$

where V_0 is the tumor volume on day 0.

When tumors reached a volume of 80-200 mm^3, animals were randomized into experimental groups and were treated as corresponded.

6.3. ADENOVIRUS ADMINISTRATION

Viral solutions for the administration *in vivo* were prepared by diluting the purified viral stocks in PBS. For the systemic administration of adenoviruses in mice, dilutions at a concentration to have 4-$5x10^{10}$ vp in a final volume of 200 µL per animal were prepared. The injection was performed with hypodermic 29 G needles via tail vein. For the intratumoral administration of adenoviruses in mice $2x10^9$ vp in 20 µL were injected per tumor and a Hamilton syringe with a

length of 25 mm and 33 G was used. For the systemic administration in hamsters, $4x10^{11}$ vp were injected through the cephalic vein with hypodermic 30 G needles in a final volume of 250 µL, whereas $2.5x10^{10}$ vp in 20 µL were administered for the intratumoral route.

6.4. TREATMENT WITH GEMCITABINE OR HYALURONIDASE

For the experiments in which gemcitabine (Gemzar) treatment was required, a dose schedule of 50 mg/kg was administered at days 0, 3, 6, and 9 by intraperitoneal injection both, in mice and hamsters.

For the study including treatment with soluble hyaluronidase, a single intratumoral administration of 100 IU/tumor of bovine testicular hyaluronidase (Sigma, St Louis, MO) diluted in PBS at a final volume of 20 µL was performed using a Hamilton syringe with a length of 25 mm and 33 G.

6.5. SAMPLE HARVESTING

The obtaining of blood samples and organs for their analysis was carried out after the sacrifice of the animals by CO_2 chamber in hamsters in the case of mice.

6.5.1. Serum for viremia analysis

Blood samples for the detection of virus in serum were obtained 6 hours after the systemic administration of the virus from the tail. After a 5 minutes centrifugation at 6500 *g*, serum was collected and titered by the anti-hexon method.

6.5.2. Blood and serum for the hematologic and biochemical analysis

Blood samples were obtained by cardiac puncture with a hypodermic 25 G needle. For hematological analysis blood samples were collected in tubes containing EDTA (BD Microtainer, K2EDTA) tubes, and were analyzed by the "Servei d'Hematologia de la Facultat de Veterinària de la Universitat Autònoma de Barcelona". For the biochemical analysis, tubes containing heparin (BD Microtainer, PST™ LH tubes) were used and the samples were centrifuged 5 minutes at 6500 *g* to obtain the serum, which was analyzed by the "Servei de Bioquímica Clínica Veterinària de la Facultat de Veterinària de la Universitat Autònoma de Barcelona".

6.5.3. Organ collection

Tumors were obtained from sacrificed animals and washed with a saline solution. Then, tumors were divided into pieces and fixed in formaldehyde 4% for 16 hours to be included in paraffin, frozen in OCT, or frozen directly in order to extract RNA.

6.5.3.1. Paraffin inclusion

Fixation of tissues in formaldehyde was followed by washing them with a saline solution in order to eliminate the fixative agent. Next, tissues underwent a battery of alcohols of crescent graduation in order to dehydrate them to allow the penetration of paraffin. Tissues were submerged for 1 hour in ethanol 70%, for 2 hours in ethanol 96%, and then in new 96% ethanol overnight. Next day, tissues went through a battery consisting of 3 absolute ethanol (1.5 hours each) and then were submerged into xylol for 1.5 hours more. Finally, they were submerged into liquid paraffin at 65°C overnight and the next day they were included in blocks.

6.5.3.2. OCT inclusion

OCT inclusion was performed directly after collecting the sample. The tumors were placed in *Criomold* (Tissue-Tek Sakura) molds in which a cryoprotective matrix of OCT (Tissue-Tek Sakura) was previously added. Included tissues were frozen immediately in dry ice and stored at -80°C.

7. QUANTIFICATION OF ANTIGENS EXPRESSION BY QUANTITATIVE RT-PCR

Total RNA from frozen tumors was extracted using the RNAeasy Plus Mini Kit (Qiagen) according to manufacturer's indications. The obtained RNA was quantified by measuring the absorbance at 260 nm in a nanodrop spectrophotometer (NanoDrop technologies) from 1 µL of the RNA solution. Moreover, the quality of the RNA was analyzed by running the samples in a 1% agarose electrophoresis gel in TBE buffer (Tris-borate, EDTA 1mM). That electrophoresis allowed the observation of the 28S, 18S and 5S bands corresponding to the ribosomal RNA and indicating the integrity of the samples.

cDNA was obtained from RNA samples after a reverse transcription reaction using the High Capacity cDNA Reverse Transcription Kit (Applied Biosystems) and following the manufacturer's indications. Obtained cDNA was used as template to perform a real-time PCR with SYBR Green (Roche Molecular Biochemicals). For this, 2µL of the DNA sample were mixed with 5 µL of Master SYBR Green, 0.4 µL of the specific oligonucleotides at 5 µM, and ddH_2O up to 10 µL of final volume. Real-time PCR was run on a LightCycler instrument (Roche Molecular Biochemicals). 43

cycles of amplification with denaturation at 95°C for 10 seconds followed by annealing at 60°C for 20 seconds and extension at 72°C for 20 seconds were done after an initial incubation at 95°C for 10 minutes. Specific primers for mouse gp100, OVA, and the house-keeping gene mouse β-actin were used (**Table 6**).

Gene	Forward oligonucleotide	Reverse oligonucleotide
Mouse gp100	5′-CCAGCCCATTGCTGCCCACA	5′-CTGTGTCCTGCCAAGGCGGG
OVA	5′-GCCTGATGAAGTCTCAGGCC	5′-AAGCAGGCAGAGAGGTGGTA
Mouse β-actin	5′-GGGGGTTGAGGTGTTGAG	5′-GTCTCAAGTCAGTGTACAGGCC

Table 6. Oligonucleotides used for the amplification of gp100, OVA, and β-actin genes.

The dC_t values were calculated after subtracting the mean C_t values of β-actin gene from the receptor gene mean C_t values.

For the detection of the expression of the gp100 and OVA genes in cell lines the same protocol was followed by using as a starting material $3x10^6$ cells instead of frozen tumor tissue. Moreover, a regular PCR was performed instead of a RT-PCR using the same oligonucleotides and the presence of the specific band was assessed by running a 1% agarose electrophoresis gel.

8. HISTOLOGY

8.1. IMMUNOHISTOCHEMISTRY IN PARAFFINIZED SECTIONS

Paraffin-embedded blocks were cut into 4-µm thick sections with a microtome and deposited into poly-L-lysine treated slides. Sections were deparaffinized by subjecting them to a battery of 4 xylols (10 minutes each), 3 absolute ethanol, 3 96% ethanol, 1 70% ethanols, and 1 50% ethanol (5 minutes each). Finally the sections were rehydrated by submerging them in ddH_2O. Next, endogenous peroxidase activity was blocked by incubation for 10 minutes in 0.3 % H_2O_2. Antigens masked during routine fixation were retrieved by submerging the slides in sodium citrate solution (pH 6.0) and heating during 12 minutes. Then, sections were washed thrice with ddH_2O during 5 minutes and then once in PBS for 5 minutes. Sections were blocked in order to reduced unspecific binding with Normal Goat Serum diluted 1:5 in PBS 1% BSA for 1 hour at RT. All the incubations were performed in a humidity chamber. Primary antibody incubation was performed using an anti-gp100 antibody (Ab787 HMB45, Abcam, Cambridge, UK) diluted 1:40 overnight at 4°C. After washing thrice with PBS 0.2% Triton-X100 for 5 minutes, the sections were covered with anti-mouse Envision$^+$-System-HRP (Dako Laboratories, Glostrup, Denmark) and incubated 1 hour at RT. Next, slides were washed 3 times more with PBS 0.2% Triton X-100 and developed by

covering the sections with the chromogenic substrate DAB+ (Envision Kit, Dako Cytomation K3468) during approximately 30 seconds, until a brown precipitated appeared. The reaction was stopped by rinsing the slides with tap water for 10 minutes. Finally, the sections were counterstained with hematoxylin, rehydrated and mounted in DPX (VWR International).

8.2. IMMUNOFLUORESCENCE IN FROZEN SECTIONS

OCT preserved samples at -80°C were cut into 5-µm thick sections with a cryostat that maintained the samples at -20°C. The sections were deposited at RT into poly-L-lysine treated slides and kept at -80°C until their processing.

In this work immunofluorescence staining has been performed in frozen sections of tumors in order to detect adenovirus presence. The detection of adenovirus in frozen tissues is quicker and easier than in paraffin-embedded section. However, it has the disadvantage that the structure and morphology of the tissues is poorly preserved.

The sections were temperate for 30 minutes at RT and then were fixed by immersion in a 4% formaldehyde solution for 30 minutes. Following a 2 minutes wash with ddH_2O and another one for 10 minutes in PBS 0.05% Tween-20, the sections were covered with a blocking solution containing 1:5 horse serum diluted in PBS for 30 minutes at RT in a humidity chamber. Then, blocking solution was removed and the sections were covered with a 1:100 dilution of the primary antibody which was a rabbit polyclonal against E1A adenovirus-2/5 (sc-430, Santa Cruz, CA, USA) in PBS 0.05% Tween-20. This incubation was carried out during 1 hour at RT. Then, the sections were washed thrice with PBS 0.05% Tween-20 and incubated for 1 hour more with the secondary antibody, which was an anti-rabbit Alexa-488 (Invitrogen, CA, USA), diluted 1:300 in PBS 0.05% Tween-20. Finally, sections were washed again with PBS 0.05% Tween-20 and mounted with mounting media containing DAPI (DAKO) in order to stain cell nucleus. The images were taken with a fluorescence microscope Olympus BX60 and a digital camera Olympus U-RFL-T, using the SPOT Advanced 3.2.4 software (Diagnostic instruments).

9. IMMUNOLOGY TECHNIQUES

9.1. IMMUNOCYTOCHEMISTRY

For the detection of gp100 expression in B16 cells, an immunocytochemistry (ICC) protocol was used. Cells were grown over sterilized glass coverslips placed into 24-well plates. When the cells had a confluence of about 60%, medium was removed and the cells were fixed by incubating them with a cold 4% paraformaldehyde solution for 15 minutes at RT. Then, the fixation solution

was removed and the cells were washed twice with ice-cold PBS. Since gp100 protein is intracellular, an additional step of permeabilization was required. With this aim, cells were incubated for 10 minutes with PBS containing 0.25% Triton X-100. Cells were washed twice again with PBS for 5 minutes and a blocking step was performed by incubating the cells in a PBS 0.05% Tween-20 10% FBS solution. Next, cells were washed 3 times in PBS for 5 minutes and incubated with the primary antibody anti-gp100 (Ab787 HMB45, Abcam, Cambridge, UK) diluted 1:40 in PBS 0.05% Tween-20 10% FBS for 1 hour at RT. The primary antibody was decanted, 3 more washes with PBS were performed and cells were incubated for 1 hour at RT with the secondary antibody anti-mouse Alexa 488 (Invitrogen, CA, USA) diluted 1:300 in PBS 0.05% Tween-20 10% FBS. Finally, coverslips were washed 3 times with PBS in dark and mounted with mounting media containing DAPI (Vectashield, Vector Laboratories LTD., UK). The images were taken with a fluorescence microscope Olympus BX60 and a digital camera Olympus U-RFL-T, using the SPOT Advanced 3.2.4 software (Diagnostic instruments).

9.2. IMMUNOFLUORESCENCE CELL STAINING AND FLOW CYTOMETRY

For the evaluation of the processing and presentation of the exogenous epitopes incorporated in oncolytic adenoviruses we used as a tool the monoclonal antibody 25D1.16, which specifically recognize the complexes formed by the MHC class I molecules H-2K^b bound to the OVA$_{257}$ peptide, restricted for this HLA haplotype. Importantly, this antibody did not recognize empty H-2K^b molecules or molecules bound to other peptides (Porgador *et al.*, 1997).

Moreover, immunofluorescence cell staining of CAR, H-2K^b, H-2D^b, and HLA-A2.1 have also been performed. Levels of surface MHC class I molecules were evaluated at basal conditions or after being treated with adenovirus or IFN-γ. Cell staining was performed in 1.5 mL tubes or 96-well plates with U bottoms, depending on the number of samples.

Generally, cells were seeded in 24-well plates and, in the case of adherent cells, were trypsinized at the moment of the staining and resuspended in FACS buffer (PBS 10% FBS 0.01% sodium azide). Cells were pelleted by centrifugation for 5 minutes at 1000 *g* and 4°C, washed twice with FACS buffer (PBS 10% FBS and 0.01% sodium azide) and incubated with the corresponding primary antibodies. Direct staining was performed in the case of H-2D^b and H-2K^b/OVA$_{257}$ since the primary antibody were already conjugated to a fluorochrome, and incubations were carried out for 30 minutes at 4°C and in a final volume of 50 µL. In the other cases, indirect staining was performed by resuspending the cell pellet in 100 µL of the hybridoma supernatant and incubating 30 minutes at 4°C. After the incubation, 3 washes were performed

with FACS buffer and in the indirect staining a second incubation of 30 minutes at 4°C in a final volume of 50 µL with an appropriate secondary antibody was needed. Finally, samples were washed again 3 times with FACS buffer, resuspended in 350 µL of final volume, and analyzed by flow cytometry. The primary and secondary antibodies used and their corresponding dilutions are summarized in **Table 7.**

Antibody	Antigen	Specie	Dilution	Manufacturer
SN RmaB	CAR	Mouse hybridoma	1	ATCC
SN Y3	H-2K^b	Mouse hybridoma	1	ATCC
PE-labeled KH95	H-2D^b	Mouse monoclonal	1:40	BD Pharmingen
SN PA2.1	HLA-A2.1	Mouse hybridoma	1	(Parham and Bodmer, 1978)
PE-labeled 25D1.16	H-2K^b/OVA$_{257}$	Mouse monoclonal	1:500	Biolegend
Alexa488 antimouse	Mouse IgG	Goat antimouse	1:500	Molecular Probes

Table 7.Primary and secondary antibodies used for the flow cytometry detections.

In the cases were the cells were treated with murine IFN-γ (Preprotech), this cytokine was added to media of the corresponding wells at a concentration of 200 IU/mL 48 hours before the analysis. In the cases were the cells were treated with adenovirus, they were infected 24 hours before the analysis. The cells were infected with the corresponding virus at a MOI of 100 TU/cell for B16CAR and TRAMPC2 or 200 TU/cell for P815K^b. 4 hours after the infection, medium was removed, the cells were washed with PBS, fresh medium was added, and the cells were incubated overnight. Alternatively, cells were pulsed overnight before the flow analysis with OVA$_{257}$ (SIINFEKL) or gp100$_{25}$ (KVPRNQDWL) peptides (GenScript, Pisacatawey, NJ, USA) at 1 µM. For the inhibition experiments, the infection of P815K^b cells was carried out in the presence or not of lactacystin (LC) (Enzo Life Sciences, NY) or brefeldin A (BFA) (Sigma, St Louis, MO) inhibitors at 10 µM or 10 µg/mL, respectively.

A Gallios™ (Beckman Coulter) cytometer was used for the analysis. 10000 events were analyzed for each sample and FlowJo v7.6.5 (Tree Star, Inc.) software was used for the analysis of the data.

9.3. MICE IMMUNIZATION

The administration of the different adenoviruses for the immunization of mice was performed directly, by the intravenous administration of 3x10^{10} vp in 200 µL of PBS or indirectly by the subcutaneous administration of infected cells. For the last protocol, B16CAR or TRAMPC2 cell lines were cultured as usual in 15 cm plates *in vitro*, and at the day of implantation, cells were

trypsinized and resuspended in DMEM 5% FBS. Cells were infected in suspension at a MOI of 100 TU/cell during 4 hours at 37°C and in continuous agitation. Then, cells were centrifuged for 5 minutes at 500 *g* and resuspended in the appropriate volume of PBS in order to have $1x10^6$ cells in 200 µL. Finally, infected cells were implanted in the flank of the mice. 7 days later, animals were euthanized and spleens were harvested to analyze antigen-specific responses as described below or were challenged by the subcutaneous implantation $1x10^6$ B16CAR-OVA cells given subcutaneously in a final volume of 200 µL.

9.4. ISOLATION OF SPLENOCYTES

The whole process was carried out in sterile conditions. Spleens were harvested from sacrificed animals and were placed in 15 mL conical Falcon tubes containing 5 mL of RPMI medium supplemented with 10% FBS and 1% P/S. A cell strainer (40-100 µm) was placed in a 6 cm plate and the spleens were mechanically disrupted with the flat portion of a syringe plunger until no fragments remained. The medium was passed several times through the cell strainer and the cell suspension was transferred to a clean 15 mL conical Falcon tube. The disrupted tissue was then centrifuged at 500 *g* for 10 minutes and the supernatant was removed. In order to lyse the red blood cells, the pellet was resuspended in 2 mL of ACK lysis buffer (Ammonium chloride NH_4Cl 150 mM, potassium bicarbonate $KHCO_3$ 10 mM, EDTA 1 mM, pH 7.2). The suspension was incubated at RT for 3 minutes, the tube was filled with fresh medium, and centrifuged again at 500 *g* for 10 minutes. The supernatant was removed and the cell pellet was resuspended in PBS. 2 more washes were performed with PBS to discard any tissue debris. Finally, the cells were counted with the automatic cell counter TC20™ and brought to a concentration of $2.5x10^6$ cells/mL for the ELISpot analysis.

9.5. ELISPOT

CTL specific responses were evaluated by anti-IFN-γ Enzyme-linked immunospot assay (ELISPot). This method is based on the measurement of the frequency of cytokine-secreting cells at a single-cell level in response to the stimulation with a specific antigen by employing the sandwich enzyme-linked immunosorbent assay (ELISA) technique.

All steps until the development of the plates were performed under sterile conditions. 96-well polyvinylidene fluoride membrane ELISPOT plates (Multiscreen plates, Millipore, Billerica, MA) were treated with 15 µL of 35% ethanol per well for 1 minute. Then, 5 washes with ddH_2O were performed and plates were incubated overnight at 4°C with a murine IFN-γ-specific capture antibody (clone AN-18, BD 551309, San Jose, CA) at 4 µg/mL diluted in PBS at a final volume of

100 µL/well. The day after, the antibody was discarded and plates were washed 5 times with PBS and blocked with 200 µL/well of supplemented RPMI medium for 2 hours at RT. During this incubation, the splenocytes were isolated as explained above and 100 µL of a $2.5x10^6$ cells/mL cell suspension were added to each well ($2.5x10^5$ cells/well). The peptides that were used for the stimulation of the splenocytes were: $E1b_{192}$ (VNIRNCCYI), Hex_{418} (GGVINTETL), OVA_{257} (SIINFEKL), and $gp100_{25}$ (KVPRNQDWL). $E1b_{192}$, Hex_{418}, and $gp100_{25}$ have affinity for H-$2D^b$, whereas OVA_{257} have affinity for H-$2D^b$. All the peptides were synthesised by GenScript USA Inc. (Piscataway, NJ, USA) at 95% purity and re-suspended following the manufacturer's instructions. Stimulation with the peptides was performed at a final concentration of 1 µM. Phorbol-myristate-acetate (PMA at 15 ng/mL) plus ionomycin (250 ng/mL) were used as positive control of stimulation and media only as negative control, at 100 µL/well. Plates were incubated with the splenocytes for at least 18 hours at 37°C and 5% CO_2. From that moment, sterility was not required. Cells and medium were removed and the plates were washed 5 times with PBS. Then, the biotinilated anti-IFNγ secondary antibody (clone RA-6A2, BD 55156, San Jose, CA) was added at a concentration of 1 µg/mL in PBS 0.5% FBS at a final volume of 100 µL/well and incubated for 2 hours at RT. Next, the antibody was removed and the plates were washed 5 times with PBS. The streptavidin-ALP (ExtrAvidin Ref E2636-2ML Sigma E2636, Sant Louis, MO) was then added diluted 1:2500 in PBS 0.5% FBS (100 µL/well) and then incubated for 1 hour at RT. Again, 5 washes with PBS were performed and finally 50 µL/well of the substrate BCIP/NBT solution (Ref B1911-100ML, Sigma, St. Louis, MO) was added. Plates were developed for 15-30 minutes until spots emerged and the plate was washed with tap water to stop the reaction. Plates were left to dry overnight and spots were counted using the AID EliSpot reader classic (ELR07 de AID GmbH, Straßberg, Germany).

9.6. STATISTICAL ANALYSIS

The graphs and statistic tests were performed with GraphPad Prism v5 software (GraphPad Software, Inc.). Unpaired two-tailed Student's *t*-test was used for the comparison of means between two groups. When more than two groups were compared, one-way ANOVA test with a tukey post-hoc test was used. If more than two groups and more than one variable were compared (ELISpot), two-way ANOVA with a Bonferroni post-hoc test was used.

Survival curves were obtained with the same software and *logrank* Mantel-Cox test was used to determine statistically significant differences.

The statistic significance was defined at a *p* value lower than 0.05.

RESULTS

Chapter 1

1. COMBINATION OF THE REPLACEMENT OF HSG-BINDING MOTIF WITH RGD AND EXPRESSION OF HYALURONIDASE IN AN ONCOLYTIC ADENOVIRUS

1.1. GENERATION AND CHARACTERIZATION OF THE ONCOLYTIC ADENOVIRUS ICOVIR-17K

Different studies have associated the mutation of the putative HSG-binding motif KKTK in the *shaft* of the fiber with the abrogation of liver transduction in several species (Smith *et al.*, 2003a; Smith *et al.*, 2003b; Nicol *et al.*, 2004). However, the insertion of tumor targeting peptides in the HI-loop of these *shaft*-modified fibers does not rescue viral infection of tumor cells (Bayo-Puxan *et al.*, 2006; Kritz *et al.*, 2007; Rittner *et al.*, 2007). Our group previously described that the replacement of the KKTK domain with an RGD motif improved the tumor-to-liver ratio *in vivo* in the context of a non-replicative adenovirus (Bayo-Puxan *et al.*, 2009) and increased bioavailability and antitumor efficacy in an oncolytic adenovirus background (Rojas *et al.*, 2011). On the other hand, our group also reported the expression of hyaluronidase by oncolytic adenoviruses as a mechanism to improve intratumoral spread across the ECM (Guedan *et al.*, 2010).

In this work, we present the combination of the RGDK retargeting modification of the fiber and the expression of PH20 hyaluronidase in a novel oncolytic adenovirus, named ICOVIR-17K. These modifications were incorporated in the genome of ICOVIR-15, an oncolytic adenovirus developed in our laboratory which we currently use as a platform for the insertion of transgenes and other modifications (Rojas *et al.*, 2010). ICOVIR-15 has a compact genome which contains three genetic mutations compared to the wild type adenovirus type 5 (Adwt or Ad5). First, it has a deletion of the CR2 domain of E1A (Δ24 deletion) that eliminates pRB binding and hence E1A capability to release E2F from the E2F-pRB complex present in non-cycling normal cells. Second, it contains eight E2F-1-binding sites and one Sp1-binding site inserted in the E1A promoter, thus rendering E1A transcription dependent on RB-pathway deregulation. These two modifications confer selective replication in tumor cells. The third modification is the insertion of the integrin-binding RGD motif at the HI-loop of the fiber *knob* to enhance its infectivity. A schematic representation of the genomes of the adenoviruses used in this study and the RGDK mutation are shown in **Figure 13a** and **Figure 13b**, respectively.

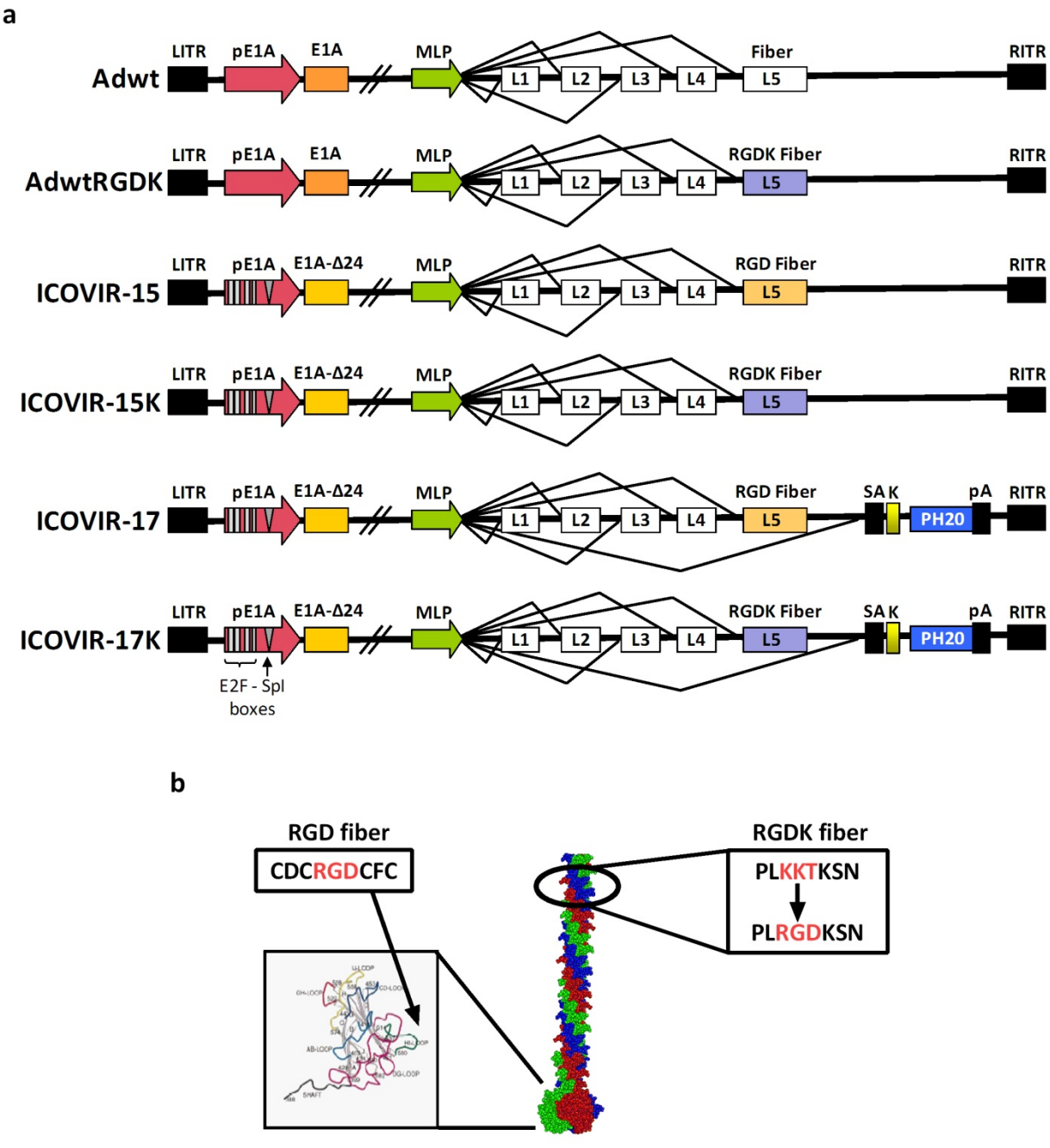

Figure 13. Adenoviruses used in this study. **(**a) Schematic representation of the genomes of the different viruses used. Main genetic modifications of each virus are highlighted. Adwt is the human Ad5 wild type virus; Adwt-RGDK is the wild type virus with the same genetic modification of the capsid described for ICOVIR-17K, the RGDK modification. ICOVIR-15, ICOVIR-15K, ICOVIR-17, and ICOVIR-17K are oncolytic adenoviruses which contain the modified E1a promoter (including four E2F boxes and one Sp1 box) and the truncated E1A protein to confer selectivity for tumor cells. ICOVIR-17 and ICOVIR-17K contain the PH20 hyaluronidase expression cassette, whereas ICOVIR-15K has the same modification in the fiber shaft of the capsid than ICOVIR-17K. ICOVIR-15 and ICOVIR-17, however, differ on the position of the RGD insertion in the fiber protein, which is in the HI-loop of the knob instead of replacing the KKTK domain in the shaft. (b) Schematic representation of fiber mutations RGD and RGDK. RGD fiber, contained in ICOVIR-15 and ICOVIR-17, incorporates the motif CDCRGDCFC (RGD-4C) in the HI-loop of the *knob* domain of the fiber. In the viruses containing the RGDK fiber, namely AdwtRGDK, ICOVIR-15K, and ICOVIR-17K, this insertion is deleted and the RGD is incorporated replacing the KKTK of the *shaft* of the fiber.

The plasmid containing ICOVIR-17K genome was constructed by homologous recombination in yeast and it was transfected into HEK293 cells to generate the virus. Then, viral DNA was extracted and the whole genome was sequenced to confirm that the sequence was the expected one. **Table 8** shows a description of the specific locations and sequences of ICOVIR-17K relevant genetic modifications.

Mutation	Sequence	Positions
E2F boxes	TTTCGCGGCAAA	439-450; 456-468; 501-512; 518-530
Sp1 box	CCGCCC	560-565
D24 deletion	CTTACCTGCCACGAGGCTGGCTTT	1097
RGDK mutation	CGA GGA GAC	31457-31465
IIIa splicing acceptor	GTACTAAGCGGTGATGTTTCTGATCAG	32975-33001
Kozak sequence	CCACC	33002-33006
Human hyaluronidase	PH20 ORF	33007-34479
Poly-A sequence	TAAACTTTATTTTTCAATTG	34480-34499

Table 8. Genetic modifications of ICOVIR-17K compared to Adenovirus Reference Material Ad5 (GenBank: AY339865.1).

Hyaluronidase expression was demonstrated by the digestion of hyaluronic acid (HA) solutions with supernatants of cells infected with ICOVIR-17K and the control viruses: ICOVIR-15K (negative control) or ICOVIR-17 (positive control). Digested samples were analyzed by two different techniques: the analysis of generated micro-oligosaccharides by electrophoresis in acrylamide gel (**Figure 14a**) and a turbidimetric enzymatic assay which consisted of the precipitation of digestion products with an acid buffer and subsequent OD measurement (**Figure 14b**). As expected, both techniques detected presence of hyaluronidase at similar levels in supernatants of cells infected with ICOVIR-17 or ICOVIR-17K, whereas ICOVIR-15K supernatants were negative for hyaluronidase activity.

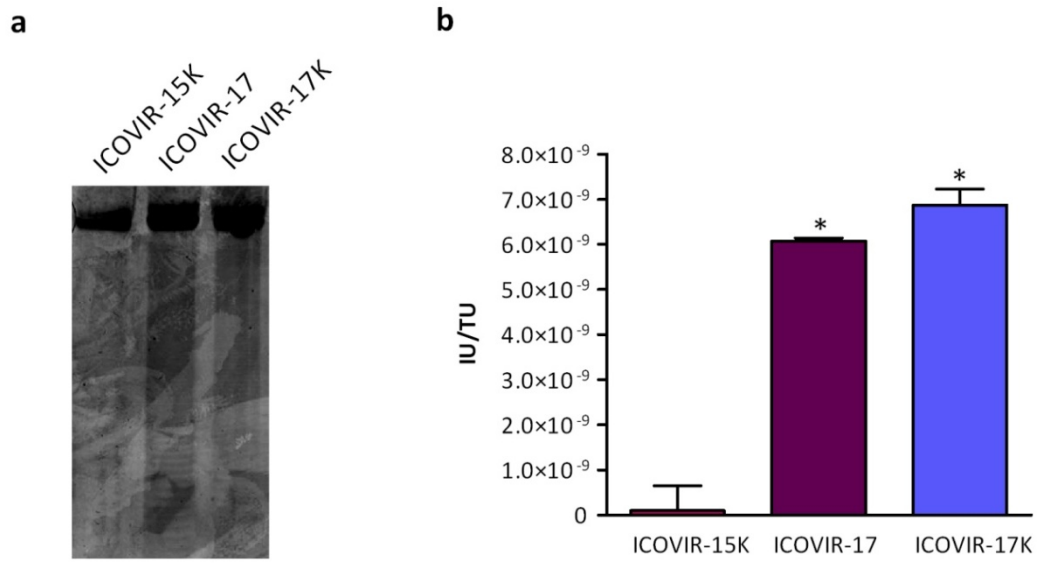

Figure 14. Analysis of hyaluronidase expression by ICOVIR-17K. A549 cells were infected with the corresponding viruses and 72 hours later supernatants were collected, concentrated and incubated with a HA solution. (a) The digested samples were analyzed by polyacrylamide gel electrophoresis and the presence of hyaluronidase was evidenced by a dark smear below high molecular weight band corresponding to HA degradation products. (b) OD_{600} was also measured for the digested samples. Absorbance negatively correlates with hyaluronic acid degradation, which reflects hyaluronidase activity of analyzed samples, and concentration was calculated thanks to a standard curve made with known concentrations of soluble hyaluronidase. Mean +SD is plotted. Significance was assessed by a two-tailed Student's unpaired t-test. *, $p<0.05$ compared to ICOVIR-15K. SN, supernatant; HA, hyaluronic acid or hyaluronan; IU, International Units of enzyme; TU, transducing units.

In addition, a genomic stability assay of ICOVIR-17K was performed by doing several passages of the virus in non-permissive human fibroblast cultures. The selective pressure to which the virus is subjected in the experimental conditions may cause modifications or rearrangements in the engineered virus genome. Therefore, the integrity of ICOVIR-17K was assessed by checking the restriction pattern after digestion of the viral genome at each passage with different restriction enzymes. Digestion with *HindIII* permits the detection of PH20 loss, in which case, a 904 bp band would disappear. On the other hand, *SacII* restriction allows the assessment of RGDK fiber loss by the appearance of two bands of 5800 bp and 1900 bp instead of one band of 8014 bp. Digestion of the viral DNA obtained from four different passages with both restriction enzymes showed the expected patterns (**Figure 15a**). Moreover, the cytotoxicity of the virus after every passage was analyzed without detecting significant differences in the IC_{50} value (**Figure 15b**).

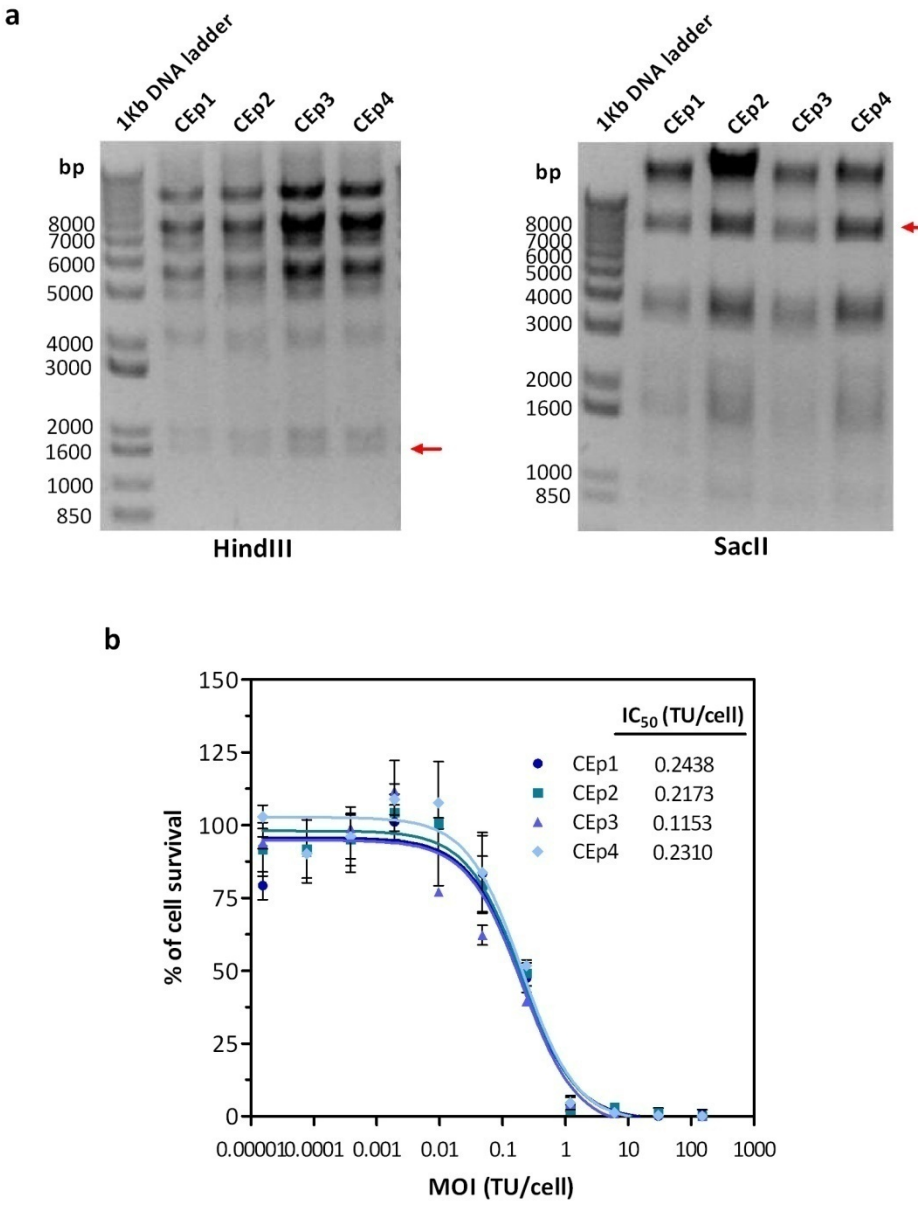

Figure 15. Genetic stability of ICOVIR-17K. (a) Restriction pattern of viral genome DNA with *HindIII* and *SacII* restriction enzymes. Viral DNA was extracted from cell extracts of ICOVIR-17K (CEp1, CEp2, CEp3, and CEp4) generated by successive passages in overconfluent arrested human fibroblasts. Digestion products (CEp1-CEp4) and a DNA marker (1 Kb DNA Ladder) were run in a 1% agarose gel. Relevant bands confirming the presence of the genetic modifications in ICOVIR-17K genome are marked with red arrows in the gels: namely, the 904 bp band in *HindIII* corresponding to PH20 hyaluronidase and the 8014 bp band in *SacII* corresponding to the RGDK fiber. (b) A549 cells were infected with serial dilutions of CEp1-CEp4 and on day 5 post-infection, cell viability was determined and IC_{50} values were calculated. Mean ±SD is plotted. Significance was assessed by extra sum-of-squares F test. CE, cell extract; p, passage; MOI, multiplicity of infection; TU, transducing units.

Once the virus was well-characterized, amplified and purified, we proceeded to evaluate toxicity, selectivity and oncolytic potency of ICOVIR-17K in different *in vitro* and *in vivo* models, in order to assess the gain provided by the combination of the modifications contained in the genome of this oncolytic adenovirus.

1.2. TOXICITY OF ICOVIR-17K

Regarding the safety in a clinical application, we evaluated the selectivity and toxicity of the oncolytic adenovirus ICOVIR-17K in different models, *in vitro* and *in vivo*.

1.2.1. Replication selectivity in pancreatic islets *in vitro*

In order to evaluate the selectivity of ICOVIR-17K for tumor cells *in vitro*, a replication experiment was performed in healthy human pancreatic islets. This model was chosen given the proximity of these cells to tumor cells in pancreatic cancer patients, since they would be potential candidates for treatment in a clinical setting. In addition, this model mimics quiescent cells in most organs *in vivo*. Pancreatic islets were infected at a multiplicity of infection (MOI) of 200 with the non-replicative virus AdTLRGDK, the wild type Ad5 AdwtRGDK, the oncolytic adenovirus ICOVIR-15, or with ICOVIR-17K. The proper infection of the islets was confirmed by GFP expression on day 3 post-infection in the samples infected with the GFP-expressing adenoviral vector AdTLRGDK, as it is shown in **Figure 16a**. Viral production yields of the cell extracts were determined on day 6 post-infection. The same background virus progeny level was detected in the samples infected with the oncolytic adenoviruses ICOVIR-15 and ICOVIR-17K than with the non-replicative negative control (AdTLRGDK), whereas wild type adenovirus (AdwtRGDK) replicated in normal human pancreatic islets (**Figure 16b**).

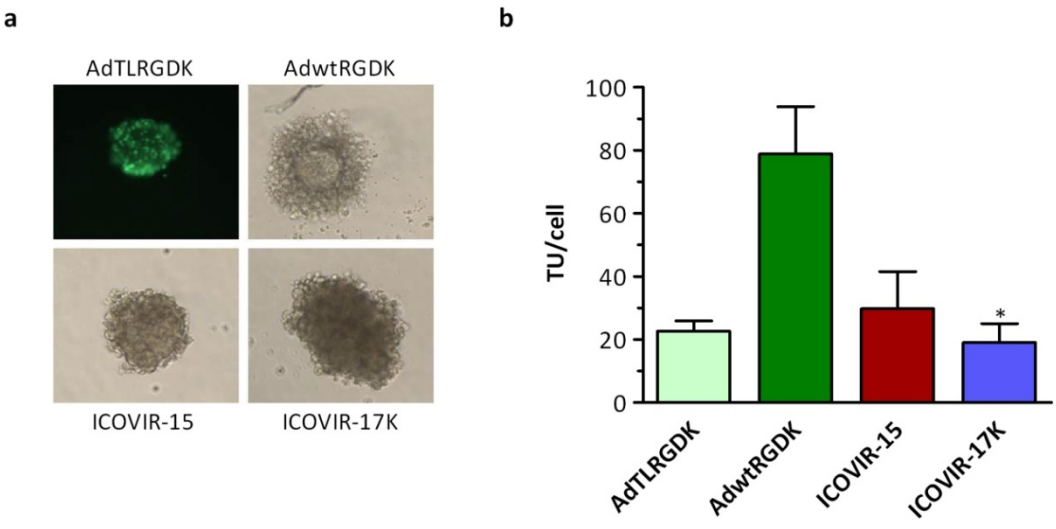

Figure 16. Selectivity *in vitro* in human pancreatic islets. Human primary pancreatic islets were infected with AdTLRGDK (non-replicative GFP-expressing adenoviral vector), AdwtRGDK (wild type non-tumor selective adenovirus), ICOVIR-15, or ICOVIR-17K (tumor selective replicating adenoviruses) at 200 MOI. (a) Different panels show pictures of islets infected with the different viruses on day 3. The first panel shows GFP expression by islet cells infected with AdTLRGDK. Original magnification 200X. (b) Total viral production from samples collected on day 6 post-infection measured by an anti-hexon staining-based method using HEK293 cells. Mean +SD is plotted. Significance was assessed by a two-tailed Student's unpaired t-test. *, $p<0.05$ compared to AdwtRGDK. TU, transducing units.

1.2.2. Toxicity profile in mice

In vivo toxicity after intravenous administration of ICOVIR-17K was first assessed in mice. This route of administration was chosen since it is the one that provides major exposure of the virus to the organism, and consequently the highest possible toxicity associated.

Balb/C immunocompetent mice were injected with PBS or $5x10^{10}$ viral particles of ICOVIR-17 (selected for comparative studies as it is the most efficacious parental virus) or ICOVIR-17K via tail vein. Weight loss, liver enzymes (aspartate aminotransferase, AST, and alanine aminotransferase, ALT), hematological parameters and platelet counts were determined at different time points after virus injection. Wild type adenovirus 5 (Adwt) was included in this study as a control, but given the high toxicity associated to its administration, the animals were sacrificed at day 3.

Body weight of the animals was monitored after systemic administration of the viruses. By day 3 post-injection, Adwt-injected animals already presented a body weight reduction of 9%, whereas in animals injected with ICOVIR-17K this reduction was significantly lower at this time point. The maximum percentage of body weight loss after the administration of oncolytic adenoviruses was observed at day 7 and corresponded to a percentage of 9%. In contrast to Adwt treatment, this loss was reversible and the animals started to recover from this day until the end of the experiment (**Figure 17a)**.

It has been widely described that systemic administration of adenovirus causes an elevation in blood transaminase levels (Aghi and Martuza, 2005). For this reason, we analyzed AST and ALT concentration in serum samples of mice at different time points. At day 7 post-administration moderate non-significant increases in both, AST (2.9-fold for ICOVIR-17 and 2.4-fold for ICOVIR-17K) and ALT levels (12-fold for ICOVIR-17 and 9-fold for ICOVIR-17K) were detected, but at later time points this parameter was normal for all groups (**Figure 17b**).

Clinical trials in humans also revealed hematological alterations after systemic treatment such as a decrease in platelet concentration or lymphocytes counts (Nemunaitis *et al.*, 2001a). Thrombocytopenia was observed until day 7 post-administration, when animals started to recover (**Figure 18a**). Moreover, non-significant increases in monocytes and neutrophils counts were detected at this time point (**Figure 18b**).

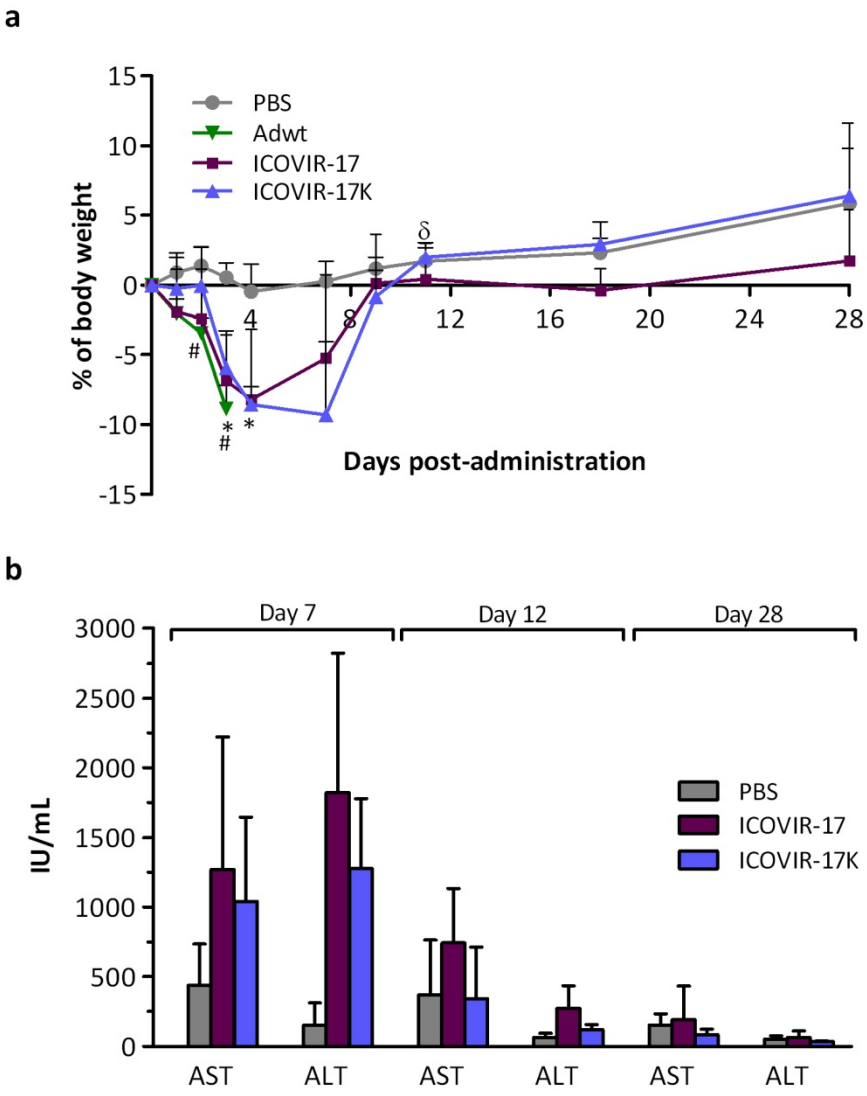

Figure 17. Toxicity after systemic administration of ICOVIR-17K in immunocompetent mice. The average values for (a) body weight variation and (b) serum transaminase levels in Balb/C peripheral blood at indicated time points after intravenous administration of PBS or $5x10^{10}$ viral particles per mouse of Adwt (wild-type Ad5), ICOVIR-17 or ICOVIR-17K are shown. Adwt-injected mice were sacrificed at day 3 due to lethal toxicity. Mean values +SD are depicted. *, ICOVIR-17K significant ($p<0.05$) by two-tailed unpaired Student's t-test, compared to PBS group. #, ICOVIR-17K significant ($p<0.05$) compared to Adwt. δ, ICOVIR-17K significant ($p<0.05$) compared to ICOVIR-17 group. ALT, alanine aminotransferase; AST, aspartate aminotransferase; IU, International units; PBS, phosphate-buffered saline.

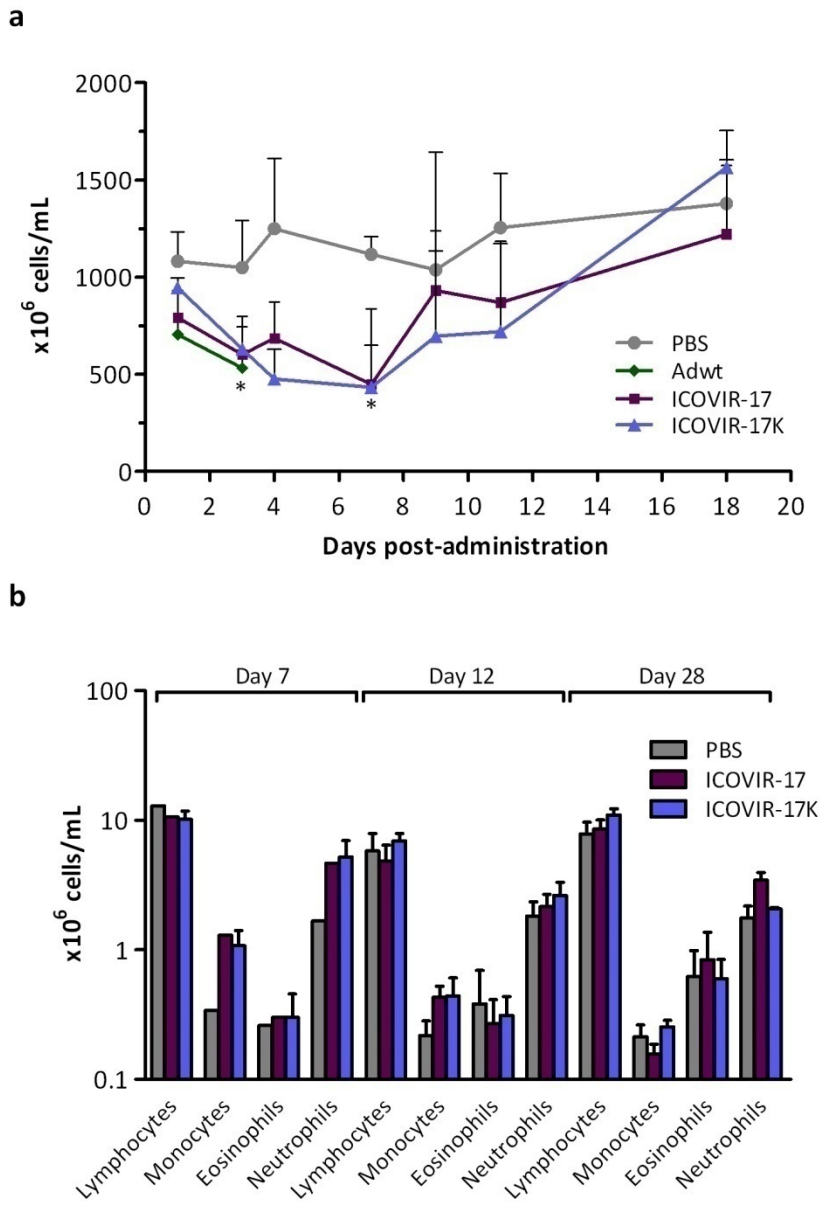

Figure 18. Hematological profile after systemic administration of ICOVIR-17K in immunocompetent mice. The average values for (a) platelets concentration and (b) blood cell counts in Balb/C peripheral blood at indicated time points after intravenous administration of PBS or $5x10^{10}$ viral particles per mouse of Adwt (wild-type Ad5), ICOVIR-17 or ICOVIR-17K are shown. Adwt-injected mice were sacrificed at day 3 due to lethal toxicity. Mean values +SD are depicted. *, ICOVIR-17K significant ($p<0.05$) by two-tailed unpaired Student's t-test, compared to PBS group. PBS, phosphate-buffered saline.

Remarkably, at the later time points analyzed all the parameters were normal. Moreover, no significant differences were detected between ICOVIR-17 and ICOVIR-17K groups at any time point, indicating that the RGDK modification does not provide an additional toxicity even though it was described to increase persistence in blood. At the same time, the fact that this mutation is supposed to decrease liver transduction does not reduce hepatic toxicity either.

1.2.3. Toxicity profile in Syrian hamsters

To further characterize the toxicity of ICOVIR-17K after intravenous administration, an additional study was performed in Syrian hamsters (*Mesocricetus auratus*). This species is considered more permissive to human adenovirus replication than mice, and consequently it allows the evaluation of the effects of viral replication in normal tissues (Thomas *et al.*, 2006). Hamsters were injected with PBS or $4x10^{11}$ viral particles of ICOVIR-17K in a single administration via cephalic vein. Since no differences were observed between ICOVIR-17 and ICOVIR-17K in mice, no further comparison with ICOVIR-17 was considered in order to reduce animal number according to ethical criteria. Body weight loss was monitored daily and, at different time points after the administration, subgroups of animals were sacrificed and hematology and clinical chemistry of the blood were studied.

Significant body weight loss was observed from day 1 to day 5 post-administration, reaching the maximum percentage at day 3 (6.5%). Animals started to gain weight from this day until the end of the experiment, when no significant differences were detected between treated and non-treated groups (**Figure 19a**).

As happened in mice, the most notable alterations observed on day 7 post-administration were a moderate elevation of transaminase levels (3.4-fold for AST and 7.8-fold for ALT) (**Figure 19b**) and thrombocytopenia (1.7-fold reduction in platelet concentration) (**Figure 20a**). With regard to the rest of hematological parameters only a slight increase in lymphocytes concentration was observed at this time point (**Figure 20b**). On day 34 post-administration all the parameters were normalized and no significant differences were observed between groups, indicating a reversible toxicity profile similar to the one observed in mice.

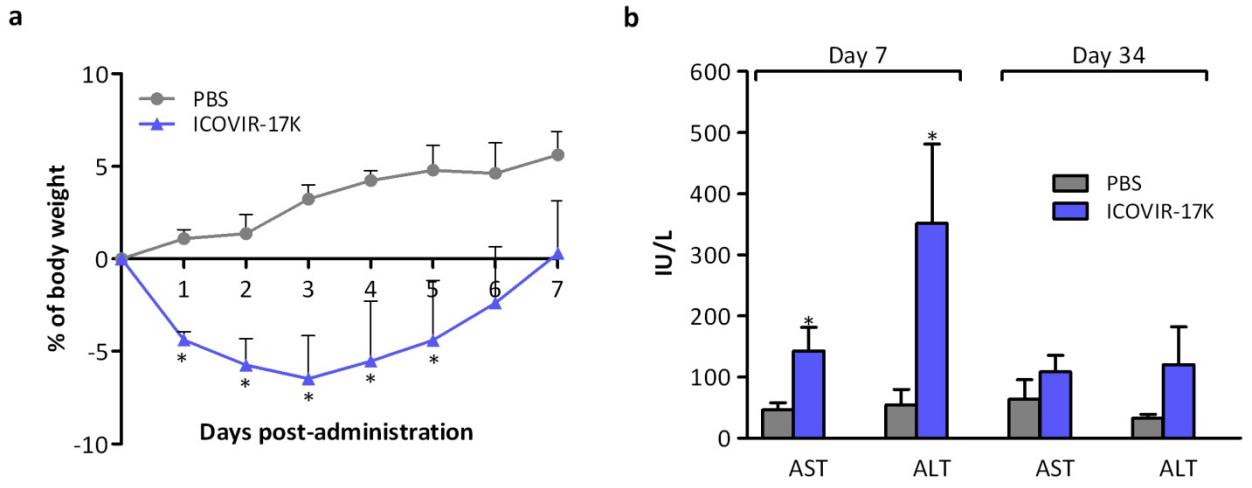

Figure 19. Toxicity after systemic administration of ICOVIR-17K in Syrian hamster. The average values for (a) body weight variation and (b) serum transaminase levels in hamsters peripheral blood at indicated time points after intravenous administration of PBS or $4x10^{11}$ viral particles per animal of ICOVIR-17K are shown. Mean values +SD are depicted. *, ICOVIR-17K significant ($p<0.05$) by two-tailed unpaired Student's t-test, compared to PBS group. ALT, alanine aminotransferase; AST, aspartate aminotransferase; IU, International units; PBS, phosphate-buffered saline.

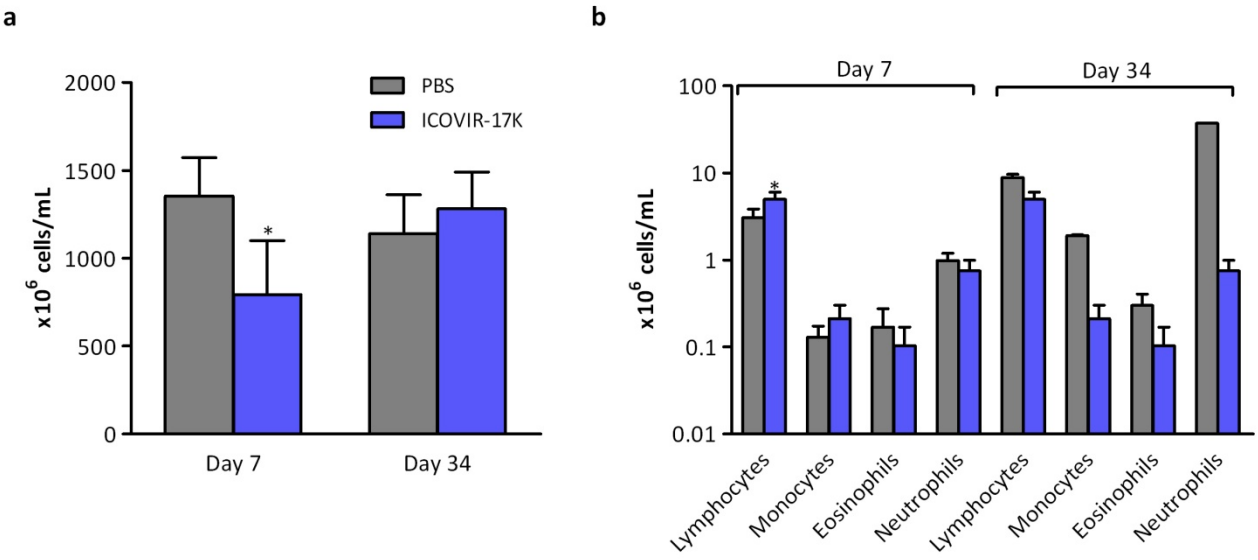

Figure 20. Hematological profile after systemic administration of ICOVIR-17K in Syrian hamster. The average values for (a) platelets concentration and (b) blood cell counts in hamsters peripheral blood at indicated time points after intravenous administration of PBS or $4x10^{11}$ viral particles per animal ICOVIR-17K are shown. Mean values +SD are depicted. *, ICOVIR-17K significant ($p<0.05$) by two-tailed unpaired Student's t-test, compared to PBS group; PBS, phosphate-buffered saline.

1.3. ONCOLYTIC POTENCY OF ICOVIR-17K

Once it was demonstrated that the RGDK modification does not provide additional toxicity compared to a virus containing the RGD motif in the HI-loop of the fiber, ICOVIR-17, and that the toxicity profile was the typical one associated to the systemic administration of oncolytic adenoviruses, we proceeded to characterizing the oncolytic potency. In this regard, our group previously described that in the context of the oncolytic adenovirus ICOVIR-15K, this mutation increased antitumor efficacy *in vivo* (Rojas *et al.*, 2011). To evaluate oncolytic potency of ICOVIR-17K, several models have been used *in vitro* and *in vivo*.

1.3.1. Viral production in tumor cell lines

For the different *in vitro* assays, ICOVIR-15K (that has the KKTK to RGDK fiber *shaft* replacement), ICOVIR-17 (that expresses hyaluronidase) or the wild-type AdwtRDGK were used as control (Guedan *et al.*, 2010; Rojas *et al.*, 2011). To measure the possible effect of the combination of RGDK and hyaluronidase on viral production yield, the producer cell line A549 was infected with the different viruses and total production (Cell Extract, CE) and released virus (supernatant, SN) were quantified at different time points post-infection (0, 24, 48 and 72 hours) in a single-round replication experiment. As shown in **Figure 21**, although AdwtRGDK was released earlier than the three oncolytic adenoviruses, all the viruses were produced at similar levels at 72 hours post-infection.

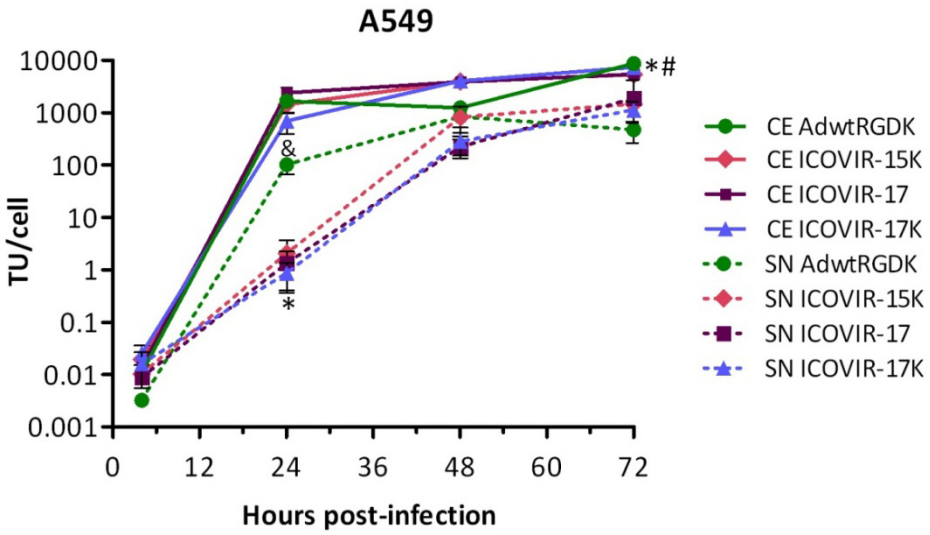

Figure 21. Viral productivity in the producer A549 (human lung adenocarcinoma) cell line. Monolayers of cells were infected at 25 TU/cell, allowing 100% of infection. At indicated time points (4, 24, 48, and 72 hours post-infection) CE and SN samples were collected and virus production was determined according to an anti-hexon staining-based method. Mean +SD is represented. *, ICOVIR-17K significant ($p<0.05$) by two-tailed unpaired Student's t-test, compared to AdwtRGDK group. #, ICOVIR-17K significant ($p<0.05$) by two-tailed unpaired Student's t-test, compared to ICOVIR-15K. &, ICOVIR-17K significant ($p<0.05$) by two-tailed unpaired Student's t-test, compared to ICOVIR-17 group. TU, transducing units; CE, cell extract; SN, supernatant.

To further characterize viral fitness of ICOVIR-17K, total production yield was also analyzed in a panel of four tumor cell lines, including melanoma and pancreatic adenocarcinoma (from human and hamster origins) tumor types. Despite a minor delay on replication in two of the cell lines at 24 hours post-infection, at later time points (48 and 72 hours), ICOVIR-17K production was similar to control viruses (**Figure 22**, **different panels)**.

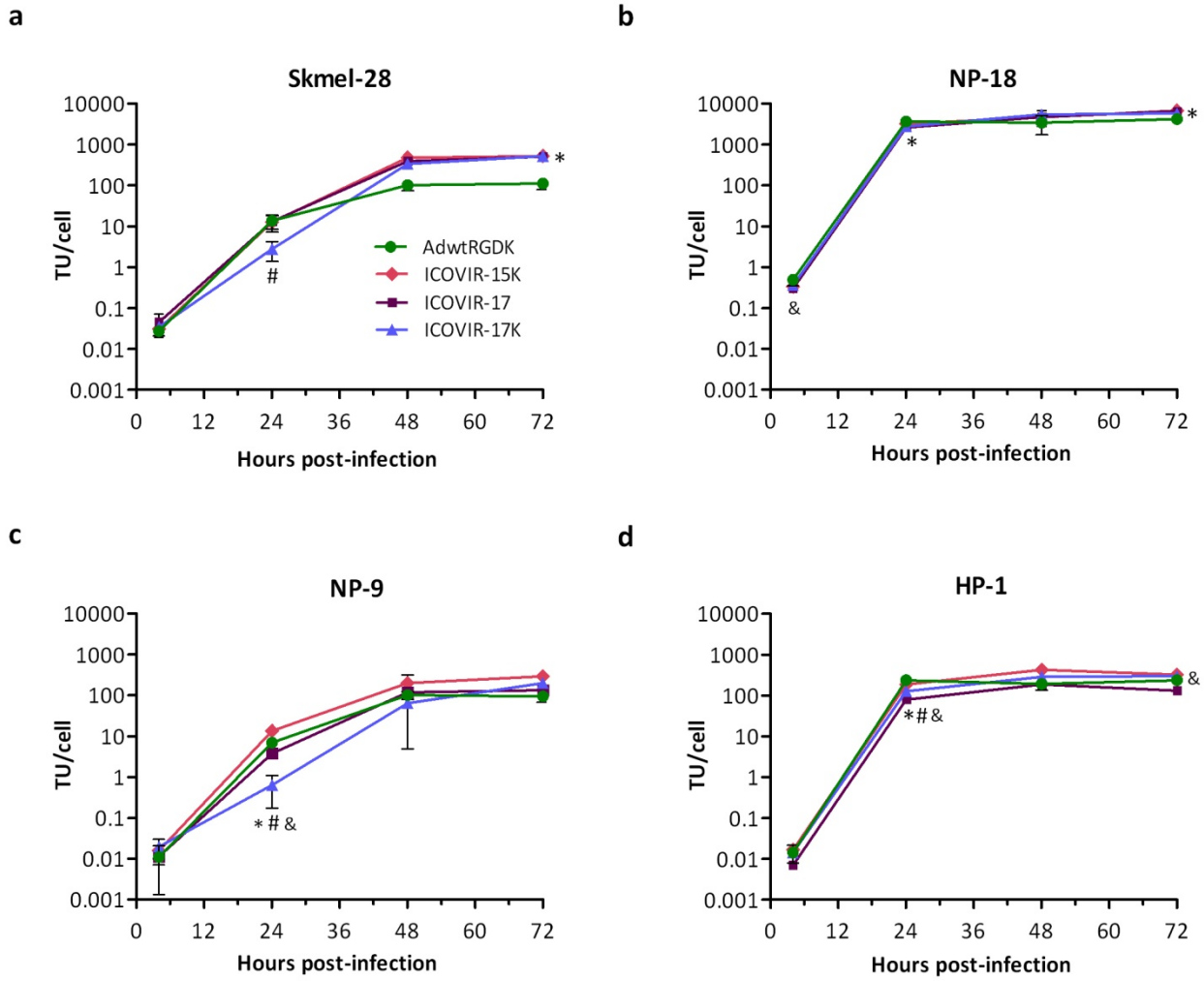

Figure 22. Viral production of ICOVIR-17K in tumor cells. (a) Skmel-28, (b) NP-18, (c) NP-9, or (d) HP-1 cell lines were infected at a high MOI allowing 100% of infection with ICOVIR-15K, ICOVIR-17 or ICOVIR-17K. At indicated time points, cell extracts were harvested and titrated by an anti-hexon staining-based method. Mean values ±SD are shown. *, ICOVIR-17K significant ($p<0.05$) compared to AdwtRGDK group ; #, ICOVIR-17K significant ($p<0.05$) compared to ICOVIR-15K group; &, ICOVIR-17K significant ($p<0.05$) compared to ICOVIR-17 group by two-tailed unpaired Student's t-test.

1.3.2. Plaque size assay

A plaque assay was used to evaluate the impact of the mutations on virus propagation, since it allows the measurement of the ability of a single infectious virus to form a plaque on a confluent monolayer culture of cells in multiple rounds of replication. Monolayers of A549 cells were

infected with the different viruses and 6 days later plaques were stained with MTT and their sizes were compared. As **Figure 23** shows, there were no differences between ICOVIR-17K and control parental viruses.

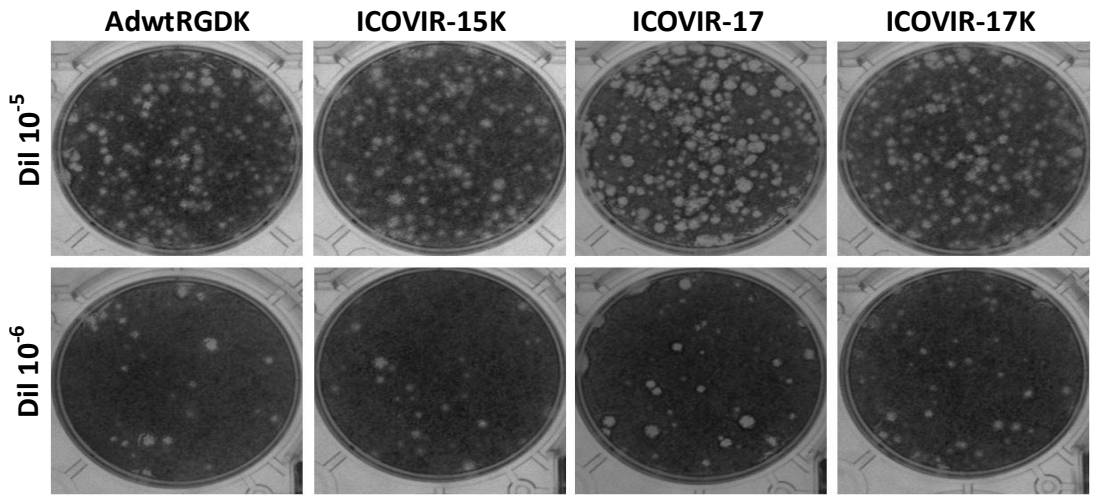

Figure 23. Comparative plaque sizes of AdwtRGDK, ICOVIR-15K, ICOVIR-17 and ICOVIR-17K in A549 infected cells. A549 monolayers were infected with 1/10 dilutions of the different viruses and covered with an agarose overlay in order to avoid the propagation of virus progeny through the monolayer and obtain isolated plaques. 6 days post-infection, plaques associated to clonal virus replication were stained with MTT. Dil, dilution; CE: cell extract.

1.3.3. Cytotoxicity in tumor cell lines

In vitro cytotoxicity was evaluated in a panel of 14 tumor cell lines as an index of virus replication potency and the ability of these viruses to propagate within multiple rounds of replication. Cells were infected with a broad range of MOIs and 5-8 days later percentage of cell viability was determined. Calculated IC_{50} values were highly variable depending on the cell line tested and different cytotoxic profiles could be distinguished. Tested adenoviruses presented a similar cytotoxic profile in 4 out of the 14 cell lines (NP-18, Rwp-1, NP-31, and HP-1). In another 4 cell lines (NP-9, BxPC-3, SCC-25, and SCC-29), AdwtRGDK was significantly more cytotoxic than the 3 oncolytic adenoviruses, whereas in another 2 (Skmel-28, and MiaPaCa-2) the wild-type virus was worse than the tumor-selective viruses. In one cell line (Panc-1), ICOVIR-17 was clearly more cytotoxic than the 3 adenoviruses containing the RGDK modification in the capsid. Finally, in 2 cell lines (A549 and FaDu), ICOVIR-17K and ICOVIR-15K presented the same cytotoxic profile, whereas AdwtRGDK and ICOVIR-17 had significantly lower IC_{50} values. Overall, the *in vitro* potency of ICOVIR-17K was similar to that of the other oncolytic adenoviruses. Importantly, the relative IC_{50} values compared to ICOVIR-15K, which has exactly the same capsid than ICOVIR-17K, ranged from 0.8 to 3.24-fold, being equivalent to 1 in 11 out of 14 cell lines tested (**Figure 24a** and **b**).

a

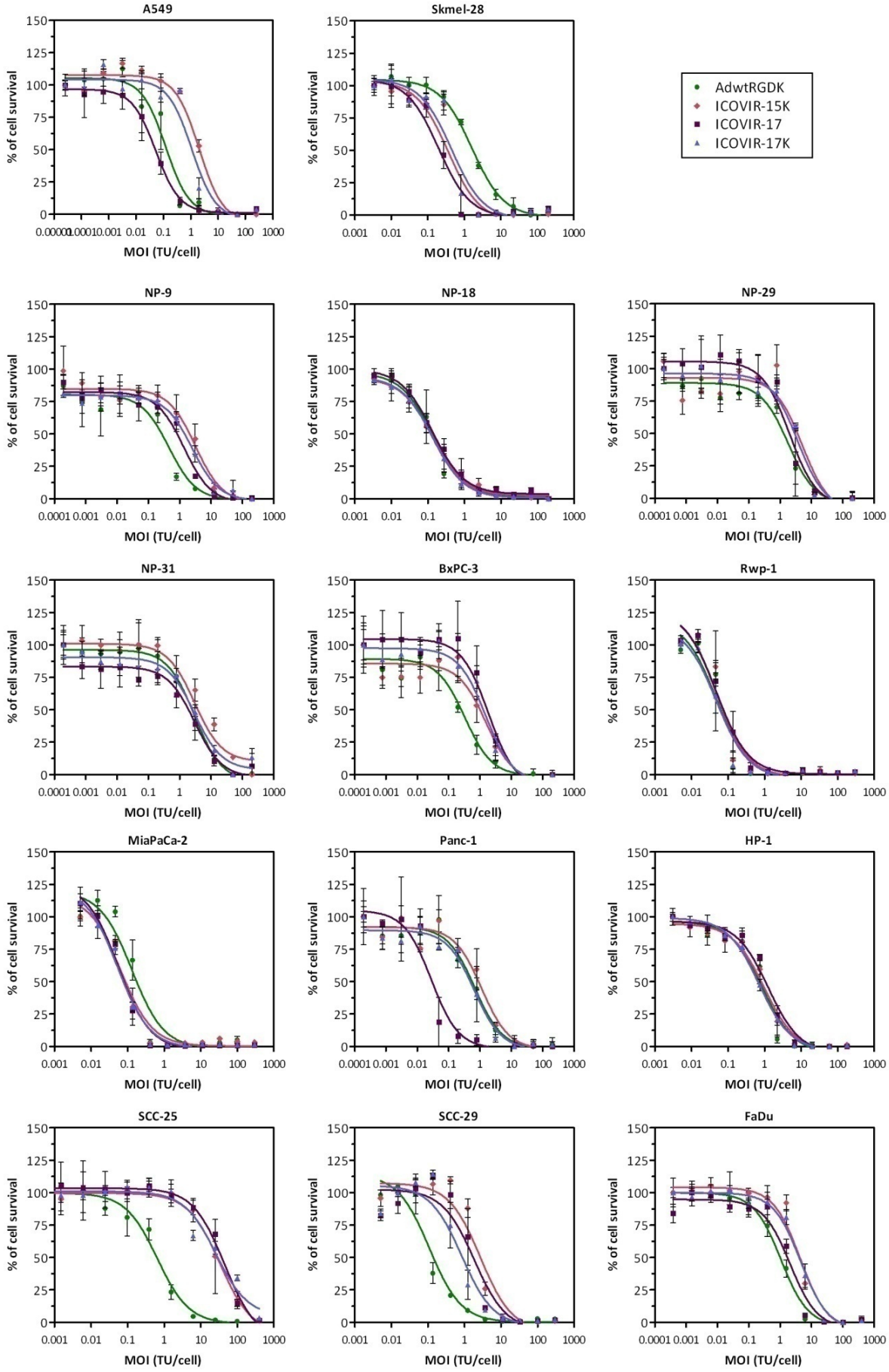
A549
Skmel-28
NP-9
NP-18
NP-29
NP-31
BxPC-3
Rwp-1
MiaPaCa-2
Panc-1
HP-1
SCC-25
SCC-29
FaDu
% of cell survival
MOI (TU/cell)
AdwtRGDK
ICOVIR-15K
ICOVIR-17
ICOVIR-17K

b

Tumor type	Cell line	IC_{50} (TU/cell)				Citotoxicity increase vs		
		AdwtRGDK	ICOVIR-15K	ICOVIR-17	ICOVIR-17K	AdwtRGDK	ICOVIR-15K	ICOVIR-17
Human lung adenocarcinoma	A549	0.1214	2.032	0.05307	1.103	0.11*	1.84*	0.05*
Human melanoma	Skmel-28	1.644	0.3622	0.1978	0.4519	3.64*	0.80	0.44*
Human pancreatic adenocarcinoma	NP-18	0.1197	0.136	0.1436	0.1435	0.83	0.95	1.00
	NP-9	0.4497	3.177	1.364	2.476	0.18*	1.28	0.55*
	NP-29	1.817	5.103	1.991	3.653	0.50*	1.40	0.55
	NP-31	2.508	5.903	2.165	3.084	0.81	1.91	0.70*
	BxPC-3	0.3267	1.541	1.870	1.501	0.22*	1.03	1.25
	Rwp-1	0.04836	0.05303	0.06003	0.03504	1.38	1.51	1.71
	MiaPaca-2	0.1316	0.06583	0.05571	0.05391	2.44*	1.22	1.03
	Panc-1	0.6797	1.115	0.02761	0.6435	1.06	1.73	0.04*
Hamster pancreatic adenocarcinoma	HP-1	0.8609	0.9875	1.260	0.7097	1.21	1.39*	1.78*
Human head and neck adenocarcinoma	SCC-29	0.1103	2.738	1.857	0.8444	0.13*	3.24*	2.20*
	SCC-25	0.6500	33.42	45.17	26.15	0.02*	1.28	1.73
	FaDu	1.056	4.433	2.079	4.480	0.24*	0.99	0.46*

Figure 24. Comparative cytotoxicity *in vitro* in a panel of tumor cell lines. Different cell lines were infected with serial dilutions of AdwtRGDK, ICOVIR-15K, ICOVIR-17, or ICOVIR-17K, and on day 5-8 post-infection, cell viability was determined by BCA staining. (a) Dose-response curves obtained by non-linear regression and (b) IC_{50} values for each virus are represented. Cytotoxicity increases versus parental viruses AdwtRGDK, ICOVIR-15K, and ICOVIR-17 are also represented. * Significant ($p<0.05$) by extra sum-of-squares F test. MOI, multiplicity of infection; TU, transducing units.

1.3.4. Amount of virus in blood after systemic administration

Previous work from our group demonstrated that ICOVIR-15K presents extended blood persistence after intravenous administration at early time points (Rojas *et al.*, 2011).

With the aim to assess if ICOVIR-17K maintains this property, nude mice were administered intravenously with PBS or $4.5x10^{10}$ viral particles of ICOVIR-17 or ICOVIR-17K and 6 hours later blood samples were collected and virus amount was quantified by the anti-hexon staining method. Accordingly to what was previously described, animals injected with ICOVIR-17K presented 2.5-fold increase in viral load compared to those treated with ICOVIR-17, although this difference was not statistically significant (**Figure 25**).

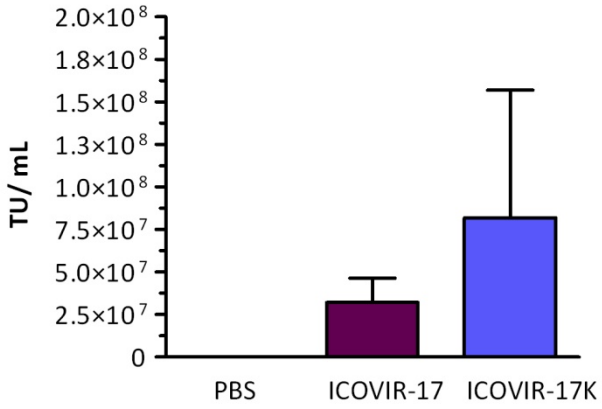

Figure 25. Viral load in blood after single intravenous administration. Nude mice carrying NP-18 human pancreatic cancer xenograft tumors were injected systemically with PBS or $4.5x10^{10}$ viral particles of ICOVIR-17 or ICOVIR-17K. Blood samples were collected by tail-vein sampling 6 hours post-administration and viral functional titer was quantified from sera according to an anti-hexon staining-based method in HEK293 cells. Significance was assessed by a two-tailed Student's unpaired t-test even though no statistically significant differences were detected. TU, transducing units; PBS, phosphate-buffered saline.

1.3.5. Antitumor activity *in vivo*

1.3.5.1. Antitumor efficacy in xenograft mice models

The antitumor efficacy of ICOVIR-17K was compared to that of its non RGDK-counterpart ICOVIR-17 after systemic administration in two different human xenograft tumor models in mice: Skmel-28 and NP-18. Subcutaneous tumors of these cell lines were implanted in nude mice and when they reached an appropriate tumor volume, mice were intravenously injected with PBS or $4.5x10^{10}$ viral particles of ICOVIR-17 or ICOVIR-17K.

In Skmel-28-bearing mice, significant antitumor efficacy was observed from day 25 post-administration and maintained throughout the study (for up to 83 days) in ICOVIR-17K-treated animals, whereas after a similar curve of initial antitumor activity, a relapse was observed by day 53 post-treatment in the ICOVIR-17 group. Statistical differences in the percentage of tumor growth between both groups were observed from day 53 post-treatment until the end of the study, when tumor size was 2.4-fold larger in the ICOVIR-17-treated animals than in the ICOVIR-17K-injected ones (**Figure 26a**). Moreover, 50% of ICOVIR-17K-treated tumors were regressing at this final time point. A similar result was observed in mice bearing NP-18 tumors, in which a greater control of the tumor growth was observed in the animals treated with ICOVIR-17K than with ICOVIR-17. These differences were significant from day 30 to day 49 post-administration, when the study ended (**Figure 26b**).

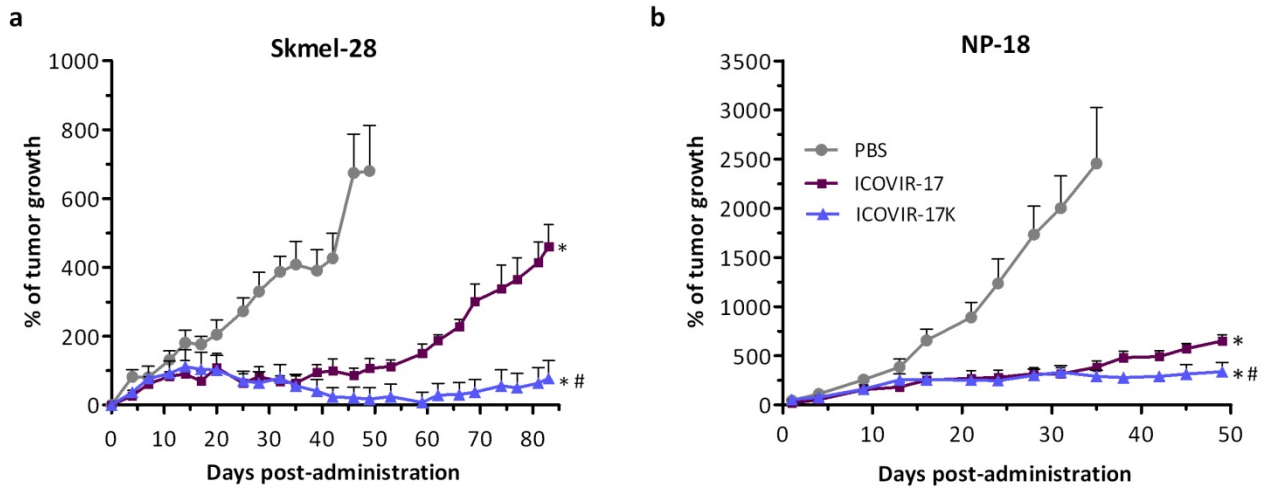

Figure 26. Antitumor activity upon systemic administration. Nude mice bearing subcutaneous xenografts of (a) Skmel-28 (melanoma) or (b) NP-18 (pancreatic carcinoma) tumors were injected intravenously with vehicle or $4.5x10^{10}$ viral particles per mouse of ICOVIR-17 or ICOVIR-17K. Mean percentage of tumor growth value +SEM is plotted (n=10 tumors/group). *, ICOVIR-17 and ICOVIR-17K significant $p<0.05$ by two-tailed unpaired Student's *t*-test compared with mice injected with PBS (from day 25 in Skmel-28 model and from day 16 in NP-18 model). #, ICOVIR-17K significant $p<0.05$ by two-tailed unpaired Student's *t*-test compared with mice injected with ICOVIR-17 (from day 53 to day 83 in Skmel-28 model and from day 30 to day 49 in NP-18 model). PBS, phosphate-buffered saline.

Besides controlling tumor growth, treatment with ICOVIR-17K was also able to increase mice survival in both tumor models, Skmel-28 and NP-18. Intravenous administration of ICOVIR-17 significantly improved survival of PBS-treated animals from 40 to 75 days in Skmel-28 model. Importantly, the mean survival of ICOVIR-17K-treated animals reached 82.1 days, being this difference statistically significant compared to ICOVIR-17-injected mice (**Figure 27a**). Regarding NP-18 model, ICOVIR-17 doubled survival time of control animals (from 18.6 days to 36.8). ICOVIR-17K increased this time to 48.8 days, even though this was not statistically different to ICOVIR-17 group (**Figure 27b**).

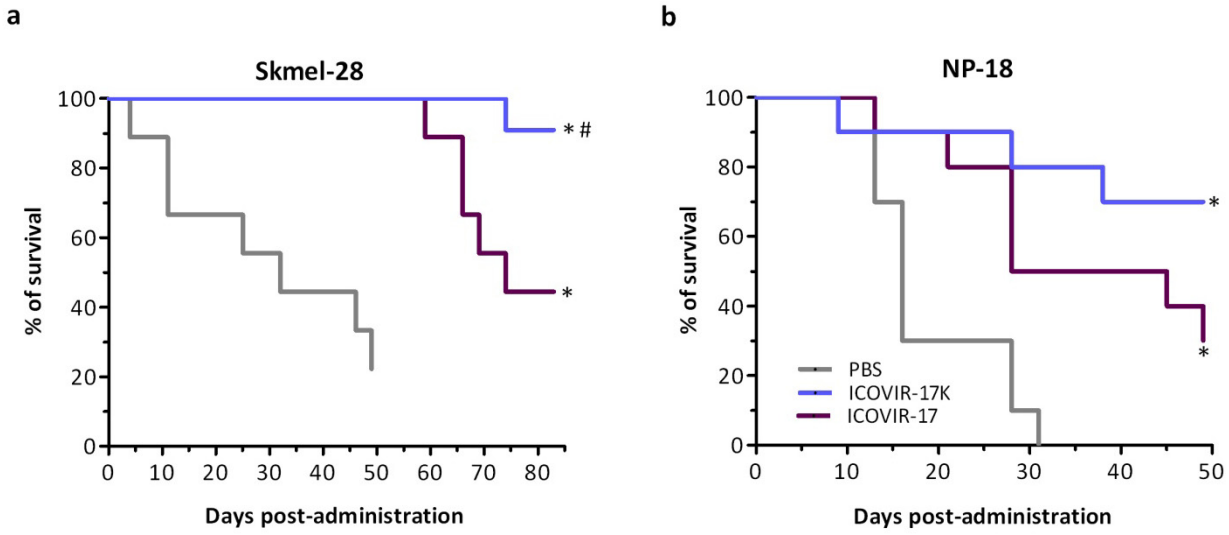

Figure 27. Kaplan-Meier survival curves upon systemic administration. Nude mice bearing subcutaneous xenografts of (a) Skmel-28 (melanoma) or (b) NP-18 (pancreatic carcinoma) tumors were injected intravenously with vehicle or $4.5x10^{10}$ viral particles per mouse of ICOVIR-17 or ICOVIR-17K. Kaplan-Meier curves are plotted. End-point was established at 500 mm^3 of tumor volume for Skmel-28 model and at 1000 mm^3 for NP-18 model. * significant ($p<0.05$) by log-rank test compared with PBS group; #, significant ($p<0.05$) by log-rank test compared with ICOVIR-17 group. PBS, phosphate-buffered saline.

Our group and others have previously reported that the intratumoral administration of hyaluronidase enhances the efficacy of oncolytic adenoviruses *in vivo* (Ganesh *et al.*, 2008; Guedan *et al.*). We wanted to test if the expression of hyaluronidase by the virus itself was better than the coadministration of both, virus and soluble hyaluronidase.

With this aim, mice bearing 150 mm^3 Skmel-28 tumors were treated with a single intravenous injection of PBS or $4.5x10^{10}$ viral particles of ICOVIR-17K or ICOVIR-15K, the last one in combination with an intratumoral injection of 100 IU per tumor of testicular bovine hyaluronidase. Although both treatments could significantly control tumor growth compared to PBS from day 12 until the end of the study, ICOVIR-17K administration induced a greater reduction of tumor growth than the combination of ICOVIR-15K and hyaluronidase. This

difference was significant from day 15 to the end of the study on day 50 post-injection (**Figure 28a**).

However, when the same experiment was performed administering the virus in one single intratumoral injection of $2x10^9$ viral particles per tumor, the efficacy advantage of ICOVIR-17K was lost (**Figure 28b**). We hypothesize that intravenous administration of oncolytic adenoviruses allows a better and more disseminated intratumoral distribution pattern of the virus, permitting hyaluronidase expression occur within all tumor mass. In contrast, when the virus is injected intratumorally in one single point, the expression of hyaluronidase is restricted and its effect is localized, as well as with the soluble hyaluronidase injection.

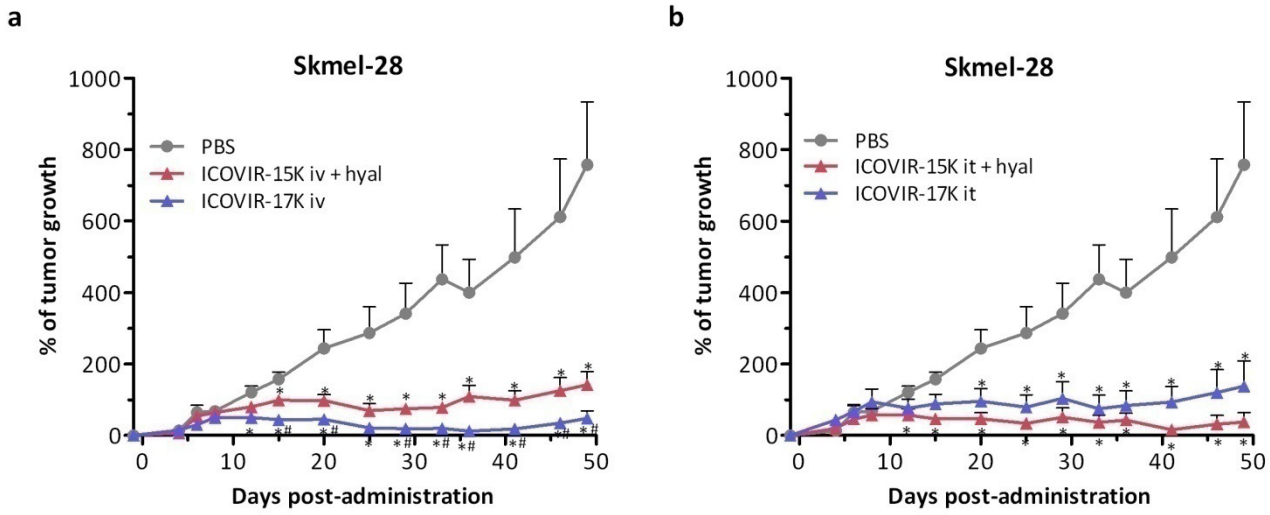

Figure 28. Comparative antitumor activity of ICOVIR-17K and the combination of ICOVIR-15K and soluble hyaluronidase. (a) Nude mice carrying Skmel-28 subcutaneous xenograft tumors were injected intravenously with PBS or $4.5x10^{10}$ viral particles of ICOVIR-17K or ICOVIR-15K in combination with a single intratumoral injection of 100 IU of soluble hyaluronidase. (b) Nude mice carrying Skmel-28 subcutaneous xenograft tumors were injected with a single intratumoral administration of PBS or $2x10^9$ viral particles of ICOVIR-17K or ICOVIR-15K in combination with a single intratumoral injection of 100 IU of soluble hyaluronidase. Mean percentage of tumor growth value +SEM is plotted (n=7-13 tumors/group). *, significant $p<0.05$ compared with mice injected with PBS . #, significant $p<0.05$ compared with mice injected with ICOVIR-15K + hyal group, by two-tailed unpaired Student's *t*-test. PBS, phosphate-buffered saline; iv, intravenous; it, intratumoral; hyal, hyaluronidase.

With regard to mice survival, in the intravenous setting the treatment with ICOVIR-17K was the only one that could significantly increase survival time, whereas combined treatment of ICOVIR-15K and soluble hyaluronidase had no effect compared to control group (**Figure 29a**). In the intratumoral setting, both treatments increased survival versus control group, but no advantage could be seen with ICOVIR-17K administration (**Figure 29b**).

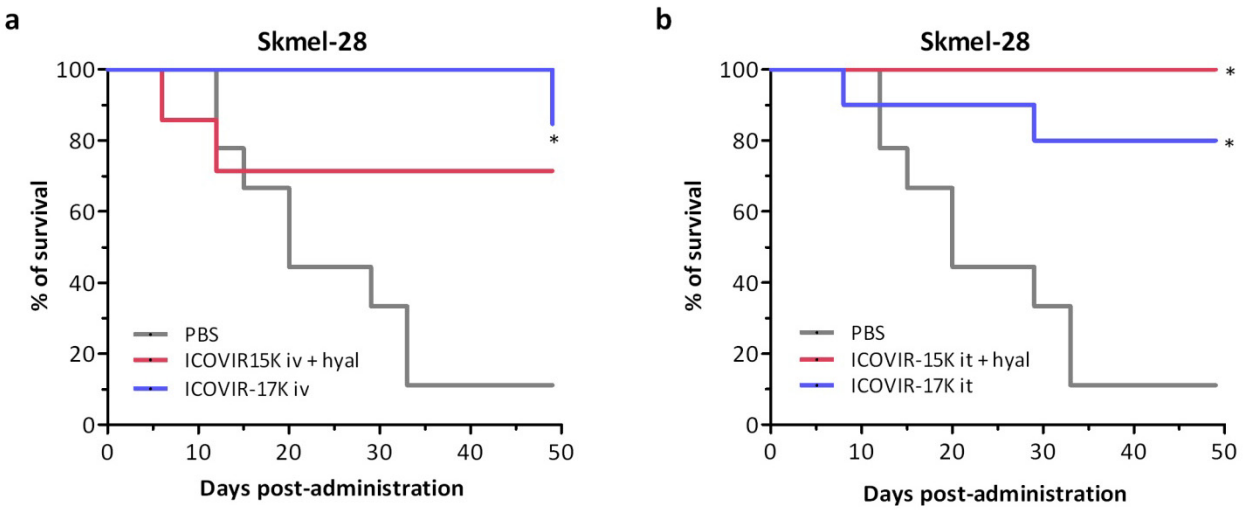

Figure 29. Comparative Kaplan-Meier survival curves of ICOVIR-17K and the combination of ICOVIR-15K and soluble hyaluronidase. (a) Nude mice carrying Skmel-28 subcutaneous xenograft tumors were injected intravenously with PBS or $4.5x10^{10}$ viral particles of ICOVIR-17K or ICOVIR-15K in combination with a single intratumoral injection of 100 IU of soluble hyaluronidase. (b) Nude mice carrying Skmel-28 subcutaneous xenograft tumors were injected with a single intratumoral administration of PBS or $2x10^{9}$ viral particles of ICOVIR-17K or ICOVIR-15K in combination with a single intratumoral injection of 100 IU of soluble hyaluronidase. Kaplan-Meier curves are plotted. End-point was established at 500 mm^3 of tumor volume. * Significant ($p<0.05$) by log-rank test compared with PBS group. PBS, phosphate-buffered saline; iv, intravenous; it, intratumoral; hyal, hyaluronidase.

So far, we have demonstrated a better antitumor activity of ICOVIR-17K after systemic administration when compared to the virus expressing hyaluronidase but with the RGD motif in the HI-loop, ICOVIR-17, and to the combination of ICOVIR-15K and soluble hyaluronidase. However, in terms of clinical application, the intratumoral route of administration was also considered interesting to evaluate. To reduce animal number for ethical reasons, no further comparison with any other virus was considered.

Mice carrying Skmel-28 or NP-9 human xenograft tumors were treated with a single intratumoral injection of PBS or $2x10^{9}$ viral particles for Skmel-28 and NP-9. A significant reduction in tumor growth could be seen in both models and, at the end of the studies, the mean tumor size of ICOVIR-17K-treated groups was 4.2- and 1.6-fold smaller compared to non-treated tumors in Skmel-28 and NP-9 models, respectively (**Figure 30a** and **b**).

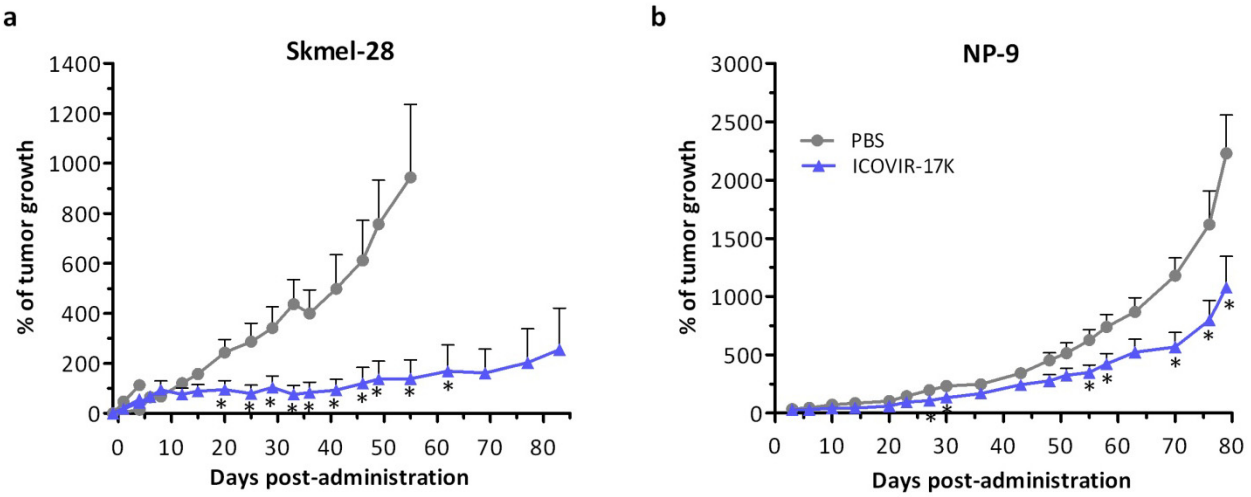

Figure 30. Antitumor activity upon intratumoral administration. Nude mice bearing subcutaneous xenografts of (a) Skmel-28 (melanoma) or (b) NP-9 (pancreatic carcinoma) tumors recieved a single intratumoral injection of PBS or $2x10^9$ viral particles of ICOVIR-17K per tumor. Mean percentage of tumor growth value +SEM is plotted (n=10 tumors/group). *, Significant $p<0.05$ by two-tailed unpaired Student's *t*-test compared with mice injected with PBS. PBS, phosphate-buffered saline.

Remarkably, intratumoral administration of ICOVIR-17K was also able to significantly increase survival in the models tested in comparison with non-treated animals (**Figure 31a** and **b**).

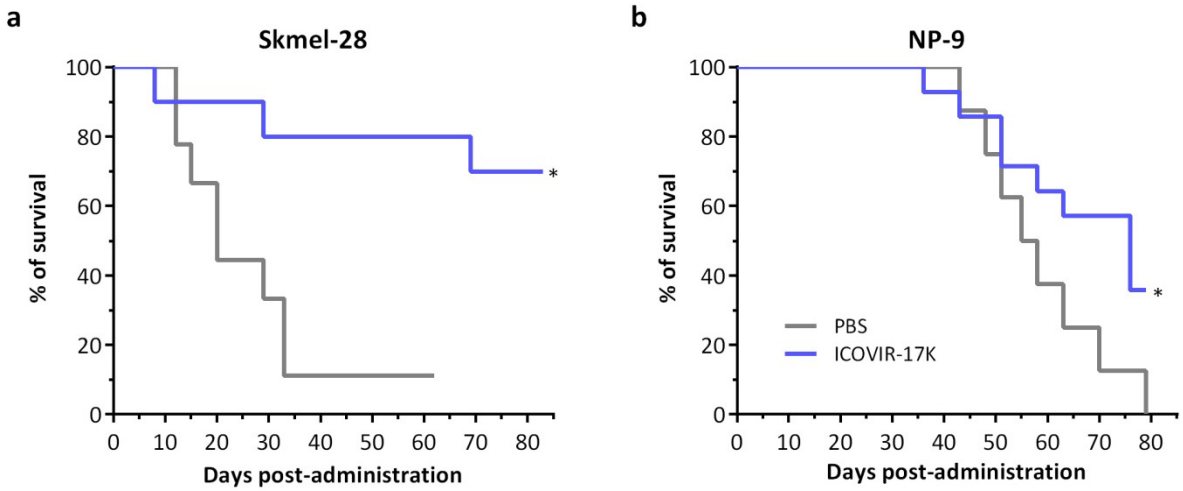

Figure 31. Kaplan-Meier survival curves upon systemic administration. Nude mice bearing subcutaneous xenografts of (a) Skmel-28 (melanoma) or (b) NP-9 (pancreatic carcinoma) tumors were injected intratumorally with PBS or $2x10^9$ viral particles per tumor of ICOVIR-17K. Kaplan-Meier curves are plotted. End-point was established at 500 mm^3 of tumor volume. *, Significant ($p<0.05$) by log-rank test compared with PBS group. PBS, phosphate-buffered saline.

1.3.5.2. Antitumor efficacy in a Syrian hamster model

Since mice are not permissive to Ad5 replication, a Syrian hamster model was included to evaluate the antitumor efficacy in the presence of an intact immune system. As it was done in mice, the antitumor activity of ICOVIR-17K was compared to that of ICOVIR-17 after systemic administration. HP-1 hamster pancreatic tumors were implanted subcutaneously in hamsters and when they reached a volume of about 250 mm^3, the animals were treated with a single intravenous dose of PBS or $4x10^{11}$ viral particles of ICOVIR-17 or ICOVIR-17K.

Both treatments induced a statistically significant control of tumor growth compared to the control group, despite this efficacy was discrete. Although in the case of ICOVIR-17K this difference was only significant at two time points (days 11 and 22), a similar behaviour was observed for the two oncolytic adenoviruses, and no significant differences were detected between them. At the end of the experiment, the mean tumor volume of non-treated group almost doubled the ones of treated animals (**Figure 32a**). However, as **Figure 32b**, shows any of the treatments could significantly increase the survival of the hamsters, evidencing the particular difficulty of this model.

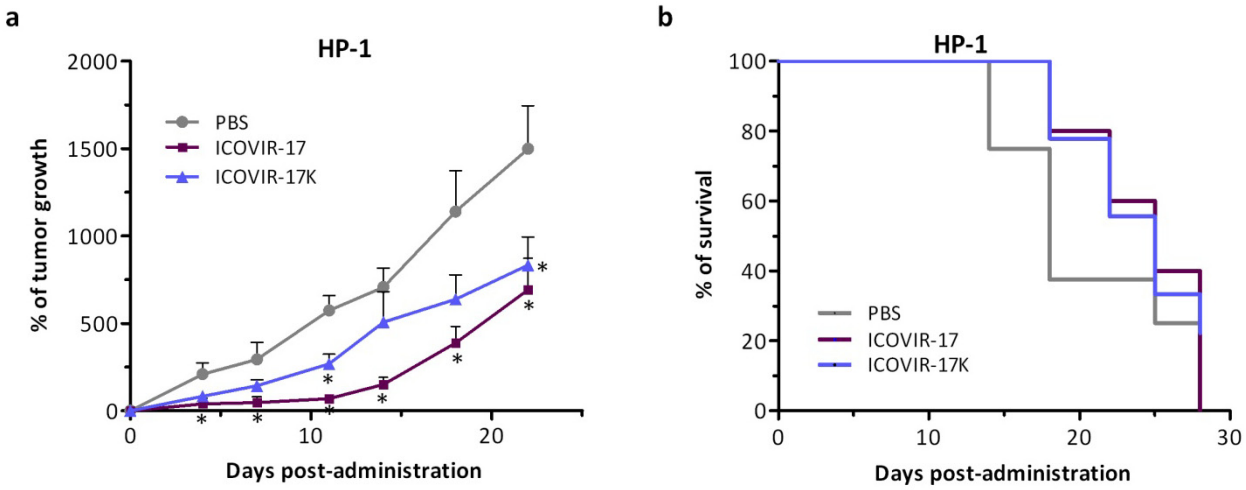

Figure 32. Antitumor activity and survival upon systemic administration in Syrian hamsters. Syrian hamsters bearing subcutaneous tumors of HP-1 (hamster pancreatic carcinoma) were injected intravenously with PBS or $4x10^{11}$ viral particles of ICOVIR-17 or ICOVIR-17K. (a) Mean percentage of tumor growth value +SEM is plotted (n=6-10 tumors/group). *, Significant $p<0.05$ by two-tailed unpaired Student's *t*-test compared with hamsters injected with PBS. (b) Kaplan-Meier curves are plotted. End-point was established at 2000 mm^3 of tumor volume. *, Significant ($p<0.05$) by log-rank test compared with PBS group. PBS, phosphate-buffered saline.

Antitumor activity in the intratumoral setting was also studied in hamsters, and the efficacy of a single injection of $2.5x10^{10}$ viral particles of ICOVIR-17K was compared to the efficacy of three injections of the same dose in consecutive days. The aim of this study was to evaluate if multiple administrations of the virus were able to improve the antitumor activity in hamster, as we had seen it was quite insensitive to the single administration schedule, at least in the intravenous setting.

A unique injection of ICOVIR-17K virus was able to significantly reduce tumor growth from day 9 post administration until the end of the study by day 28, when tumor volume was 2.1-fold smaller in treated animals. Surprisingly, the triple administration had no effect on tumor growth, and the tumors from this group followed exactly the same course than the ones from PBS group (**Figure 33a**). Moreover, the analysis of survival curves showed the same result: only the treatment with a single administration of ICOVIR-17K had a significant effect in prolonging survival with respect to PBS group (**Figure 33b**).

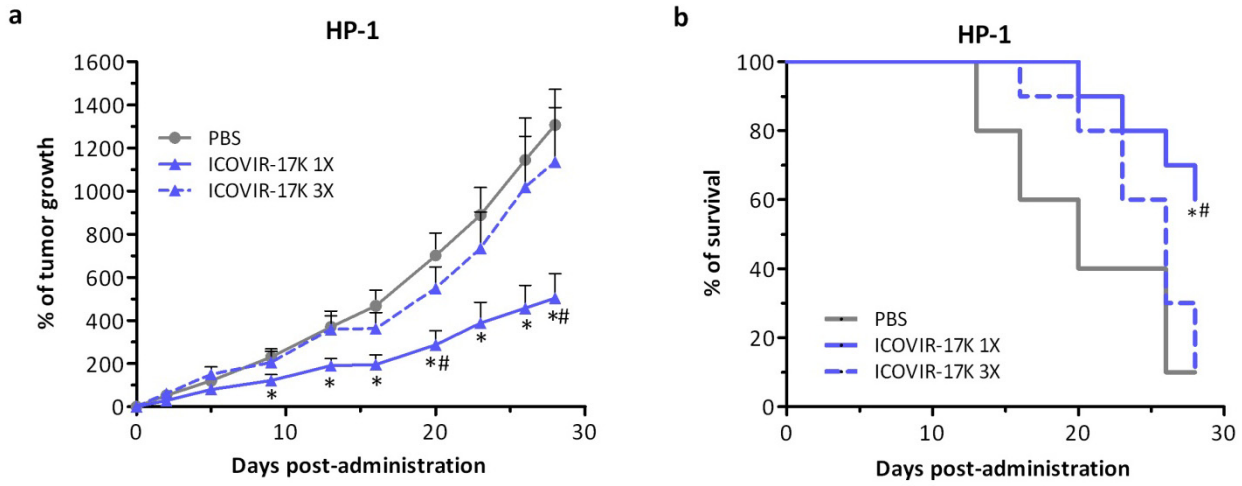

Figure 33. Antitumor activity and survival upon intratumoral administration in Syrian hamsters. Syrian hamsters bearing subcutaneous tumors of HP-1 (hamster pancreatic carcinoma) were injected intratumorally with PBS, a single administration (1X) or 3 administrations (3X) in consecutive days at a dose of $2.5x10^{10}$ viral particles of ICOVIR-17K. (a) Mean percentage of tumor growth value +SEM is plotted (n=10 tumors/group). *, Significant $p<0.05$ compared with hamsters injected with PBS. #, significant $p<0.05$ compared to hamsters receiving three doses of ICOVIR-17K, by two-tailed unpaired Student's *t*-test (b) Kaplan-Meier curves are plotted. End-point was established at 1500 mm^3 of tumor volume. * Significant ($p<0.05$) compared with PBS group. #, significant ($p<0.05$) compared to hamsters receiving three doses of ICOVIR-17K, by log-rank test. PBS, phosphate-buffered saline; 1X, one administration; 3X, triple administration.

In fact, immune staining of the viral protein E1A in frozen tumor sections revealed no presence of virus in the triple-administered animals, whereas virus was detected in tumors injected with a single dose on days 7 and 28 post-administration (**Figure 34**, **different panels**).

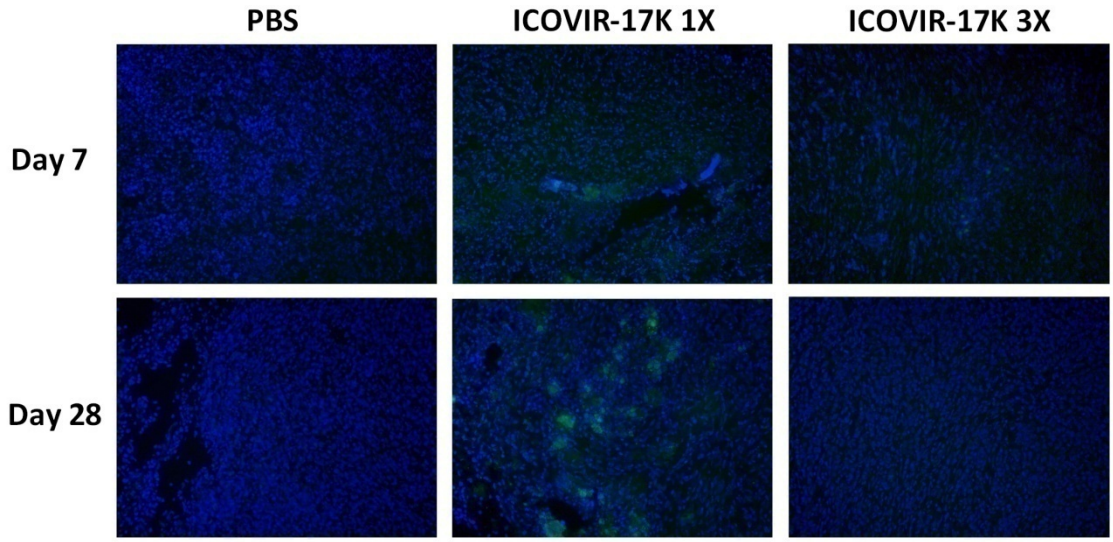

Figure 34. Virus detection in HP-1 tumors by immune staining of E1A. HP-1 tumors treated intratumorally with PBS, a single administration (1X) or 3 administrations (3X) in consecutive days of $2.5x10^{11}$ viral particles of ICOVIR-17K were obtained 7 and 28 days post-injection and were frozen in OCT. Adenovirus immunodetection was performed in frozen sections with an antiadenovirus antibody and counterstained with DAPI. Representative sections of tumors are shown. Original magnification ×200. PBS, phosphate-buffered saline; 1X, one administration; 3X, triple administration.

One possible reason to explain this unexpected result is that the triple administration of the virus is much more immunogenic than the unique injection, and the virus is quickly eliminated by the immune system, even considering its intratumoral location.

1.4. COMBINATION OF ICOVIR-17K AND GEMCITABINE

Different studies have reported that hyaluronidase administration prior to some chemotherapeutic drugs such as gemcitabine enhances their antitumor effect (Baumgartner *et al.*, 1998; Klocker *et al.*, 1998; Pillwein *et al.*, 1998). Gemcitabine is a chemotherapeutic drug licensed as a first line treatment of adult patients with locally advanced or metastatic adenocarcinoma of the pancreas. The abundant stroma content and the hyaluronic acid accumulation in these tumors raise the interstitial fluid pressure and compress the blood vessels, limiting drug delivery. Hyaluronidase ablates stromal hyaluronan, normalizing the interstitial pressure and improving the penetration of the drug to the tumor (Provenzano *et al.*, 2012; Jacobetz *et al.*, 2013).

Having in mind that other oncolytic adenoviruses have shown promising results in combination with chemotherapy in clinical trials (Hecht *et al.*, 2003), we decided to study the effect of the combination of our hyaluronidase-expressing virus and gemcitabine.

1.4.1. Toxicity of ICOVIR-17K and gemcitabine combination

Since the first concern we had was if the gemcitabine provided an additive toxicity to the oncolytic adenovirus ICOVIR-17K, we performed toxicology studies in mice and hamsters.

1.4.1.1. Toxicity profile in mice

Mice were treated with ICOVIR-17K, intravenously at $4x10^{10}$ viral particles per animal or intratumorally at a dose of $2x10^{9}$ viral particles per tumor, alone or in combination with gemcitabine at a dose schedule of 50 mg/kg on days 0, 3, 6, and 9. Body weight was monitored after the administration of the virus. Gemcitabine treatment alone did not have any significant effect on body weight compared to PBS-injected animals. As reported in previous sections, virus administration caused a transient body weight loss of about 10% that was recovered on day 10 post-injection. Importantly, the addition of gemcitabine did not significantly increase the body weight loss caused by the virus alone (**Figure 35a**). Intratumoral administration of ICOVIR-17K did not have any significant effect on body weight loss, regardless of whether it was combined with gemcitabine or not (**Figure 35b**).

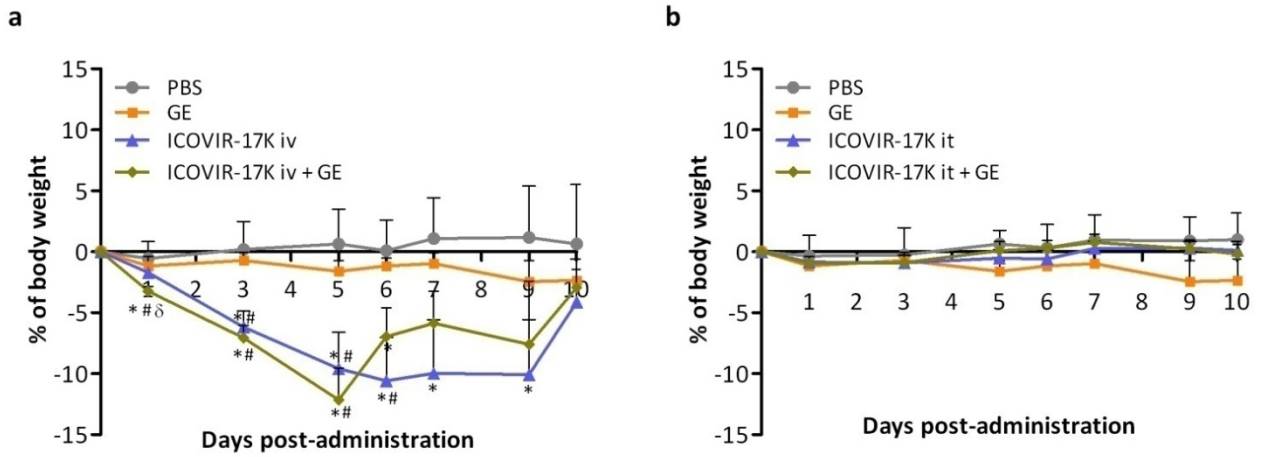

Figure 35. Body weight variation in nude mice upon the administration of ICOVIR-17K in combination with gemcitabine. Nude mice bearing xenograft tumors of NP-9 were administered with ICOVIR-17K by (a) intravenous or (b) intratumoral injection ($4x10^{10}$ viral particles per animal or $2x10^{9}$ viral particles per tumor, respectively) alone or in combination with intraperitoneal GE at 50 mg/kg (at days 0, 3, 6 and 9). Animals were monitored daily for body weight until day 10 post-administration. Mean values of body weight variation +SD are depicted. *, ICOVIR-17K significant ($p<0.05$) by compared to PBS group ; #, ICOVIR-17K significant ($p<0.05$) compared to GE group; δ, ICOVIR-17K significant ($p<0.05$) compared to ICOVIR-17K group, by two-tailed unpaired Student's t-test. GE: gemcitabine; iv, intravenous; it, intratumoral. PBS, phosphate-buffered saline.

1.4.1.2. Toxicology profile in Syrian hamsters

Syrian hamsters were administered with PBS, gemcitabine by intraperitoneal injection at a dose schedule of 50 mg/kg on days 0, 3, and 6, with an intravenous dose of $4x10^{11}$ viral particles of ICOVIR-17K, or with the combination of both treatments. Body weight of animals was monitored daily. On day 7 post-administration hamsters were sacrificed and liver enzymes (AST and ALT), creatinine levels and hematological parameters were determined.

Gemcitabine alone had no significant effect on body weight compared to PBS-treated animals. When combined with ICOVIR-17K, a maximum body weight loss was observed on day 4, reaching a percentage of 7.2%. However, body weight loss was not significantly different from that observed in hamsters treated with the virus alone. After day 4 animals started to gain weight and, although at the end of the study animals treated with ICOVIR-17K (alone or with gemcitabine) had not reached the body weight of PBS-injected animals, the general tendency suggested signs of recovery (**Figure 36a**).

With regard to the biochemistry parameters, differences were not observed between ICOVIR-17K group and ICOVIR-17K in combination with gemcitabine, and the toxicological events were the same that we have seen previously for ICOVIR-17K treatment alone, consisting in a moderate elevation of transaminase levels (**Figure 36b**).

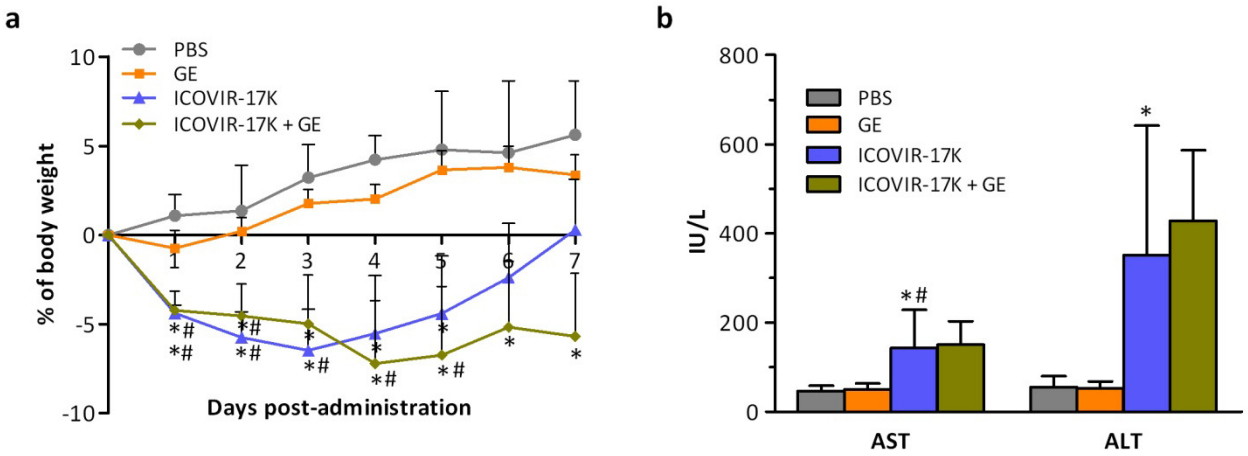

Figure 36. Toxicity upon systemic administration of ICOVIR-17K in combination with gemcitabine in Syrian hamsters. The average values for (a) body weight variation and (b) serum transaminase levels in hamsters peripheral blood on day 7 after the intravenous administration of PBS or $4x10^{11}$ viral particles per hamster of ICOVIR-17K alone or in combination with intraperitoneal GE at a dose schedule of 50 mg/kg on days 0, 3 and 6 are shown. Mean values +SD are plotted. *, Significant ($p<0.05$) compared to PBS group. #, Significant ($p<0.05$) compared to GE group, by two-tailed unpaired Student's t-test. ALT, alanine aminotransferase; AST, aspartate aminotransferase; IU, International units; PBS, phosphate-buffered saline.

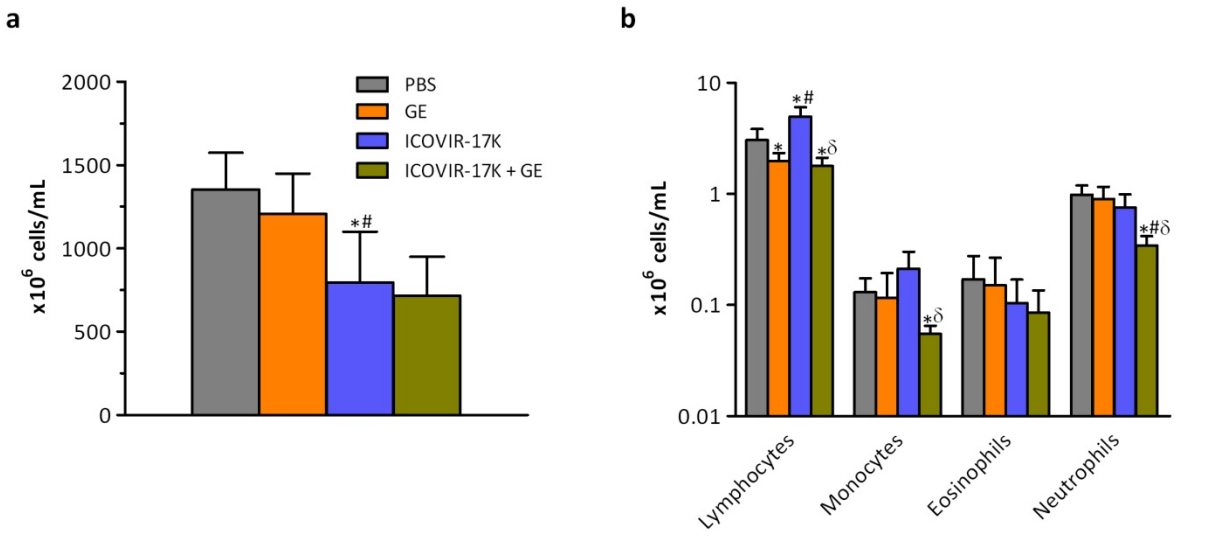

Figure 37. Hematological profile upon systemic administration of ICOVIR-17K in Syrian hamsters. The average values for (a) platelets concentration and (b) blood cell counts in hamsters peripheral blood at indicated time points after intravenous administration of PBS or $4x10^{11}$ viral particles per hamster of ICOVIR-17K alone or in combination with intraperitoneal GE at a dose schedule of 50 mg/kg at days 0, 3 and 6 are shown. Mean values +SD are plotted. *, Significant ($p<0.05$) compared to PBS group. #, Significant ($p<0.05$) compared to GE group. δ, Significant ($p<0.05$) compared to ICOVIR-17K group, by two-tailed unpaired Student's t-test. ALT, alanine aminotransferase; AST, aspartate aminotransferase; IU, International units; PBS, phosphate-buffered saline.

Differences between virus alone and virus plus gemcitabine were found in the hematologic parameters. While in the ICOVIR-17K group an increase in lymphocyte counts was detected, in the two groups treated with gemcitabine lymphopenia, which is a known effect of this drug, was observed. Moreover, a reduction of monocytes and neutrophils counts was detected in the group of the combined treatment compared to the other ones (**Figure 37b**). Platelets were not further affected by gemcitabine beyond the normal effect of the virus, which is a plaquetopenia at early time points (**Figure 37a**).

To conclude, cumulative toxicity was not observed in mice or hamsters treated with the combination of ICOVIR-17K with gemcitabine.

1.4.1.3. Oncolytic potency of the combination of ICOVIR-17K and gemcitabine

1.4.1.3.1. Cytotoxicity in tumor cell lines in vitro

Some studies have reported that gemcitabine reduces adenovirus production *in vitro,* since it is a nucleoside analogue which inhibits DNA synthesis (Nelson *et al.*, 2009). However, synergy has also been observed via several mechanisms such as the E1A-induced sensitization of cancer cells to gemcitabine (Bhattacharyya *et al.*, 2011; Onimaru *et al.*, 2011), increased infectivity due to coxsackievirus-adenovirus receptor and integrin overexpression (Nelson *et al.*, 2009;

Bhattacharyya *et al.*, 2011), or activation of promoters that regulate replication of the oncolytic adenovirus (Onimaru *et al.*, 2011).

Cytotoxicity experiments in different tumor cell lines were performed in order to see if the addition of gemcitabine was able to decrease the IC_{50} value of the virus alone. First of all, regarding the specific sensitivity of the different cell lines to gemcitabine and in order to decide the concentration to use for each one, cytotoxicity of this drug alone was evaluated (**Figure 38a** and **b**). Concentrations of gemcitabine close to the IC_{50} values were chosen for following studies.

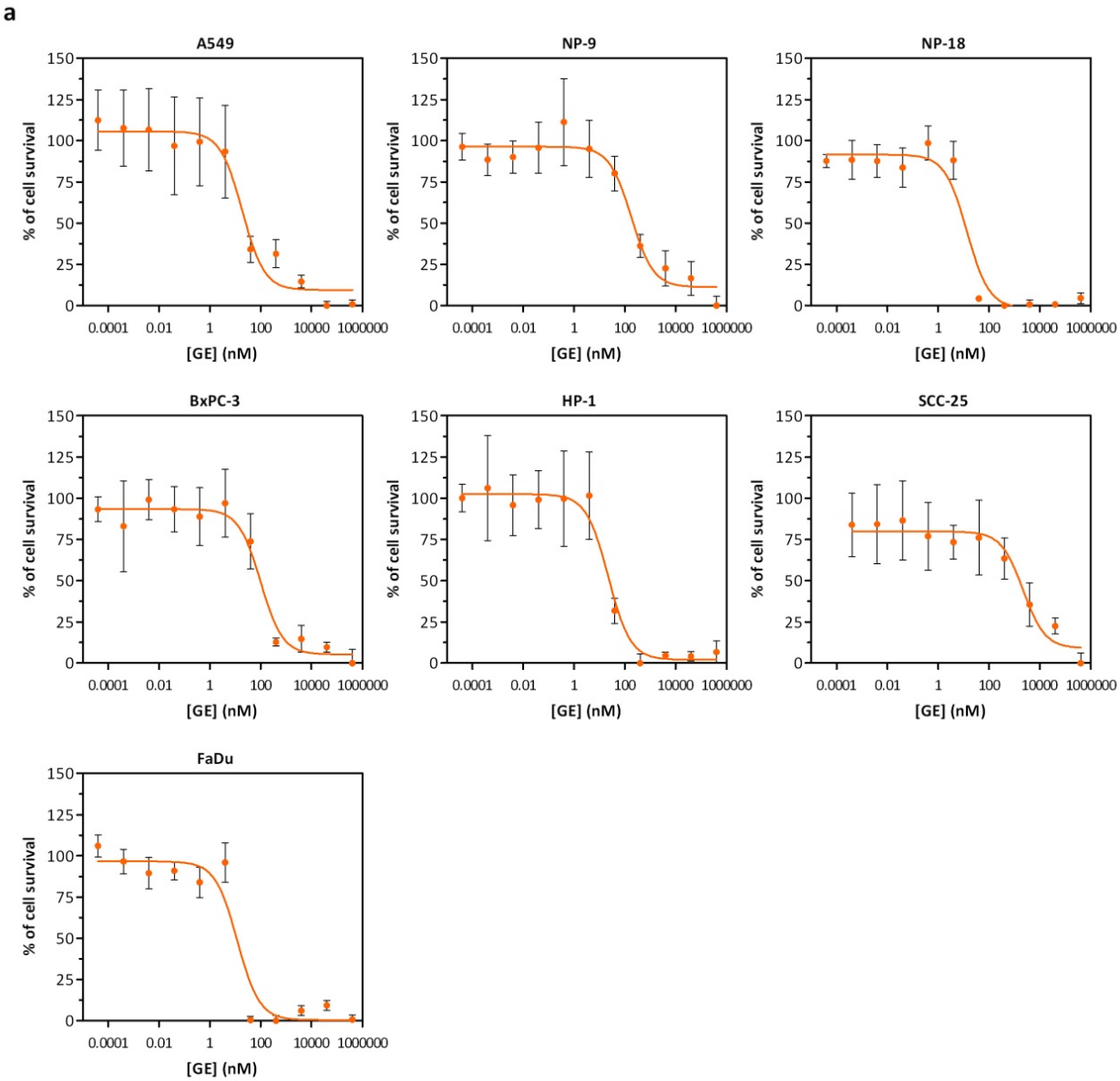

b

Tumor type	Cell line	IC_{50} GE (nM)
Human lung adenocarcinoma	A549	18.90
Human pancreatic adenocarcinoma	NP-9	178.30
	NP-18	13.52
	BxPC-3	99.20
Hamster pancreatic adenocarcinoma	HP-1	22.41
Human head and neck adenocarcinoma	SCC-25	2183
	FaDu	12.08

Figure 38. Cytotoxicity of gemcitabine in a panel of tumor cell lines *in vitro*. Different cell lines were treated with serial dilutions of GE starting at 400 µM during 6 days and cell viability was determined by BCA staining. (a) Dose-response curves are shown. Mean values of percent survival ±SD are plotted. (b) IC_{50} values of gemcitabine in a panel of tumor cell lines *in vitro*.

Cytotoxicity assays were performed by infecting a panel of tumor cell lines with serial dilutions of ICOVIR-17K and treating them or not with gemcitabine at the concentration indicated in **Figure 39b**. The percentage of cell survival was determined on day 5-8 post-infection for the cells infected with ICOVIR-17K and the ones infected and treated with gemcitabine. In order to remove the effect of gemcitabine, this percentage was normalized with that of cells treated with gemcitabine alone (**Figure 39a**). Results showed that the combined treatment significantly lowered IC_{50} values with a range of 2.6 to 32.8-fold increases in cytotoxicity compared to virus alone in 5 cell lines tested (**Figure 39b**). In conclusion, we demonstrated that ICOVIR-17K was able to induce chemosensitization to gemcitabine.

a

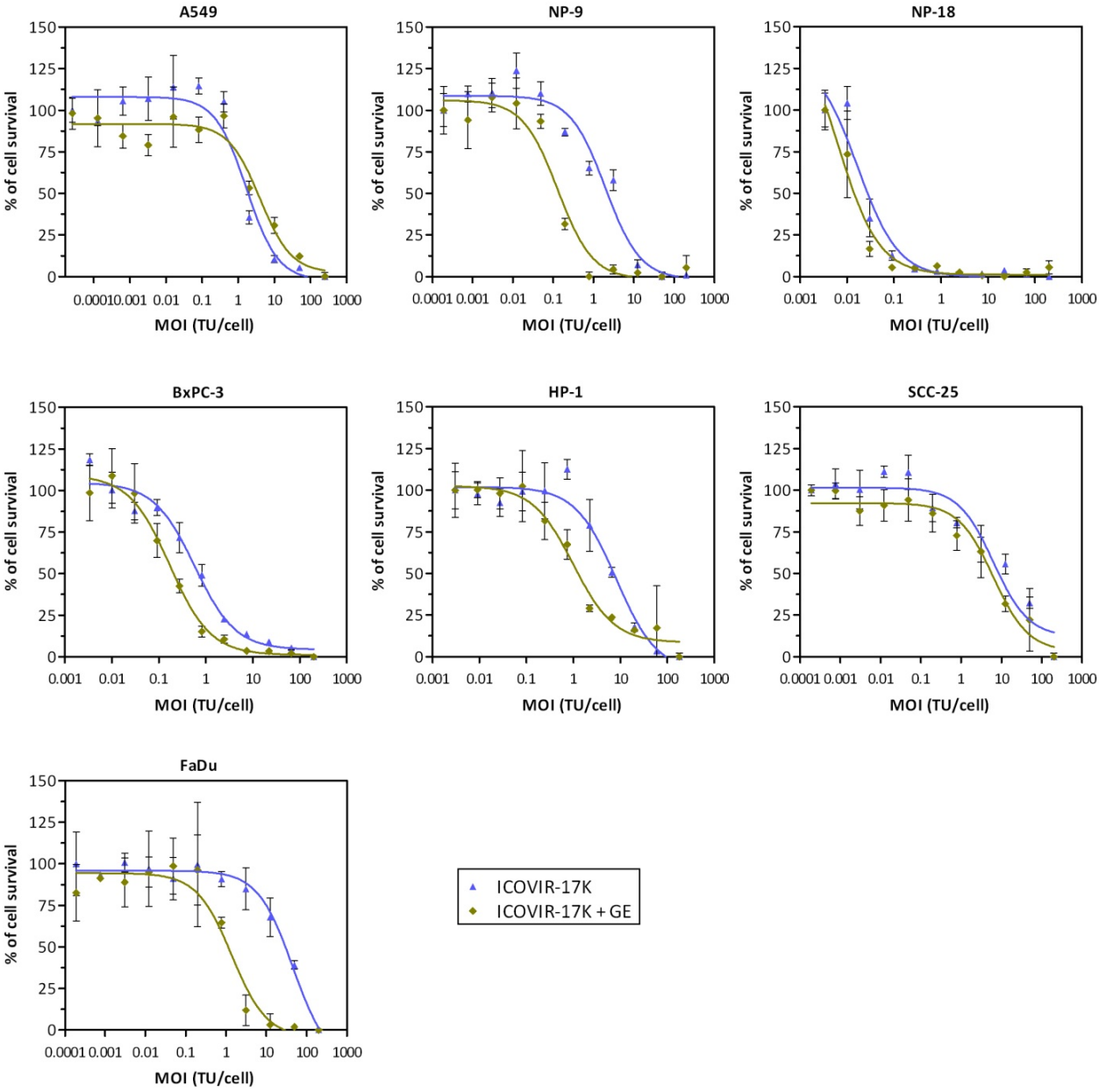
A549
NP-9
NP-18
BxPC-3
HP-1
SCC-25
FaDu
% of cell survival
MOI (TU/cell)
ICOVIR-17K
ICOVIR-17K + GE

b

Tumor type	Cell line	[GE] (nM)	IC_{50} (TU/cell)		Cytotoxicity fold-increase
			ICOVIR-17K	ICOVIR-17K + GE	
Human lung adenocarcinoma	A549	25	1.689	3.951	0.4
Human pancreatic adenocarcinoma	NP-9	250	1.968	0.1296	15.2*
	NP-18	15	0.01680	0.006529	2.6*
	BxPC-3	100	0.5802	0.1706	3.4*
Hamster pancreatic adenocarcinoma	HP-1	25	8.262	0.9945	8.3*
Human head and neck adenocarcinoma	SCC-25	1000	8.650	5.440	1.6
	FaDu	15	45.81	1.396	32.8*

Figure 39. Cytotoxicity of ICOVIR-17K in combination with gemcitabine *in vitro* in a panel of tumor cell lines. Different cell lines were infected with serial dilutions of ICOVIR-17K and treated or not with GE at a dose close to IC_{50} value for each cell line. On day 5-8 post-infection, cell viability was determined by BCA staining for the virus alone and for the combination, and normalized with the percentage of cell survival of the cells treated with GE alone. (a) Dose-response curve. Mean values of percent survival ±SD are plotted. (b) The concentration of GE used for each cell line is indicated in the table. IC_{50} values of ICOVIR-17K alone or in combination with GE are shown, as well as the cytotoxicity fold-increase provided by GE addition. *, ICOVIR-17K + GE significant ($p<0.05$) compared to ICOVIR-17K alone group by extra sum-of-squares F test. MOI, multiplicity of infection; TU, transducing units; GE, gemcitabine.

1.4.1.4. Antitumor activity in vivo

Antitumor activity of ICOVIR-17K in combination with gemcitabine was assessed in a human NP-9 pancreatic xenograft model after intravenous or intratumoral administration of the virus. Nude mice bearing subcutaneous tumors of about 90 mm^3 were treated with intraperitoneal gemcitabine at a dose schedule of 50 mg/kg on days 0, 3, 6 and 9, being day 0 the day of virus administration. ICOVIR-17K was injected systemically at a dose of $4x10^{10}$ viral particles per animal or intratumorally at $2x10^9$ viral particles per tumor.

In the systemic setting, gemcitabine and ICOVIR-17K treatments showed significant antitumor activity after day 36 and 20, respectively, compared to PBS-treated group. Importantly, the combination of both treatments was able to significantly improve the efficacy with respect to either treatment alone (**Figure 40a**). Furthermore, 5 out of 7 tumors in the combined treatment were regressing at the end of the study, of which 3 completely disappeared.

In contrast, when the virus was injected intratumorally, the differences between groups were modest. Gemcitabine treatment alone did not have any significant effect in terms of percentage of tumor growth compared to PBS-injected tumors. Both virus treatments, regardless of whether

administered concomitantly with gemcitabine, were able to significantly reduce tumor growth. However, no significant differences were observed between them in this setting (**Figure 40b**). In spite of the lack of significant differences, almost 50% of tumors treated with ICOVIR-17K plus gemcitabine had disappeared by the end of the experiment (5 out of 12), whereas no tumors had disappeared in the group treated with virus alone.

The lack of chemosensitization observed by ICOVIR-17K in this intratumoral administration setting can be explained by a limited dissemination of the virus, given the single intratumoral injection used. This precludes wide expression of hyaluronidase that may facilitate the entrance gemcitabine penetration. In contrast, intravenous administration allows ICOVIR-17K to spread more efficiently and results in a significant chemosensitizitation associated with decreased hyaluronan content in the whole tumor.

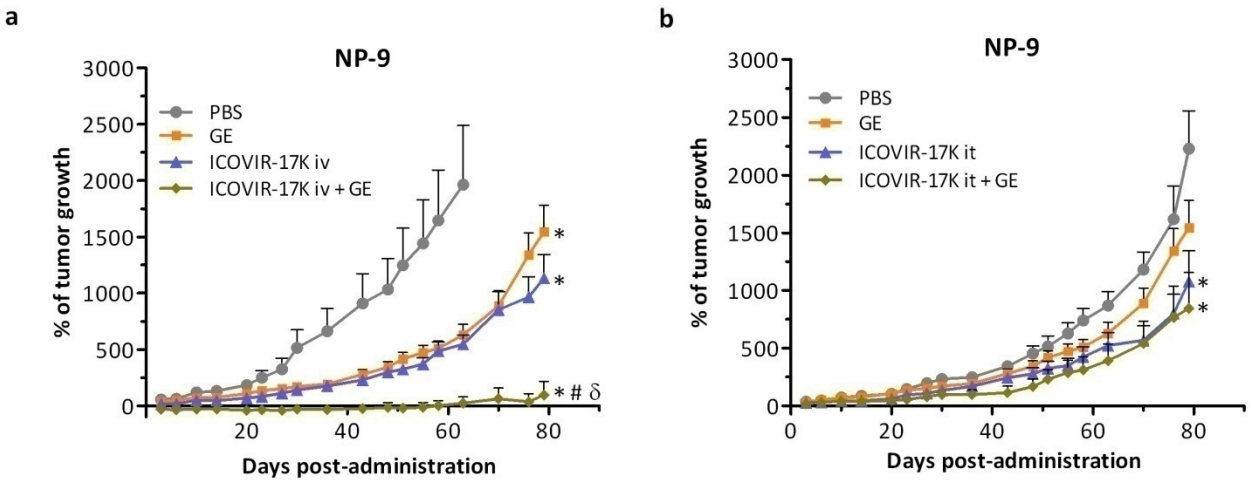

Figure 40. Antitumor activity of ICOVIR-17K in combination with gemcitabine *in vivo*. Nude mice bearing xenograft tumors of NP-9 were administered with ICOVIR-17K by (a) intravenous or (b) intratumoral injection ($4x10^{10}$ viral particles per animal or $2x10^{9}$ viral particles per tumor, respectively) alone or in combination with intraperitoneal GE at 50 mg/kg (at days 0, 3, 6 and 9). Tumor growth was monitored. Mean values of percentage of tumor growth +SEM are depicted (n=7-14 tumors/group). *, significant ($p<0.05$) compared to PBS group; #, significant ($p<0.05$) compared to GE group; δ, significant ($p<0.05$) compared to ICOVIR-17K group, by by two-tailed unpaired Student's t-test. GE: gemcitabine; iv, intravenous; it, intratumoral; PBS, phosphate-buffered saline.

Gemcitabine treatment could not significantly increase survival time compared to mock-treated animals. However, the treatment with ICOVIR-17K, alone or in combination with gemcitabine, and upon both administration routes, intravenous or intratumoral, had a significant effect increasing survival time. Moreover, in the case of intravenous administration of the virus, the addition of gemcitabine to the treatment prolonged survival from 74 days observed for the virus alone, to 79 days, even though such difference was not statistically significant. For the

intratumoral setting, the survival time was the same for both treatments including virus and equivalent to 66 days (**Figure 41a** and **b**).

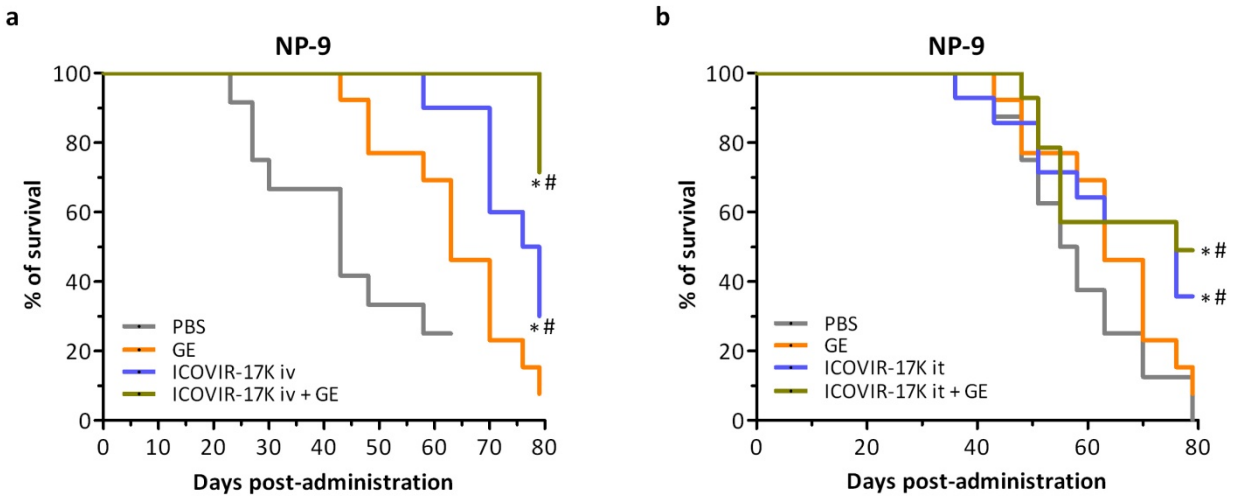

Figure 41. Kaplan-Meier survival curves upon the administration of ICOVIR-17K in combination with gemcitabine *in vivo*. Nude mice bearing xenograft tumors of NP-9 were administered with ICOVIR-17K by (a) intravenous or (b) intratumoral injection ($4x10^{10}$ viral particles per animal or $2x10^{9}$ viral particles per tumor, respectively) alone or in combination with intraperitoneal GE at 50 mg/kg (on days 0, 3, 6 and 9). Kaplan-Meier curves are plotted. End-point was established at 500 mm^3 of tumor volume. *, significant ($p<0.05$) compared with PBS group. #, significant ($p<0.05$) compared with GE group, by log-rank test. GE: gemcitabine; iv, intravenous; it, intratumoral; PBS, phosphate-buffered saline.

Chapter 2

2. INSERTION OF EXOGENOUS EPITOPES IN THE E3-19K OF ONCOLYTIC ADENOVIRUSES TO ENHANCE TAP-INDEPENDENT PRESENTATION AND IMMUNOGENICITY

Downregulation on cell surface expression of major histocompatibility complex (MHC) class I is frequently associated to tumor cell immune evasion. Among defects at different levels, one of the most frequent is the downregulation of the transporter associated with antigen processing (TAP) that translocates peptides generated by the proteosome into the endoplasmatic reticulum (ER) to be loaded onto empty MHC-I molecules (Leone *et al.*, 2013). One strategy that has been proposed to solve this problem is to link immunogenic peptides to ER-targeting signals to promote their TAP-independent presentation (Lu *et al.*, 2001; Lu *et al.*, 2004).

On the other hand, oncolytic adenoviruses have been used to promote immune responses against tumors by expressing and/or displaying tumor-associated antigens (TAAs). However, the strong immunodominance of virus antigens masks responses against tumor epitopes.

With the aim to enhance the immunogenicity of exogenous epitopes presented by oncolytic adenoviruses in TAP-defective tumor cells, we propose the use of the ER-resident adenoviral protein E3-19K as a carrier of tumor epitopes across the ER membrane.

2.1. GENERATION AND CHARACTERIZATION OF THE ONCOLYTIC ADENOVIRUSES

We inserted two different exogenous epitopes in the E3-19K gene, after the ER-targeting signal, and separated by linkers cleavable by the transgolgi network protease furin (RVKR) to facilitate the proteasome-independent processing of the epitopes. The first of them was the $OVA_{257-264}$ (SIINFEKL) epitope of ovalbumin protein from chicken egg whites, which is presented by the H-$2K^b$ MHC class I molecule and has been widely used as a model epitope since it is highly immunogenic (Maecker *et al.*, 1998; Werlen *et al.*, 2000). The second epitope was the $hgp100_{25-33}$ (KVPRNQDWL) from the human melanoma TAA gp100 which, in contrast to $OVA_{257-264}$, has an associated intrinsic immunotolerance since it is a self-antigen. The homologous murine and human epitopes of gp100 (amino acids 25–33) are presented in the context of the MHC class I molecule H-$2D^b$ and differ in the three NH_2-terminal amino acids. This difference confers greater avidity on MHC class I binding of the human peptide, thereby increasing its ability to break tolerance to the murine self-antigen gp100 or also known as Pmel17 (Overwijk *et al.*, 1998).

In order to do comparative studies, another oncolytic adenovirus has been constructed inserting the same epitopes in the HI-loop of the fiber and separated by classical GS-flexible linkers (GSGSR). The fiber, as well as the other viral proteins excluding E3-19K, is processed in the cytoplasm by the proteasome according to the classical MHC-I pathway, so it does not need furin linkers. A schematic representation of the modifications included in each virus is shown in **Figure 42**.

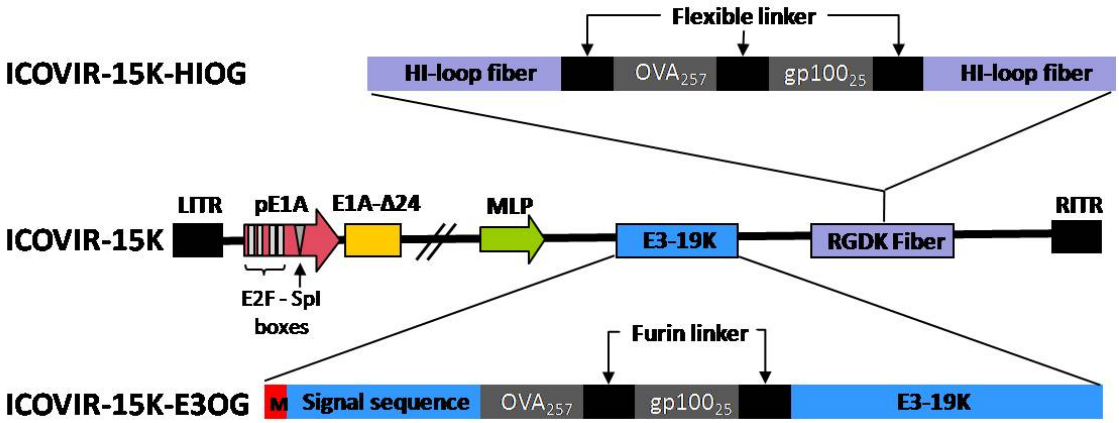

Figure 42. Schematic representation of the genomes of the different viruses. ICOVIR-15K contains the modified E1a promoter (including four E2F boxes and one Sp1 box) and the truncated E1A protein to confer selectivity for tumor cells. It also incorporates the motif CDCRGDCFC (RGD-4C) replacing the putative HSG-binding domain, KKTK (RGDK modification). The epitopes OVA_{257} and $gp100_{25}$ have been incorporated within the HI-loop domain of the fiber and are flanked by GS-flexible linkers to generate ICOVIR-15K-HIOG. The same epitopes were inserted after the ER-targeting signal sequence of the E3-19K flanked by furin-linkers for the construction of ICOVIR-15K-E3OG. LITR, left inverted terminal repeat; RITR, right inverted terminal repeat; MLP, major late promoter.

Plasmids containing the genomes of the oncolytic adenoviruses presented in this section were generated by homologous recombination in bacteria and then transfected into HEK293 cells for virus generation.

Once the viruses were generated, a cytotoxicity assay was performed in the A549 cell line in order to confirm that the new oncolytic adenoviruses did not suffer any potency loss associated to the incorporated mutations compared to the parental virus ICOVIR-15K. ICOVIR-15K-HIOG and ICOVIR-15K-E3OG showed similar IC_{50} values to that of ICOVIR-15K, without detecting any statistically significant difference between them (**Figure 43a** and **b**).

a

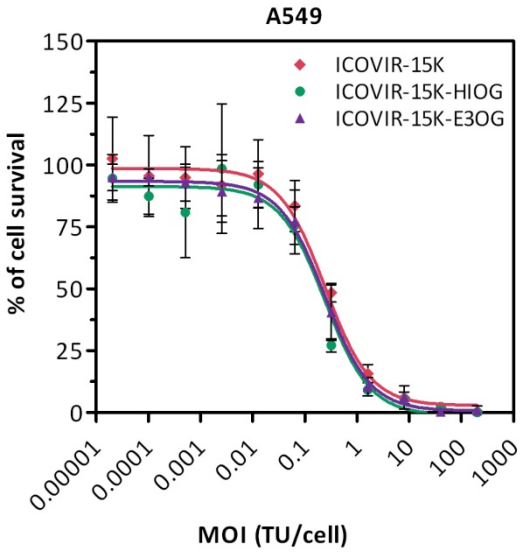

b

Virus	IC_{50} (TU/cell)	Cytotoxicity fold-increase versus ICOVIR-15K
ICOVIR-15K	0.3218	-
ICOVIR-15K-HIOG	0.1846	1.7
ICOVIR-15K-E3OG	0.2464	1.3

Figure 43. Cytotoxicity in A549 cells. (a) Dose-response curves obtained by non-linear regression. A549 cells were infected with 1:5 serial dilutions of ICOVIR-15K, ICOVIR-15K-HIOG and ICOVIR-15K-E3OG starting at 300 MOI and cell viability was determined by BCA staining on day 6 post-infection. Mean ±SD is plotted (b) IC_{50} values for each virus are represented. Cytotoxicity increase versus parental virus ICOVIR-15K is also represented. * significant ($p<0.05$) compared to ICOVIR-15K. MOI, multiplicity of infection; TU, transducing units.

2.2. MURINE MODELS FOR THE ANALYSIS OF IMMUNOVIROTHERAPY OF CANCER

Since OVA_{257} and $gp100_{25}$ epitopes are specifically recognized by H-$2K^b$ and H-$2D^b$ murine MHC class I molecules respectively, tumor mouse cell lines from *b* H2 haplotype origin were required as models for this study, *in vitro* and *in vivo*. Moreover, since the goal of this project was to evaluate immune responses, common models to study efficacy of oncolytic adenoviruses such as immunodeficient mice carrying xenografted human tumors were not appropriate, and immunocompetent mice carrying murine tumors were needed instead.

Since human adenoviruses replication is species-specific, the usefulness of these models to evaluate oncolysis is limited. In order to conduct this project, parameters such as the infectivity,

viral productivity or MHC class I surface levels have been characterized in different murine tumor cell lines. In some cases, these cell lines have been modified to become suitable for the experiments.

For *in vitro* experiments, B16 melanoma and TRAMPC2 prostatic adenocarcinoma tumor cell lines were used since its TAP deficiency has been previously described. Moreover, the expression of TAP and other molecules of MHC class I processing pathway can be enhanced by the incubation with interferon-γ (IFN) in both of them, allowing a TAP-positive or negative environment depending on the presence or absence of this cytokine (Seliger *et al.*, 2001; Martini *et al.*, 2010).

2.2.1. Infectivity and viral production assays

The first parameter that we wanted to characterize was the infectivity *in vitro* of B16 and TRAMPC2 cell lines. Previous observations in our laboratory and others determined the poor infectivity by adenovirus of B16 cell line. Therefore, we have used the cell line B16CAR, which was stably transfected with the coxsackievirus adenovirus receptor, CAR, in order to increase the efficacy of transduction by adenoviruses (Tosch *et al.*, 2008). Regarding TRAMPC2, different published studies performed with adenoviruses support the susceptibility of this cell line to be infected (Dzojic *et al.*, 2006; Danielsson *et al.*, 2011; Freytag *et al.*, 2013). After demonstrating CAR expression in B16CAR by flow cytometry (**Figure 44a**), infectivity assays were performed by infecting each cell line with two adenoviral vectors expressing GFP (one containing the wild type capsid, AdTL, and another containing the RGDK mutation, AdTLRGDK) at different MOIs and analyzing the percentage of infected cells 24 hours post-infection by flow cytometry (**Figure 44b**) and also by microscopy (**Figure 44c**).

Results in B16CAR showed that at the lowest MOI, 25 TU/cell, 60% of the cells were infected, whereas 100% of infectivity was observed at 100 MOI, indicating a good infectivity profile of this cell line. Importantly, only mild differences between both capsids were observed at the lowest MOIs, where a negligible loss of infectivity was perceived upon the infection with the RGDK virus.

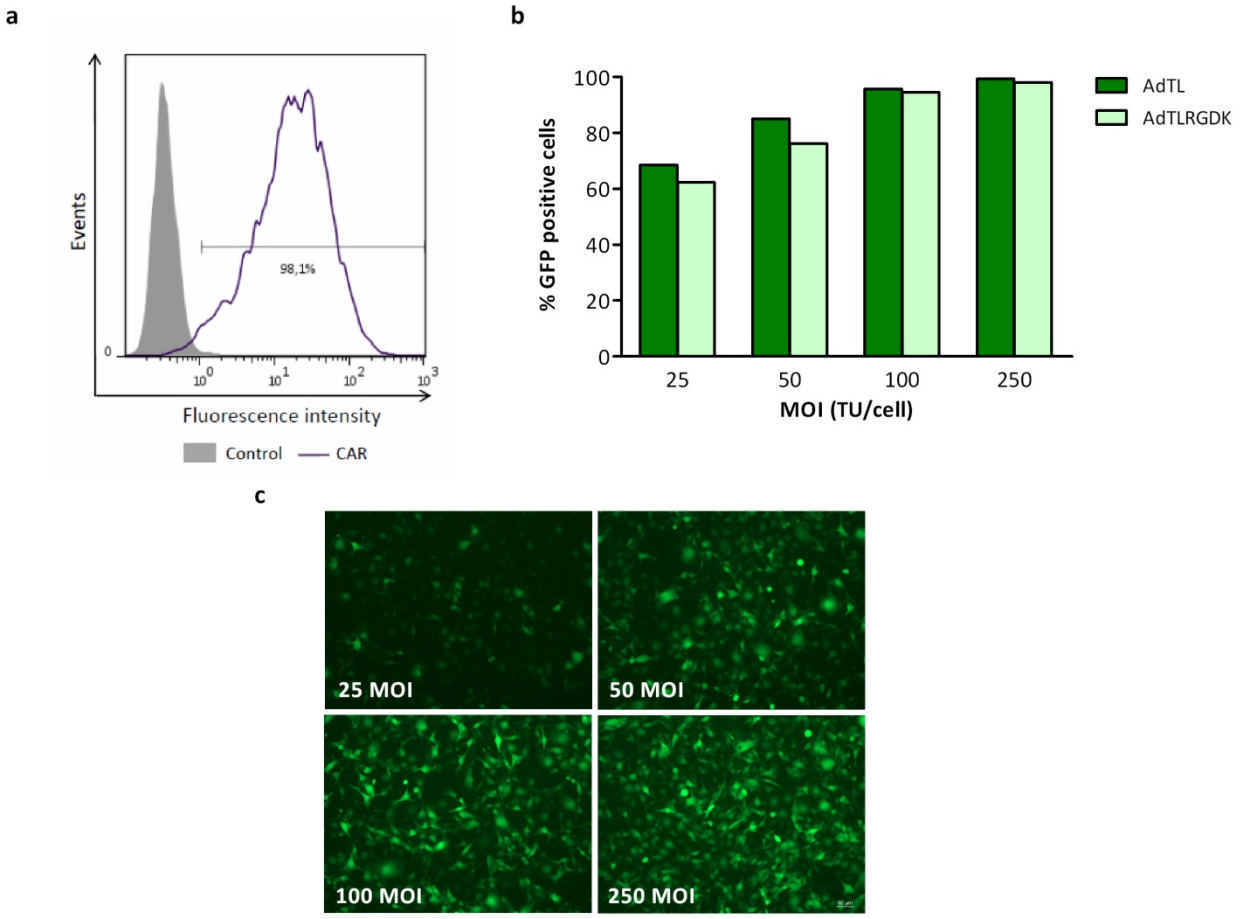

Figure 44. CAR expression and infectivity of B16CAR. (a) B16CAR cells were stained with anti-CAR hybridoma and analyzed by flow cytometry. Fluorescence intensity and percentage of positive cells is shown. B16CAR cells were infected at different MOI with the GFP-expressing adenoviral vectors AdTL and AdTLRGDK. 24 hours post-infection, fluorescence was analyzed by (b) microscopic observation (original magnification 100X) and by (c) flow cytometry. Percentage of GFP positive cells is plotted. MOI, multiplicity of infection. TU, transducing unit.

The infectivity of TRAMPC2 was much lower than that of B16CAR. Only about 60% of infected cells were observed at the highest MOI of 200 TU/cell, independently of the capsid of the virus. However, at this condition some mortality associated to cytotoxicity was observed, so the chosen MOI for the different studies was 100 TU/cell, allowing around 40% of infectivity (**Figure 45**, **different panels**).

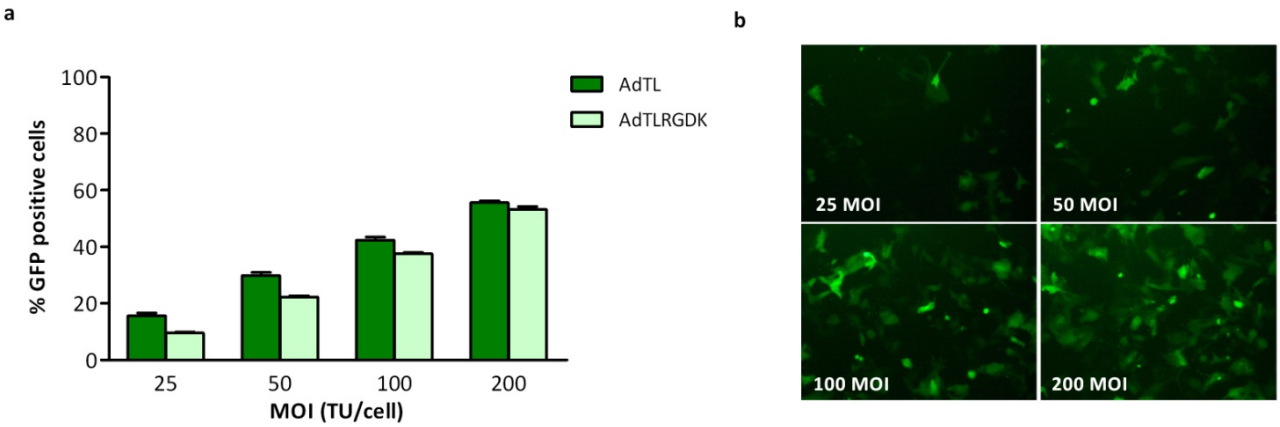

Figure 45. Infectivity of TRAMPC2. (a) TRAMPC2 cells were infected at different MOI with the GFP-expressing adenoviral vectors AdTL and AdTLRGDK. 24 hours post-infection, fluorescence was analyzed by (b) microscopic observation (original magnification 100X) and by (c) flow cytometry. Percentage of GFP positive cells is plotted. MOI, multiplicity of infection. TU, transducing unit.

The next step was to characterize viral production yields of each cell line in order to know if they could be used for oncolysis evaluation besides immune responses. B16CAR and TRAMPC2 cells were infected with the parental virus ICOVIR-15K and 72 hours post-infection viral yields were quantified from cell extracts. A549 cells were included as a control of a permissive human cell line. Whereas, A549 were able to produce almost $2x10^4$ TU/cell, neither B16CAR nor TRAMPC2 produced significant levels of virus 72 hours post-infection, concluding that these cells do not represent a good model to study direct oncolytic effect of human adenoviruses (**Figure 46**). However, they are still useful for immunologic assays.

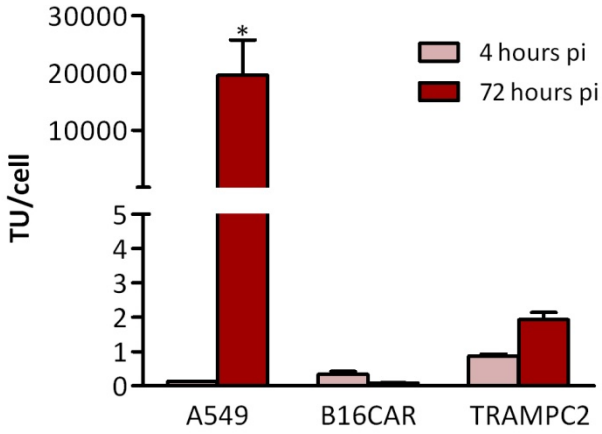

Figure 46. Viral production yield in murine cell lines. A549, B16CAR and TRAMPC2 cells were infected at 25, 100 and 100 TU/cell. 4 hours post-infection, cells were washed three times with PBS and cell extract samples were obtained to determine basal levels of virus. At 72 hours post-infection new cell extract samples were collected. Viral yields were quantified at these time points by an anti-hexon staining based method. Mean values +SD are plotted. TU, transducing units. pi, post-infection.

2.2.2. MHC class I surface expression levels

It was interesting for us to quantify basal MHC class I surface levels of these cell lines in the presence or absence of IFN-γ, especially of H-2K^b and H-2D^b, since the exogenous epitopes included in the oncolytic adenoviruses are restricted for these molecules.

As it is shown in **Figure 47**, TRAMPC2 expressed higher levels of H-2K^b than B16CAR at basal conditions (52.4% compared to 38.4%). However, when IFN-γ is added to the medium, H-2K^b levels reached 100% of expression in both cell lines. Moreover, infection by adenovirus did not affect H-2K^b expression in any case. This result was expected since it is described that E3-19K does not bind to this MHC class I haplotype (Tanaka and Tevethia, 1988).

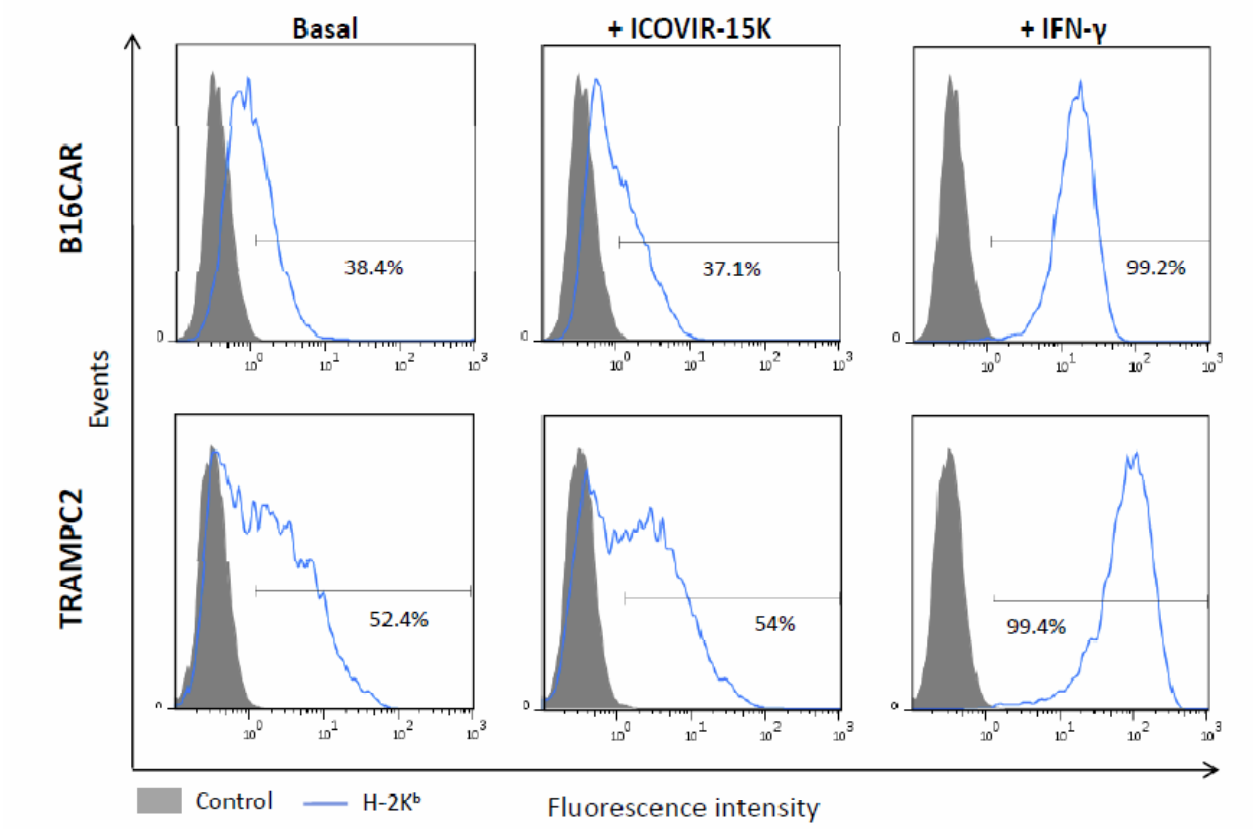

Figure 47. H-2K^b levels in B16CAR and TRAMPC2 cell lines. Monolayers of B16CAR and TRAMPC2 cells seeded in 24-well plates. IFN- γ-treated cells were incubated for 48 hours at 200 U/mL and were analyzed 24 hours later. Virus-treated cells were infected with ICOVIR-15K at 100 MOI during 4 hours, then washed 3 times with PBS and incubated 24 hours in fresh medium. Then, the cells were stained with the anti-H-2K^b hybridoma Y3 and analyzed by flow cytometry. Fluorescence intensity histograms are plotted and the percentage of positive cells is indicated in the graph.

Regarding H-2D^b molecules, surface basal levels were extremely low. This observation was previously reported by other groups (Kaluza *et al.*, 2012). In this case, the effect of E3-19K in binding MHC class I molecules should be seen, however since detected basal levels were

practically negligible (4% of positive cells), we were not able to detect any difference. Even in the presence of IFN-γ, they barely reach 60% of expression in B16CAR cell line**.** In the case of TRAMPC2, these low basal levels of H-2D^b were also detected. As happened in B16CAR, no differences could be observed between basal conditions and infected cells, and the inducibility of these molecules by IFN-γ was also limited to the ~25% of the cells (**Figure 48**, **different panels)**.

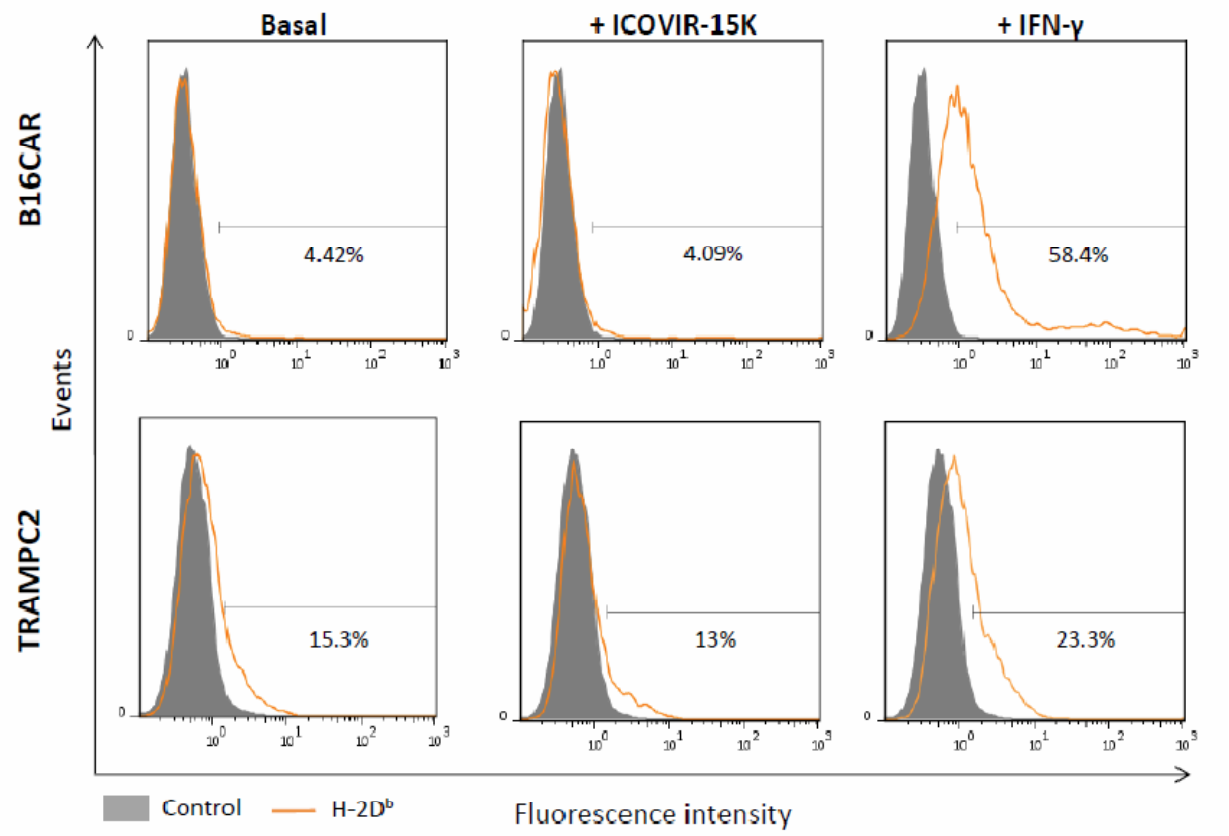

Figure 48. H-2D^b levels in B16CAR and TRAMPC2 cell lines. Monolayers of B16CAR and TRAMPC2 cells seeded in 24-well plates. IFN- γ-treated cells were incubated for 48 hours at 200 U/mL and were analyzed 24 hours later. Virus-treated cells were infected with ICOVIR-15K at 100 MOI during 4 hours, then washed 3 times with PBS and incubated 24 hours in fresh medium. Then, the cells were stained with an anti-H-2D^b and analyzed by flow cytometry. Fluorescence intensity histograms are plotted and the percentage of positive cells is indicated in the graph.

2.2.3. Tumor model for *in vivo* studies

A tumor model which expresses both antigens targeted by our oncolytic adenoviruses, OVA and gp100, was also required. B16CAR is a melanoma cell line which naturally overexpresses gp100 (Peter *et al.*, 2001). In order to have a model which also expresses OVA, we generated the B16CAROVA cell line by the transfection of B16CAR cells with the expression plasmid pAcNeoOVA (Moore *et al.*, 1988). This plasmid expresses OVA gene and also contains the

selection gene Neo, which provides resistance to G418 antibiotic, that was used to select and maintain the transfected OVA-expressing cells.

Once the cell line was generated, we confirmed that it maintained the same levels of H-2K^b and CAR expression than the parental cell line B16CAR (**Figure 49**).

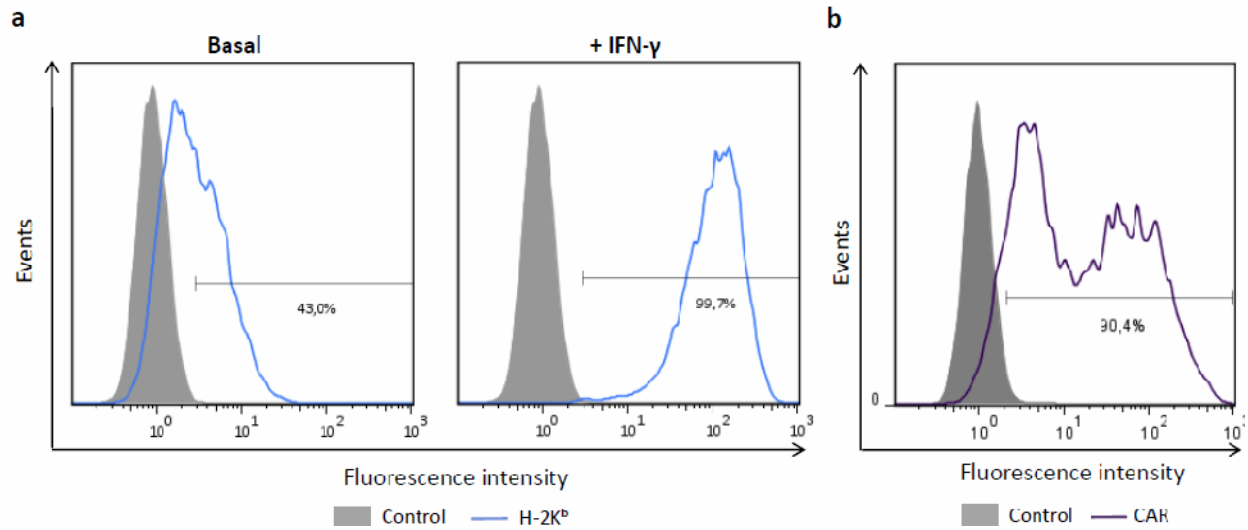

Figure 49. B16CAROVA characterization. Monolayers of B16CAROVA were incubated or not with IFN-γ at 200 U/mL during 48 hours and stained with the (a) anti-H-2K^b hybridoma Y3 or (b) anti-CAR hybridoma. Cells were analyzed by flow cytometry. Fluorescence intensity is represented and the percentage of positive cells is indicated in the graph.

Afterwards, OVA expression was confirmed by specific PCR after retrotranscription of RNA extracted from B16 (parental cell line), B16CAR (parental cell line transfected with CAR), B16OVA (parental cell line transfected with OVA) and B16CAROVA (parental cell line transfected with CAR and OVA). As expected, the specific band corresponding to OVA was only detected in B16OVA and B16CAROVA samples (**Figure 50a**). The same technique was used to confirm gp100 expression, and in this case, all four cell lines tested were positive (**Figure 50b**). This result was also confirmed by immunocytofluorescence, in which A549 cell line was used as negative control (**Figure 50c**).

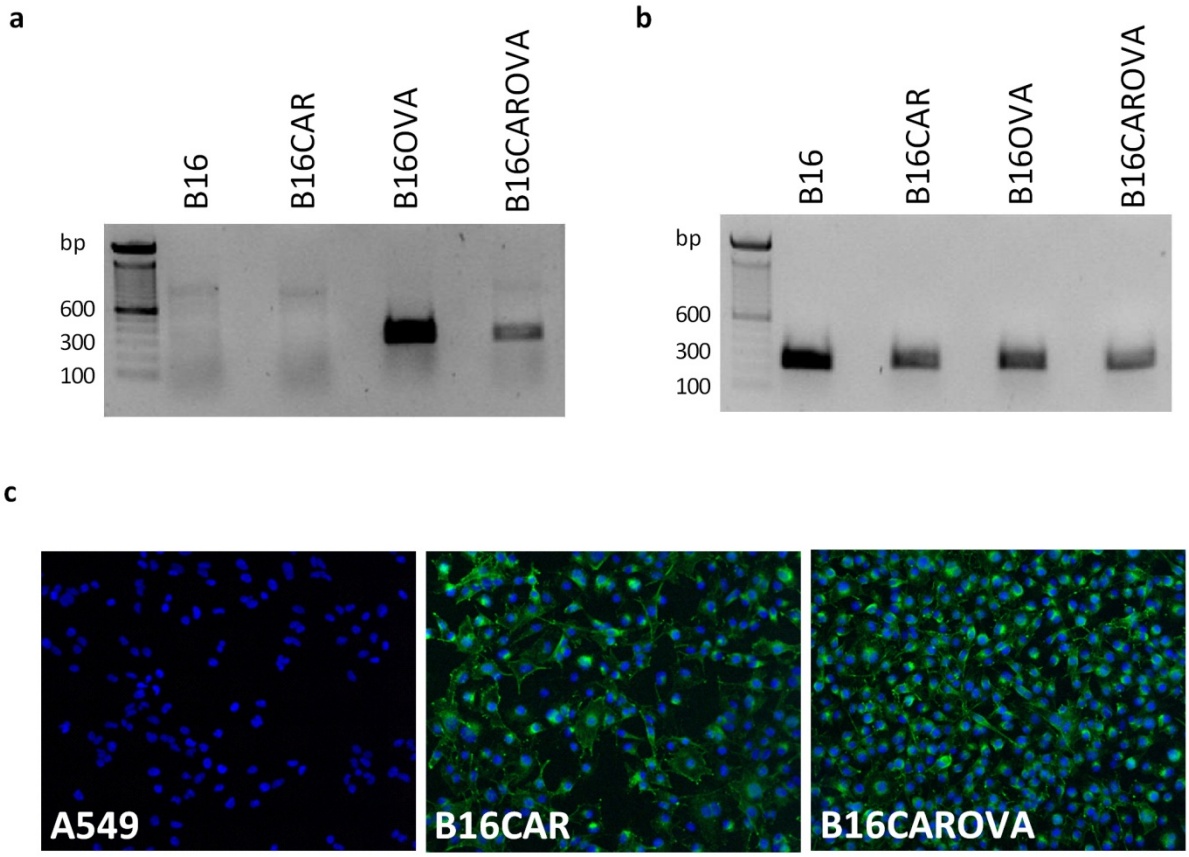

Figure 50. Antigen expression by B16CAROVA tumor cells. RNA was extracted from B16 (parental cell line), B16CAR, B16OVA, and B16CAROVA cells. This RNA was retrotranscribed to cDNA and specific oligonucleotides were used to amplify fragments of (a) OVA (band corresponding to 292 bp) or (b) gp100 (236 bp band). (c) Immune staining of gp100 was performed in cultured cells. A549 were used as negative control. bp, base pairs.

2.3. PROCESSING AND PRESENTATION OF THE EXOGENOUS EPITOPES *IN VITRO*

The availability of an antibody that specifically recognizes complexes formed by OVA_{257} epitope bound to the murine MHC-I molecule H-$2K^b$ allowed the study of the processing and presentation of this epitope *in vitro*.

2.3.1. Presentation of OVA_{257} upon infection of TAP-deficient tumor cell lines *in vitro*

B16CAR and TRAMPC2 tumor cell lines were infected with the different oncolytic adenoviruses: the parental virus ICOVIR-15K, the virus containing the epitopes in the HI-loop, ICOVIR-15K-HIOG, and the one that has the epitopes in the E3-19K, ICOVIR-15K-E3OG. After 24 hours of infection, cells were stained with a PE-labeled anti-K^b/OVA antibody and fluorescence was analyzed by flow cytometry. As negative and positive controls, cells were incubated with peptides corresponding to $gp100_{25}$ (which was irrelevant for this experiment as it is not H-$2K^b$ restricted) or OVA_{257} epitopes, respectively. Since deficiencies in MHC class I pathway in these

cell lines are IFN-γ inducible, the experiment was performed in the presence or absence of this cytokine.

An unexpected finding was that, in the absence of IFN-γ, thus the TAP-deficient environment, complexes formed by H-2K^b MHC class I molecules and OVA$_{257}$ could only be detected in the surface of B16CAR cells incubated with the peptide alone, which was the positive control. The infection with the OVA$_{257}$ displaying/expressing adenoviruses was not able to promote the processing and presentation of this epitope, at least at sufficient levels to be detected by this technique. However, when IFN-γ was added to the cells, OVA$_{257}$ was processed and presented in a percentage of about 30% of cells infected with the virus containing the epitopes in the E3-19K, ICOVIR-15K-E3OG, while no presentation of this epitope was detected either in the negative controls (cells incubated with gp100$_{25}$ peptide or infected with ICOVIR-15K parental virus) or in the cells infected with the virus displaying the epitopes in the HI-loop, ICOVIR-15K-HIOG (**Figure 51a**). Despite deficiencies in TAP expression had been reported in B16 cells, downregulation of other components of the MHC-I pathway such as tapasin are also responsible for the low MHC class I molecules displayed on the cell surface (Seliger *et al.*, 2001). Taking this into account and combined with the low K^b/OVA presentation in the positive control of cells incubated with the peptide alone (which is supposed to be the maximum levels of OVA$_{257}$ presentation), it may explain the reason why, although ICOVIR-15K-E3OG should be able to process and present the epitope in a TAP-independent manner, no K^b/OVA staining was detected by this technique. Nevertheless, the induction of MHC class I pathway components expression by incubation with IFN-γ, elevated the K^b/OVA staining to 100%. Of note, ICOVIR-15K-HIOG was not able to induce OVA$_{257}$ presentation in this condition either, although the fiber protein is processed by the proteasome following the classical pathway. Strikingly, even in this scenario, where no deficiency in the MHC class I pathway is supposed to occur, the location of the epitopes in E3-19K protein provided a great advantage to the processing and presentation of the exogenous epitope.

Similar results were observed in the TRAMPC2 model. Importantly, OVA$_{257}$ presentation was also observed in the IFN-γ-depleted conditions after the infection with ICOVIR-15K-E3OG, and at similar levels to the presentation in cells incubated with the peptide alone (**Figure 51b**). Probably, this could be explained by the higher basal surface levels of H-2K^b expression in TRAMPC2 cell line compared to B16CAR.

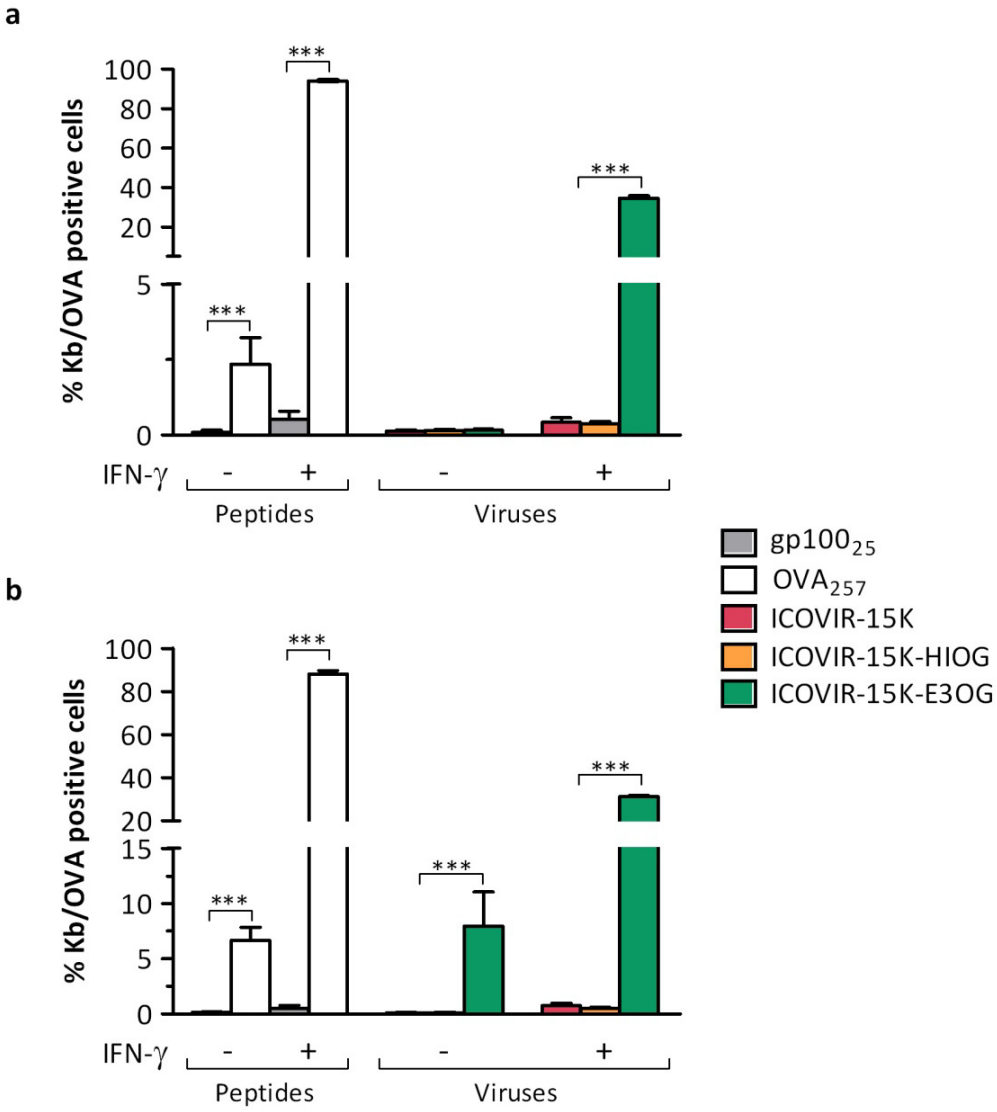

Figure 51. H-2K^b/OVA presentation *in vitro*. (a) B16CAR or (b) TRAMPC2 cells were infected at 100 MOI with ICOVIR-15K, ICOVIR-15K-HIOG or ICOVIR-15K-E3OG or incubated with gp100$_{25}$ or OVA$_{257}$ peptides as negative or positive control, respectively. 24 hours later, cells were tripsinized and stained with anti-Kb/OVA antibody (25-D1.16) for 30 minutes in ice. Fluorescence was analyzed by flow cytometry. In the IFN-γ positive conditions, this cytokine was added 24 hours prior to the infection (that is, 48 hours before the analysis). Mean values of percentage of Kb/OVA positive cells +SD are plotted. ***, p<0.0001 by one-way ANOVA test and Tukey post-hoc test. IFN-γ, interferon gamma.

2.3.2. Mechanisms of TAP-independency

In order to further explore and understand the mechanisms responsible for the increased surface presentation of OVA$_{257}$ epitope in TAP-deficient tumor cells when they were infected with an oncolytic adenovirus which genetically incorporates this epitope into E3-19K adenoviral protein, different approximations were followed.

2.3.2.1. Expression levels of fiber and E3-19K in infected murine cell lines

One hypothesis to explain this important advantage provided by the location of the exogenous epitopes in E3-19K rather than the fiber was that mouse cells can express early proteins, such as E3-19K, after the infection with human adenoviruses, but expression of late proteins, such as fiber, might be hampered. This would favor immunogenicity from E3-19K regardless of the putative TAP-independency of the epitopes.

Expression of both fiber and E3-19K was analyzed by western blot in B16CAR and TRAMPC2 mouse tumor cell lines after the infection with the parental virus, ICOVIR-15K. As a positive control of an adenovirus-permissive cell line, A549 human cells were used. Even though both proteins analyzed were expressed in higher levels in A549 infected cells than in B16CAR or TRAMPC2, fiber and E3-19K expression was detected in all cell lines 24 hours post-infection with no higher E3-19K levels in any case (**Figure 52**). This evidence denied the postulated hypothesis based on differential expression, strengthening our initial hypothesis based on the location of exogenous epitopes in ER-targeted E3-19K to overcome TAP deficiencies in tumor cells.

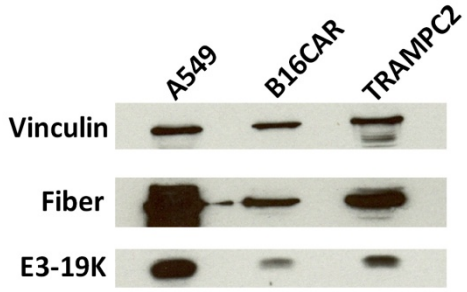

Figure 52. Fiber and E3-19K expression in murine cell lines. B16CAR and TRAMPC2 murine cell lines were infected at 100 MOI with ICOVIR-15K virus. A549 human cell line was used as positive control of adenoviral gene expression and was infected with ICOVIR-15K at 25 MOI. 24 hours after the infection, cells were harvested, lysed and expression of E3-19K and fiber was analyzed by Western Blot. Vinculin was used as loading control.

2.3.2.2. TAP-independent presentation demonstrated by using mutant adenoviruses and inhibitors

A more directed way to demonstrate the importance of E3-19K ER-localization and furin sites for the TAP-independent epitope presentation was based on the use of mutant viruses and inhibitors. One mutant virus was constructed by deleting the E3-19K ER-targeting signal sequence from the NH2-terminal of the protein in order to avoid its traffic to the ER and, consequently, the TAP-independent processing pathway. This virus was named ICOVIR-15K-SSdelE3OG. Additionally, the furin-sensitive linkers of ICOVIR-15K-SSdelE3OG (RVKR) were replaced by non-

cleavable sequences (VRVV) to avoid the processing of the epitopes in the secretory compartments, generating the adenovirus ICOVIR-15K-SSdelE3OGFR. **Figure 53** shows a schematic representation of the modifications included in the mutant adenoviruses.

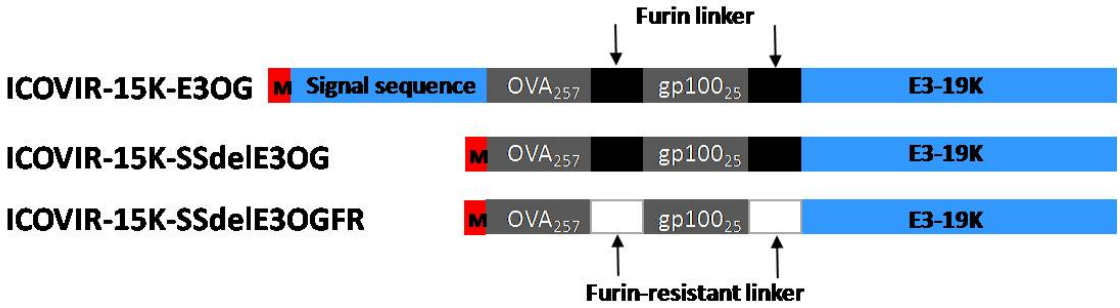

Figure 53. Schematic representation of the construction of the mutant adenoviruses. Two additional mutant viruses were constructed by deleting the ER-targeting signal sequence (ICOVIR-15K-SSdelE3OG) and by combining this deletion with the replacement of the furin linkers by furin-resistant linkers (ICOVIR-15K-SSdelE3OGFR). M, methionine.

To check that these additional modifications were not affecting the viability of the adenoviruses, cytotoxicity in A549 cell line was tested in comparison with the parental virus ICOVIR-15K.

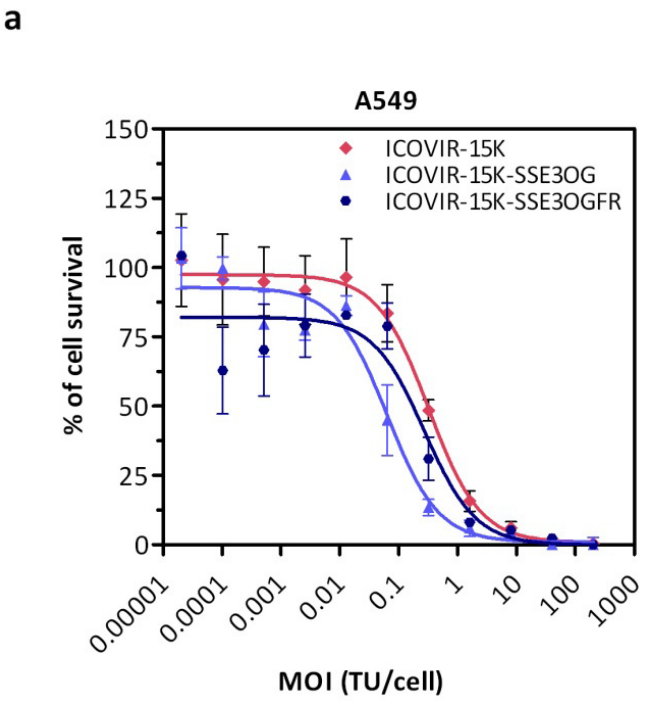

b

Virus	IC_{50} (TU/cell)	Cytotoxicity fold-increase versus ICOVIR-15K
ICOVIR-15K	0.3218	-
ICOVIR-15K-SSdelE3OG	0.06335	5.1 *
ICOVIR-15K-SSdelE3OGFR	0.2733	1.2

Figure 54. Cytotoxicity of control adenoviruses in A549 cells. (a) Dose-response curves obtained by non-linear regression. A549 cells were infected with 1:5 serial dilutions of ICOVIR-15K, ICOVIR-15K-SSdelE3OG or ICOVIR-15K-SSdelE3OGFR starting at 300 MOI and cell viability was determined by BCA staining on day 6 post-infection. Mean ±SD is plotted (b) IC_{50} values for each virus are represented. Cytotoxicity increase versus parental virus ICOVIR-15K is also represented. * significant ($p<0.05$) compared to ICOVIR-15K by extra sum-of-squares F test. MOI, multiplicity of infection; TU, transducing units.

Surprisingly, whereas ICOVIR-15K-SSdelE3OGFR presented a similar IC_{50} value than the parental virus, ICOVIR-15K-SSdelE3OG resulted significantly more cytotoxic, with a 5-fold lower IC_{50} value than ICOVIR-15K. However, we did not consider this difference relevant for K^b/OVA presentation studies (**Figure 54a** and **b**).

The main function of E3-19K is to bind and to retain the heavy chains of MHC class I molecules in the ER, preventing CTL response to adenoviral infection (Cox *et al.*, 1991; Hermiston *et al.*, 1993; Jackson *et al.*, 1993). Despite this interaction is described for human MHC class I and some murine haplotypes, H-$2K^b$ surface expression is not affected by the infection with adenovirus, indicating that E3-19K is not interacting with this molecule (Tanaka and Tevethia, 1988). Since we wanted to demonstrate that the deletion of the ER-targeting signal sequence changed the intracellular localization of E3-19K from the ER to the cytoplasm, human HLA-A2 levels in TRAMPC2-A2 cells (TRAMPC2 cells stably transfected with HLA-A2) infected with the different adenoviruses were determined. As it is shown in **Figure 55a**, HLA-A2 levels significantly decreased from 90% to 70% when the cells were infected with the viruses containing the wild type version of E3-19K protein. However, when they were infected with the viruses containing the deletion of the ER-targeting signal, surface expression of HLA-A2 reached almost the same levels than in non-infected cells (85%). This demonstrates that, in this case, the signal sequence-deleted E3-19K was not interacting with HLA-A2. Furthermore, no reduction of H-$2K^b$ levels was observed after the infection with any of the adenoviruses, regardless of whether E3-19K was wild type or mutated (**Figure 55b**).

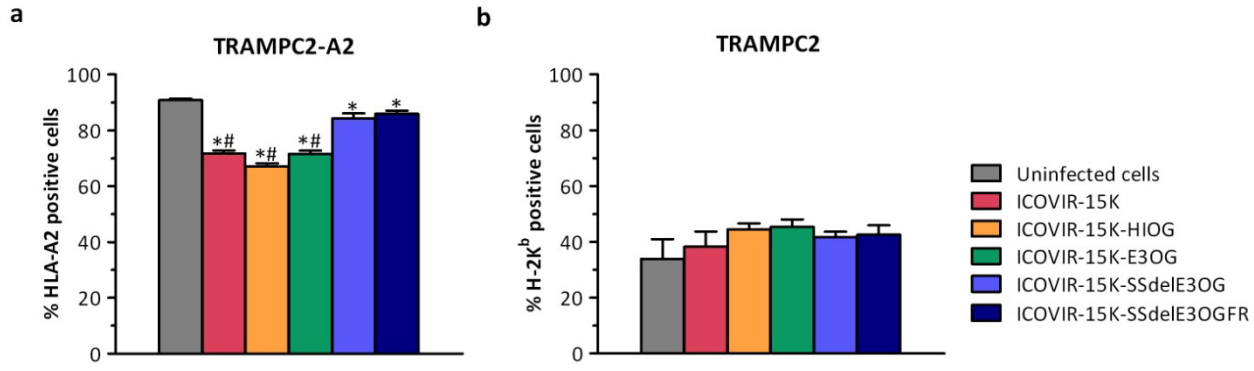

Figure 55. MHC-I levels in TRAMPC2 after the infection with different adenoviruses. (a) TRAMPC2-A2 or (b) TRAMPC2 were infected with the different adenoviruses at 100 MOI. 24 hours post-infection, HLA-A2 and H-2K^b MHC-I surface levels were quantified by flow cytometry. Mean values of percentage of positive cells +SD are plotted. *, significant ($p<0.05$) with respect to uninfected cells. #, significant ($p<0.05$) with respect to ICOVIR-15K-SSdelE3OG and ICOVIR-15K-SSdelE3OGFR, according to one-way ANOVA test and Tukey post-hoc test.

The ideal scenario to perform OVA$_{257}$ presentation experiments with these control viruses was a TAP-deficient cell line with no other affected component of the epitope presentation pathway, in contrast to the previously used tumor cell lines B16CAR and TRAMPC2. We had two different cell lines available which met the desired characteristics: T2-K^b and RMA/S. However, given the lymphoblastic origin of both cell lines, adenoviruses were not able to infect them. In an attempt to increase the infectivity of these cell lines, the adenoviruses ICOVIR-15K-SSdelE3OG and ICOVIR-15K-SSdelE3OGFR were reconstructed by changing RGD position from the shaft of the fiber (RGDK mutation) to the HI-loop of the fiber (RGD mutation) which is supposed to increase infectivity in this kind of cells. However, we did not succeed in this goal (results not shown). Given the unavailability of an infectable TAP-deficient cell line, these experiments were performed in the TAP-competent cell line P815K^b, which is a mouse lymphoblast-like mastocytoma cell line stably transduced with H-2K^b gene, and which has been widely used in immunological studies. To induce a TAP-deficient scenario, different inhibitors were included. Given the unavailability of a TAP inhibitor, the classical pathway of antigen processing was blocked by a highly specific proteasome inhibitor, lactacystin (LC), which was used to force TAP-independent pathways. Brefeldin A (BFA) was used as positive control of inhibition since it blocks protein transport from the ER to the Golgi apparatus.

The results obtained in B16CAR and TRAMPC2 were reproduced in P815K^b, detecting almost 40% of OVA$_{257}$ presentation in cells infected with ICOVIR-15K-E3OG while no presentation was detected after the infection with ICOVIR-15K-HIOG (**Figure 56a**). The deletion of the ER-targeting signal sequence of the E3-19K caused a 50% reduction in the presentation of OVA$_{257}$ peptide when compared to the virus containing the signal sequence. Moreover, upon infection with a

virus in which this deletion of the ER-targeting signal was combined with the replacement of the furin-sensitive linkers by furin-resistant linkers, the surface expression of H-2K^b/OVA$_{257}$ complexes was completely abrogated, evidencing the implication of the TAP-independent presentation pathway (**Figure 56b**). Importantly, the presentation of OVA$_{257}$ upon the infection of the cells with ICOVIR-15K-E3OG was not affected by proteasome inhibition with LC, demonstrating that OVA$_{257}$ processing was not dependent on the classical presentation pathway. However, we found that the inhibition of the proteasome further reduced the presentation of OVA$_{257}$ by the signal sequence-deleted adenovirus, suggesting that, in this case, the TAP-dependent pathway was involved. As expected, the treatment of the cells with BFA, which was the positive control of inhibition, completely abrogated the surface presentation of H-2K^b/OVA$_{257}$ complexes upon the infection with all viruses (**Figure 56b**).

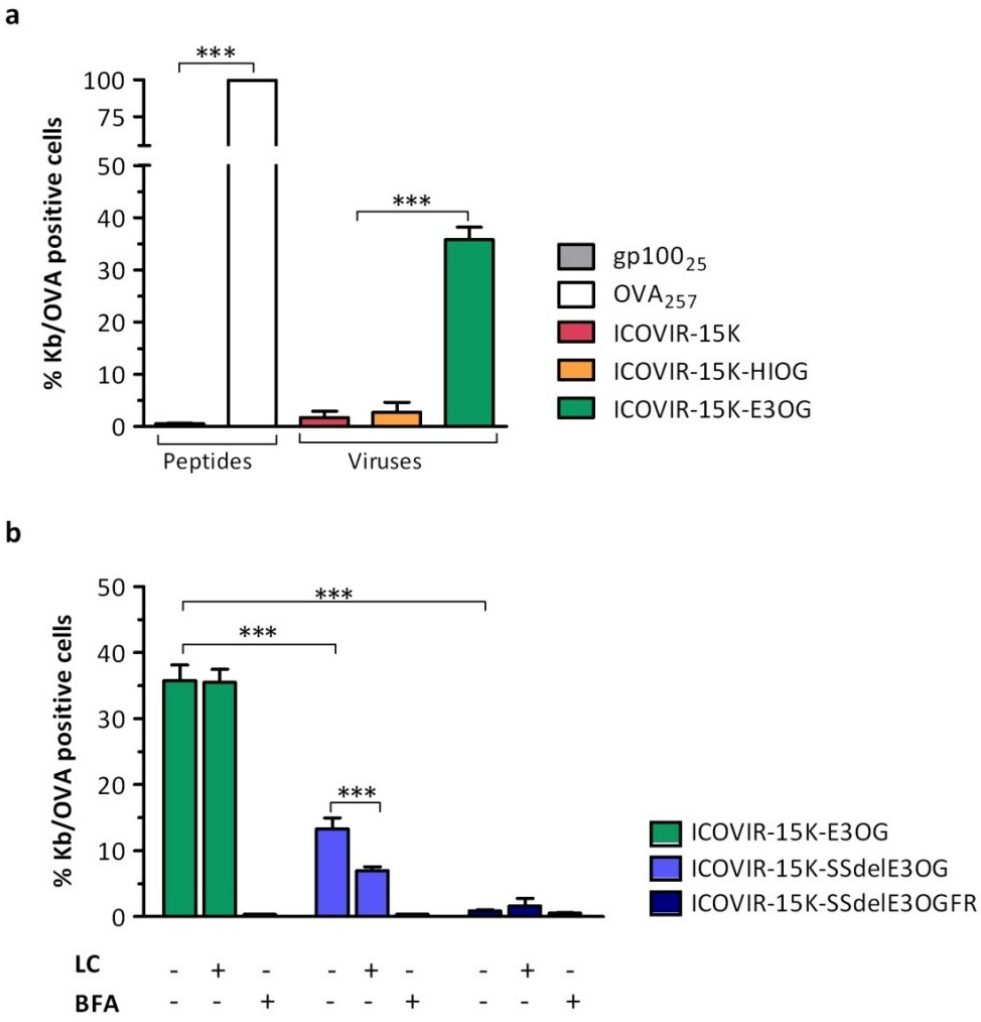

Figure 56. Analysis of the TAP-independent mechanisms. (a) P815K^b cells were infected at 200 MOI with the different adenoviruses or incubated with gp100$_{25}$ and OVA$_{257}$ peptides as negative and positive control, respectively, during 24 hours. (b) P815K^b cells were infected at 200 MOI with the mutant adenoviruses and lactacystin (LC) or brefeldin A (BFA) were added to the cells during 24 hours at 10 µM and 5 µg/mL respectively. Then, cells were stained with anti-Kb/OVA antibody (25-D1.16) for 30 minutes in ice. Fluorescence was analyzed by flow cytometry. ***, p<0.0001 by one-way ANOVA test and Tukey post-hoc test. LC, lactacystin; BFA, brefeldin A.

2.4. SPECIFIC CTL IMMUNE RESPONSES GENERATED UPON THE IMMUNIZATION OF IMMUNOCOMPETENT MICE WITH THE ONCOLYTIC ADENOVIRUSES

Once the TAP-independent mechanism of presentation of the epitopes located in the E3-19K and that this location is much more efficient than the HI-loop of the fiber was demonstrated, the next step was to evaluate if this location was able to generate an immune response against the exogenous epitopes *in vivo,* and in such case, if the responses were comparable to the generated by viral epitopes.

2.4.1. Specific CTL immune responses upon intravenous immunization

In a first approach, C57BL/6 immunocompetent mice were injected intravenously with PBS or $3x10^{10}$ viral particles of ICOVIR-15K-HIOG or ICOVIR-15K-E3OG. On day 7 post-administration mice were sacrificed, spleens removed, and splenocytes obtained. Presence of specific T cells was analyzed by anti-IFN-γ ELISpot, which allows the simultaneous evaluation of the response against different epitopes. As a positive control of anti-adenovirus immune response we used an epitope from the early protein E1B, which is immunodominant in mice, $E1b_{192}$ (Toes *et al.*, 1995) and another one from the late protein hexon, Hex_{418}, that has been previously defined by our group to have a high affinity for $H\text{-}2D^b$ by in-silico epitope prediction informatic softwares (Gil-Hoyos, 2014). Splenocytes were also stimulated with the peptides of interest: OVA_{257} and $gp100_{25}$.

After this protocol of single direct intravenous immunization, the dominant immune response was generated against E1b. An unexpected finding, since E1b is not modified in any of these viruses, was that significantly lower responses against the viral epitope were detected in the animals injected with ICOVIR-15K-E3OG. Lower responses were detected against the hexon, since it is a late protein expressed at lower levels in mouse cells. Specific responses against OVA_{257} epitope were detected in both groups, regardless of the exogenous epitope location. However, these responses were low and not statistically significant compared to the PBS group. No specific response was detected against $gp100_{25}$ in any group (**Figure 57**). Note that, in this intravenous immunization with viruses, no tumors are present in the animals and therefore we could not expect an advantage of the TAP-independent epitope presentation.

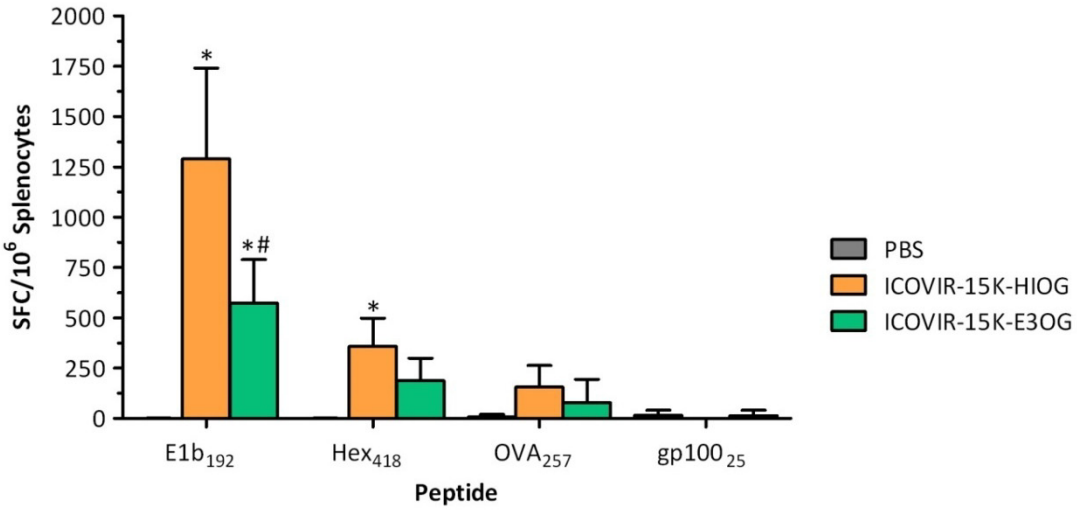

Figure 57. Analysis of the immune response upon systemic immunization. C57BL/6 immunocompetent mice were injected intravenously with PBS or $3x10^{10}$ viral particles of ICOVIR-15K-HIOG or ICOVIR-15K-E3OG. 7 days after the immunization, animals were sacrificed and splenocytes were isolated and analyzed by anti-IFN-γ ELISpot technique. Mean + SD is plotted (n=3-4 animals/group). *, significant ($p<0.05$) compared to PBS group. #, significant ($p<0.05$) compared to ICOVIR-15K-HIOG group, according to a two-way ANOVA test.

2.4.2. Specific CTL immune responses upon immunization by subcutaneous implantation of infected TAP-deficient cells

In order to create a scenario in which the effect of the TAP-independent epitope processing pathway was potentiated, animals were immunized subcutaneously with the TAP-deficient tumor cells, B16CAR or TRAMPC2, infected with the parental adenovirus ICOVIR-15K, ICOVIR-15K-HIOG or ICOVIR-15K-E3OG. Moreover, this setting also mimics the oncolytic situation, in which the virus would be inside the tumor cells. One week after the immunization, mice were sacrificed and the splenocytes were analyzed by ELISpot. Even though the virus was administered inside the tumor cells, we could also found response against viral antigens. In the case of the response against the late protein hexon epitope Hex_{418}, it was much lower compared to the direct virus injection in blood in both models. In contrast, the response against the early epitope $E1b_{192}$ was similar to the one obtained with direct virus injection, and no significant differences between viruses were observed in this case.

Focusing on the exogenous epitopes, epitope location in E3-19K was more immunogenic than in the fiber: higher levels of OVA_{257} -specific IFN-γ secretion were detected from splenocytes of animals immunized with the virus containing the epitopes in E3-19K compared to animals immunized with the virus displaying the epitopes in the HI-loop of the fiber. This observation was consistent in both tumor models, B16CAR and TRAMPC2. In the first one, specific immune response against OVA_{257} epitope was only significant for the ICOVIR-15K-E3OG group compared

to the mock group (**Figure 58a**). In an attempt to correct for the high variability of the response among animals, the response against the exogenous epitopes was plotted in relation to the anti-E1b response for each animal (tumor-to-viral immune response ratio), since $E1b_{192}$ is immunodominant in H-2^b mice and we assumed that the response mounted against it would be the highest achievable response. In this plotting, the response against OVA was significant for both groups of viruses displaying the epitopes when compared to mock or ICOVIR-15K groups. Of note, the anti-OVA response in animals immunized with B16CAR cells infected with ICOVIR-15K-E3OG was significantly higher compared to all other groups (**Figure 58b**). More remarkable were the results observed in TRAMPC2, model in which differences between the viruses incorporating the epitopes in different locations were more pronounced (**Figure 59a** and **b**).

Regarding $gp100_{25}$ epitope, different results were observed in both models. In the case of B16CAR, no activation of specific CTLs was observed with splenocytes from animals immunized with ICOVIR-15K-E3OG, whereas the immunization of these animals with ICOVIR-15K-HIOG was able to generate significant immune response against gp100 (**Figure 58c**). In contrast, similar results to those found for OVA_{257} were observed in TRAMPC2 model for $gp100_{25}$ epitope, with a significantly higher immune response in animals immunized with ICOVIR-15K-E3OG than with ICOVIR-15K-HIOG (**Figure 59c**). It is important to highlight that this result demonstrates that the immunization with an adenovirus incorporating this peptide could break immunotolerance to the self-antigen gp100.

It is also worth noticing that the plotting of the tumor-to-viral epitopes immune response ratio, which is the response generated against exogenous epitopes relative to the viral epitope $E1b_{192}$, allows the assessment of the putative immunodominance shift. In the case of specific anti-OVA_{257} immune responses, the levels of anti-viral responses in both models (i.e. 100%) after the immunization with the virus presenting the epitopes in a TAP-independent manner were almost reached, thus compensating virus epitope immunodominance (**Figure 58b** and **Figure 59b**). This observation provides clear evidences that the novel location for exogenous epitopes in E3-19K is capable of changing the immunodominance of viral epitopes in favor of exogenous epitopes.

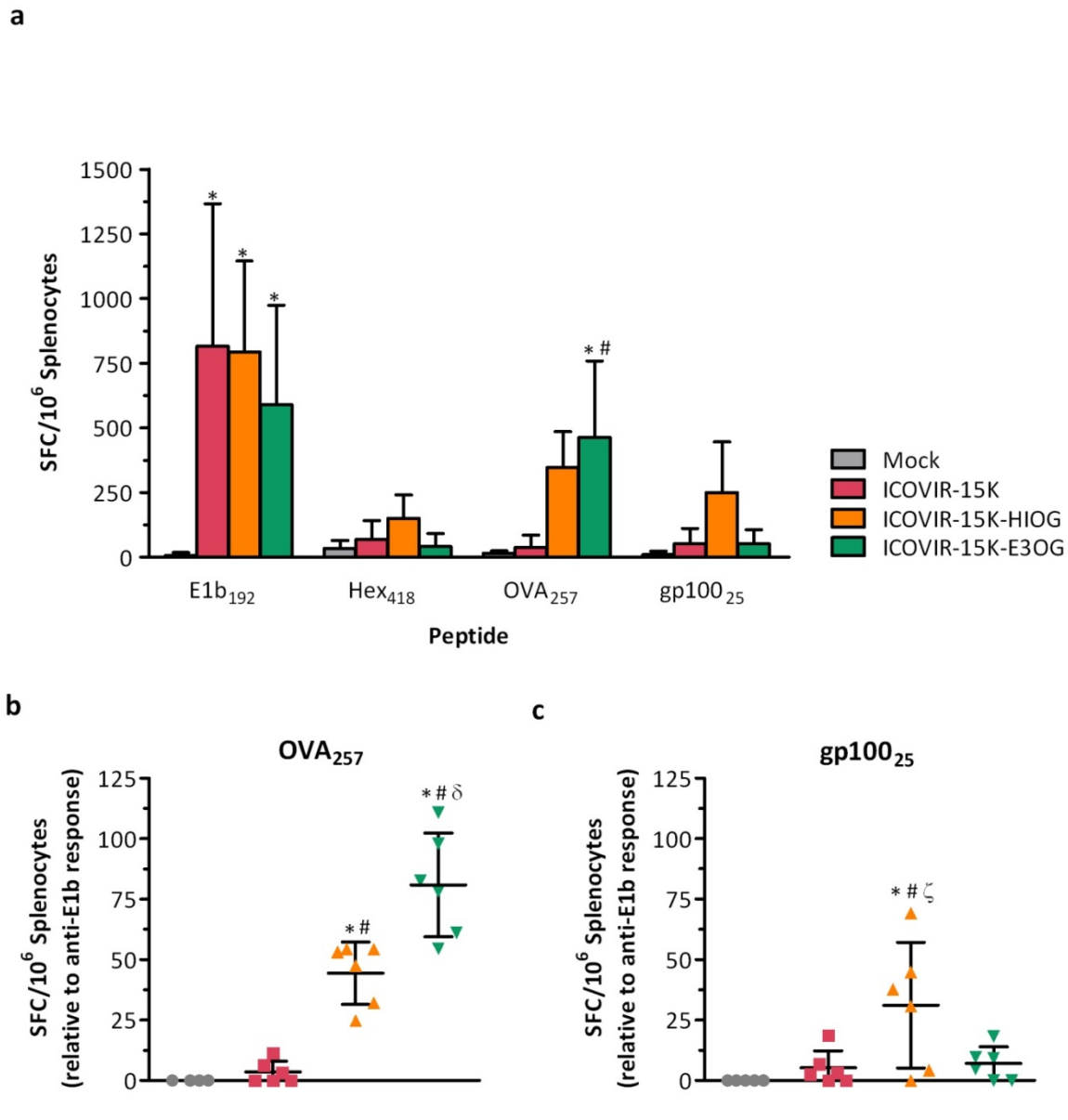

Figure 58. Immune response generated *in vivo* after the immunization with infected B16CAR cells. C57BL/6 immunocompetent mice were injected subcutaneously with $1x10^6$ cells per flank of B16CAR cells which had been previously infected during 4 hours at 100 MOI with the parental virus, ICOVIR-15K, or the viruses containing the epitopes, ICOVIR-15K-HIOG or ICOVIR-15K-E3OG. As negative control (mock), uninfected cells were used. 7 days post-implantation, mice were sacrificed and splenocytes were isolated and analyzed by anti-IFN-γ ELISpot. (a) Spots forming colonies (SFC) per each $1x10^6$ splenocytes are represented. Mean +SD is plotted (n=5-6 animals/group). *, significant ($p<0.05$) compared to mock group. #, significant ($p<0.05$) compared to ICOVIR-15K group, according to a two-way ANOVA test. (b) Specific immune response against OVA_{257} and $gp100_{25}$ epitopes is represented relative to the immune response against $E1b_{192}$ for each animal, since response against E1b is the maximum that any animal can achieve and it is linearly correlated to anti-OVA and anti-gp100 responses. Mean ± SD is plotted (n=5-6 animals/group). *, significant ($p<0.05$) compared to mock group. #, significant ($p<0.05$) compared to ICOVIR-15K group. δ, significant ($p<0.05$) compared to ICOVIR-15K-HIOG group. ζ, significant ($p<0.05$) compared to ICOVIR-15K-E3OG group according to one-way ANOVA test.

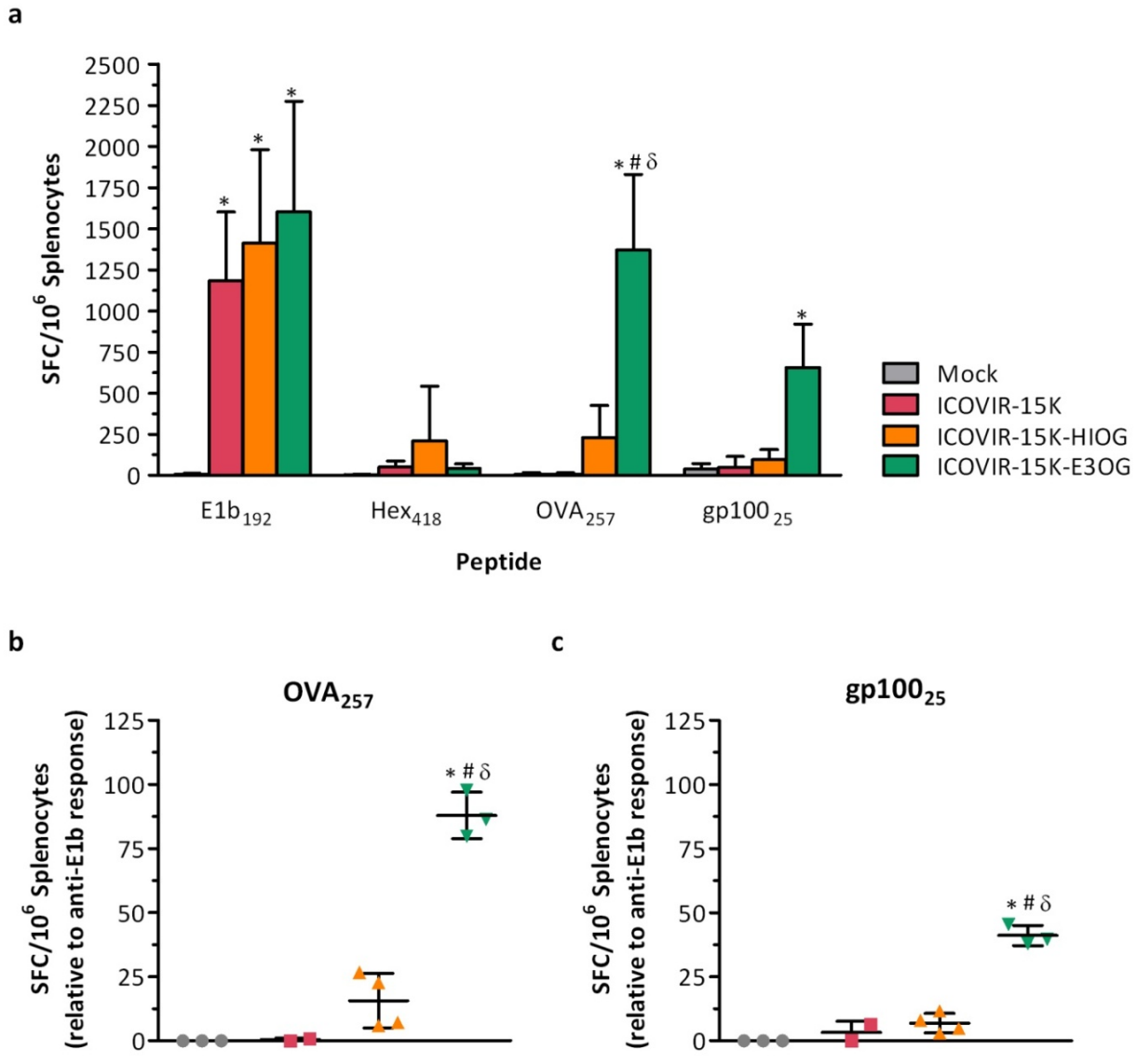

Figure 59. Immune response generated *in vivo* after the immunization with infected TRAMPC2 cells. C57BL/6 immunocompetent mice were injected subcutaneously with $1x10^6$ cells per flank of TRAMPC2 cells which had been previously infected during 4 hours at 100 MOI with the parental virus, ICOVIR-15K, or the viruses containing the epitopes, ICOVIR-15K-HIOG or ICOVIR-15K-E3OG. As negative control (mock), uninfected cells were used. 7 days post-implantation, mice were sacrificed and splenocytes were isolated and analyzed by anti-IFN-γ ELISpot. (a) Spots forming colonies (SFC) per each $1x10^6$ splenocytes are represented. Mean + SD is plotted (n=2-5 animals/group). *, significant ($p<0.05$) compared to mock group. #, significant ($p<0.05$) compared to ICOVIR-15K group. δ, significant ($p<0.05$) compared to ICOVIR-15K-HIOG group, according to a two-way ANOVA test. (b) Specific immune response against OVA_{257} and $gp100_{25}$ epitopes is represented relative to the immune response against $E1b_{192}$ for each animal, since response against E1b is the maximum that any animal can achieve and it is linearly correlated to anti-OVA and anti-gp100 responses. Mean ± SD is plotted (n=5-6 animals/group). *, significant ($p<0.05$) compared to mock group. #, significant ($p<0.05$) compared to ICOVIR-15K group. δ, significant ($p<0.05$) compared to ICOVIR-15K-HIOG group according to one-way ANOVA test.

2.4.3. Antitumor efficacy of the specific CTL immune responses generated upon immunization by subcutaneous implantation of infected TAP-deficient cells in a murine model of melanoma

The next step was to test if the exogenous epitope-specific immune responses had also antitumor properties in a tumor-challenge experiment. Even though the results on OVA_{257} presentation *in vitro* and also on the generation of specific CTL immune responses *in vivo* were better in TRAMPC2, the B16CAR model was chosen for the evaluation of antitumor activity. This choice was based on the fact that B16CAR already expresses high levels of the melanoma-associated antigen gp100, and that we had available the OVA-expressing B16CAROVA cell line. In contrast, TRAMPC2 cell line does not express gp100 nor OVA antigens. Therefore, C57BL/6 immunocompetent mice were immunized, as previously, by subcutaneous administration of B16CAR cells infected with the different viruses. One week after the immunization, B16CAROVA tumors were implanted subcutaneously in the flanks of the mice. Animals were monitored three times per week in order to control tumor formation and growth. For all groups, tumors started to appear after day 7 post-implantation. However, whereas on day 12 post-implantation 100% of the tumors had appeared in animals from mock, ICOVIR-15K, and ICOVIR-15K-HIOG groups, only 60% of tumors had appeared in the ICOVIR-15K-E3OG group at this time point. Nevertheless, by the end of the experiment, all tumors implanted had been formed, indicating that the immunization with cells infected with ICOVIR-15K-E3OG was not able to completely prevent tumor growth, although it delayed its appearance (**Figure 60a**). With regard to tumor growth, tumors from animals immunized with B16CAR infected with the parental oncolytic adenovirus ICOVIR-15K or with the virus containing the epitopes in the HI-loop, ICOVIR-15K-HIOG, followed the same course than in animals immunized with uninfected cells (mock group). Strikingly, the immunization with ICOVIR-15K-E3OG-infected B16CAR cells was able to significantly reduce tumor growth compared to the other groups. Moreover, the mean size of these tumors was almost 4 times smaller than mock-treated animals and around 3-fold smaller than tumors from ICOVIR-15K or ICOVIR-15K-HIOG groups (**Figure 60b**). Kaplan-Meier survival curves analysis revealed that the only treatment that could significantly increase the survival time compared to the other 3 groups was that of ICOVIR-15K-E3OG (**Figure 60c**).

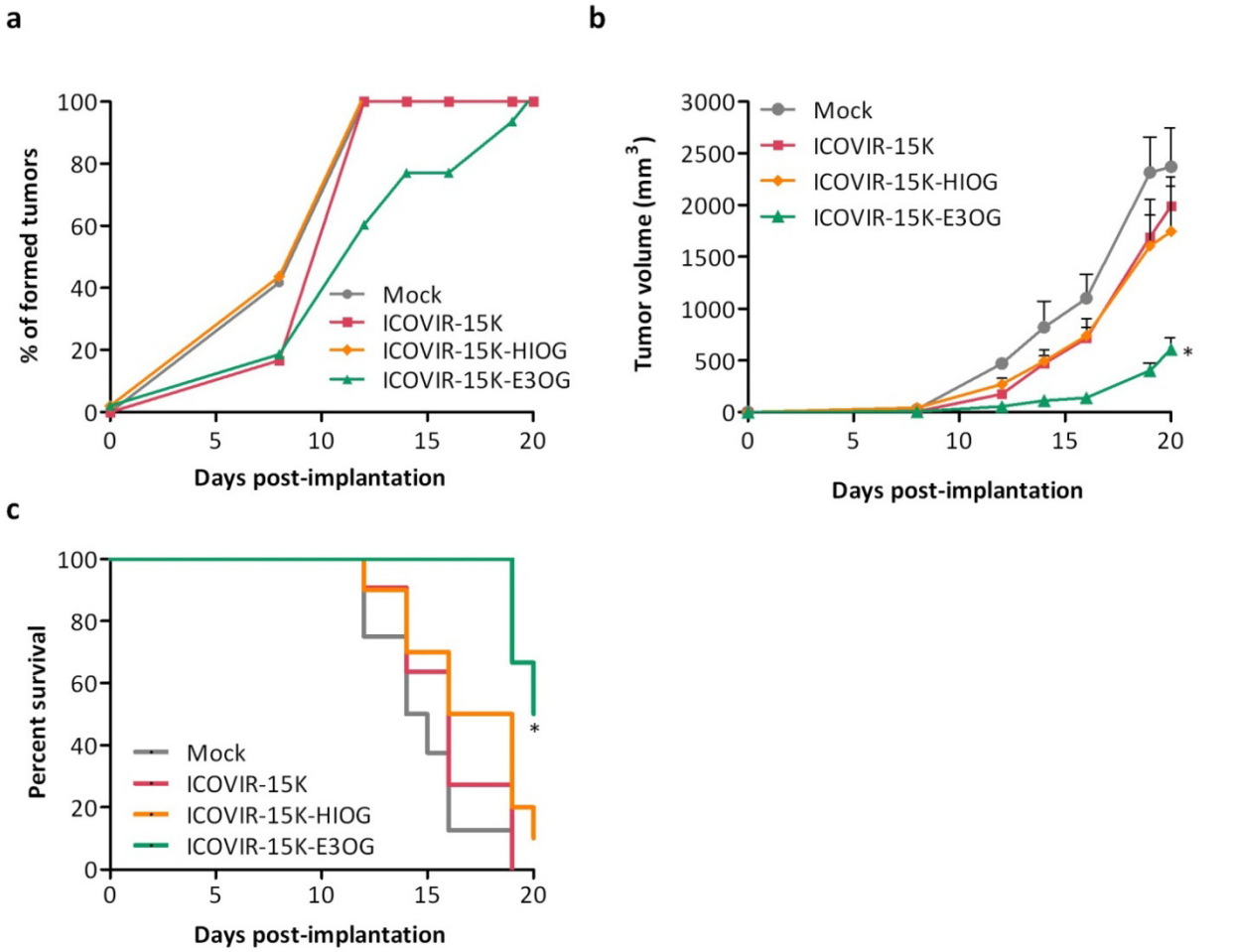

Figure 60. Efficacy of the antitumor immune response in B16CAROVA tumors model. C57BL/6 immunocompetent mice were injected subcutaneously with $1x10^6$ cells per flank of B16CAR cells which had been previously infected during 4 hours at 100 MOI with the parental virus, ICOVIR-15K, or the viruses containing the epitopes, ICOVIR-15K-HIOG or ICOVIR-15K-E3OG. As negative control (mock), uninfected cells were used. 7 days after the immunization, B16CAROVA tumors were implanted subcutaneously in both flanks of the immunized animals ($1x10^6$ cells/flank) and tumor growth was monitored. (a) Percentage of formed tumors after the implantation of B16CAROVA cells for each group is plotted. (b) Mean values of tumor volume per group +SEM are plotted (n=10-12 tumors/group) *, significant ($p<0.05$) from day 12 compared to mock group. #, significant ($p<0.05$) from day 12 compared to ICOVIR-15K group. δ, significant ($p<0.05$) from day 12 compared to ICOVIR-15K-HIOG group by two-tailed unpaired Student's *t*-test.. (c) Kaplan-Meier survival curves are represented. *, significant ($p<0.05$) by log-rank test compared with mock group.

At the end of the study, on day 20 post-implantation of B16CAROVA tumors, mice were sacrificed and spleens and tumors were collected. Splenocytes were analyzed by ELISpot for specific immune responses against the virus epitopes $E1b_{192}$ and Hex_{418}, and the exogenous epitopes OVA_{257} and $gp100_{25}$. However, stimulation of the splenocytes with these peptides did not generate secretion of IFN-γ, indicating the absence of specific CTLs against the epitopes tested, at least in the spleen and at this time point (**Figure 61b**). We hypothesize that specific CTLs might be inside the tumors and close to lymphatic nodes and, consequently, the ELISpot analysis should have been done with these cells instead of splenocytes. One observation which might support this hypothesis is that total number of isolated splenocytes was significantly lower

in ICOVIR-15K-E3OG group than in the others, indicating that specific T cells could have migrated to the tumor site (**Figure 61a**).

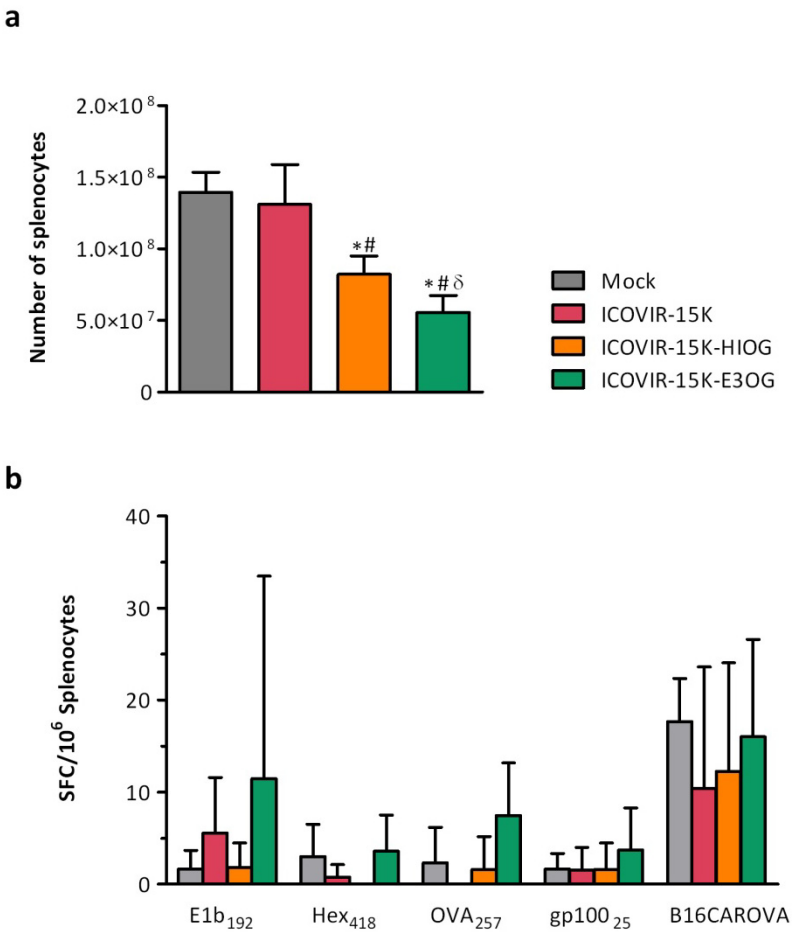

Figure 61. Analysis of the immune response at the end of the antitumor study. C57BL/6 immunocompetent mice were injected subcutaneously with $1x10^6$ cells per flank of B16CAR cells which had been previously infected during 4 hours at 100 MOI with the parental virus, ICOVIR-15K, or the viruses containing the epitopes, ICOVIR-15K-HIOG or ICOVIR-15K-E3OG. As negative control (mock), uninfected cells were used. 7 days after the immunization, B16CAROVA tumors were implanted subcutaneously in both flanks of the immunized animals ($1x10^6$ cells/flank). On day 20 post-implantation, mice were sacrificed and splenocytes were isolated. (a) Total number of viable splenocytes obtained from the spleen of the animals of each group. (b) Splenocytes were analyzed by anti-IFN-γ ELISpot for immune responses against $E1b_{192}$, Hex_{418}, OVA_{257} and $gp100_{25}$. B16CAROVA cells were used also to stimulate the splenocytes. Spots forming colonies (SFC) per each $1x10^6$ splenocytes are represented. Mean+SD is plotted (n=6 animals/group). *, significant ($p<0.05$) compared to mock group. #, significant ($p<0.05$) compared to ICOVIR-15K group. δ, significant ($p<0.05$) compared to ICOVIR-15K-HIOG group by two-tailed unpaired Student's *t*-test.

Despite the substantial antitumor activity observed in animals immunized with ICOVIR-15K-E3OG-infected B16CAR cells, this treatment did not completely prevent the appearance of tumors or induced, complete regressions. Since our designed immunotherapy only targeted two different antigens, OVA and gp100, we hypothesized that tumors which continue growing might have lost or downregulated such antigens to escape the therapy. To confirm this hypothesis, total RNA was extracted from tumors, retrotranscribed to cDNA and both antigens were quantified by quantitative Real Time PCR and normalized with the housekeeping gene β-actin. The results

showed that, although gp100 expression levels were the same for all tumors (**Figure 62a**), result that was confirmed by immunohistochemical staining of paraffin tumor sections (**Figure 62c**), OVA expression in tumors of animals immunized with ICOVIR-15K-E3OG-infected B16CAR was significantly reduced compared to the other groups (**Figure 62b**).

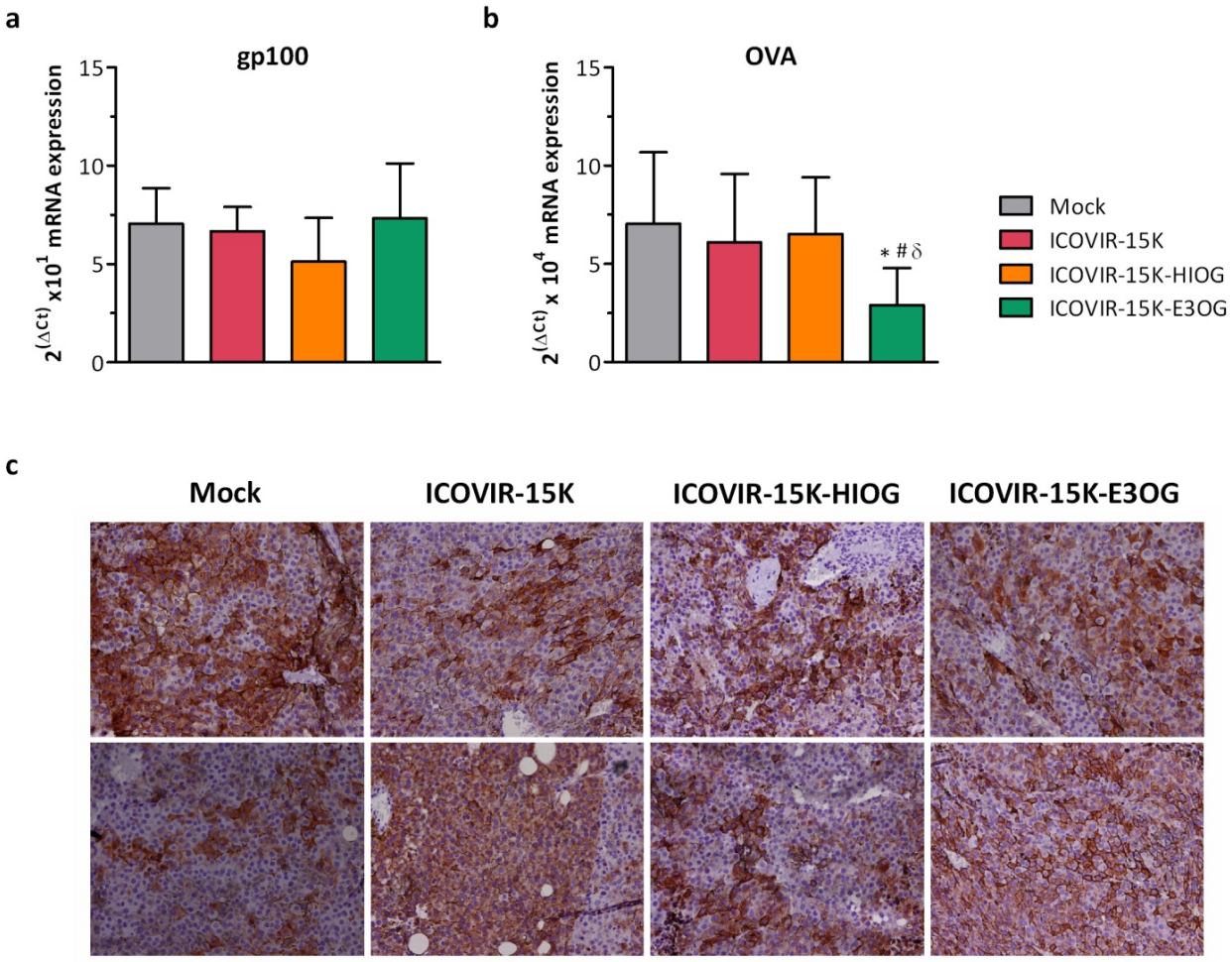

Figure 62. Analysis of OVA and gp100 antigens expression in escaped tumors. C57BL/6 immunocompetent mice were injected subcutaneously with 1x10^6 cells per flank of B16CAR cells which had been previously infected during 4 hours at 100 MOI with the parental virus, ICOVIR-15K, or the viruses containing the epitopes, ICOVIR-15K-HIOG or ICOVIR-15K-E3OG. As negative control (mock), uninfected cells were used. 7 days after the immunization, B16CAROVA tumors were implanted subcutaneously in both flanks of the immunized animals (1x10^6 cells/flank). On day 20 post-implantation, mice were sacrificed and tumors were collected. RNA was extracted from frozen tumors and retrotranscribed to cDNA. Specific real-time PCR was used to amplify and quantify (a) gp100 and (b) OVA mRNA expression levels. $2^{(\Delta Ct)}$ mRNA expression value +SD is plotted. (c) Immunohistochemistry of gp100 was performed in paraffin embedded tumor sections. Original magnification, 200X.

DISCUSSION

1. ICOVIR-17K AS A POTENTIAL CLINICAL CANDIDATE

Oncolytic viruses can potentially eliminate tumor cells directly by lysis or indirectly by immune responses. Antitumor immunity is so appealing that most viruses in clinical trials are armed with immunostimulatory genes (Bartlett *et al.*, 2013; Elsedawy and Russell, 2013). Nevertheless, improving oncolytic traits should not be underestimated and the arrival of the virus to the tumors and intratumoral spread are important factors to be considered (Russell *et al.*, 2012).

The first chapter of this thesis has focused on the development of an oncolytic adenovirus with improved tumor targeting and spread within tumors to become a clinical candidate. Aiming at this goal, two different modifications previously described by our group addressing both of these issues were combined in a single oncolytic adenovirus, ICOVIR-17K: the KKTK to RGDK replacement to improve the persistence in blood of the virus and its antitumor activity after systemic administration (Bayo-Puxan *et al.*, 2009; Rojas *et al.*, 2011), and the expression of hyaluronidase to enhance the intratumoral spread (Guedan *et al.*, 2010). We hypothesized that combining these two modifications in a highly active oncolytic adenovirus of broad applicability as our previously-described ICOVIR-15 (Rojas *et al.*, 2010) would generate an interesting candidate for clinical development. In this context, it is worth highlighting that DNX-2401 (formerly Ad-D24RGD) (Fueyo *et al.*, 2000), a parental virus to ICOVIR-15, has received fast-track designation from the FDA after promising results in a phase I trial in glioblastoma.

A suitable oncolytic adenovirus to be developed in the clinical setting should accomplish several requirements. It has to be genetically stable, be produced at high yields, possess a tolerable selectivity/toxicity profile, and present a potent antitumor activity. After the generation of the oncolytic adenovirus ICOVIR-17K, all these parameters were evaluated in different models.

The insertion of transgenes increases the genome size and could cause packaging defects. ICOVIR-15 genome only exceeds the wild-type Ad5 genome in 151 bp, so it still allows the incorporation of up to ~2 Kb of foreign DNA. In fact, our group has previously armed ICOVIR-15 with different transgenes like the nitroreductase NfsA (~800 bp), the fusogenic protein GALV (~2000 bp), or the PH20 hyaluronidase (~1500 bp) without compromising viral replication (Guedan *et al.*, 2010; Rojas *et al.*, 2010; Guedan *et al.*, 2012). Moreover, it has been described that certain mutations of the KKTK motif of the shaft domain affect the bending or structure of the fiber (Bayo-Puxan *et al.*, 2006; Kritz *et al.*, 2007), which are thought to be required for the efficient receptor interactions to occur (Wu *et al.*, 2003). Neither the replacement of the KKTK by RGDK motif in the adenoviral vector AdTL or in ICOVIR-15K had a negative effect in the viability of

the viruses (Bayo-Puxan *et al.*, 2009; Rojas *et al.*, 2011). However, when together in the same adenovirus, the RGDK mutation and the insertion of the hyaluronidase gene seemed to negatively affect replication at early time points (24 hours post-infection) in some of the cell lines tested (**Figure 21** and **Figure 22**). Nevertheless, at a time point when the first round of replication is completed (72 hours post-infection), the viral yield was the same for ICOVIR-17K and for the virus containing each modification separately, showing normal replication efficiency in all tumor cell lines tested. Comparing the viral yields among different cell lines, the maximum amount of produced virus was obtained in A549 (which is the cell line used for the amplification of the adenoviruses) and almost reached 7500 TU/cell. These levels were only approximated by NP-18 cell line, which achieved 5800 TU/cell of viral production. Viral yields obtained in NP-19, Skmel-28, and HP-1 were 10-fold lower and ranged from 200 and 500 TU/cell. These differences could be related basically to the growing nature of each cell line, which means that in human cell lines with faster growing rates such as A549 and NP-18, viral cycle is also faster, and higher amounts of virus can be achieved *in vitro*. In contrast, NP-9 and Skmel-28 cell lines, present a slower growth rate, producing less amount of virus during the same time. Finally, the low productivity of HP-1 could be explained by its non-human origin and poor permissiveness to human adenovirus replication, topic which is going to be further discussed below.

Another parameter that was tested in order to evaluate the fitness of ICOVIR-17K was the cytotoxicity *in vitro* (**Figure 24**). Of note, as happened with viral production yields, there was a high variability of IC_{50} values among cell lines, ranging from 0.035 (Rwp-1) to 26.15 (SCC-25) TU/cell for ICOVIR-17K. However, since in the specific case of cytotoxicity assay several rounds of replication take place, other reasons more than the cell growth rate are involved. The first observation is that in several cell lines, significant differences between the wild-type adenovirus (AdwtRGDK) and the oncolytic adenoviruses (ICOVIR-15K, ICOVIR-17, or ICOVIR-17K) were detected. In some cases, the non-selective adenovirus was more cytotoxic than the tumor-selective ones (NP-9, BxPC-3, SCC-25, and SCC-29), whereas in other cases it was less cytotoxic (Skmel-28, and MiaPaCa-2). Since the E1A promoter included in the oncolytic adenoviruses is activatable by free E2F-1, levels of this transcription factor among cell lines could have an impact on the activation of the viral cycle in each case. According to this statement, in cell lines with higher levels of E2F-1 the viruses with modified E1A promoters would have an advantage on the activation of viral cell cycle, whereas in the opposite case, the wild-type virus would be benefited. Importantly, in the majority of cell lines tested the cytotoxicity was similar between non-selective and tumor-selective viruses. Comparing the three oncolytic adenoviruses between them, two additional factors might be implicated. On the one hand, the comparison between ICOVIR-17K

and ICOVIR-17 allowed the evaluation of the RGDK mutation relevance. The importance of the integrins and/or HSG on the binding and entry of the adenovirus in the cell and the levels of expression of these receptors in each cell line could affect successive rounds of infection. Indeed, ICOVIR-17 (which was the only virus tested containing the RGD motif in the HI-loop of the fiber) was more cytotoxic than the rest of the adenovirus (all containing the RGDK-mutated fiber) in the cell line Panc-1. In spite of this observation, ICOVIR-17K was equally or more cytotoxic than ICOVIR-17 in 8 out of the 14 cell lines tested. On the other hand, the comparison between ICOVIR-17K and ICOVIR-15K allowed the assessment of the importance of hyaluronidase on the cytotoxicity. These two adenoviruses presented similar IC_{50} values in 11 out of 14 cell lines tested. This result was not surprising since the effect of hyaluronidase was expected to be relevant *in vivo* rather than in cell monolayers *in vitro*, where the potential role of the extracellular matrix is limited. In summary, overall virus yields and cytotoxicity *in vitro* revealed unaffected viability of ICOVIR-17K compared to parental viruses containing RGDK or hyaluronidase modifications separately.

For safety in clinical development we were concerned about the tumor-selective replication of ICOVIR-17K. Impaired viral replication was demonstrated *in vitro* in a model of human pancreatic islets (**Figure 16**). This model was especially relevant since patients with pancreatic cancer are potential candidates for the treatment with ICOVIR-17K and it was important to know if this treatment could cause damage to healthy tissue surrounding the tumor. Moreover, results obtained in pancreatic islets could be extrapolated to most healthy tissues in the body that stay quiescent.

Once the virus was characterized *in vitro*, we proceeded to evaluate its behavior *in vivo*. The lack of an appropriate animal model to evaluate oncolytic adenoviruses is one of the main drawbacks for the progress in the field. This problem derives from the fact that adenoviruses are fairly species-specific and consequently, human adenovirus replicate very poorly in murine cell lines (Jogler *et al.*, 2006). Therefore, the use of immunosuppressed mice with human xenograft tumors is almost the unique choice to evaluate the toxicology and oncolytic potency of adenoviruses. However, the role of the immune system and the effect of the virus on normal tissues cannot be assessed in this model.

Other animal species such as the pig, the cotton rat or the Syrian hamster have been described as semi-permissive for Ad5 replication (Jogler *et al.*, 2006; Steel *et al.*, 2007). Among them, the most feasible to handle in the laboratory is the Syrian hamster. Unfortunately, a major drawback of this model is the general lack of hamster-specific reagents.

For safety studies of ICOVIR-17K, both immunocompetent mice and hamsters were used. Mice are poorly permissive to Ad5 replication; nevertheless, this animal model allows the evaluation of toxicity associated to the capsid and the expression of early adenoviral genes such as E1A. Syrian hamsters are considered semi-permissive to human adenovirus replication and have been used to evaluate the toxicological events related to the expression of late adenoviral genes (Thomas *et al.*, 2006). Despite differential permissiveness of the two models, a similar toxicity profile was observed in both species, suggesting that it is independent of viral replication. The observed toxicity was mainly due to direct infection of liver cells and the consequent expression of early viral proteins. Importantly, since ICOVIR-17K replication is impaired in normal (and in murine) tissues, toxicity was transient and disappeared once the levels of viral proteins decreased in initially infected cells. Accordingly, the adverse events observed were restored to normal at the last time point analyzed in mice and hamsters.

The results on ICOVIR-17K presented in this thesis were complemented by later studies performed by Dr. Marta Giménez-Alejandre for VCN Biosciences company, and were published together (Rodriguez-Garcia *et al.*, 2014). These studies consisted mainly in GLP (Good Laboratory Practice) toxicology and biodistribution analysis in hamsters, performed at TNO Triskelion facilities (Netherlands) (**Figure 63**). The toxicology profile that we observed previously was confirmed by the results obtained in the GLP study, even though different time points were analyzed. A dramatic increase in transaminase levels (65.1-fold for AST and 23.8-fold for ALT) was observed at day 2 post-injection, compared to the 3.4-fold for AST and 7.8-fold for ALT observed at day 7 in our experiment. These results indicated that a peak of toxicity occurs at the first days and then decreases progressively, reaching basal levels at day 8 post-injection (**Figure 63a**). Moreover, biodistribution studies were also consistent with the toxicology profile. Highest levels of viral genomes were detected in the liver at early time points, which is in agreement with previous reports (Bernt *et al.*, 2003; Shayakhmetov *et al.*, 2004; Thomas *et al.*, 2006; Page *et al.*, 2007; Ying *et al.*, 2009), whereas at later time points only residual traces of viral DNA were observed in liver as well as in other non-target organs (**Figure 63b**). These results are especially relevant since they were obtained in the Syrian hamster model, in which certain level of virus replication occurs.

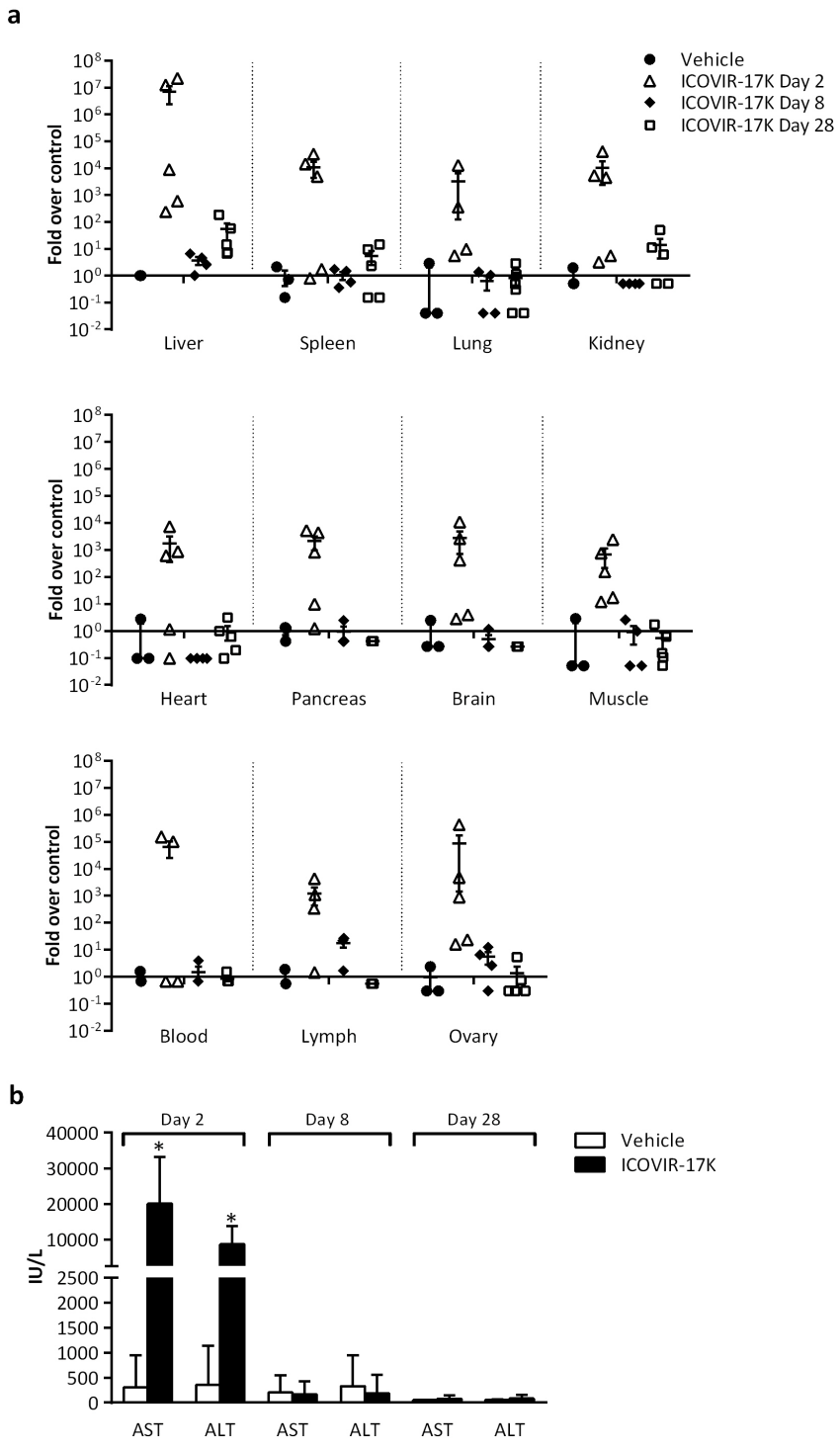

Figure 63. GLP Toxicity and biodistribution study in Syrian hamsters. Immunocompetent Syrian hamsters were treated intravenously with $4x10^{11}$ vp of ICOVIR-17K and sacrificed at indicated time points. (a) Viral amount in different organs was quantified by real-time PCR. ICOVIR-17K genome copies in 100 nanograms of total DNA for vehicle group was set as 1 (control) and data are expressed as number of genome copies fold over control ±SEM (n=4-18 samples/group). (b) The average values for serum transaminase levels are shown. Mean values +SD are depicted. *, ICOVIR-17K significant ($p<0.05$) by Kruskall-Wallis test, compared to vehicle group. ALT, alanine aminotransferase; AST, aspartate aminotransferase; IU, International units.

In summary, ICOVIR-17K toxicology data obtained in the preclinical studies is similar to the previously described for ICOVIR-15, ICOVIR-15K and, ICOVIR-17 (Guedan *et al.*, 2010; Rojas *et al.*, 2011). The detected alterations match with the most common toxicity events reported after systemic administration of adenoviruses in clinical trials (Nemunaitis *et al.*, 2001a; Zhang *et al.*, 2001; Muruve, 2004; Small *et al.*, 2006).

The assessment of the oncolytic potency of ICOVIR-17K was also performed in both animal models. Compared to a virus which has the RGD motif inserted in the HI-loop, the RGDK fiber *shaft* mutation significantly improved the antitumor activity of ICOVIR-17 after a single intravenous administration in two different immunodeficient mice-human tumor xenograft models (Skmel-28 melanoma, and NP-18 pancreatic carcinoma) (**Figure 26**). This improved antitumor efficacy of ICOVIR-17K could be related to the 2.5-fold increase detected in the viremia of injected animals at 6 hours post-administration, which may increase the amount of virus available to reach the tumor sites (**Figure 25**). Even though this increase was not statistically significant in our experiment, the same observation was reported by Dr. Juan José Rojas in the comparison of ICOVIR-15 to ICOVIR-15K (Rojas, 2010). Moreover, this higher viremia of the oncolytic adenoviruses containing the RGDK mutation, especially at early time points, was confirmed in later studies in comparison with their RGD-counterpart viruses, which was consistent with a longer persistence in blood (Rojas *et al.*, 2011; Rodriguez-Garcia *et al.*, 2014). Overall, the better antitumor activity of ICOVIR-17K in two different tumor models is very relevant since ICOVIR-17 was already the result of a series of steps to optimize oncolytic potency, and until the moment it was our most efficacious virus (Guedan *et al.*, 2010).

Efficacy via intratumoral administration was also evaluated as this route has been commonly used to treat tumor types such as pancreatic adenocarcinoma, glioblastoma, and head and neck adenocarcinoma. A single intratumoral injection of ICOVIR-17K significantly reduced tumor growth and increased survival when compared to control group in melanoma Skmel-28 and pancreatic carcinoma NP-9 tumor models (**Figure 30**). Nonetheless, the antitumor activity observed in NP-9 model was lower than in the Skmel-28 model. It is worth mentioning that for Skmel-28, the antitumor efficacy obtained after intravenous administration of ICOVIR-17K was better than upon intratumoral injection (**Figure 26** and **Figure 30**). One feasible reason is that the distribution of the virus within the tumor is more homogenous when given systemically than when injected in one point of the tumor. In NP-9, the limited antitumor activity could be related to the lower viral production yields of ICOVIR-17K in this cell line *in vitro* compared to Skmel-28 (200 TU/cell versus 527 TU/cell, respectively) (**Figure 22**). Moreover, 5.5-fold higher IC_{50} values were also observed in NP-9 than in Skmel-28 (2.476 TU/cell compared to 0.4519 TU/cell) (**Figure 24**).

Despite the encouraging results obtained in mice with xenograft tumors in terms of efficacy, these models are extremely artificial since the role of the immune system, that might be either beneficial or detrimental for the antitumor activity, cannot be determined. For this reason, antitumor activity studies were performed in Syrian hamsters carrying syngenic tumors. Various

hamster tumor cell lines have been reported as permissive for the replication of Ad5, even though this productivity is about 10 to 100-fold lower than in the A549 human cell line (Wold and Toth, 2012). This observation was reproduced in our hands; whereas A549 was able to achieve viral yields of 8700 TU/cell, the pancreatic adenocarcinoma hamster cell line HP-1 could only produce 240 TU/cell of Ad5 (**Figure 21** and **Figure 22d**), which means 36-fold less productivity. This poor replication of the virus together with the difficulty of reaching tumors after systemic administration of oncolytic adenoviruses lead to the observation of only marginal antitumor activity of ICOVIR-17K. However, to our knowledge, this is the first evidence of antitumor activity after intravenous administration of oncolytic adenoviruses in Syrian hamsters, given that most reports in the literature involve intratumoral (Thomas *et al.*, 2006; Spencer *et al.*, 2009) or intraperitoneal administration (Spencer *et al.*, 2009). We also characterized the efficacy of ICOVIR-17K upon the intratumoral route of administration, finding a better antitumor response. It was surprising to find that repeated administrations of the oncolytic adenovirus in three consecutive days not only failed to improve efficacy compared to a single injection but also had no therapeutic effect compared to non-treated animals (**Figure 32**). Consistent with this result, no presence of the virus in tumors was detected in the thrice-administered group at days 7 and 28 post-injection by immune-staining of frozen tumor sections (**Figure 34**). This lack of efficacy after repeated administration was supported also by other study in our group in which the virus was administered three times each 9 days instead of in consecutive days (Personal communication, Dr. Marta Giménez-Alejandre). However, it does not correlate with some studies in the literature in which antitumor activity was reported after intratumoral injections given in 6 consecutive days (Thomas *et al.*, 2008a; Dhar *et al.*, 2009a). Hamsters develop an anti-adenoviral immune response which causes viral clearance and prevents subsequent infection of tumor cells even after intratumoral administration. *A priori*, it could be thought that the effects of neutralizing antibodies (NAbs) might be reduced within the tumor microenvironment. In this sense, Bramson *et al*. reported that pre-existing immunity in a mice model does not affect vector efficacy after intratumoral injection (Bramson *et al.*, 1997). Dhar and colleagues also demonstrated that the effect of pre-existing NAbs on antitumor activity upon intratumoral administration of the virus in immunocompetent hamsters was negligible (Dhar *et al.*, 2009a). However, the same group reported the presence of infiltrating NAbs inside the tumors after intratumoral injection of the oncolytic adenovirus and, furthermore, that the amount of virus in tumors was inversely related with the intratumoral NAbs titer, suggesting its implication in the clearance of the virus (Dhar *et al.*, 2009a). The lack of effect of pre-existing immunity on the antitumor activity could be explained since the generation of NAbs is so rapid after virus administration that pre-existing neutralizing antibodies do not further affect the antitumor

activity (Dhar *et al.*, 2009b). Nevertheless, Thomas and colleagues demonstrated the importance of NAbs in preventing antitumor activity by immunosuppressing the hamsters with cyclophosphamide (CPA). This drug acts by suppressing cytotoxic T lymphocytes, helper lymphocytes and NAbs-mediated responses, and was able to increase the antitumor efficacy of oncolytic adenoviruses by allowing sustained viral replication and oncolysis (Thomas *et al.*, 2008b). Importantly, in CPA-immunosuppressed animals (that were not able to mount an immune response based on NAbs), the presence of pre-existing NAbs against adenovirus had a detrimental effect on the antitumor efficacy of the oncolytic virus. Taking all together, the rational to explain our lack of antitumor activity upon repeated administrations, in disagreement with the results published by other groups, could be related to the dosage used. In our case, the three consecutive injections consisted of $2.5x10^{10}$ vp (equivalent to $6x10^{8}$ TU, taking into account the vp/TU ratio of the viral stock used) compared to $1x10^{10}$ TU on 6 consecutive days used by Dhar and Thomas, which means a 33-fold difference in total dose. The higher doses used in the referenced studies might overcome the presence of NAbs, whereas the lower dose used in our studies would be rapidly neutralized by the pre-existing intratumoral NAbs. In conclusion, the rapid generation of an immune response against the virus injected in the first place would prevent the activity of subsequent injections, at least at the tested dose schedule. Certainly, efficacy studies in Ad5 seropositive models and in combination with immunomodulatory agents will be needed to better understand the potential and limitations of ICOVIR-17K, as well as the study of the NAbs titer in serum and inside the tumors generated after single or repeated administrations of the virus.

Arming oncolytic viruses with extracellular matrix (ECM) degrading enzymes is a commonly exploited strategy to enhance viral penetration of solid tumors (Smith *et al.*, 1997). Different proteins that modulate the configuration of ECM such as decorin, relaxin, metalloprotease 9, or chondroitinase ABC have been used to increase viral spread and antitumor efficacy of oncolytic viruses in different tumor models (Kim *et al.*, 2006; Ganesh *et al.*, 2007; Choi *et al.*, 2010; Dmitrieva *et al.*, 2011; Schafer *et al.*, 2012) . The choice of the appropriate enzyme may depend on the type of tumor to be treated, taking into account specific ECM compositions. For instance, high levels of hyaluronic acid are present in almost 87% of pancreatic adenocarcinomas (Kultti *et al.*, 2012; Jacobetz *et al.*, 2013), which is one of the cancer types with worst prognosis. Therefore, hyaluronidase expression by ICOVIR-17K can provide a particular advantage to treat this tumor type. In addition, early clinical trials have demonstrated that hyaluronidase enhances the efficacy of chemotherapy in cancer patients (Baumgartner *et al.*, 1998). Preclinical studies by Provenzano and coworkers have attributed the beneficial effect of hyaluronidase to a lower insterstitial

pressure in HA-depleted tumors, leading to blood vessel decompression and increased vascular permeability, thereby favoring the penetration of drugs to the tumor core (Provenzano *et al.*, 2012). The administration of hyaluronidase expressed from an oncolytic virus provides further advantages compared to recombinant enzymes. ICOVIR-17K restricts transgene expression to the tumor sites and, consequently, may limit systemic side effects. In fact, a phase II clinical trial testing PEGPH20 in combination with chemotherapy (NCT01839487) was transiently halted recently because of the associated toxicity. Moreover and in contrast to recombinant enzymes which have a relatively short half-life and may require readministrations, a sustained delivery of hyaluronidase could be achieved with a replicating virus. Besides the imaginable hurdles associated to the toxicity and half-life of recombinant hyaluronidase, we were able to demonstrate that in terms of antitumor activity the expression of hyaluronidase by the oncolytic adenovirus ICOVIR-17K was significantly better than the coadministration of soluble hyaluronidase and ICOVIR-15K, at least when the viruses were injected intravenously (**Figure 28**). Importantly, this is the first demonstration of this issue, since previous studies were focused on the demonstration that the antitumor activity of an oncolytic adenovirus could be enhanced by its coadministration with hyaluronidase as well as by its expression from the virus. However, these studies did not compare both strategies between them (Ganesh *et al.*, 2008; Guedan *et al.*, 2010). From a different point of view, this result is also relevant in drug development terms, since the exigencies for the development of two combined treatments are much more demanding.

On the other hand, the studies performed with hyaluronidase in combination with gemcitabine strongly suggest the possibility of combining ICOVIR-17K with this drug, which is the current standard-of-care treatment in pancreatic ductal adenocarcinoma. Moreover, synergistic and/or additive effects between oncolytic adenoviruses and chemotherapeutic drugs including gemcitabine have been reported both at preclinical (You *et al.*, 2000; Raki *et al.*, 2005; Bhattacharyya *et al.*, 2011) and clinical (Hecht *et al.*, 2003) levels. Following these rationales, preliminary studies were performed with ICOVIR-17K and gemcitabine both *in vitro* and *in vivo*. Significantly higher cytotoxicity was observed with the combination of increasing doses of ICOVIR-17K with a fixed concentration of gemcitabine than with the virus alone in 5 out of 7 tumor cell lines tested, with differences ranging from 2.6- to 32.8-fold. It is important to highlight also that the combination of ICOVIR-17K and gemcitabine significantly reduced the IC_{50} values of the virus alone in all the pancreatic cell lines tested.

Studies performed in mice and Syrian hamsters only showed mild cumulative toxicity of ICOVIR-17K and gemcitabine. Importantly, significantly improved antitumor activity was displayed by the combined treatment compared with each treatment alone in a xenograft model of NP-9 pancreatic carcinoma tumors in nude mice. The intravenous administration of ICOVIR-17K together with intraperitoneal gemcitabine was able to cause the complete regression of almost 50% of the tumors, a result that has been only seen in this setting. Nevertheless, when the virus was injected intratumorally this advantage was lost, probably because expression of hyaluronidase might be localized in one focus of the tumor (the injection site) and the penetration of intraperitoneally administered gemcitabine to the tumors might be less efficient. However, studies performed *a posteriori* in hamsters carrying syngenic HP-1 pancreatic carcinoma tumors showed again that the combined treatment had a significantly better antitumor activity than ICOVIR-17K, in this case upon repeated intratumoral administrations, or gemcitabine separately, which only had marginal antitumor effects (Personal communication, Dr. Marta Giménez-Alejandre). The feasibility of the combination of ICOVIR-17K with chemotherapeutic drugs is highly relevant, since the attainment of a successful treatment for this kind of diseases will probably come from the combination of different therapeutic strategies. Additionally, the combination with gemcitabine could be interesting from an immunotherapeutic point of view. It is well characterized that gemcitabine administration cause a reduction of absolute lymphocyte counts, observation that our results also supported (**Figure 37b**). However, it has been reported that this effect is selectively detrimental on the B-lymphocyte subset, whereas antitumor specific T-cell responses were augmented (Nowak *et al.*, 2002). Interestingly, this reduction in B-cell populations might have an additional effect in reducing the undesirable generation of NAbs. Moreover, gemcitabine is described to selectively deplete MDSC and regulatory T cells, both having immunosuppressive functions (Le *et al.*, 2009; Rettig *et al.*, 2011). These observations suggest a favorable setting for the establishment of specific antitumor immune responses provided by gemcitabine, which can also account for the explanation of the better antitumor activity of the combination of oncolytic adenoviruses and gemcitabine in immunocompetent models.

Despite the notable improvement of antitumor activity obtained with ICOVIR-17K, complete tumor regression were rarely seen. Besides ECM and malignant cells, solid tumors contain stromal cells such as cancer-associated fibroblasts (CAFs), endothelial, and inflammatory cells which physically limit viral spread. In this sense, it would be interesting to combine the enzymatic degradation of the ECM by hyaluronidase with a strategy directed to eliminate stromal cells. Lopez and colleagues have described the use of specific promoters, such as the SPARC promoter,

to allow for virus replication in tumor and stromal cells (Lopez *et al.*, 2012). Alternatively, our group recently described that the truncation of the i-leader adenoviral protein enhanced the release and cytotoxicity of the virus in CAFs *in vitro* and increased its antitumor activity *in vivo* (Puig-Saus *et al.*, 2012). Importantly, this oncolytic adenovirus showed synergistic antitumor efficacy combined with gemcitabine in the Syrian hamster model, and the incorporation of this mutation to ICOVIR-17K would be an interesting approach (Puig-Saus *et al.*, 2014).

In conclusion, ICOVIR-17K addresses two of the main limitations in the treatment of cancer with oncolytic adenoviruses: tumor targeting and spread across the ECM barrier. Altogether, the present study supports ICOVIR-17K (named now VCN-01) as a potential candidate for clinical development. Currently, two phase I clinical trials are ongoing; one in pancreatic cancer by endoscopic ultrasound-guided intratumoral injection and another one targeting different tumor types by intravenous administration (EudraCT 2012-005555-16 and EudraCT 2012-005556-42).

2. INCREASING THE IMMUNOGENICITY OF TUMOR EPITOPES INCORPORATED IN ONCOLYTIC ADENOVIRUSES AS AN STRATEGY TO INCREASE ANTITUMOR ACTIVITY

In the second chapter of this thesis we have explored the usefulness of oncolytic adenoviruses from a more “immunocentric” point of view. In this approach, the oncolytic adenovirus is used to disrupt the immunotolerance status in tumors and to promote the development of antitumor specific immune responses. To achieve this goal, it is also important to develop a potent and tumor-selective viral platform. Potency is required since large tumors may need extensive tumor debulking by viral infection and replication in order to be rejected by CTLs. Moreover, tumor cell death produced by oncolytic viruses promotes the release of danger signals that recruit immune cells and tumor-associated antigens (TAAs) that are uptaken by DCs and crosspresented to $CD8^+$ T cells. Selectivity is needed to prevent off-target virus or immune-mediated damage. In this regard, the work presented in the first chapter of this thesis was focused on the development of such selective and potent oncolytic adenovirus. Since the better oncolytic vaccine would ideally combine potent viral oncolysis with an effective and long-lasting antitumor immune response (Lichty *et al.*, 2014), the second chapter has been focused on the stimulation of specific antitumor immune responses by oncolytic adenoviruses using the ICOVIR-15K oncolytic platform (Rojas *et al.*, 2011).

Several strategies have been developed by different groups towards immunotherapy with oncolytic adenoviruses. One unspecific but widely used approach is to arm oncolytic viruses with immunomodulatory transgenes such as GM-CSF in order to improve the immune stimulating properties of the virus. An alternative and more directed strategy to elicit immune responses against specific tumor antigens is the expression or display of TAAs or their immunogenic epitopes by oncolytic viruses. However, both strategies share the same key limitation that need to be overcome: the bias of the response towards viral antigens instead of the less immunogenic tumor antigens.

Adenoviruses are attractive to be used as vaccine platforms against several infectious diseases and even cancer since they are able to induce high innate and adaptive immune responses. E1/E3-deleted replication-deficient adenoviruses are the most commonly used platforms, and additional deletions in E2 and E4 regions have been done to accommodate larger amounts of foreign DNA. However, *gutless* adenoviruses are gaining interest in the vaccination field since, as they lack all the adenovirus genes, have a higher capacity for the insertion of transgenes and induce superior transgene-specific immune response compared to first generation vectors (Harui *et al.*, 2004; Weaver *et al.*, 2013). Adenoviral vectors encoding for antigens from the causing agents of diseases such as AIDS, influenza, malaria, or ebola (van Kampen *et al.*, 2005; Buchbinder *et al.*, 2008; Chuang *et al.*, 2013; Richardson *et al.*, 2013) among others have been developed and tested in human trials. In the cancer vaccination field, TAAs including Her2, Trp-2, gp100, MART-1, PSA, CEA, or WT1 have also been expressed from adenoviral vectors (Rosenberg *et al.*, 1998; Hartman *et al.*, 2008; Gabitzsch *et al.*, 2010; Karan *et al.*, 2011). Nevertheless, the use of this kind of platforms in virotherapy is not feasible as a conditionally replicating adenovirus is needed to selectively kill cancer cells. Therefore, a different strategy rather than deleting adenoviral genes was required to overcome the high immunogenicity of vector antigens.

An additional hurdle that needs to be taken into account is that defects in components of the antigen processing pathway of tumor cells, such as the transporter associated to antigen processing (TAP), also impair the generation of specific immune responses against TAAs carried by oncolytic viruses. Membrane-translocating signals have been used to deliver CTL epitopes to the cytoplasm of APCs in order to be processed by the MHC class I antigen processing pathway, since they are not very efficient in processing exogenous antigens. Two of the most commonly used carriers derive from the HIV-tat protein (Kim *et al.*, 1997) and the *Antennapedia* homeodomain (AntpHD) (Schutze-Redelmeier *et al.*, 1996). Lu and collaborators reported that these constructs consisting of epitopes linked to membrane-translocating sequences were also able to generate epitopes through a TAP-independent fashion that have the ability to cross the

endoplasmic reticulum (ER) membrane and translocate into this compartment. This characteristic has been used for the design of vaccines for the treatment or prevention of several infectious diseases in order to promote the generation and presentation of MHC class I-restricted epitopes and the activation of specific CTL responses. In the field of cancer, the TAP-deficiency of tumor cells makes this strategy even more appealing.

The fact that most viruses express proteins which block TAP in order to evade immune recognition of infected cells accounts for the importance of this transporter in the generation of antiviral immunity. An ideal viral anticancer vaccine vector should have low intrinsic CTL immunogenicity and efficiently present tumor-specific epitopes. Aiming at this goal, Raafat and colleagues developed a vaccinia virus (VV)-based vaccine combining the expression of the protein ICP47 of herpes simplex virus (HSV), that acts by blocking TAP in order to prevent the presentation of viral epitopes by MHC class I, with the expression of an ER-targeted minigene including different tumor-associated epitopes to promote their TAP-independent presentation (Raafat *et al.*, 2012). Curiously, the membrane-translocating sequence that they used in that work was from the N-terminal of the E3-19K protein of the adenovirus, taking advantage of its ER localization. Furthermore, the main function of E3-19K is homologous to that of ICP47 and aims at preventing MHC class I molecules surface expression by means of directly binding them and also by interacting with TAP, even that interactions do not occur simultaneously (Bennett *et al.*, 1999).

Thus, in this work we propose to do both, reduce the immunogenicity of viral epitopes that need to be processed by the TAP-dependent pathway and increase the immunogenicity of tumor-associated epitopes by making them TAP-independent: by attaching the tumor-associated epitopes to E3-19K. Moreover, this strategy benefits from the TAP-deficiency on tumor cells to enhance the response against tumor antigens carried by oncolytic adenoviruses bypassing the necessity of TAP to transport the epitopes to the ER. In addition, APCs are also poorly efficient in processing exogenous antigens through the MHC class I pathway. Therefore, the additional blocking of TAP by E3-19K may benefit the presentation of the TAP-independent tumor-associated epitopes in detriment of viral epitopes. However, the downregulation of MHC class I molecules due to the direct binding of E3-19K in the ER can affect the presentation of both kind of epitopes: viral and tumor. It has been reported that even if binding of MHC class I molecules depends on the ER-retention motif of E3-19K (Cox *et al.*, 1991; Gros *et al.*, 2008), this motif is not required for the interaction with TAP since mutants with truncated C-terminal forms of the protein are still able to interact with TAP and interfere with tapasin function (Bennett *et al.*, 1999). Previous work of our group described a mutation named T1 selected from randomly

mutagenized adenoviruses on the basis of improved potency and that corresponded to a truncation in the E3-19K which resulted in the loss of the ER-retention motif and consequently in an impaired retention of MCH class I (Gros *et al.*, 2008). Therefore, we decided to include this T1 mutation in the oncolytic adenovirus incorporating the epitopes in the E3-19K to avoid the retaining of the MHC class I molecules whereby it still blocks TAP. However, *in vitro* we could not detect any improvement in the presentation of OVA_{257} by this virus (data not shown). The reason of this *a priori* unexpected result, is that the OVA_{257} epitope is H-$2K^b$-restricted, and it is reported in the literature that E3-19K is not able to bind this HLA haplotype (Tanaka and Tevethia, 1988). In contrast, E3-19K binds to H-$2D^b$ molecules, the haplotype to which $gp100_{25}$ epitope is restricted. Since we did not have tools to evaluate the presentation of $gp100_{25}$ *in vitro*, we included the virus combining the epitopes in the E3-19K with the T1 mutation in an immunization experiment *in vivo*. However, we could not see an improvement of the immunogenicity of the epitope $gp100_{25}$ by the incorporation of the T1 mutation into the adenovirus that has the epitope in the E3-19K. Consequently, we decided to move on only with the oncolytic adenovirus without the T1 mutation in order to reduce the number of animals in the studies (data not shown). Nevertheless, we consider important to test the potential of T1 mutation in the future with more appropriated epitopes.

In this study we have compared the strategy of promoting the TAP-independent presentation of the epitopes by inserting them in the E3-19K to a more classical approach which consists in the incorporation of the epitopes in the capsid of the oncolytic adenovirus. The proteins of the capsid of the adenovirus that have been reported to allow the insertion of exogenous epitopes until now are: the penton base, the protein IX, the hexon, and the fiber *knob*. Protein IX allows the incorporation of large polypeptides, so as an advantage, this protein can be used to display fragments of the antigen rather than just the immunogenic epitopes. However, protein IX is a minor and poorly immunogenic protein, and according to our experience, its modification affects the viability of the adenovirus (unpublished results). The hexon is the most abundant and immunogenic protein of the capsid. Most neutralizing antibodies are directed against this protein so its modification can contribute to the success of repeated administrations. Moreover, the modification of some regions of the hexon precludes the binding of this protein to blood coagulation factors, and previous results from our group indicated that the abrogation of the binding of hexon to factor X reduced the antitumor activity of oncolytic adenoviruses, suggesting the implication of blood factors in second rounds of infection inside the tumors (Gimenez-Alejandre *et al.*, 2008). Finally, the fiber *knob* has shown to accommodate a wide range of exogenous peptides of up to 83 amino acids (Belousova *et al.*, 2002). Regarding the

immunogenicity of epitopes incorporated in each capsid protein, Krause and collaborators reported a comparative study of the immune response elicited by the epitope HA from hemagglutinin of influenza A virus in the four different possible proteins of the capsid. They found that the major humoral and cellular immune responses were generated against HA when it was incorporated in the fiber *knob*, regardless if the immunization was performed according to the same number of viral particles or to the same number of epitope copies (Krause *et al.*, 2006). Based on this, we chose the HI-loop domain of the fiber *knob* to incorporate the tumor-associated epitopes OVA_{257} and $gp100_{25}$.

K^b/OVA_{257} presentation studies *in vitro* in TAP-deficient tumor cell lines showed that the only virus that could promote the processing and presentation of the epitope at levels high enough to be detected by the monoclonal antibody 25D1.16 (specific for the complexes formed by H-$2K^b$ molecules and OVA_{257} peptide) was the one containing the epitopes in the E3-19K (**Figure 51**). This advantage was clearly seen in both tumor cell lines, B16CAR and TRAMPC2, in the presence of IFN-γ, where no deficiencies in the MHC class I antigen processing pathway are supposed to occur, suggesting that the blocking of TAP by the virus itself is able to have an effect on the presentation of the carried epitopes. In the TAP-deficient conditions (i.e. absence of IFN-γ), K^b/OVA_{257} complexes were detected only in TRAMPC2 tumor model (**Figure 51b**). However, this result is highly relevant as it suggests the TAP-independent presentation of the peptide. Strikingly, no detectable levels of presentation of OVA_{257} were detected upon the infection of the cells displaying the epitopes in the capsid. This observation seems to indicate that, in this case in which exogenous epitopes are processed by the classical MHC class I antigen processing pathway as if they were viral antigens, there is a competition between tumor and viral epitopes to be presented on the cell surface. However, by making these tumor epitopes TAP-independent, they have an advantage over the immunodominant viral epitopes.

The importance of TAP-independency was assessed by the generation of mutant viruses in which the ER-targeting signal sequence of the E3-19K was deleted. In the same way, to evaluate the relevance of the furin-linkers, they were replaced by furin-resistant linkers. The deletion of the membrane-translocating sequence significantly reduced up to 50% the presentation of OVA_{257} in the surface of TAP-competent cells, indicating that the TAP-independent processing pathway played a relevant role also in the presence of intact antigen processing machinery. The importance of the activity of furin protease in the ER and the TGN was also clear, since its replacement further reduced up to negligible levels the presentation of OVA_{257} upon the infection by the virus without the ER-targeting signal (**Figure 56a**). Interestingly, both observations support the implication of the TAP-independent pathway in the presentation of the

epitope *in vitro* even in TAP-competent cells, in which proteosomal cleavage and TAP are fully functional. This statement was also supported by the results from Lu and collaborators, as they found that their multiepitope vaccine containing furin-resistant linkers failed to generate CTL epitopes even in TAP-competent cells (Lu *et al.*, 2004). When a TAP-deficient situation was mimicked in the TAP-competent cell line P815K^{b} by the inhibition of the proteasome, the presentation of OVA_{257} induced by the virus with the ER-targeting signal sequence deleted was further reduced. However, the presentation of the epitope induced by the virus containing the wild type E3-19K resulted unaffected by proteasome inhibition, demonstrating that the processing in this case was not dependent on the classical MHC class I pathway, whereas in the control without ER-targeting signal proteasome activity was involved (**Figure 56b**).

The relevance of this project lies on the demonstration that the immunodominance of antigens contained in an oncolytic adenovirus could be modified. The idea of the immunodominance might be seen as a "ranking" of epitopes in which the most immunogenic or the ones with higher affinities for the MHC class I molecules are located in the first positions whereas the less immunogenic occupy the lower positions. According to the evaluation of specific CTL immune responses upon immunization by subcutaneous implantation of infected TRAMPC2 cells, response generated against the epitopes OVA_{257} and $gp100_{25}$ by the adenovirus displaying them in the capsid was 6- and 14-fold lower than the response against the viral epitope $E1b_{192}$, respectively. In contrast, the oncolytic adenovirus carrying the epitopes in the E3-19K was able to elicit the same levels of responses against OVA_{257} than those against $E1b_{192}$ and only 2.5-fold lower against the less immunogenic $gp100_{25}$ than against the viral epitope. This result indicates an improvement in the tumor-to-viral immune response ratio provided by the fusion of the tumor epitopes to the E3-19K. In agreement with the results obtained *in vitro*, this may suggest that in the case of the virus displaying the epitopes on the capsid, they have to compete with viral epitopes to be presented, whereas the virus carrying the epitopes in the E3-19K promotes its TAP-independent processing, providing an advantage compared to the viral epitopes. Even though in this case $E1b_{192}$ might be still in the first place of the "ranking" since the higher responses detected are against this epitope, the non-viral epitopes OVA_{257} and $gp100_{25}$ could have advanced several positions by making them TAP-independent, probably bypassing many other subdominant viral epitopes. The results in the B16CAR tumor model were consistent with this hypothesis for the OVA_{257} epitope, whereas in the case of $gp100_{25}$ we were not able to find an improvement by the incorporation of the epitopes in the E3-19K. We attribute this observation to the nature of the B16CAR cell line, which does not represent a good model for several reasons that will be discussed later on. Importantly, this is the second demonstration by

our group that immunodominance is susceptible to be manipulated and modified. The work by Gil aimed at reducing the immunogenicity of the adenoviral capsid by silencing the most immunodominant epitopes of the hexon protein and at the same time at increasing the immune response against a melanoma-associated epitope displayed also by the hexon (Gil-Hoyos, 2014). These approaches are highly innovative since they tackle a crucial aspect of virotherapy with oncolytic adenoviruses which is the high immunogenicity of the viral proteins *per se* and that is often overlooked.

A priori, one advantage of the incorporation of tumor epitopes in the capsid of the adenovirus should be that gene expression is not necessary to generate an immune response (Kafri *et al.*, 1998). This is very important in the context of neutralizing antibodies that block gene expression and which are quite common in humans. Moreover, the incorporation of immunogenic epitopes of the tumor antigens in the capsid of adenoviral vectors has shown to allow prime and boost regimen with the same viral vector. Worgall and collaborators reported that repeated administrations of an adenoviral vector displaying *P. aeruginosa* epitopes in the hexon boosted the immune response against the epitopes, whereas no boosting response was detected against β-galactosidase transgene expressed by the same vector. According to our results, none of these advantages could be seen. The display of the epitopes on the capsid was not better than their TAP-independent presentation by the E3-19K protein in any case. *In vitro*, no presentation of OVA_{257} was detected in the cell surface upon their infection with the virus ICOVIR-15K-HIOG, not even in the case were the cells were treated with IFN-γ, restoring the MHC class I antigen presentation pathway (**Figure 51**). *In vivo*, immunization of the animals with cells infected with the adenovirus displaying the epitopes in the capsid was able to elicit specific $CD8^+$ immune responses against both epitopes in B16CAR model, whereas almost negligible responses were detected in the TRAMPC2 model. In spite of the encouraging results in the B16CAR model, these responses were not reflected in the antitumor efficacy study, where the virus displaying the epitopes in the HI-loop of the fiber had no effect on the growth of B16CAR-OVA tumors compared to the mock group or to the oncolytic adenovirus without the epitopes. Strikingly, even the advantage provided by the oncolytic adenovirus ICOVIR-15K-E3OG in this model was not very obvious, the anti-epitope immune responses elicited by this virus were the only that had an impact on the control of tumor growth until day 16 post-implantation, when most tumors started to relapse (**Figure 60**). Possible reasons for this observation are discussed below.

Historically, immunotherapy has been focused on the activation of antitumor-specific $CD8^+$ CTLs, as it has been assumed that they play a major role in tumor-killing. However, different studies claim a more direct participation of helper $CD4^+$ T cells in mediating other significant

antitumor effector functions (Hung *et al.*, 1998). It has been reported that $CD4^+$ T cells can enhance the infiltration of $CD8^+$ T cells into tumors, promote long-term maintenance of activated $CD8^+$ T cells by producing cytokines such as IL-2 or IFN-γ, and alter the immunosuppressive tumor microenvironment. Shafer-Weaver and collaborators found that the administration of tumor-specific $CD4^+$ T-cells resulted in an enhanced immunity to TRAMP tumors by two different mechanisms: the activation of tumor resident APCs *in situ* and the prevention of the tolerization of $CD8^+$ T cells (Shafer-Weaver *et al.*, 2009). Consequently, an effective cancer vaccination might also require the stimulation of both, $CD4^+$ and $CD8^+$ T cell responses. In this sense, the strategy proposed here allows the combination of dominant MHC class I and class II- restricted epitopes in tandem. In fact, in the work by Lu *et al.* they combine different epitopes connected by furin-linkers and linked to a membrane-translocating signal sequence derived from HIV-I Tat protein to generate a multiepitope peptide vaccine (Lu *et al.*, 2004). They showed that MHC class I and II epitopes were efficiently generated by this vaccine and were able to induce both $CD4^+$ and $CD8^+$ T cell responses *in vivo*. More importantly, these antitumor immune responses were effective at increasing mice survival. These published results supports the feasibility of successfully including CD4 epitopes in combination to CD8 epitopes in the E3-19K of oncolytic adenovirus to generate more potent and long-lasting antitumor immune responses.

Moreover, epitopes from several tumor-associated antigens can be also combined. Targeting many antigens has the advantage of increasing the coverage of the vaccine and also to avoid the emerging of antigen-escape variants. Genomic instability is a very common feature of tumors, and the loss of its characteristic antigens frequently occurs to evade the recognition by the immune system. In this regard, Kaluza and collaborators found that adoptive transfer of anti-OVA CTLs led to tumor regression of B16-OVA tumors followed by eventual tumor recurrence associated to the loss of the targeted antigen, OVA (Kaluza *et al.*, 2011). In an attempt to overcome this limitation, the same group proposed the combination of these anti-OVA CTLs with anti-gp100 CTLs, targeting in this way two different antigens. In this setting, tumor relapse was not associated to the loss of antigen expression, which was maintained in escaped tumors (Kaluza *et al.*, 2012). Although we used the same epitopes as in that study, this result is in contradiction with ours. We found that relapsing tumors expressed lower levels of OVA whether gp100 levels remained constant among all the groups (**Figure 62**). We hypothesized then that given the low immunogenicity of the self-antigen gp100 together with the extremely high immunogenicity of the exogenous antigen OVA, the antitumor immune response is biased toward OVA_{257} epitope. This statement is in agreement with the specific CTL immune responses generated after the immunization of mice with the subcutaneous administration of infected TAP-deficient tumor cell

lines. In this setting we observed that the specific CTL responses generated against OVA_{257} were much higher than the responses against $gp100_{25}$. This observation was especially notable in B16CAR model, in which almost negligible specific responses were raised against the melanoma-specific epitope (**Figure 58**). We postulate that these differences could be related to distinct furin levels among cell lines, since the release of the $gp100_{25}$ peptide requires more furin cleavages compared to the OVA_{257} epitope. However, we could not demonstrate this hypothesis. On the other hand, the lower response generated against $gp100_{25}$ and its presumably poor contribution to antitumor efficacy is in agreement with the study by Kaluza *et al.*, in which they observed very poor antitumor effect upon the treatment of B16-OVA-bearing mice with CTLs specific for this epitope, regardless of the high levels of expression of gp100 in this cell line (Kaluza *et al.*, 2012). They attributed this observation to two reasons. On the one hand, to the low H-$2D^b$ levels expressed by B16 cells that may preclude the exposition of the epitope in the cell surface, avoiding its recognition by specific CTLs. This low surface expression of H-$2D^b$ in B16 cells was confirmed in our results (**Figure 48**). In addition to this fact, the two viral epitopes tested in ELISpot assays ($E1b_{192}$ and Hex_{418}) are also H-$2D^b$-restricted, so a direct competition between these epitopes and $gp100_{25}$ epitope might be taking place. However, a study by Riond and collaborators demonstrated that, even though *in vitro* H-$2D^b$ levels were undetectable in B16 cells, a rapid upregulation of the same can be achieved after engraftment of the cells *in vivo* by different routes (Riond *et al.*, 2009). On the other hand, the $gp100_{25}$ peptide used in this study derives from the human gp100 protein, which has been reported to have higher affinity for MHC class I molecules than the mouse homologue (Overwijk *et al.*, 1998). Although there is cross-reactivity between human and mouse epitopes, the responsiveness to the endogenous mouse epitope is lower than to the human one (Kaluza *et al.*, 2012).

As it has been mentioned in *section 3.5.1.1.*, the concept of immunodominance implies that the immune response is directed mainly towards a few antigenic determinants even in the presence of many different and complex antigens. In the specific case of our work, since OVA_{257} is highly immunodominant because of its exogenous nature, the response against $gp100_{25}$ might be hindered. Evidently, the virus presented in this work containing OVA_{257} and $gp100_{25}$ is not a therapeutic agent but a proof of concept virus. The model epitope OVA_{257} was selected because of the availability of reagents and the elevated knowledge and amounts of studies published with it. However, we are aware about the highly artificial nature of this setting. We postulate that in a truly therapeutic setting in which the expression of several self-tumor-associated antigens with similar affinities for MHC molecules and putatively similar immunogenicities, the immune response would be more fairly distributed among different epitopes. The important result to

emphasize in this sense is that in TRAMPC2 model *in vivo* the immunotolerance against the poorly immunogenic and self-antigen gp100 could be broken by the virus containing the epitopes in the E3-19K (**Figure 59**), demonstrating that it is feasible to generate CTL-mediated immune responses against auto-antigens by means of this strategy.

Overall, the major challenge of this strategy is the proper choice of tumor-associated epitopes. Wilms Tumor antigen 1 (WT1) was classified by a pilot priorization project as the best tumor-associated antigen among a list of 75 antigens. This classification was performed according to criteria that an ideal cancer antigen must accomplish including: therapeutic function, immunogenicity, and specificity, between others (Cheever *et al.*, 2009). However, we incorporated two epitopes that were described as the most immunogenic from this tumor-associated antigen in the HI-loop of the fiber of an oncolytic adenovirus and it failed in eliciting specific CTL immune responses against them and also in the control of tumor growth of WT1-expressing TRAMPC2 tumors (data not shown). At that point, we concluded that this tumor-associated epitopes were not immunogenic enough. However, the results obtained with the model OVA_{257} in the same localization indicate that the problem might be related to the position of the epitope within the adenovirus capsid rather than with the antigen *per se*. Curiously, gp100 is also in the upper part of this priorization ranking occupying the 16^{th} position. Nevertheless, taking our results into account, it does not seem a highly immunogenic antigen. In addition, it is not completely tumor-specific as normal melanocytes also express gp100. According to immunogenicity and specificity parameters, the best tumor antigens might be viral antigens in tumors originated by virus infections. However, only 15 up to 20% of cancers are linked to infections according to the America Cancer Society (http://www.cancer.org). Lately, the identification of specific somatic mutations in individual tumors by exome sequencing is gaining interest in immunotherapy field for the development of personalized vaccines. Detected neoantigens are valuable targets for immunotherapy since they are highly tumor-specific. Unfortunately, this strategy seems unlikely at the moment for our approach, since it would be time and money-consuming to develop a new personalized oncolytic adenovirus for each individual patient and generate it in the proper conditions to be used in humans. However, mutanome-based vaccination analysis is an extremely interesting approach that might be feasible in the near future.

2.1. MODELS FOR IMMUNOVIROTHERAPY

For the evaluation of the immune responses generated by the oncolytic adenoviruses described in Chapter 2, having an immunocompetent animal model was critical. Since the epitopes that we evaluated in this work ($E1b_{192}$, Hex_{418}, OVA_{257}, and $gp100_{25}$) were H-2^b-restricted, C57BL/6 immunocompetent mice (H-2^b haplotype) were appropriate to assess specific immune responses elicited against them. However, as mentioned in Chapter 1, effects of the oncolytic adenovirus *per se* in normal tissues cannot be determined in this model.

More importantly, since we claim that immunogenic cell death caused by oncolytic virus replication in tumor cells is critical for the triggering of antitumor immune responses, a murine tumor cell line permissive to adenovirus replication was needed. Even though there is literature about murine cell lines allowing human adenovirus replication (Ganly *et al.*, 2000b; Hallden *et al.*, 2003), viral productivity in these cell lines is extremely low in our hands. For instance, Halldén and collaborators described that the lung carcinoma cell line from mice CMT-64 was able to produce 1116 TU/cell (Hallden *et al.*, 2003), whereas we barely observed 3 TU/cell viral yields in the same cell line (data not shown). In the specific case of our study, B16CAR and TRAMPC2 were the used murine cancer cell lines, since both have been described to present defects in antigen processing at the level of TAP (Riond *et al.*, 2009; Martini *et al.*, 2010). However, negligible viral yields were obtained in productivity assays with those cell lines (**Figure 46**). Infectivity of melanoma B16 cell line was previously improved by means of the stable transfection of the cells with the adenovirus receptor CAR (Tosch *et al.*, 2009), reaching 100% of infectivity at an MOI of 100 (**Figure 44**). Lower percentages of infectivity were observed in TRAMPC2 after their infection at the same MOI (40%), even though this level of infection was considered sufficient for the virus to be produced (**Figure 45**). Therefore, according to the results presented here, the uptake of the virus by murine cells was not the limiting factor, nor it was the expression of early and late genes, demonstrated by western blot in both cancer cell lines (**Figure 52**). Several attempts to increase virus productivity of murine cell lines have been carried out in our group including the selection of clones with increased viral replication. Unfortunately, these efforts did not succeed in finding a model with acceptable levels of viral production (data not shown). Thereby, we decided to move on with B16CAR and TRAMPC2 models.

Defects in MHC class I antigen processing pathway in B16CAR and TRAMPC2 cell lines could be restored by the incubation of the cells with IFN-γ *in vitro*, so we could have a TAP-deficient and TAP-competent scenario in the same cell line by adding or not this cytokine to the media. Nevertheless, since we wanted to demonstrate the TAP-independent presentation of the

exogenous epitopes carried by the E3-19K protein, the ideal scenario would be to have paired cell lines wild type or mutated only for TAP genes. RMA/S were selected from mutagenized RMA cells (Rauscher virus-induced T lymphoma tumor cell line) on the basis of low surface expression of MHC class I molecules (Karre *et al.*, 1986). This cell line has a mutated TAP2 gene and consequently TAP complex is not functional. Although both cell lines were available they were hardly infected with adenovirus (data not shown) due to their T cell origin. The same happened with the TAP-mutated T2-K^b cell line (human B-lymphoblast and T-lymphoblast hybrid stably transfected with H-$2K^b$) (data not shown). In an attempt to increase the infectivity of these cell lines we used agents such as polybrene that had shown to induce better transduction of adenoviruses *in vitro* (Miralles *et al.*, 2012). Moreover, we also changed the localization of the RGD motif from the KKTK domain of the fiber *shaft* to the HI-loop of the fiber in the viruses incorporating the epitopes in the E3-19K since this RGD-fiber has shown better infectivity than RGDK-fiber in this kind of cell lines. Unfortunately, we were not able to achieve sufficient levels of infectivity with any of these strategies (data not shown). The only choice was then to use a TAP-competent cell line in which a MHC class I classical antigen presentation pathway was blocked, in this case, by the inhibition of the proteasome by lactacystin.

Although the results obtained in the OVA_{257} presentation experiments *in vitro* and also in the evaluation of specific CTL immune responses upon immunization by subcutaneous implantation of infected cells were better in TRAMPC2 than in B16CAR, the latter was chosen for antitumor activity studies. The reason for this election was that this melanoma cell line expresses high levels of the melanoma tumor-associated antigen gp100 (**Figure 50**), and we only had to transfect exogenously the expression plasmid containing OVA gene. In contrast, TRAMPC2 did not express gp100 (data not shown) nor OVA. Thus, B16CAR-OVA was the model of choice for the antitumor activity experiments despite its limitations. In addition to the lack of replication of human adenovirus in mouse cells, the fast-growing rate of syngenic cell line-based tumor models is also a limiting factor for the testing of our strategy in a therapeutic setting. Therefore, the effect of virus-induced oncolysis, which presumably would further enhance the efficacy of the vaccination, could not be assessed in this experimental model.

Another difficulty of B16 melanoma model is the expression of Fas ligand by this cell line, which may contribute to the evasion from immune attack and to the maintenance of immune privileged conditions in tumors, limiting the efficacy of the elicited CTL immune responses (Hahne *et al.*, 1996). Whether human melanomas also expresses Fas ligand or not is controversial as the work by Hahne *et al*. reported the expression of this ligand in human samples, whereas a later

publication by Chappell and colleagues failed to detect the expression of Fas ligand in any of the 26 human melanoma cell lines that they evaluated (Chappell *et al.*, 1999).

3. OUTLOOK AND FUTURE PERSPECTIVE

Oncolytic viruses are promising anticancer agents. Encouraging results have been obtained lately in the clinics especially with T-Vec or Pexa-Vec, which are HSV and VV-based oncolytic viruses, respectively, engineered to express the immunostimulatory transgene GM-CSF with the aim to stimulate antitumor specific immune responses.

Historically, there are two different views regarding the role that the immune system plays in the efficacy of oncolytic viruses: the virocentric and the immunocentric (Alemany and Cascallo, 2009). Virocentrics sees the immune system as an enemy since the immune response generated against the virus can rapidly eliminate it from the bloodstream and also from the tumor microenvironment before doing its job. For them, the immunosuppressive state in tumors is beneficial to allow intratumoral viral replication. On the other hand, immunocentrics consider the immune system an ally and use oncolytic viruses as immune stimulators to disrupt the immunotolerant state of tumors and elicit antitumor specific immune responses. The immunogenic cell death produced by oncolytic viruses causes a release of danger signals that recruits immune cells to the tumor sites, where liberated tumor-associated antigens are captured and cross-presented to CTLs. Importantly, the stimulation of specific antitumor immune responses by these agents is basic, since a memory response that may prevent future relapses is established.

Although *a priori* these two thoughts seem to be confronted, they are not as far apart from each other. Efficient tumor targeting, selective replication and potency are three traits that an oncolytic virus has to accomplish for both, virocentric and immunocentric approaches. For virocentrics the virus needs to reach all the tumor nodules to replicate in and eliminate them. Moreover the replication must be tumor selective in order to avoid off-target damage. Finally, the most potent the virus is the best antitumor activity will be achieved. For immunocentrics tumor targeting is important since viral replication in tumors is needed to promote an immunogenic kind of cell death. In addition, this replication must be restricted to tumor cells in order to focus the immune system on tumor sites and prevent immune-mediated toxicity. Finally, large tumors may require the help of highly efficient viral replication to debulk them before being completely rejected by CTLs.

This thesis combined these two distinct views. The first project aimed at improving the tumor targeting and increasing the potency of the adenovirus by enhancing its intratumoral spread by means of combining a capsid targeting modification with the expression of the extracellular matrix-degrading enzyme hyaluronidase. The goal of the second project was to stimulate the generation of specific immune responses against tumor-associated epitopes incorporated in the oncolytic adenovirus by promoting its TAP-independent processing and presentation. At the same time, taking into account that the success of this approach would depend on a delicate balance between antiviral and antitumor immune responses, this second project handled the problem of the high immunodominance of adenoviral antigens that could mask antitumor immune responses.

Importantly, both projects are not mutually exclusive, and might eventually be combined in one single oncolytic adenovirus. We strongly think that the combination of virocentric and immunocentric approaches is key to maximize the opportunities of success of oncolytic adenoviruses.

CONCLUSIONS

Chapter 1

1. The combination of RGDK fiber modification and hyaluronidase expression in ICOVIR-17K does not have a negative impact on viral replication or cytotoxic potency *in vitro*.

2. ICOVIR-17K is tumor-selective and shows a transient acute toxicity profile *in vivo* after systemic administration in immunocompetent mice and hamsters, which does not differ from the oncolytic adenovirus without the RGDK modification, ICOVIR-17.

3. ICOVIR-17K exhibit significant antitumor efficacy when administered systemically or intratumorally in different tumor models in nude mice and immunocompetent hamsters, and shows superior oncolytic potency than ICOVIR-17.

4. The antitumor efficacy of ICOVIR-17K was improved *in vitro* and *in vivo* when combined with gemcitabine, especially in pancreatic carcinoma cell lines, without significantly increase the toxicity of the treatment.

Chapter 2

5. The insertion of tumor-associated epitopes into the ER-targeted adenovirus protein E3-19K promotes a TAP-independent processing that increases their presentation on infected cells *in vitro* compared to the display of the epitopes on the fiber protein of the capsid.

6. The fusion of tumor-associated epitopes to the E3-19K of an oncolytic adenovirus induces higher specific antitumor immune responses than the incorporation of the same epitopes on the capsid after the immunization of immunocompetent mice with infected-TAP-deficient tumor cells.

7. The localization of tumor-associated epitopes in the E3-19K of an oncolytic adenovirus increases the tumor-to-viral immune response ratio compared to the display of the same epitopes on the capsid, improving the immunogenicity of the exogenous epitopes.

8. Specific antitumor immune responses triggered by the immunization of mice with TAP-deficient tumor cells infected with the oncolytic adenovirus containing tumor-associated epitopes in the E3-19K controls tumor growth after challenging with tumors expressing the targeted tumor-associated antigens.

REFERENCES

A

AGHI, M., and MARTUZA, R.L. (2005). Oncolytic viral therapies - the clinical experience. Oncogene **24**, 7802-7816.

ALEMANY, R., and CASCALLO, M. (2009). Oncolytic viruses from the perspective of the immune system. Future Microbiol **4**, 527-536.

ALEMANY, R., and CURIEL, D.T. (2001). CAR-binding ablation does not change biodistribution and toxicity of adenoviral vectors. Gene therapy **8**, 1347-1353.

ALEMANY, R., SUZUKI, K., and CURIEL, D.T. (2000). Blood clearance rates of adenovirus type 5 in mice. J Gen Virol **81**, 2605-2609.

ALTOMONTE, J., WU, L., MESECK, M., CHEN, L., EBERT, O., GARCIA-SASTRE, A.*, et al.* (2009). Enhanced oncolytic potency of vesicular stomatitis virus through vector-mediated inhibition of NK and NKT cells. Cancer Gene Ther **16**, 266-278.

ARUGA, A., ARUGA, E., TANIGAWA, K., BISHOP, D.K., SONDAK, V.K., and CHANG, A.E. (1997). Type 1 versus type 2 cytokine release by Vbeta T cell subpopulations determines in vivo antitumor reactivity: IL-10 mediates a suppressive role. J Immunol **159**, 664-673.

B

BARTLETT, D.L., LIU, Z., SATHAIAH, M., RAVINDRANATHAN, R., GUO, Z., HE, Y.*, et al.* (2013). Oncolytic viruses as therapeutic cancer vaccines. Mol Cancer **12**, 103.

BAUERSCHMITZ, G.J., LAM, J.T., KANERVA, A., SUZUKI, K., NETTELBECK, D.M., DMITRIEV, I.*, et al.* (2002). Treatment of ovarian cancer with a tropism modified oncolytic adenovirus. Cancer Res **62**, 1266-1270.

BAUMGARTNER, G., GOMAR-HOSS, C., SAKR, L., ULSPERGER, E., and WOGRITSCH, C. (1998). The impact of extracellular matrix on the chemoresistance of solid tumors--experimental and clinical results of hyaluronidase as additive to cytostatic chemotherapy. Cancer Lett **131**, 85-99.

BAYO-PUXAN, N., CASCALLO, M., GROS, A., HUCH, M., FILLAT, C., and ALEMANY, R. (2006). Role of the putative heparan sulfate glycosaminoglycan-binding site of the adenovirus type 5 fiber shaft on liver detargeting and knob-mediated retargeting. J Gen Virol **87**, 2487-2495.

BAYO-PUXAN, N., GIMENEZ-ALEJANDRE, M., LAVILLA-ALONSO, S., GROS, A., CASCALLO, M., HEMMINKI, A.*, et al.* (2009). Replacement of adenovirus type 5 fiber shaft heparan sulfate proteoglycan-binding domain with RGD for improved tumor infectivity and targeting. Hum Gene Ther **20**, 1214-1221.

BECKENLEHNER, K., BANNKE, S., SPRUSS, T., BERNHARDT, G., SCHONENBERG, H., and SCHIESS, W. (1992). Hyaluronidase enhances the activity of adriamycin in breast cancer models in vitro and in vivo. J Cancer Res Clin Oncol **118**, 591-596.

BELOUSOVA, N., KRENDELCHTCHIKOVA, V., CURIEL, D.T., and KRASNYKH, V. (2002). Modulation of adenovirus vector tropism via incorporation of polypeptide ligands into the fiber protein. J Virol **76**, 8621-8631.

BENNETT, E.M., BENNINK, J.R., YEWDELL, J.W., and BRODSKY, F.M. (1999). Cutting Edge: Adenovirus E19 Has Two Mechanisms for Affecting Class I MHC Expression1. The Journal of Immunology **162**, 5049-5052.

BENNINK, J.R., and YEWDELL, J.W. (1988). Murine cytotoxic T lymphocyte recognition of individual influenza virus proteins. High frequency of nonresponder MHC class I alleles. J Exp Med **168**, 1935-1939.

BERK, A.J. (1986). Adenovirus promoters and E1A transactivation. Annu Rev Genet **20**, 45-79.

BERNT, K.M., NI, S., GAGGAR, A., LI, Z.Y., SHAYAKHMETOV, D.M., and LIEBER, A. (2003). The effect of sequestration by nontarget tissues on anti-tumor efficacy of systemically applied, conditionally replicating adenovirus vectors. Mol Ther **8**, 746-755.

BETT, A.J., DUBEY, S.A., MEHROTRA, D.V., GUAN, L., LONG, R., ANDERSON, K.*, et al.* (2010). Comparison of T cell immune responses induced by vectored HIV vaccines in non-human primates and humans. Vaccine **28**, 7881-7889.

BHATTACHARYYA, M., FRANCIS, J., EDDOUADI, A., LEMOINE, N.R., and HALLDEN, G. (2011). An oncolytic adenovirus defective in pRb-binding (dl922-947) can efficiently eliminate pancreatic cancer cells and tumors in vivo in combination with 5-FU or gemcitabine. Cancer Gene Ther **18**, 734-743.

BIRNBOIM, H.C., and DOLY, J. (1979). A rapid alkaline extraction procedure for screening recombinant plasmid DNA. Nucleic Acids Res **7**, 1513-1523.

BISCHOFF, J.R., KIRN, D.H., WILLIAMS, A., HEISE, C., HORN, S., MUNA, M.*, et al.* (1996). An adenovirus mutant that replicates selectively in p53-deficient human tumor cells. Science **274**, 373-376.

BLUM, J.S., WEARSCH, P.A., and CRESSWELL, P. (2013). Pathways of antigen processing. Annu Rev Immunol **31**, 443-473.

BORTOLANZA, S., BUNUALES, M., OTANO, I., GONZALEZ-ASEGUINOLAZA, G., ORTIZ-DE-SOLORZANO, C., PEREZ, D.*, et al.* (2009). Treatment of pancreatic cancer with an oncolytic adenovirus expressing interleukin-12 in Syrian hamsters. Mol Ther **17**, 614-622.

BRAMSON, J.L., HITT, M., GAULDIE, J., and GRAHAM, F.L. (1997). Pre-existing immunity to adenovirus does not prevent tumor regression following intratumoral administration of a vector expressing IL-12 but inhibits virus dissemination. Gene therapy **4**, 1069-1076.

BREITBACH, C.J., BURKE, J., JONKER, D., STEPHENSON, J., HAAS, A.R., CHOW, L.Q.M.*, et al.* (2011). Intravenous delivery of a multi-mechanistic cancer-targeted oncolytic poxvirus in humans. Nature **477**, 99-102.

BRESSY, C., and BENIHOUD, K. (2014). Association of oncolytic adenoviruses with chemotherapies: an overview and future directions. Biochem Pharmacol **90**, 97-106.

BRIDLE, B.W., STEPHENSON, K.B., BOUDREAU, J.E., KOSHY, S., KAZDHAN, N., PULLENAYEGUM, E.*, et al.* (2010). Potentiating Cancer Immunotherapy Using an Oncolytic Virus. Mol Ther **18**, 1430-1439.

BRISTOL, J.A., ZHU, M., JI, H., MINA, M., XIE, Y., CLARKE, L.*, et al.* (2003). In vitro and in vivo activities of an oncolytic adenoviral vector designed to express GM-CSF. Mol Ther **7**, 755-764.

BUCHBINDER, S.P., MEHROTRA, D.V., DUERR, A., FITZGERALD, D.W., MOGG, R., LI, D*., et al.* (2008). Efficacy assessment of a cell-mediated immunity HIV-1 vaccine (the Step Study): a double-blind, randomised, placebo-controlled, test-of-concept trial. Lancet **372**, 1881-1893.

BUNUALES, M., GARCIA-ARAGONCILLO, E., CASADO, R., QUETGLAS, J.I., HERVAS-STUBBS, S., BORTOLANZA, S*., et al.* (2012). Evaluation of monocytes as carriers for armed oncolytic adenoviruses in murine and Syrian hamster models of cancer. Hum Gene Ther **23**, 1258-1268.

BURKE, J.M., LAMM, D.L., MENG, M.V., NEMUNAITIS, J.J., STEPHENSON, J.J., ARSENEAU, J.C*., et al.* (2012). A first in human phase 1 study of CG0070, a GM-CSF expressing oncolytic adenovirus, for the treatment of nonmuscle invasive bladder cancer. J Urol **188**, 2391-2397.

BURNET, M. (1957). Cancer; a biological approach. I. The processes of control. Br Med J **1**, 779-786.

C

CAMPOS, S.K., PARROTT, M.B., and BARRY, M.A. (2004). Avidin-based targeting and purification of a protein IX-modified, metabolically biotinylated adenoviral vector. Mol Ther **9**, 942-954.

CASCALLO, M., ALONSO, M.M., ROJAS, J.J., PEREZ-GIMENEZ, A., FUEYO, J., and ALEMANY, R. (2007). Systemic toxicity-efficacy profile of ICOVIR-5, a potent and selective oncolytic adenovirus based on the pRB pathway. Mol Ther **15**, 1607-1615.

CASCALLO, M., CAPELLA, G., MAZO, A., and ALEMANY, R. (2003). Ras-dependent oncolysis with an adenovirus VAI mutant. Cancer Res **63**, 5544-5550.

CASCALLO, M., GROS, A., BAYO, N., SERRANO, T., CAPELLA, G., and ALEMANY, R. (2006). Deletion of VAI and VAII RNA genes in the design of oncolytic adenoviruses. Hum Gene Ther **17**, 929-940.

CASTELO-BRANCO, P., PASSER, B.J., BUHRMAN, J.S., ANTOSZCZYK, S., MARINELLI, M., ZAUPA, C*., et al.* (2010). Oncolytic herpes simplex virus armed with xenogeneic homologue of prostatic acid phosphatase enhances antitumor efficacy in prostate cancer. Gene therapy **17**, 805-810.

CERULLO, V., DIACONU, I., ROMANO, V., HIRVINEN, M., UGOLINI, M., ESCUTENAIRE, S*., et al.* (2012). An oncolytic adenovirus enhanced for toll-like receptor 9 stimulation increases antitumor immune responses and tumor clearance. Mol Ther **20**, 2076-2086.

CERULLO, V., PESONEN, S., DIACONU, I., ESCUTENAIRE, S., ARSTILA, P.T., UGOLINI, M*., et al.* (2010). Oncolytic adenovirus coding for granulocyte macrophage colony-stimulating factor induces antitumoral immunity in cancer patients. Cancer Res **70**, 4297-4309.

CODY, J.J., and DOUGLAS, J.T. (2009). Armed replicating adenoviruses for cancer virotherapy. Cancer Gene Ther **16**, 473-488.

COUGHLAN, L., ALBA, R., PARKER, A.L., BRADSHAW, A.C., MCNEISH, I.A., NICKLIN, S.A*., et al.* (2010). Tropism-modification strategies for targeted gene delivery using adenoviral vectors. Viruses **2**, 2290-2355.

COX, J.H., BENNINK, J.R., and YEWDELL, J.W. (1991). Retention of adenovirus E19 glycoprotein in the endoplasmic reticulum is essential to its ability to block antigen presentation. J Exp Med **174**, 1629-1637.

CRIPE, T.P., DUNPHY, E.J., HOLUB, A.D., SAINI, A., VASI, N.H., MAHLLER, Y.Y*., et al.* (2001). Fiber knob modifications overcome low, heterogeneous expression of the coxsackievirus-adenovirus receptor that limits adenovirus gene transfer and oncolysis for human rhabdomyosarcoma cells. Cancer Res **61**, 2953-2960.

CURTISS, L.K., and KRUEGER, R.G. (1975). The relative immunodominance of haptenic determinants on a complex hapten phage conjugate. Immunochemistry **12**, 949-957.

CHAPPELL, D.B., ZAKS, T.Z., ROSENBERG, S.A., and RESTIFO, N.P. (1999). Human melanoma cells do not express Fas (Apo-1/CD95) ligand. Cancer Res **59**, 59-62.

CHEEVER, M.A., ALLISON, J.P., FERRIS, A.S., FINN, O.J., HASTINGS, B.M., HECHT, T.T*., et al.* (2009). The prioritization of cancer antigens: a national cancer institute pilot project for the acceleration of translational research. Clin Cancer Res **15**, 5323-5337.

CHEN, C.S., DOLOFF, J.C., and WAXMAN, D.J. (2014). Intermittent metronomic drug schedule is essential for activating antitumor innate immunity and tumor xenograft regression. Neoplasia **16**, 84-96.

CHEN, H., VINNAKOTA, R., and FLINT, S.J. (1994). Intragenic activating and repressing elements control transcription from the adenovirus IVa2 initiator. Mol Cell Biol **14**, 676-685.

CHEN, H.L., GABRILOVICH, D., TAMPE, R., GIRGIS, K.R., NADAF, S., and CARBONE, D.P. (1996). A functionally defective allele of TAP1 results in loss of MHC class I antigen presentation in a human lung cancer. Nat Genet **13**, 210-213.

CHEN, W., and MCCLUSKEY, J. (2006). Immunodominance and immunodomination: critical factors in developing effective CD8+ T-cell-based cancer vaccines. Adv Cancer Res **95**, 203-247.

CHIOCCA, E.A., ABBED, K.M., TATTER, S., LOUIS, D.N., HOCHBERG, F.H., BARKER, F*., et al.* (2004). A phase I open-label, dose-escalation, multi-institutional trial of injection with an E1B-Attenuated adenovirus, ONYX-015, into the peritumoral region of recurrent malignant gliomas, in the adjuvant setting. Mol Ther **10**, 958-966.

CHOI, I.-K., LI, Y., OH, E., KIM, J., and YUN, C.-O. (2013). Oncolytic Adenovirus Expressing IL-23 and p35 Elicits IFN-Î³- and TNF-Î±-Co-Producing T Cell-Mediated Antitumor Immunity. PLoS One **8**, e67512.

CHOI, I.K., LEE, Y.S., YOO, J.Y., YOON, A.R., KIM, H., KIM, D.S*., et al.* (2010). Effect of decorin on overcoming the extracellular matrix barrier for oncolytic virotherapy. Gene therapy **17**, 190-201.

CHUANG, I., SEDEGAH, M., CICATELLI, S., SPRING, M., POLHEMUS, M., TAMMINGA, C*., et al.* (2013). DNA prime/Adenovirus boost malaria vaccine encoding P. falciparum CSP and

AMA1 induces sterile protection associated with cell-mediated immunity. PLoS One **8**, e55571.

D

DANIELSSON, A., DZOJIC, H., RASHKOVA, V., CHENG, W.S., and ESSAND, M. (2011). The HDAC inhibitor FK228 enhances adenoviral transgene expression by a transduction-independent mechanism but does not increase adenovirus replication. PLoS One **6**, e14700.

DE LA SALLE, H., SAULQUIN, X., MANSOUR, I., KLAYME, S., FRICKER, D., ZIMMER, J.*, et al.* (2002). Asymptomatic deficiency in the peptide transporter associated to antigen processing (TAP). Clin Exp Immunol **128**, 525-531.

DECHECCHI, M.C., MELOTTI, P., BONIZZATO, A., SANTACATTERINA, M., CHILOSI, M., and CABRINI, G. (2001). Heparan sulfate glycosaminoglycans are receptors sufficient to mediate the initial binding of adenovirus types 2 and 5. J Virol **75**, 8772-8780.

DEL VAL, M., IBORRA, S., RAMOS, M., and LAZARO, S. (2011). Generation of MHC class I ligands in the secretory and vesicular pathways. Cell Mol Life Sci **68**, 1543-1552.

DEPACE. (1912). Sulla scomparsa di un enorme cancro vegetante del collo dell'utero senza cura chirurgica. . Ginecologia **9**, 82–89.

DEWEESE, T.L., VAN DER POEL, H., LI, S., MIKHAK, B., DREW, R., GOEMANN, M.*, et al.* (2001). A phase I trial of CV706, a replication-competent, PSA selective oncolytic adenovirus, for the treatment of locally recurrent prostate cancer following radiation therapy. Cancer Res **61**, 7464-7472.

DHAR, D., SPENCER, J.F., TOTH, K., and WOLD, W.S. (2009a). Effect of preexisting immunity on oncolytic adenovirus vector INGN 007 antitumor efficacy in immunocompetent and immunosuppressed Syrian hamsters. J Virol **83**, 2130-2139.

DHAR, D., SPENCER, J.F., TOTH, K., and WOLD, W.S. (2009b). Pre-existing immunity and passive immunity to adenovirus 5 prevents toxicity caused by an oncolytic adenovirus vector in the Syrian hamster model. Mol Ther **17**, 1724-1732.

DIACONU, I., CERULLO, V., HIRVINEN, M.L., ESCUTENAIRE, S., UGOLINI, M., PESONEN, S.K.*, et al.* (2012). Immune response is an important aspect of the antitumor effect produced by a CD40L-encoding oncolytic adenovirus. Cancer Res **72**, 2327-2338.

DIAS, J.D., HEMMINKI, O., DIACONU, I., HIRVINEN, M., BONETTI, A., GUSE, K.*, et al.* (2012). Targeted cancer immunotherapy with oncolytic adenovirus coding for a fully human monoclonal antibody specific for CTLA-4. Gene therapy **19**, 988-998.

DIAZ, R.M., GALIVO, F., KOTTKE, T., WONGTHIDA, P., QIAO, J., THOMPSON, J.*, et al.* (2007). Oncolytic immunovirotherapy for melanoma using vesicular stomatitis virus. Cancer Res **67**, 2840-2848.

DIGHE, A.S., RICHARDS, E., OLD, L.J., and SCHREIBER, R.D. (1994). Enhanced in vivo growth and resistance to rejection of tumor cells expressing dominant negative IFN gamma receptors. Immunity **1**, 447-456.

DMITRIEV, I., KRASNYKH, V., MILLER, C.R., WANG, M., KASHENTSEVA, E., MIKHEEVA, G.*, et al.* (1998). An adenovirus vector with genetically modified fibers demonstrates expanded tropism via utilization of a coxsackievirus and adenovirus receptor-independent cell entry mechanism. J Virol **72**, 9706-9713.

DMITRIEVA, N., YU, L., VIAPIANO, M., CRIPE, T.P., CHIOCCA, E.A., GLORIOSO, J.C.*, et al.* (2011). Chondroitinase ABC I-mediated enhancement of oncolytic virus spread and antitumor efficacy. Clin Cancer Res **17**, 1362-1372.

DOCK, G. (1904). THE INFLUENCE OF COMPLICATING DISEASES UPON LEUKAEMIA.*. The American Journal of the Medical Sciences **127**, 563-592.

DOHERTY, P.C., BIDDISON, W.E., BENNINK, J.R., and KNOWLES, B.B. (1978). Cytotoxic T-cell responses in mice infected with influenza and vaccinia viruses vary in magnitude with H-2 genotype. J Exp Med **148**, 534-543.

DONG, H., STROME, S.E., SALOMAO, D.R., TAMURA, H., HIRANO, F., FLIES, D.B.*, et al.* (2002). Tumor-associated B7-H1 promotes T-cell apoptosis: a potential mechanism of immune evasion. Nat Med **8**, 793-800.

DORFMAN, A., and OTT, M.L. (1948). A turbidimetric method for the assay of hyaluronidase. J Biol Chem **172**, 367-375.

DUDLEY, M.E., WUNDERLICH, J.R., ROBBINS, P.F., YANG, J.C., HWU, P., SCHWARTZENTRUBER, D.J.*, et al.* (2002). Cancer regression and autoimmunity in patients after clonal repopulation with antitumor lymphocytes. Science **298**, 850-854.

DUNN, G.P., BRUCE, A.T., IKEDA, H., OLD, L.J., and SCHREIBER, R.D. (2002). Cancer immunoediting: from immunosurveillance to tumor escape. Nat Immunol **3**, 991-998.

DUNN, G.P., KOEBEL, C.M., and SCHREIBER, R.D. (2006). Interferons, immunity and cancer immunoediting. Nat Rev Immunol **6**, 836-848.

DZOJIC, H., LOSKOG, A., TOTTERMAN, T.H., and ESSAND, M. (2006). Adenovirus-mediated CD40 ligand therapy induces tumor cell apoptosis and systemic immunity in the TRAMP-C2 mouse prostate cancer model. Prostate **66**, 831-838.

E

EIKENES, L., TARI, M., TUFTO, I., BRULAND, O.S., and DE LANGE DAVIES, C. (2005). Hyaluronidase induces a transcapillary pressure gradient and improves the distribution and uptake of liposomal doxorubicin (Caelyx) in human osteosarcoma xenografts. Br J Cancer **93**, 81-88.

EINFELD, D.A., BROUGH, D.E., ROELVINK, P.W., KOVESDI, I., and WICKHAM, T.J. (1999). Construction of a pseudoreceptor that mediates transduction by adenoviruses expressing a ligand in fiber or penton base. J Virol **73**, 9130-9136.

ELSEDAWY, N.B., and RUSSELL, S.J. (2013). Oncolytic vaccines. Expert Rev Vaccines **12**, 1155-1172.

F

FANG, J., NAKAMURA, H., and MAEDA, H. (2011). The EPR effect: Unique features of tumor blood vessels for drug delivery, factors involved, and limitations and augmentation of the effect. Adv Drug Deliv Rev **63**, 136-151.

FOWLER, N.L., and FRAZER, I.H. (2004). Mutations in TAP genes are common in cervical carcinomas. Gynecologic Oncology **92**, 914-921.

FRAHM, N., DECAMP, A.C., FRIEDRICH, D.P., CARTER, D.K., DEFAWE, O.D., KUBLIN, J.G.*, et al.* (2012). Human adenovirus-specific T cells modulate HIV-specific T cell responses to an Ad5-vectored HIV-1 vaccine. The Journal of Clinical Investigation **122**, 359-367.

FREYTAG, S.O., BARTON, K.N., and ZHANG, Y. (2013). Efficacy of oncolytic adenovirus expressing suicide genes and interleukin-12 in preclinical model of prostate cancer. Gene therapy **20**, 1131-1139.

FREYTAG, S.O., KHIL, M., STRICKER, H., PEABODY, J., MENON, M., DEPERALTA-VENTURINA, M.*, et al.* (2002). Phase I study of replication-competent adenovirus-mediated double suicide gene therapy for the treatment of locally recurrent prostate cancer. Cancer Res **62**, 4968-4976.

FREYTAG, S.O., STRICKER, H., PEGG, J., PAIELLI, D., PRADHAN, D.G., PEABODY, J.*, et al.* (2003). Phase I study of replication-competent adenovirus-mediated double-suicide gene therapy in combination with conventional-dose three-dimensional conformal radiation therapy for the treatment of newly diagnosed, intermediate- to high-risk prostate cancer. Cancer Res **63**, 7497-7506.

FUEYO, J., GOMEZ-MANZANO, C., ALEMANY, R., LEE, P.S., MCDONNELL, T.J., MITLIANGA, P.*, et al.* (2000). A mutant oncolytic adenovirus targeting the Rb pathway produces anti-glioma effect in vivo. Oncogene **19**, 2-12.

FUJIWARA, T., KAGAWA, S., KISHIMOTO, H., ENDO, Y., HIOKI, M., IKEDA, Y.*, et al.* (2006). Enhanced antitumor efficacy of telomerase-selective oncolytic adenoviral agent OBP-401 with docetaxel: preclinical evaluation of chemovirotherapy. Int J Cancer **119**, 432-440.

G

GABITZSCH, E.S., XU, Y., BALINT, J.P., JR., HARTMAN, Z.C., LYERLY, H.K., and JONES, F.R. (2010). Anti-tumor immunotherapy despite immunity to adenovirus using a novel adenoviral vector Ad5 [E1-, E2b-]-CEA. Cancer Immunol Immunother **59**, 1131-1135.

GABRILOVICH, D.I., ISHIDA, T., NADAF, S., OHM, J.E., and CARBONE, D.P. (1999). Antibodies to vascular endothelial growth factor enhance the efficacy of cancer immunotherapy by improving endogenous dendritic cell function. Clin Cancer Res **5**, 2963-2970.

GADOLA, S.D., MOINS-TEISSERENC, H.T., TROWSDALE, J., GROSS, W.L., and CERUNDOLO, V. (2000). TAP deficiency syndrome. Clin Exp Immunol **121**, 173-178.

GAJEWSKI, T.F., SCHREIBER, H., and FU, Y.X. (2013). Innate and adaptive immune cells in the tumor microenvironment. Nat Immunol **14**, 1014-1022.

GALANIS, E., OKUNO, S.H., NASCIMENTO, A.G., LEWIS, B.D., LEE, R.A., OLIVEIRA, A.M*., et al.* (2005). Phase I-II trial of ONYX-015 in combination with MAP chemotherapy in patients with advanced sarcomas. Gene therapy **12**, 437-445.

GALON, J., COSTES, A., SANCHEZ-CABO, F., KIRILOVSKY, A., MLECNIK, B., LAGORCE-PAGES, C*., et al.* (2006). Type, density, and location of immune cells within human colorectal tumors predict clinical outcome. Science **313**, 1960-1964.

GAMBOTTO, A., TUTING, T., MCVEY, D.L., KOVESDI, I., TAHARA, H., LOTZE, M.T*., et al.* (1999). Induction of antitumor immunity by direct intratumoral injection of a recombinant adenovirus vector expressing interleukin-12. Cancer Gene Ther **6**, 45-53.

GANESH, S., GONZALEZ-EDICK, M., GIBBONS, D., VAN ROEY, M., and JOOSS, K. (2008). Intratumoral coadministration of hyaluronidase enzyme and oncolytic adenoviruses enhances virus potency in metastatic tumor models. Clin Cancer Res **14**, 3933-3941.

GANESH, S., GONZALEZ EDICK, M., IDAMAKANTI, N., ABRAMOVA, M., VANROEY, M., ROBINSON, M*., et al.* (2007). Relaxin-expressing, fiber chimeric oncolytic adenovirus prolongs survival of tumor-bearing mice. Cancer Res **67**, 4399-4407.

GANLY, I., KIRN, D., ECKHARDT, G., RODRIGUEZ, G.I., SOUTAR, D.S., OTTO, R*., et al.* (2000a). A phase I study of Onyx-015, an E1B attenuated adenovirus, administered intratumorally to patients with recurrent head and neck cancer. Clin Cancer Res **6**, 798-806.

GANLY, I., MAUTNER, V., and BALMAIN, A. (2000b). Productive replication of human adenoviruses in mouse epidermal cells. J Virol **74**, 2895-2899.

GAO, J.Q., KANAGAWA, N., XU, D.H., HAN, M., SUGITA, T., HATANAKA, Y*., et al.* (2008). Combination of two fiber-mutant adenovirus vectors, one encoding the chemokine FKN and another encoding cytokine interleukin 12, elicits notably enhanced anti-tumor responses. Cancer Immunol Immunother **57**, 1657-1664.

GARBER, K. (2006). China approves world's first oncolytic virus therapy for cancer treatment. Journal of the National Cancer Institute **98**, 298-300.

GARCIA-CASTRO, J., ALEMANY, R., CASCALLO, M., MARTINEZ-QUINTANILLA, J., ARRIERO MDEL, M., LASSALETTA, A*., et al.* (2010). Treatment of metastatic neuroblastoma with systemic oncolytic virotherapy delivered by autologous mesenchymal stem cells: an exploratory study. Cancer Gene Ther **17**, 476-483.

GASTON, D.C., ODOM, C.I., LI, L., MARKERT, J.M., ROTH, J.C., CASSADY, K.A*., et al.* (2013). Production of Bioactive Soluble Interleukin-15 in Complex with Interleukin-15 Receptor Alpha from a Conditionally-Replicating Oncolytic HSV-1. PLoS One **8**, e81768.

GIETZ, R.D., and WOODS, R.A. (2002). Transformation of yeast by lithium acetate/single-stranded carrier DNA/polyethylene glycol method. Methods Enzymol **350**, 87-96.

GIL-HOYOS, R. (2014). Modificación genética de la immunodominancia epitópica del adenovirus para potenciar la respuesta immune contra epítopos no virales. Doctoral thesis, Universidad de Barcelona.

GIL-TORREGROSA, B.C., CASTANO, A.R., LOPEZ, D., and DEL VAL, M. (2000). Generation of MHC class I peptide antigens by protein processing in the secretory route by furin. Traffic **1**, 641-651.

GIL-TORREGROSA, B.C., RAUL CASTANO, A., and DEL VAL, M. (1998). Major histocompatibility complex class I viral antigen processing in the secretory pathway defined by the trans-Golgi network protease furin. J Exp Med **188**, 1105-1116.

GIMENEZ-ALEJANDRE, M., CASCALLO, M., BAYO-PUXAN, N., and ALEMANY, R. (2008). Coagulation factors determine tumor transduction in vivo. Hum Gene Ther **19**, 1415-1419.

GRAHAM, F.L., SMILEY, J., RUSSELL, W.C., and NAIRN, R. (1977). Characteristics of a human cell line transformed by DNA from human adenovirus type 5. J Gen Virol **36**, 59-74.

GRILL, J., VAN BEUSECHEM, V.W., VAN DER VALK, P., DIRVEN, C.M., LEONHART, A., PHERAI, D.S*., et al.* (2001). Combined targeting of adenoviruses to integrins and epidermal growth factor receptors increases gene transfer into primary glioma cells and spheroids. Clin Cancer Res **7**, 641-650.

GROS, A., MARTINEZ-QUINTANILLA, J., PUIG, C., GUEDAN, S., MOLLEVI, D.G., ALEMANY, R*., et al.* (2008). Bioselection of a gain of function mutation that enhances adenovirus 5 release and improves its antitumoral potency. Cancer Res **68**, 8928-8937.

GUEDAN, S., GRASES, D., ROJAS, J.J., GROS, A., VILARDELL, F., VILE, R*., et al.* (2012). GALV expression enhances the therapeutic efficacy of an oncolytic adenovirus by inducing cell fusion and enhancing virus distribution. Gene therapy **19**, 1048-1057.

GUEDAN, S., ROJAS, J.J., GROS, A., MERCADE, E., CASCALLO, M., and ALEMANY, R. (2010). Hyaluronidase expression by an oncolytic adenovirus enhances its intratumoral spread and suppresses tumor growth. Mol Ther **18**, 1275-1283.

GUERRA, N., TAN, Y.X., JONCKER, N.T., CHOY, A., GALLARDO, F., XIONG, N*., et al.* (2008). NKG2D-deficient mice are defective in tumor surveillance in models of spontaneous malignancy. Immunity **28**, 571-580.

H

HAHNE, M., RIMOLDI, D., SCHROTER, M., ROMERO, P., SCHREIER, M., FRENCH, L.E*., et al.* (1996). Melanoma cell expression of Fas(Apo-1/CD95) ligand: implications for tumor immune escape. Science **274**, 1363-1366.

HALLDEN, G., HILL, R., WANG, Y., ANAND, A., LIU, T.C., LEMOINE, N.R*., et al.* (2003). Novel immunocompetent murine tumor models for the assessment of replication-competent oncolytic adenovirus efficacy. Mol Ther **8**, 412-424.

HALLENBECK, P.L., CHANG, Y.N., HAY, C., GOLIGHTLY, D., STEWART, D., LIN, J*., et al.* (1999). A novel tumor-specific replication-restricted adenoviral vector for gene therapy of hepatocellular carcinoma. Hum Gene Ther **10**, 1721-1733.

HAMID, O., VARTERASIAN, M.L., WADLER, S., HECHT, J.R., BENSON, A., 3RD, GALANIS, E*., et al.* (2003). Phase II trial of intravenous CI-1042 in patients with metastatic colorectal cancer. J Clin Oncol **21**, 1498-1504.

HANAHAN, D., and WEINBERG, R.A. (2011). Hallmarks of cancer: the next generation. Cell **144**, 646-674.

HARALAMBIEVA, I., IANKOV, I., HASEGAWA, K., HARVEY, M., RUSSELL, S.J., and PENG, K.W. (2007). Engineering oncolytic measles virus to circumvent the intracellular innate immune response. Mol Ther **15**, 588-597.

HARRINGTON, L.E., MOST RV, R., WHITTON, J.L., and AHMED, R. (2002). Recombinant vaccinia virus-induced T-cell immunity: quantitation of the response to the virus vector and the foreign epitope. J Virol **76**, 3329-3337.

HARTMAN, Z.C., APPLEDORN, D.M., and AMALFITANO, A. (2008). Adenovirus vector induced innate immune responses: impact upon efficacy and toxicity in gene therapy and vaccine applications. Virus Res **132**, 1-14.

HARUI, A., ROTH, M.D., KIERTSCHER, S.M., MITANI, K., and BASAK, S.K. (2004). Vaccination with helper-dependent adenovirus enhances the generation of transgene-specific CTL. Gene therapy **11**, 1617-1626.

HECHT, J.R., BEDFORD, R., ABBRUZZESE, J.L., LAHOTI, S., REID, T.R., SOETIKNO, R.M*., et al.* (2003). A phase I/II trial of intratumoral endoscopic ultrasound injection of ONYX-015 with intravenous gemcitabine in unresectable pancreatic carcinoma. Clin Cancer Res **9**, 555-561.

HEDLEY, S.J., CHEN, J., MOUNTZ, J.D., LI, J., CURIEL, D.T., KOROKHOV, N*., et al.* (2006). Targeted and shielded adenovectors for cancer therapy. Cancer Immunol Immunother **55**, 1412-1419.

HEISE, C., HERMISTON, T., JOHNSON, L., BROOKS, G., SAMPSON-JOHANNES, A., WILLIAMS, A*., et al.* (2000). An adenovirus E1A mutant that demonstrates potent and selective systemic anti-tumoral efficacy. Nat Med **6**, 1134-1139.

HENDERSON, R.A., MICHEL, H., SAKAGUCHI, K., SHABANOWITZ, J., APPELLA, E., HUNT, D.F*., et al.* (1992). HLA-A2.1-associated peptides from a mutant cell line: a second pathway of antigen presentation. Science **255**, 1264-1266.

HEO, J., REID, T., RUO, L., BREITBACH, C.J., ROSE, S., BLOOMSTON, M*., et al.* (2013). Randomized dose-finding clinical trial of oncolytic immunotherapeutic vaccinia JX-594 in liver cancer. Nat Med **19**, 329-336.

HERMISTON, T.W., TRIPP, R.A., SPARER, T., GOODING, L.R., and WOLD, W.S. (1993). Deletion mutation analysis of the adenovirus type 2 E3-gp19K protein: identification of sequences within the endoplasmic reticulum lumenal domain that are required for class I antigen binding and protection from adenovirus-specific cytotoxic T lymphocytes. J Virol **67**, 5289-5298.

HERNANDEZ-ALCOCEBA, R., PIHALJA, M., QIAN, D., and CLARKE, M.F. (2002). New oncolytic adenoviruses with hypoxia- and estrogen receptor-regulated replication. Hum Gene Ther **13**, 1737-1750.

HINZ, S., TRAUZOLD, A., BOENICKE, L., SANDBERG, C., BECKMANN, S., BAYER, E*., et al.* (2000). Bcl-XL protects pancreatic adenocarcinoma cells against CD95- and TRAIL-receptor-mediated apoptosis. Oncogene **19**, 5477-5486.

HSIEH, C.L., YANG, L., MIAO, L., YEUNG, F., KAO, C., YANG, H.*, et al.* (2002). A novel targeting modality to enhance adenoviral replication by vitamin D(3) in androgen-independent human prostate cancer cells and tumors. Cancer Res **62**, 3084-3092.

HUANG, B., PAN, P.Y., LI, Q., SATO, A.I., LEVY, D.E., BROMBERG, J.*, et al.* (2006). Gr-1+CD115+ immature myeloid suppressor cells mediate the development of tumor-induced T regulatory cells and T-cell anergy in tumor-bearing host. Cancer Res **66**, 1123-1131.

HUANG, J., and SCHNEIDER, R.J. (1991). Adenovirus inhibition of cellular protein synthesis involves inactivation of cap-binding protein. Cell **65**, 271-280.

HUANG, T.G., SAVONTAUS, M.J., SHINOZAKI, K., SAUTER, B.V., and WOO, S.L.C. (2002). Telomerase-dependent oncolytic adenovirus for cancer treatment. Gene therapy **10**, 1241-1247.

HUEBNER, R.J., ROWE, W.P., SCHATTEN, W.E., SMITH, R.R., and THOMAS, L.B. (1956). Studies on the use of viruses in the treatment of carcinoma of the cervix. Cancer **9**, 1211-1218.

HUNG, K., HAYASHI, R., LAFOND-WALKER, A., LOWENSTEIN, C., PARDOLL, D., and LEVITSKY, H. (1998). The central role of CD4(+) T cells in the antitumor immune response. J Exp Med **188**, 2357-2368.

HUNTER-CRAIG, I., NEWTON, K.A., WESTBURY, G., and LACEY, B.W. (1970). Use of vaccinia virus in the treatment of metastatic malignant melanoma. Br Med J **2**, 512-515.

I

IKEGAMI-KAWAI, M., and TAKAHASHI, T. (2002). Microanalysis of hyaluronan oligosaccharides by polyacrylamide gel electrophoresis and its application to assay of hyaluronidase activity. Anal Biochem **311**, 157-165.

J

JACKSON, M.R., NILSSON, T., and PETERSON, P.A. (1993). Retrieval of transmembrane proteins to the endoplasmic reticulum. J Cell Biol **121**, 317-333.

JACOBETZ, M.A., CHAN, D.S., NEESSE, A., BAPIRO, T.E., COOK, N., FRESE, K.K.*, et al.* (2013). Hyaluronan impairs vascular function and drug delivery in a mouse model of pancreatic cancer. Gut **62**, 112-120.

JAGER, E., RINGHOFFER, M., KARBACH, J., ARAND, M., OESCH, F., and KNUTH, A. (1996). Inverse relationship of melanocyte differentiation antigen expression in melanoma tissues and CD8+ cytotoxic-T-cell responses: evidence for immunoselection of antigen-loss variants in vivo. Int J Cancer **66**, 470-476.

JIANG, H., WHITE, E.J., RIOS-VICIL, C.I., XU, J., GOMEZ-MANZANO, C., and FUEYO, J. (2011). Human adenovirus type 5 induces cell lysis through autophagy and autophagy-triggered caspase activity. J Virol **85**, 4720-4729.

JOFFRE, O.P., SEGURA, E., SAVINA, A., and AMIGORENA, S. (2012). Cross-presentation by dendritic cells. Nat Rev Immunol **12**, 557-569.

JOGLER, C., HOFFMANN, D., THEEGARTEN, D., GRUNWALD, T., UBERLA, K., and WILDNER, O. (2006). Replication properties of human adenovirus in vivo and in cultures of primary cells from different animal species. J Virol **80**, 3549-3558.

JOHNSON, L., SHEN, A., BOYLE, L., KUNICH, J., PANDEY, K., LEMMON, M.*, et al.* (2002). Selectively replicating adenoviruses targeting deregulated E2F activity are potent, systemic antitumor agents. Cancer Cell **1**, 325-337.

JOHNSTON, J.H., and SIMMONS, D.A. (1968). The immunochemistry of Shigella flexneri O-antigens: an analysis of the immunodominant sugars in lipopolysaccharides from smooth strains. J Pathol Bacteriol **95**, 477-480.

JUNE, C.H. (2007). Adoptive T cell therapy for cancer in the clinic. J Clin Invest **117**, 1466-1476.

K

KAFRI, T., MORGAN, D., KRAHL, T., SARVETNICK, N., SHERMAN, L., and VERMA, I. (1998). Cellular immune response to adenoviral vector infected cells does not require de novo viral gene expression: implications for gene therapy. Proc Natl Acad Sci U S A **95**, 11377-11382.

KAKLAMANIS, L., TOWNSEND, A., DOUSSIS-ANAGNOSTOPOULOU, I.A., MORTENSEN, N., HARRIS, A.L., and GATTER, K.C. (1994). Loss of major histocompatibility complex-encoded transporter associated with antigen presentation (TAP) in colorectal cancer. Am J Pathol **145**, 505-509.

KALUZA, K.M., KOTTKE, T., DIAZ, R.M., ROMMELFANGER, D., THOMPSON, J., and VILE, R. (2012). Adoptive transfer of cytotoxic T lymphocytes targeting two different antigens limits antigen loss and tumor escape. Hum Gene Ther **23**, 1054-1064.

KALUZA, K.M., THOMPSON, J.M., KOTTKE, T.J., FLYNN GILMER, H.C., KNUTSON, D.L., and VILE, R.G. (2011). Adoptive T cell therapy promotes the emergence of genomically altered tumor escape variants. Int J Cancer **131**, 844-854.

KALYUZHNIY, O., DI PAOLO, N.C., SILVESTRY, M., HOFHERR, S.E., BARRY, M.A., STEWART, P.L.*, et al.* (2008). Adenovirus serotype 5 hexon is critical for virus infection of hepatocytes in vivo. Proc Natl Acad Sci U S A **105**, 5483-5488.

KAPLAN, D.H., SHANKARAN, V., DIGHE, A.S., STOCKERT, E., AGUET, M., OLD, L.J.*, et al.* (1998). Demonstration of an interferon gamma-dependent tumor surveillance system in immunocompetent mice. Proc Natl Acad Sci U S A **95**, 7556-7561.

KARAN, D., DUBEY, S., VAN VELDHUIZEN, P., HOLZBEIERLEIN, J.M., TAWFIK, O., and THRASHER, J.B. (2011). Dual antigen target-based immunotherapy for prostate cancer eliminates the growth of established tumors in mice. Immunotherapy **3**, 735-746.

KARLSEDER, J., ROTHENEDER, H., and WINTERSBERGER, E. (1996). Interaction of Sp1 with the growth- and cell cycle-regulated transcription factor E2F. Mol Cell Biol **16**, 1659-1667.

KARRE, K., LJUNGGREN, H.G., PIONTEK, G., and KIESSLING, R. (1986). Selective rejection of H-2-deficient lymphoma variants suggests alternative immune defence strategy. Nature **319**, 675-678.

KATAOKA, T., SCHROTER, M., HAHNE, M., SCHNEIDER, P., IRMLER, M., THOME, M.*, et al.* (1998). FLIP prevents apoptosis induced by death receptors but not by perforin/granzyme B, chemotherapeutic drugs, and gamma irradiation. J Immunol **161**, 3936-3942.

KAUFMAN, H.L., and BINES, S.D. (2010). OPTIM trial: a Phase III trial of an oncolytic herpes virus encoding GM-CSF for unresectable stage III or IV melanoma. Future Oncol **6**, 941-949.

KEDL, R.M., KAPPLER, J.W., and MARRACK, P. (2003). Epitope dominance, competition and T cell affinity maturation. Current Opinion in Immunology **15**, 120-127.

KELLY, E., and RUSSELL, S.J. (2007). History of oncolytic viruses: genesis to genetic engineering. Mol Ther **15**, 651-659.

KHONG, H.T., WANG, Q.J., and ROSENBERG, S.A. (2004). Identification of multiple antigens recognized by tumor-infiltrating lymphocytes from a single patient: tumor escape by antigen loss and loss of MHC expression. J Immunother **27**, 184-190.

KHURI, F.R., NEMUNAITIS, J., GANLY, I., ARSENEAU, J., TANNOCK, I.F., ROMEL, L.*, et al.* (2000a). a controlled trial of intratumoral ONYX-015, a selectively-replicating adenovirus, in combination with cisplatin and 5-fluorouracil in patients with recurrent head and neck cancer. Nat Med **6**, 879-885.

KHURI, F.R., SHIN, D.M., GLISSON, B.S., LIPPMAN, S.M., and HONG, W.K. (2000b). Treatment of patients with recurrent or metastatic squamous cell carcinoma of the head and neck: current status and future directions. Semin Oncol **27**, 25-33.

KIM, D.T., MITCHELL, D.J., BROCKSTEDT, D.G., FONG, L., NOLAN, G.P., FATHMAN, C.G.*, et al.* (1997). Introduction of soluble proteins into the MHC class I pathway by conjugation to an HIV tat peptide. J Immunol **159**, 1666-1668.

KIM, J.H., LEE, Y.S., KIM, H., HUANG, J.H., YOON, A.R., and YUN, C.O. (2006). Relaxin expression from tumor-targeting adenoviruses and its intratumoral spread, apoptosis induction, and efficacy. Journal of the National Cancer Institute **98**, 1482-1493.

KIMBALL, K.J., PREUSS, M.A., BARNES, M.N., WANG, M., SIEGAL, G.P., WAN, W.*, et al.* (2010). A phase I study of a tropism-modified conditionally replicative adenovirus for recurrent malignant gynecologic diseases. Clin Cancer Res **16**, 5277-5287.

KLOCKER, J., SABITZER, H., RAUNIK, W., WIESER, S., and SCHUMER, J. (1998). Hyaluronidase as additive to induction chemotherapy in advanced squamous cell carcinoma of the head and neck. Cancer Lett **131**, 113-115.

KOEBEL, C.M., VERMI, W., SWANN, J.B., ZERAFA, N., RODIG, S.J., OLD, L.J.*, et al.* (2007). Adaptive immunity maintains occult cancer in an equilibrium state. Nature **450**, 903-907.

KOSKI, A., KANGASNIEMI, L., ESCUTENAIRE, S., PESONEN, S., CERULLO, V., DIACONU, I.*, et al.* (2010). Treatment of cancer patients with a serotype 5/3 chimeric oncolytic adenovirus expressing GMCSF. Mol Ther **18**, 1874-1884.

KOTTKE, T., ERRINGTON, F., PULIDO, J., GALIVO, F., THOMPSON, J., WONGTHIDA, P.*, et al.* (2011). Broad antigenic coverage induced by vaccination with virus-based cDNA libraries cures established tumors. Nat Med **17**, 854-859.

KRASNYKH, V., DMITRIEV, I., MIKHEEVA, G., MILLER, C.R., BELOUSOVA, N., and CURIEL, D.T. (1998). Characterization of an adenovirus vector containing a heterologous peptide epitope in the HI loop of the fiber knob. J Virol **72**, 1844-1852.

KRAUSE, A., JOH, J.H., HACKETT, N.R., ROELVINK, P.W., BRUDER, J.T., WICKHAM, T.J.*, et al.* (2006). Epitopes expressed in different adenovirus capsid proteins induce different levels of epitope-specific immunity. J Virol **80**, 5523-5530.

KRITZ, A.B., NICOL, C.G., DISHART, K.L., NELSON, R., HOLBECK, S., VON SEGGERN, D.J.*, et al.* (2007). Adenovirus 5 Fibers Mutated at the Putative HSPG-binding Site Show Restricted Retargeting with Targeting Peptides in the HI Loop. Mol Ther **15**, 741-749.

KUHN, I., HARDEN, P., BAUZON, M., CHARTIER, C., NYE, J., THORNE, S.*, et al.* (2008). Directed evolution generates a novel oncolytic virus for the treatment of colon cancer. PLoS One **3**, e2409.

KULTTI, A., LI, X., JIANG, P., THOMPSON, C.B., FROST, G.I., and SHEPARD, H.M. (2012). Therapeutic Targeting of Hyaluronan in the Tumor Stroma. Cancers **4**, 873-903.

KURACHI, S., KOIZUMI, N., SAKURAI, F., KAWABATA, K., SAKURAI, H., NAKAGAWA, S.*, et al.* (2007). Characterization of capsid-modified adenovirus vectors containing heterologous peptides in the fiber knob, protein IX, or hexon. Gene therapy **14**, 266-274.

L

LAMONT, J.P., NEMUNAITIS, J., KUHN, J.A., LANDERS, S.A., and MCCARTY, T.M. (2000). A prospective phase II trial of ONYX-015 adenovirus and chemotherapy in recurrent squamous cell carcinoma of the head and neck (the Baylor experience). Ann Surg Oncol **7**, 588-592.

LAPTEVA, N., ALDRICH, M., WEKSBERG, D., ROLLINS, L., GOLTSOVA, T., CHEN, S.Y.*, et al.* (2009). Targeting the intratumoral dendritic cells by the oncolytic adenoviral vaccine expressing RANTES elicits potent antitumor immunity. J Immunother **32**, 145-156.

LE, H.K., GRAHAM, L., CHA, E., MORALES, J.K., MANJILI, M.H., and BEAR, H.D. (2009). Gemcitabine directly inhibits myeloid derived suppressor cells in BALB/c mice bearing 4T1 mammary carcinoma and augments expansion of T cells from tumor-bearing mice. Int Immunopharmacol **9**, 900-909.

LE, L.P., EVERTS, M., DMITRIEV, I.P., DAVYDOVA, J.G., YAMAMOTO, M., and CURIEL, D.T. (2004). Fluorescently labeled adenovirus with pIX-EGFP for vector detection. Mol Imaging **3**, 105-116.

LE, L.P., LI, J., TERNOVOI, V.V., SIEGAL, G.P., and CURIEL, D.T. (2005). Fluorescently tagged canine adenovirus via modification with protein IX-enhanced green fluorescent protein. J Gen Virol **86**, 3201-3208.

LEE, Y.S., KIM, J.H., CHOI, K.J., CHOI, I.K., KIM, H., CHO, S.*, et al.* (2006). Enhanced antitumor effect of oncolytic adenovirus expressing interleukin-12 and B7-1 in an immunocompetent murine model. Clin Cancer Res **12**, 5859-5868.

LEONE, P., SHIN, E.C., PEROSA, F., VACCA, A., DAMMACCO, F., and RACANELLI, V. (2013). MHC class I antigen processing and presenting machinery: organization, function, and defects in tumor cells. Journal of the National Cancer Institute **105**, 1172-1187.

LEONHARDT, R.M., FIEGL, D., RUFER, E., KARGER, A., BETTIN, B., and KNITTLER, M.R. (2010). Post-endoplasmic reticulum rescue of unstable MHC class I requires proprotein convertase PC7. J Immunol **184**, 2985-2998.

LI, H., HAN, Y., GUO, Q., ZHANG, M., and CAO, X. (2009a). Cancer-expanded myeloid-derived suppressor cells induce anergy of NK cells through membrane-bound TGF-beta 1. J Immunol **182**, 240-249.

LI, J.L., LIU, H.L., ZHANG, X.R., XU, J.P., HU, W.K., LIANG, M.*, et al.* (2009b). A phase I trial of intratumoral administration of recombinant oncolytic adenovirus overexpressing HSP70 in advanced solid tumor patients. Gene therapy **16**, 376-382.

LICHTENSTEIN, D.L., SPENCER, J.F., DORONIN, K., PATRA, D., MEYER, J.M., SHASHKOVA, E.V.*, et al.* (2009). An acute toxicology study with INGN 007, an oncolytic adenovirus vector, in mice and permissive Syrian hamsters; comparisons with wild-type Ad5 and a replication-defective adenovirus vector. Cancer Gene Ther **16**, 644-654.

LICHTY, B.D., BREITBACH, C.J., STOJDL, D.F., and BELL, J.C. (2014). Going viral with cancer immunotherapy. Nature reviews **14**, 559-567.

LOPEZ, M.V., RIVERA, A.A., VIALE, D.L., BENEDETTI, L., CUNEO, N., KIMBALL, K.J.*, et al.* (2012). A tumor-stroma targeted oncolytic adenovirus replicated in human ovary cancer samples and inhibited growth of disseminated solid tumors in mice. Mol Ther **20**, 2222-2233.

LU, J., HIGASHIMOTO, Y., APPELLA, E., and CELIS, E. (2004). Multiepitope Trojan Antigen Peptide Vaccines for the Induction of Antitumor CTL and Th Immune Responses. The Journal of Immunology **172**, 4575-4582.

LU, J., WETTSTEIN, P.J., HIGASHIMOTO, Y., APPELLA, E., and CELIS, E. (2001). TAP-Independent Presentation of CTL Epitopes by Trojan Antigens. The Journal of Immunology **166**, 7063-7071.

M

MAECKER, H.T., UMETSU, D.T., DEKRUYFF, R.H., and LEVY, S. (1998). Cytotoxic T cell responses to DNA vaccination: dependence on antigen presentation via class II MHC. J Immunol **161**, 6532-6536.

MAKOWER, D., ROZENBLIT, A., KAUFMAN, H., EDELMAN, M., LANE, M.E., ZWIEBEL, J.*, et al.* (2003). Phase II clinical trial of intralesional administration of the oncolytic adenovirus ONYX-015 in patients with hepatobiliary tumors with correlative p53 studies. Clin Cancer Res **9**, 693-702.

MARTINI, M., TESTI, M.G., PASETTO, M., PICCHIO, M.C., INNAMORATI, G., MAZZOCCO, M.*, et al.* (2010). IFN-gamma-mediated upmodulation of MHC class I expression activates tumor-specific immune response in a mouse model of prostate cancer. Vaccine **28**, 3548-3557.

MARTUZA, R.L., MALICK, A., MARKERT, J.M., RUFFNER, K.L., and COEN, D.M. (1991). Experimental therapy of human glioma by means of a genetically engineered virus mutant. Science **252**, 854-856.

MATZINGER, P. (1994). Tolerance, danger, and the extended family. Annu Rev Immunol **12**, 991-1045.

MAUS, M.V., GRUPP, S.A., PORTER, D.L., and JUNE, C.H. (2014). Antibody-modified T cells: CARs take the front seat for hematologic malignancies. Blood **123**, 2625-2635.

MCCONNELL, M.J., and IMPERIALE, M.J. (2004). Biology of adenovirus and its use as a vector for gene therapy. Hum Gene Ther **15**, 1022-1033.

MEIER, O., BOUCKE, K., HAMMER, S.V., KELLER, S., STIDWILL, R.P., HEMMI, S.*, et al.* (2002). Adenovirus triggers macropinocytosis and endosomal leakage together with its clathrin-mediated uptake. J Cell Biol **158**, 1119-1131.

MELLMAN, I., COUKOS, G., and DRANOFF, G. (2011). Cancer immunotherapy comes of age. Nature **480**, 480-489.

MEULENBROEK, R.A., SARGENT, K.L., LUNDE, J., JASMIN, B.J., and PARKS, R.J. (2004). Use of adenovirus protein IX (pIX) to display large polypeptides on the virion--generation of fluorescent virus through the incorporation of pIX-GFP. Mol Ther **9**, 617-624.

MICHL, P., and GRESS, T.M. (2012). Improving drug delivery to pancreatic cancer: breaching the stromal fortress by targeting hyaluronic acid. Gut **61**, 1377-1379.

MIRALLES, M., SEGURA, M.M., PUIG, M., BOSCH, A., and CHILLON, M. (2012). Efficient amplification of chimeric adenovirus 5/40S vectors carrying the short fiber protein of Ad40 in suspension cell cultures. PLoS One **7**, e42073.

MOMBURG, F., and HENGEL, H. (2002). Corking the bottleneck: the transporter associated with antigen processing as a target for immune subversion by viruses. Curr Top Microbiol Immunol **269**, 57-74.

MOORE, M.W., CARBONE, F.R., and BEVAN, M.J. (1988). Introduction of soluble protein into the class I pathway of antigen processing and presentation. Cell **54**, 777-785.

MULVIHILL, S., WARREN, R., VENOOK, A., ADLER, A., RANDLEV, B., HEISE, C.*, et al.* (2001). Safety and feasibility of injection with an E1B-55 kDa gene-deleted, replication-selective adenovirus (ONYX-015) into primary carcinomas of the pancreas: a phase I trial. Gene therapy **8**, 308-315.

MURUVE, D.A. (2004). The innate immune response to adenovirus vectors. Hum Gene Ther **15**, 1157-1166.

N

NAGARAJ, S., GUPTA, K., PISAREV, V., KINARSKY, L., SHERMAN, S., KANG, L.*, et al.* (2007). Altered recognition of antigen is a mechanism of CD8+ T cell tolerance in cancer. Nat Med **13**, 828-835.

NAGEL, H., MAAG, S., TASSIS, A., NESTLE, F.O., GREBER, U.F., and HEMMI, S. (2003). The alphavbeta5 integrin of hematopoietic and nonhematopoietic cells is a transduction receptor of RGD-4C fiber-modified adenoviruses. Gene therapy **10**, 1643-1653.

NAKASHIMA, H., KAUR, B., and CHIOCCA, E.A. (2010). Directing systemic oncolytic viral delivery to tumors via carrier cells. Cytokine Growth Factor Rev **21**, 119-126.

NELSON, A.R., DAVYDOVA, J., CURIEL, D.T., and YAMAMOTO, M. (2009). Combination of conditionally replicative adenovirus and standard chemotherapies shows synergistic antitumor effect in pancreatic cancer. Cancer Sci **100**, 2181-2187.

NEMUNAITIS, J., CUNNINGHAM, C., BUCHANAN, A., BLACKBURN, A., EDELMAN, G., MAPLES, P.*, et al.* (2001a). Intravenous infusion of a replication-selective adenovirus (ONYX-015) in cancer patients: safety, feasibility and biological activity. Gene therapy **8**, 746-759.

NEMUNAITIS, J., KHURI, F., GANLY, I., ARSENEAU, J., POSNER, M., VOKES, E.*, et al.* (2001b). Phase II trial of intratumoral administration of ONYX-015, a replication-selective adenovirus, in patients with refractory head and neck cancer. J Clin Oncol **19**, 289-298.

NEMUNAITIS, J., SENZER, N., SARMIENTO, S., ZHANG, Y.A., ARZAGA, R., SANDS, B.*, et al.* (2007). A phase I trial of intravenous infusion of ONYX-015 and enbrel in solid tumor patients. Cancer Gene Ther **14**, 885-893.

NEMUNAITIS, J., TONG, A.W., NEMUNAITIS, M., SENZER, N., PHADKE, A.P., BEDELL, C.*, et al.* (2010). A phase I study of telomerase-specific replication competent oncolytic adenovirus (telomelysin) for various solid tumors. Mol Ther **18**, 429-434.

NETTELBECK, D.M., RIVERA, A.A., BALAGUE, C., ALEMANY, R., and CURIEL, D.T. (2002). Novel oncolytic adenoviruses targeted to melanoma: specific viral replication and cytolysis by expression of E1A mutants from the tyrosinase enhancer/promoter. Cancer Res **62**, 4663-4670.

NICOL, C.G., GRAHAM, D., MILLER, W.H., WHITE, S.J., SMITH, T.A., NICKLIN, S.A.*, et al.* (2004). Effect of adenovirus serotype 5 fiber and penton modifications on in vivo tropism in rats. Mol Ther **10**, 344-354.

NILSSON, T., JACKSON, M., and PETERSON, P.A. (1989). Short cytoplasmic sequences serve as retention signals for transmembrane proteins in the endoplasmic reticulum. Cell **58**, 707-718.

NOKISALMI, P., PESONEN, S., ESCUTENAIRE, S., SARKIOJA, M., RAKI, M., CERULLO, V.*, et al.* (2010). Oncolytic adenovirus ICOVIR-7 in patients with advanced and refractory solid tumors. Clin Cancer Res **16**, 3035-3043.

NOWAK, A.K., ROBINSON, B.W., and LAKE, R.A. (2002). Gemcitabine exerts a selective effect on the humoral immune response: implications for combination chemo-immunotherapy. Cancer Res **62**, 2353-2358.

O

ONIMARU, M., OHUCHIDA, K., NAGAI, E., MIZUMOTO, K., EGAMI, T., CUI, L.*, et al.* (2011). Combination with low-dose gemcitabine and hTERT-promoter-dependent conditionally

replicative adenovirus enhances cytotoxicity through their crosstalk mechanisms in pancreatic cancer. Cancer Lett **294**, 178-186.

OVERWIJK, W.W., TSUNG, A., IRVINE, K.R., PARKHURST, M.R., GOLETZ, T.J., TSUNG, K.*, et al.* (1998). gp100/pmel 17 is a murine tumor rejection antigen: induction of "self"-reactive, tumoricidal T cells using high-affinity, altered peptide ligand. J Exp Med **188**, 277-286.

P

PAABO, S., BHAT, B.M., WOLD, W.S., and PETERSON, P.A. (1987). A short sequence in the COOH-terminus makes an adenovirus membrane glycoprotein a resident of the endoplasmic reticulum. Cell **50**, 311-317.

PAGE, J.G., TIAN, B., SCHWEIKART, K., TOMASZEWSKI, J., HARRIS, R., BROADT, T.*, et al.* (2007). Identifying the safety profile of a novel infectivity-enhanced conditionally replicative adenovirus, Ad5-delta24-RGD, in anticipation of a phase I trial for recurrent ovarian cancer. American journal of obstetrics and gynecology **196**, 389 e381-389; discussion 389 e389-310.

PAGES, F., BERGER, A., CAMUS, M., SANCHEZ-CABO, F., COSTES, A., MOLIDOR, R.*, et al.* (2005). Effector memory T cells, early metastasis, and survival in colorectal cancer. N Engl J Med **353**, 2654-2666.

PARATO, K.A., SENGER, D., FORSYTH, P.A., and BELL, J.C. (2005). Recent progress in the battle between oncolytic viruses and tumours. Nature reviews **5**, 965-976.

PARDOLL, D.M. (2012). The blockade of immune checkpoints in cancer immunotherapy. Nature reviews **12**, 252-264.

PARHAM, P., and BODMER, W.F. (1978). Monoclonal antibody to a human histocompatibility alloantigen, HLA-A2. Nature **276**, 397-399.

PARK, B.-H., HWANG, T., LIU, T.-C., SZE, D.Y., KIM, J.-S., KWON, H.-C.*, et al.* (2008). Use of a targeted oncolytic poxvirus, JX-594, in patients with refractory primary or metastatic liver cancer: a phase I trial. The Lancet Oncology **9**, 533-542.

PARRENO, M., GARRIGA, J., LIMON, A., ALBRECHT, J.H., and GRANA, X. (2001). E1A modulates phosphorylation of p130 and p107 by differentially regulating the activity of G1/S cyclin/CDK complexes. Oncogene **20**, 4793-4806.

PESONEN, S., DIACONU, I., CERULLO, V., ESCUTENAIRE, S., RAKI, M., KANGASNIEMI, L.*, et al.* (2011). Integrin targeted oncolytic adenoviruses Ad5-D24-RGD and Ad5-RGD-D24-GMCSF for treatment of patients with advanced chemotherapy refractory solid tumors. Int J Cancer **130**, 1937-1947.

PETER, I., MEZZACASA, A., LEDONNE, P., DUMMER, R., and HEMMI, S. (2001). Comparative analysis of immunocritical melanoma markers in the mouse melanoma cell lines B16, K1735 and S91-M3. Melanoma Res **11**, 21-30.

PETTIT, S.J., SEYMOUR, K., O'FLAHERTY, E., and KIRBY, J.A. (2000). Immune selection in neoplasia: towards a microevolutionary model of cancer development. Br J Cancer **82**, 1900-1906.

PILLWEIN, K., FUIKO, R., SLAVC, I., CZECH, T., HAWLICZEK, G., BERNHARDT, G.*, et al.* (1998). Hyaluronidase additional to standard chemotherapy improves outcome for children with malignant brain tumors. Cancer Lett **131**, 101-108.

PORGADOR, A., YEWDELL, J.W., DENG, Y., BENNINK, J.R., and GERMAIN, R.N. (1997). Localization, quantitation, and in situ detection of specific peptide-MHC class I complexes using a monoclonal antibody. Immunity **6**, 715-726.

PROVENZANO, P.P., CUEVAS, C., CHANG, A.E., GOEL, V.K., VON HOFF, D.D., and HINGORANI, S.R. (2012). Enzymatic targeting of the stroma ablates physical barriers to treatment of pancreatic ductal adenocarcinoma. Cancer Cell **21**, 418-429.

PUIG-SAUS, C., GROS, A., ALEMANY, R., and CASCALLO, M. (2012). Adenovirus i-leader truncation bioselected against cancer-associated fibroblasts to overcome tumor stromal barriers. Mol Ther **20**, 54-62.

PUIG-SAUS, C., LABORDA, E., RODRIGUEZ-GARCIA, A., CASCALLO, M., MORENO, R., and ALEMANY, R. (2014). The combination of i-leader truncation and gemcitabine improves oncolytic adenovirus efficacy in an immunocompetent model. Cancer Gene Ther.

R

RAAFAT, N., SADOWSKI-CRON, C., MENGUS, C., HEBERER, M., SPAGNOLI, G.C., and ZAJAC, P. (2012). Preventing vaccinia virus class-I epitopes presentation by HSV-ICP47 enhances the immunogenicity of a TAP-independent cancer vaccine epitope. Int J Cancer **131**, E659-669.

RAKI, M., KANERVA, A., RISTIMAKI, A., DESMOND, R.A., CHEN, D.T., RANKI, T.*, et al.* (2005). Combination of gemcitabine and Ad5/3-Delta24, a tropism modified conditionally replicating adenovirus, for the treatment of ovarian cancer. Gene therapy **12**, 1198-1205.

RAMESH, N., GE, Y., ENNIST, D.L., ZHU, M., MINA, M., GANESH, S.*, et al.* (2006). CG0070, a conditionally replicating granulocyte macrophage colony-stimulating factor--armed oncolytic adenovirus for the treatment of bladder cancer. Clin Cancer Res **12**, 305-313.

REID, T., GALANIS, E., ABBRUZZESE, J., SZE, D., WEIN, L.M., ANDREWS, J.*, et al.* (2002a). Hepatic arterial infusion of a replication-selective oncolytic adenovirus (dl1520): phase II viral, immunologic, and clinical endpoints. Cancer Res **62**, 6070-6079.

REID, T., WARREN, R., and KIRN, D. (2002b). Intravascular adenoviral agents in cancer patients: lessons from clinical trials. Cancer Gene Ther **9**, 979-986.

REID, T.R., FREEMAN, S., POST, L., MCCORMICK, F., and SZE, D.Y. (2005). Effects of Onyx-015 among metastatic colorectal cancer patients that have failed prior treatment with 5-FU/leucovorin. Cancer Gene Ther **12**, 673-681.

RESPA, A., BUKUR, J., FERRONE, S., PAWELEC, G., ZHAO, Y., WANG, E.*, et al.* (2011). Association of IFN-gamma signal transduction defects with impaired HLA class I antigen processing in melanoma cell lines. Clin Cancer Res **17**, 2668-2678.

RESTIFO, N.P., MARINCOLA, F.M., KAWAKAMI, Y., TAUBENBERGER, J., YANNELLI, J.R., and ROSENBERG, S.A. (1996). Loss of functional beta 2-microglobulin in metastatic melanomas

from five patients receiving immunotherapy. Journal of the National Cancer Institute **88**, 100-108.

RETTIG, L., SEIDENBERG, S., PARVANOVA, I., SAMARAS, P., CURIONI, A., KNUTH, A.*, et al.* (2011). Gemcitabine depletes regulatory T-cells in human and mice and enhances triggering of vaccine-specific cytotoxic T-cells. Int J Cancer **129**, 832-838.

RICHARDSON, J.S., PILLET, S., BELLO, A.J., and KOBINGER, G.P. (2013). Airway delivery of an adenovirus-based Ebola virus vaccine bypasses existing immunity to homologous adenovirus in nonhuman primates. J Virol **87**, 3668-3677.

RIOND, J., RODRIGUEZ, S., NICOLAU, M.L., AL SAATI, T., and GAIRIN, J.E. (2009). In vivo major histocompatibility complex class I (MHCI) expression on MHCIlow tumor cells is regulated by gammadelta T and NK cells during the early steps of tumor growth. Cancer Immun **9**, 10.

RITTNER, K., SCHREIBER, V., ERBS, P., and LUSKY, M. (2007). Targeting of adenovirus vectors carrying a tumor cell-specific peptide: in vitro and in vivo studies. Cancer Gene Ther **14**, 509-518.

RODRIGUEZ-GARCIA, A., GIMENEZ-ALEJANDRE, M., ROJAS, J., MORENO, R., BAZAN-PEREGINO, M., CASCALLO, M.*, et al.* (2014). Safety and efficacy of VCN-01, an oncolytic adenovirus combining fiber HSG-binding domain replacement with RGD and hyaluronidase expression. Clin Cancer Res.

RODRIGUEZ-ROCHA, H., GOMEZ-GUTIERREZ, J.G., GARCIA-GARCIA, A., RAO, X.M., CHEN, L., MCMASTERS, K.M.*, et al.* (2011). Adenoviruses induce autophagy to promote virus replication and oncolysis. Virology **416**, 9-15.

RODRIGUEZ, R., SCHUUR, E.R., LIM, H.Y., HENDERSON, G.A., SIMONS, J.W., and HENDERSON, D.R. (1997). Prostate attenuated replication competent adenovirus (ARCA) CN706: a selective cytotoxic for prostate-specific antigen-positive prostate cancer cells. Cancer Res **57**, 2559-2563.

ROJAS, J. J. (2010). Desenvolupament d'un adenovirus oncolític potent i selectiu com a base per a la incorporació de transgens que ajudin a l'eradicació dels tumors. Doctoral thesis, Universitat Autónoma de Barcelona.

ROJAS, J.J., CASCALLO, M., GUEDAN, S., GROS, A., MARTINEZ-QUINTANILLA, J., HEMMINKI, A.*, et al.* (2009). A modified E2F-1 promoter improves the efficacy to toxicity ratio of oncolytic adenoviruses. Gene therapy **16**, 1441-1451.

ROJAS, J.J., GIMENEZ-ALEJANDRE, M., GIL-HOYOS, R., CASCALLO, M., and ALEMANY, R. (2011). Improved systemic antitumor therapy with oncolytic adenoviruses by replacing the fiber shaft HSG-binding domain with RGD. Gene therapy **19**, 453-457.

ROJAS, J.J., GUEDAN, S., SEARLE, P.F., MARTINEZ-QUINTANILLA, J., GIL-HOYOS, R., ALCAYAGA-MIRANDA, F.*, et al.* (2010). Minimal RB-responsive E1A promoter modification to attain potency, selectivity, and transgene-arming capacity in oncolytic adenoviruses. Mol Ther **18**, 1960-1971.

ROSENBERG, S.A., RESTIFO, N.P., YANG, J.C., MORGAN, R.A., and DUDLEY, M.E. (2008). Adoptive cell transfer: a clinical path to effective cancer immunotherapy. Nature reviews **8**, 299-308.

ROSENBERG, S.A., YANG, J.C., SHERRY, R.M., KAMMULA, U.S., HUGHES, M.S., PHAN, G.Q.*, et al.* (2011). Durable complete responses in heavily pretreated patients with metastatic melanoma using T-cell transfer immunotherapy. Clin Cancer Res **17**, 4550-4557.

ROSENBERG, S.A., ZHAI, Y., YANG, J.C., SCHWARTZENTRUBER, D.J., HWU, P., MARINCOLA, F.M.*, et al.* (1998). Immunizing patients with metastatic melanoma using recombinant adenoviruses encoding MART-1 or gp100 melanoma antigens. Journal of the National Cancer Institute **90**, 1894-1900.

ROWE, W.P., HUEBNER, R.J., GILMORE, L.K., PARROTT, R.H., and WARD, T.G. (1953). Isolation of a cytopathogenic agent from human adenoids undergoing spontaneous degeneration in tissue culture. Proc Soc Exp Biol Med **84**, 570-573.

RUBINSTEIN, N., ALVAREZ, M., ZWIRNER, N.W., TOSCANO, M.A., ILARREGUI, J.M., BRAVO, A.*, et al.* (2004). Targeted inhibition of galectin-1 gene expression in tumor cells results in heightened T cell-mediated rejection; A potential mechanism of tumor-immune privilege. Cancer Cell **5**, 241-251.

RUSSELL, S.J., PENG, K.W., and BELL, J.C. (2012). Oncolytic virotherapy. Nat Biotechnol **30**, 658-670.

RUSSELL, W.C. (2009). Adenoviruses: update on structure and function. J Gen Virol **90**, 1-20.

RUX, J.J., and BURNETT, R.M. (2004). Adenovirus structure. Hum Gene Ther **15**, 1167-1176.

S

SANGRO, B., MAZZOLINI, G., RUIZ, J., HERRAIZ, M., QUIROGA, J., HERRERO, I.*, et al.* (2004). Phase I trial of intratumoral injection of an adenovirus encoding interleukin-12 for advanced digestive tumors. J Clin Oncol **22**, 1389-1397.

SCHAFER, S., WEIBEL, S., DONAT, U., ZHANG, Q., AGUILAR, R.J., CHEN, N.G.*, et al.* (2012). Vaccinia virus-mediated intra-tumoral expression of matrix metalloproteinase 9 enhances oncolysis of PC-3 xenograft tumors. BMC cancer **12**, 366.

SCHIERER, S., HESSE, A., KNIPPERTZ, I., KAEMPGEN, E., BAUR, A.S., SCHULER, G.*, et al.* (2012). Human dendritic cells efficiently phagocytose adenoviral oncolysate but require additional stimulation to mature. Int J Cancer **130**, 1682-1694.

SCHIRMBECK, R., REIMANN, J., KOCHANEK, S., and KREPPEL, F. (2008). The Immunogenicity of Adenovirus Vectors Limits the Multispecificity of CD8 T-cell Responses to Vector-encoded Transgenic Antigens. Mol Ther **16**, 1609-1616.

SCHREIBER, R.D., OLD, L.J., and SMYTH, M.J. (2011). Cancer immunoediting: integrating immunity's roles in cancer suppression and promotion. Science **331**, 1565-1570.

SCHUTZE-REDELMEIER, M.P., GOURNIER, H., GARCIA-PONS, F., MOUSSA, M., JOLIOT, A.H., VOLOVITCH, M.*, et al.* (1996). Introduction of exogenous antigens into the MHC class I

processing and presentation pathway by Drosophila antennapedia homeodomain primes cytotoxic T cells in vivo. J Immunol **157**, 650-655.

SELIGER, B., WOLLSCHEID, U., MOMBURG, F., BLANKENSTEIN, T., and HUBER, C. (2001). Characterization of the major histocompatibility complex class I deficiencies in B16 melanoma cells. Cancer Res **61**, 1095-1099.

SENZER, N.N., KAUFMAN, H.L., AMATRUDA, T., NEMUNAITIS, M., REID, T., DANIELS, G.*, et al.* (2009). Phase II clinical trial of a granulocyte-macrophage colony-stimulating factor-encoding, second-generation oncolytic herpesvirus in patients with unresectable metastatic melanoma. J Clin Oncol **27**, 5763-5771.

SERCARZ, E.E., LEHMANN, P.V., AMETANI, A., BENICHOU, G., MILLER, A., and MOUDGIL, K. (1993). Dominance and crypticity of T cell antigenic determinants. Annu Rev Immunol **11**, 729-766.

SHAFER-WEAVER, K.A., WATKINS, S.K., ANDERSON, M.J., DRAPER, L.J., MALYGUINE, A., ALVORD, W.G.*, et al.* (2009). Immunity to murine prostatic tumors: continuous provision of T-cell help prevents CD8 T-cell tolerance and activates tumor-infiltrating dendritic cells. Cancer Res **69**, 6256-6264.

SHANKARAN, V., IKEDA, H., BRUCE, A.T., WHITE, J.M., SWANSON, P.E., OLD, L.J.*, et al.* (2001). IFNgamma and lymphocytes prevent primary tumour development and shape tumour immunogenicity. Nature **410**, 1107-1111.

SHARPE, S., POLYANSKAYA, N., DENNIS, M., SUTTER, G., HANKE, T., ERFLE, V.*, et al.* (2001). Induction of simian immunodeficiency virus (SIV)-specific CTL in rhesus macaques by vaccination with modified vaccinia virus Ankara expressing SIV transgenes: influence of pre-existing anti-vector immunity. J Gen Virol **82**, 2215-2223.

SHASHKOVA, E.V., SPENCER, J.F., WOLD, W.S., and DORONIN, K. (2007). Targeting interferon-alpha increases antitumor efficacy and reduces hepatotoxicity of E1A-mutated spread-enhanced oncolytic adenovirus. Mol Ther **15**, 598-607.

SHAYAKHMETOV, D.M., GAGGAR, A., NI, S., LI, Z.Y., and LIEBER, A. (2005). Adenovirus binding to blood factors results in liver cell infection and hepatotoxicity. J Virol **79**, 7478-7491.

SHAYAKHMETOV, D.M., LI, Z.Y., NI, S., and LIEBER, A. (2004). Analysis of adenovirus sequestration in the liver, transduction of hepatic cells, and innate toxicity after injection of fiber-modified vectors. J Virol **78**, 5368-5381.

SHIN, M.S., KIM, H.S., LEE, S.H., PARK, W.S., KIM, S.Y., PARK, J.Y.*, et al.* (2001). Mutations of tumor necrosis factor-related apoptosis-inducing ligand receptor 1 (TRAIL-R1) and receptor 2 (TRAIL-R2) genes in metastatic breast cancers. Cancer Res **61**, 4942-4946.

SHIVER, J.W., FU, T.-M., CHEN, L., CASIMIRO, D.R., DAVIES, M.-E., EVANS, R.K.*, et al.* (2002). Replication-incompetent adenoviral vaccine vector elicits effective anti-immunodeficiency-virus immunity. Nature **415**, 331-335.

SIKORSKI, R.S., and HIETER, P. (1989). A system of shuttle vectors and yeast host strains designed for efficient manipulation of DNA in Saccharomyces cerevisiae. Genetics **122**, 19-27.

SINKOVICS, J., and HORVATH, J. (1993). New Developments in the Virus Therapy of Cancer: A Historical Review. Intervirology **36**, 193-214.

SIURALA, M., BRAMANTE, S., VASSILEV, L., HIRVINEN, M., PARVIAINEN, S., TAHTINEN, S.*, et al.* (2014). Oncolytic adenovirus and doxorubicin-based chemotherapy results in synergistic antitumor activity against soft-tissue sarcoma. Int J Cancer.

SMALL, E.J., CARDUCCI, M.A., BURKE, J.M., RODRIGUEZ, R., FONG, L., VAN UMMERSEN, L.*, et al.* (2006). A phase I trial of intravenous CG7870, a replication-selective, prostate-specific antigen-targeted oncolytic adenovirus, for the treatment of hormone-refractory, metastatic prostate cancer. Mol Ther **14**, 107-117.

SMITH, E., BREZNIK, J., and LICHTY, B.D. (2011). Strategies to enhance viral penetration of solid tumors. Hum Gene Ther **22**, 1053-1060.

SMITH, J.S., XU, Z., TIAN, J., STEVENSON, S.C., and BYRNES, A.P. (2008). Interaction of systemically delivered adenovirus vectors with Kupffer cells in mouse liver. Hum Gene Ther **19**, 547-554.

SMITH, K.J., SKELTON, H.G., TURIANSKY, G., and WAGNER, K.F. (1997). Hyaluronidase enhances the therapeutic effect of vinblastine in intralesional treatment of Kaposi's sarcoma. Military Medical Consortium for the Advancement of Retroviral Research (MMCARR). J Am Acad Dermatol **36**, 239-242.

SMITH, T.A., IDAMAKANTI, N., MARSHALL-NEFF, J., ROLLENCE, M.L., WRIGHT, P., KALOSS, M.*, et al.* (2003a). Receptor interactions involved in adenoviral-mediated gene delivery after systemic administration in non-human primates. Hum Gene Ther **14**, 1595-1604.

SMITH, T.A., IDAMAKANTI, N., ROLLENCE, M.L., MARSHALL-NEFF, J., KIM, J., MULGREW, K.*, et al.* (2003b). Adenovirus serotype 5 fiber shaft influences in vivo gene transfer in mice. Hum Gene Ther **14**, 777-787.

SOUTHAM, C.M., and MOORE, A.E. (1952). Clinical studies of viruses as antineoplastic agents with particular reference to Egypt 101 virus. Cancer **5**, 1025-1034.

SPENCER, J.F., SAGARTZ, J.E., WOLD, W.S., and TOTH, K. (2009). New pancreatic carcinoma model for studying oncolytic adenoviruses in the permissive Syrian hamster. Cancer Gene Ther **16**, 912-922.

SPRUSS, T., BERNHARDT, G., SCHONENBERGER, H., and SCHIESS, W. (1995). Hyaluronidase significantly enhances the efficacy of regional vinblastine chemotherapy of malignant melanoma. J Cancer Res Clin Oncol **121**, 193-202.

SRIVASTAVA, M.K., SINHA, P., CLEMENTS, V.K., RODRIGUEZ, P., and OSTRAND-ROSENBERG, S. (2010). Myeloid-derived suppressor cells inhibit T-cell activation by depleting cystine and cysteine. Cancer Res **70**, 68-77.

STANTON, R.J., MCSHARRY, B.P., ARMSTRONG, M., TOMASEC, P., and WILKINSON, G.W. (2008). Re-engineering adenovirus vector systems to enable high-throughput analyses of gene function. Biotechniques **45**, 659-662, 664-658.

STEEL, J.C., MORRISON, B.J., MANNAN, P., ABU-ASAB, M.S., WILDNER, O., MILES, B.K.*, et al.* (2007). Immunocompetent syngeneic cotton rat tumor models for the assessment of replication-competent oncolytic adenovirus. Virology **369**, 131-142.

STERN-GINOSSAR, N., GUR, C., BITON, M., HORWITZ, E., ELBOIM, M., STANIETSKY, N.*, et al.* (2008). Human microRNAs regulate stress-induced immune responses mediated by the receptor NKG2D. Nat Immunol **9**, 1065-1073.

STEWART, P.L., CHIU, C.Y., HUANG, S., MUIR, T., ZHAO, Y., CHAIT, B.*, et al.* (1997). Cryo-EM visualization of an exposed RGD epitope on adenovirus that escapes antibody neutralization. EMBO J **16**, 1189-1198.

SU, C., PENG, L., SHAM, J., WANG, X., ZHANG, Q., CHUA, D.*, et al.* (2006). Immune gene-viral therapy with triplex efficacy mediated by oncolytic adenovirus carrying an interferon-gamma gene yields efficient antitumor activity in immunodeficient and immunocompetent mice. Mol Ther **13**, 918-927.

T

TAKAHASHI, H., FEUERHAKE, F., KUTOK, J.L., MONTI, S., DAL CIN, P., NEUBERG, D.*, et al.* (2006). FAS death domain deletions and cellular FADD-like interleukin 1beta converting enzyme inhibitory protein (long) overexpression: alternative mechanisms for deregulating the extrinsic apoptotic pathway in diffuse large B-cell lymphoma subtypes. Clin Cancer Res **12**, 3265-3271.

TANAKA, Y., and TEVETHIA, S.S. (1988). Differential effect of adenovirus 2 E3/19K glycoprotein on the expression of H-2Kb and H-2Db class I antigens and H-2Kb- and H-2Db-restricted SV40-specific CTL-mediated lysis. Virology **165**, 357-366.

TAO, J., LI, Y., LIU, Y.Q., WANG, L., YANG, J., DONG, J.*, et al.* (2008). Restoration of the expression of transports associated with antigen processing in human malignant melanoma increases tumor-specific immunity. J Invest Dermatol **128**, 1991-1996.

TAUBER, B., and DOBNER, T. (2001). Adenovirus early E4 genes in viral oncogenesis. Oncogene **20**, 7847-7854.

TERABE, M., and BERZOFSKY, J.A. (2004). Immunoregulatory T cells in tumor immunity. Curr Opin Immunol **16**, 157-162.

THOMAS, M.A., SPENCER, J.F., LA REGINA, M.C., DHAR, D., TOLLEFSON, A.E., TOTH, K.*, et al.* (2006). Syrian hamster as a permissive immunocompetent animal model for the study of oncolytic adenovirus vectors. Cancer Res **66**, 1270-1276.

THOMAS, M.A., SPENCER, J.F., TOTH, K., SAGARTZ, J.E., PHILLIPS, N.J., and WOLD, W.S. (2008a). Immunosuppression enhances oncolytic adenovirus replication and antitumor efficacy in the Syrian hamster model. Mol Ther **16**, 1665-1673.

THOMAS, M.A., SPENCER, J.F., TOTH, K., SAGARTZ, J.E., PHILLIPS, N.J., and WOLD, W.S.M. (2008b). Immunosuppression Enhances Oncolytic Adenovirus Replication and Antitumor Efficacy in the Syrian Hamster Model. Mol Ther **16**, 1665-1673.

TIWARI, N., GARBI, N., REINHECKEL, T., MOLDENHAUER, G., HAMMERLING, G.J., and MOMBURG, F. (2007). A transporter associated with antigen-processing independent vacuolar pathway for the MHC class I-mediated presentation of endogenous transmembrane proteins. J Immunol **178**, 7932-7942.

TOES, R.E., OFFRINGA, R., BLOM, R.J., BRANDT, R.M., VAN DER EB, A.J., MELIEF, C.J.*, et al.* (1995). An adenovirus type 5 early region 1B-encoded CTL epitope-mediating tumor eradication by CTL clones is down-modulated by an activated ras oncogene. J Immunol **154**, 3396-3405.

TOLLEFSON, A.E., RYERSE, J.S., SCARIA, A., HERMISTON, T.W., and WOLD, W.S. (1996a). The E3-11.6-kDa adenovirus death protein (ADP) is required for efficient cell death: characterization of cells infected with adp mutants. Virology **220**, 152-162.

TOLLEFSON, A.E., SCARIA, A., HERMISTON, T.W., RYERSE, J.S., WOLD, L.J., and WOLD, W.S. (1996b). The adenovirus death protein (E3-11.6K) is required at very late stages of infection for efficient cell lysis and release of adenovirus from infected cells. J Virol **70**, 2296-2306.

TOSCH, C., GEIST, M., LEDOUX, C., ZILLER-REMI, C., PAUL, S., ERBS, P.*, et al.* (2008). Adenovirus-mediated gene transfer of pathogen-associated molecular patterns for cancer immunotherapy. Cancer Gene Ther **16**, 310-319.

TOSCH, C., GEIST, M., LEDOUX, C., ZILLER-REMI, C., PAUL, S., ERBS, P.*, et al.* (2009). Adenovirus-mediated gene transfer of pathogen-associated molecular patterns for cancer immunotherapy. Cancer Gene Ther **16**, 310-319.

TRAVERSARI, C., MEAZZA, R., COPPOLECCHIA, M., BASSO, S., VERRECCHIA, A., VAN DER BRUGGEN, P.*, et al.* (1997). IFN-gamma gene transfer restores HLA-class I expression and MAGE-3 antigen presentation to CTL in HLA-deficient small cell lung cancer. Gene therapy **4**, 1029-1035.

TSUKUDA, K., WIEWRODT, R., MOLNAR-KIMBER, K., JOVANOVIC, V.P., and AMIN, K.M. (2002). An E2F-responsive Replication-selective Adenovirus Targeted to the Defective Cell Cycle in Cancer Cells: Potent Antitumoral Efficacy but No Toxicity to Normal Cell. Cancer Research **62**, 3438-3447.

U

UYTTENHOVE, C., PILOTTE, L., THEATE, I., STROOBANT, V., COLAU, D., PARMENTIER, N.*, et al.* (2003). Evidence for a tumoral immune resistance mechanism based on tryptophan degradation by indoleamine 2,3-dioxygenase. Nat Med **9**, 1269-1274.

V

VAN KAMPEN, V., MERGET, R., and BRUNING, T. (2005). [Occupational allergies to papain]. Pneumologie **59**, 405-410.

VASEY, P.A., SHULMAN, L.N., CAMPOS, S., DAVIS, J., GORE, M., JOHNSTON, S.*, et al.* (2002). Phase I trial of intraperitoneal injection of the E1B-55-kd-gene-deleted adenovirus ONYX-015 (dl1520) given on days 1 through 5 every 3 weeks in patients with recurrent/refractory epithelial ovarian cancer. J Clin Oncol **20**, 1562-1569.

VERMA, I.M., and WEITZMAN, M.D. (2005). GENE THERAPY: Twenty-First Century Medicine. Annual Review of Biochemistry **74**, 711-738.

VESELY, M.D., KERSHAW, M.H., SCHREIBER, R.D., and SMYTH, M.J. (2011). Natural innate and adaptive immunity to cancer. Annu Rev Immunol **29**, 235-271.

VILLANUEVA, A., GARCIA, C., PAULES, A.B., VICENTE, M., MEGIAS, M., REYES, G.*, et al.* (1998). Disruption of the antiproliferative TGF-beta signaling pathways in human pancreatic cancer cells. Oncogene **17**, 1969-1978.

W

WADDINGTON, S.N., MCVEY, J.H., BHELLA, D., PARKER, A.L., BARKER, K., ATODA, H.*, et al.* (2008). Adenovirus serotype 5 hexon mediates liver gene transfer. Cell **132**, 397-409.

WANG, T., NIU, G., KORTYLEWSKI, M., BURDELYA, L., SHAIN, K., ZHANG, S.*, et al.* (2004). Regulation of the innate and adaptive immune responses by Stat-3 signaling in tumor cells. Nat Med **10**, 48-54.

WEAVER, E.A., NEHETE, P.N., NEHETE, B.P., YANG, G., BUCHL, S.J., HANLEY, P.W.*, et al.* (2013). Comparison of systemic and mucosal immunization with helper-dependent adenoviruses for vaccination against mucosal challenge with SHIV. PLoS One **8**, e67574.

WEI, M.L., and CRESSWELL, P. (1992). HLA-A2 molecules in an antigen-processing mutant cell contain signal sequence-derived peptides. Nature **356**, 443-446.

WERLEN, G., HAUSMANN, B., and PALMER, E. (2000). A motif in the alphabeta T-cell receptor controls positive selection by modulating ERK activity. Nature **406**, 422-426.

WESSELING, J.G., BOSMA, P.J., KRASNYKH, V., KASHENTSEVA, E.A., BLACKWELL, J.L., REYNOLDS, P.N.*, et al.* (2001). Improved gene transfer efficiency to primary and established human pancreatic carcinoma target cells via epidermal growth factor receptor and integrin-targeted adenoviral vectors. Gene therapy **8**, 969-976.

WICKHAM, T.J., FILARDO, E.J., CHERESH, D.A., and NEMEROW, G.R. (1994). Integrin alpha v beta 5 selectively promotes adenovirus mediated cell membrane permeabilization. The Journal of Cell Biology **127**, 257-264.

WICKHAM, T.J., MATHIAS, P., CHERESH, D.A., and NEMEROW, G.R. (1993). Integrins Î±vÎ²3 and Î±vÎ²5 promote adenovirus internalization but not virus attachment. Cell **73**, 309-319.

WICKHAM, T.J., SEGAL, D.M., ROELVINK, P.W., CARRION, M.E., LIZONOVA, A., LEE, G.M.*, et al.* (1996). Targeted adenovirus gene transfer to endothelial and smooth muscle cells by using bispecific antibodies. J Virol **70**, 6831-6838.

WOLD, W.S., CLADARAS, C., DEUTSCHER, S.L., and KAPOOR, Q.S. (1985). The 19-kDa glycoprotein coded by region E3 of adenovirus. Purification, characterization, and structural analysis. J Biol Chem **260**, 2424-2431.

WOLD, W.S., and TOTH, K. (2012). Chapter three--Syrian hamster as an animal model to study oncolytic adenoviruses and to evaluate the efficacy of antiviral compounds. Adv Cancer Res **115**, 69-92.

WOLLER, N., GURLEVIK, E., URECHE, C.I., SCHUMACHER, A., and KUHNEL, F. (2014). Oncolytic viruses as anticancer vaccines. Front Oncol **4**, 188.

WRZESINSKI, S.H., WAN, Y.Y., and FLAVELL, R.A. (2007). Transforming growth factor-beta and the immune response: implications for anticancer therapy. Clin Cancer Res **13**, 5262-5270.

WU, E., PACHE, L., VON SEGGERN, D.J., MULLEN, T.M., MIKYAS, Y., STEWART, P.L.*, et al.* (2003). Flexibility of the adenovirus fiber is required for efficient receptor interaction. J Virol **77**, 7225-7235.

WU, H., HAN, T., BELOUSOVA, N., KRASNYKH, V., KASHENTSEVA, E., DMITRIEV, I.*, et al.* (2005). Identification of sites in adenovirus hexon for foreign peptide incorporation. J Virol **79**, 3382-3390.

X

XIA, Z.J., CHANG, J.H., ZHANG, L., JIANG, W.Q., GUAN, Z.Z., LIU, J.W.*, et al.* (2004). [Phase III randomized clinical trial of intratumoral injection of E1B gene-deleted adenovirus (H101) combined with cisplatin-based chemotherapy in treating squamous cell cancer of head and neck or esophagus]. Ai Zheng **23**, 1666-1670.

XU, R.H., YUAN, Z.Y., GUAN, Z.Z., CAO, Y., WANG, H.Q., HU, X.H.*, et al.* (2003). [Phase II clinical study of intratumoral H101, an E1B deleted adenovirus, in combination with chemotherapy in patients with cancer]. Ai Zheng **22**, 1307-1310.

XU, Z., QIU, Q., TIAN, J., SMITH, J.S., CONENELLO, G.M., MORITA, T.*, et al.* (2013). Coagulation factor X shields adenovirus type 5 from attack by natural antibodies and complement. Nat Med **19**, 452-457.

XU, Z., TIAN, J., SMITH, J.S., and BYRNES, A.P. (2008). Clearance of adenovirus by Kupffer cells is mediated by scavenger receptors, natural antibodies, and complement. J Virol **82**, 11705-11713.

Y

YAMANISHI, K., TAKAHASHI, M., KURIMURA, T., UEDA, S., and MINEKAWA, Y. (1970). Studies on live mumps virus vaccine. 3. Evaluation of newly developed live mumps virus vaccine. Biken J **13**, 157-161.

YING, B., TOTH, K., SPENCER, J.F., MEYER, J., TOLLEFSON, A.E., PATRA, D.*, et al.* (2009). INGN 007, an oncolytic adenovirus vector, replicates in Syrian hamsters but not mice: comparison of biodistribution studies. Cancer Gene Ther **16**, 625-637.

YOU, L., YANG, C.T., and JABLONS, D.M. (2000). ONYX-015 works synergistically with chemotherapy in lung cancer cell lines and primary cultures freshly made from lung cancer patients. Cancer Res **60**, 1009-1013.

YU, D.C., CHEN, Y., DILLEY, J., LI, Y., EMBRY, M., ZHANG, H.*, et al.* (2001). Antitumor synergy of CV787, a prostate cancer-specific adenovirus, and paclitaxel and docetaxel. Cancer Res **61**, 517-525.

Z

ZHANG, S.N., CHOI, I.K., HUANG, J.H., YOO, J.Y., CHOI, K.J., and YUN, C.O. (2011). Optimizing DC vaccination by combination with oncolytic adenovirus coexpressing IL-12 and GM-CSF. Mol Ther **19**, 1558-1568.

ZHANG, W., and IMPERIALE, M.J. (2000). Interaction of the adenovirus IVa2 protein with viral packaging sequences. J Virol **74**, 2687-2693.

ZHANG, Y., and BERGELSON, J.M. (2005). Adenovirus receptors. J Virol **79**, 12125-12131.

ZHANG, Y., CHIRMULE, N., GAO, G.P., QIAN, R., CROYLE, M., JOSHI, B*., et al.* (2001). Acute cytokine response to systemic adenoviral vectors in mice is mediated by dendritic cells and macrophages. Mol Ther **3**, 697-707.

ZINKERNAGEL, R.M., and DOHERTY, P.C. (1975). H-2 compatability requirement for T-cell-mediated lysis of target cells infected with lymphocytic choriomeningitis virus. Different cytotoxic T-cell specificities are associated with structures coded for in H-2K or H-2D. J Exp Med **141**, 1427-1436.

ANNEX

Cancer Gene Therapy (2014) 21, 68–73

www.nature.com/cgt

ORIGINAL ARTICLE

The combination of i-leader truncation and gemcitabine improves oncolytic adenovirus efficacy in an immunocompetent model

C Puig-Saus[1], E Laborda[1,2], A Rodríguez-García[1], M Cascalló[1], R Moreno[1] and R Alemany[1]

Adenovirus (Ad) i-leader protein is a small protein of unknown function. The C-terminus truncation of the i-leader protein increases Ad release from infected cells and cytotoxicity. In the current study, we use the i-leader truncation to enhance the potency of an oncolytic Ad. *In vitro*, an i-leader truncated oncolytic Ad is released faster to the supernatant of infected cells, generates larger plaques, and is more cytotoxic in both human and Syrian hamster cell lines. In mice bearing human tumor xenografts, the i-leader truncation enhances oncolytic efficacy. However, in a Syrian hamster pancreatic tumor model, which is immunocompetent and less permissive to human Ad, antitumor efficacy is only observed when the i-leader truncated oncolytic Ad, but not the non-truncated version, is combined with gemcitabine. This synergistic effect observed in the Syrian hamster model was not seen *in vitro* or in immunodeficient mice bearing the same pancreatic hamster tumors, suggesting a role of the immune system in this synergism. These results highlight the interest of the i-leader C-terminus truncation because it enhances the antitumor potency of an oncolytic Ad and provides synergistic effects with gemcitabine in the presence of an immune competent system.

Cancer Gene Therapy (2014) **21,** 68–73; doi:10.1038/cgt.2013.85; published online 17 January 2014

Keywords: gemcitabine; intratumoral spread; oncolytic adenovirus; oncolytic potency; Syrian hamster; viral release

INTRODUCTION

Despite the promising use of oncolytic adenovirus (Ad) in cancer therapy, over 20 clinical trials with different oncolytic Ads by intravenous or intratumoral administration have shown good safety but modest efficacy.[1] One of the main barriers to oncolytic Ads efficacy is the virus spread through the tumor mass.[2] Several strategies have been proposed to enhance intratumoral spread: the use of ECM-degrading enzymes, enhancing permissivity of the virus to stromal cells and enhancing the cytotoxicity or the release of the virus from the infected cells.[3–5]

After a bioselection of random mutants with enhanced cytotoxicity in cancer-associated fibroblasts, we previously identified the iLG397T i-leader C-terminal truncating mutation.[6] The iLG397T mutation enhanced Ad release in cancer-associated fibroblast and tumor cells, and apoptosis-independent cytotoxicity. *In vivo,* an Ad with the truncated i-leader disseminated better through the tumor, enhancing its antitumor efficacy, especially when tumors were embedded with human fibroblasts.[6] Similar i-leader truncated Ad mutants have been identified after bioselection in cancer cell lines.[7,8] The convergence between different bioselection processes highlights the importance of the i-leader truncation for Ad potency.

For a virotherapeutic use, it is necessary to restrict virus replication to tumor cells. ICOVIR-15 is an oncolytic Ad that presents an appealing efficacy/toxicity ratio. To restrict its replication to tumor cells, it has the Δ24 deletion that abrogates E1A binding to pRb and the insertion of four palindromic E2F-binding sites and one Sp-1 binding site in the E1A endogenous promoter to control E1A-Δ24 transcription upon pRb deregulation. Moreover, ICOVIR-15 has an RGD peptide inserted in the HI-loop that enhances the targeting to tumor cells.[9]

Aiming at the generation of a more potent oncolytic Ad, we have introduced the iLG397T mutation into ICOVIR-15 to obtain ICOVIR-15i. We demonstrate that the iLG397T mutation maintains its phenotype in an E1A-transcriptionally regulated oncolytic Ad providing enhanced release, cytotoxicity and antitumor activity *in vivo* in a human lung adenocarcinoma xenograft tumor model.

To date, it is clear that accelerating virus release improves spreading through the tumor and antitumor activity in human tumor xenografts in immunodeficient mice.[10–12] However, Ad is highly immunogenic and studying the interactions with the immune system is critical for the application of Ads in the clinic.[13] This may be especially relevant for a fast-release Ad mutant, as it could induce higher immune responses than wild-type Ad.[5]

Syrian hamsters have been proposed as an immunocompetent semi-permissive model to study the antitumor efficacy and toxicity of oncolytic Ads.[14,15] To date, no significant differences in antitumor activity with fast-release mutants in this model have been shown. However, the Ads studied have their immunomodulatory functions compromised due to total or partial E3 deletions.[11,16] In the present work, we study the role of i-leader truncation in the context of an oncolytic Ad that preserves all the E3 immune evasion functions, in an immunocompetent pancreatic cancer model in Syrian hamsters, alone or combined with gemcitabine. Gemcitabine shows synergy with several oncolytic Ad.[17–20] In hamster, we found a synergistic effect of gemcitabine with the fast-release oncolytic Ad ICOVIR-15i. These results provide valuable data for the translation to the clinic of fast-release oncolytic Ads.

[1]Translational Research Laboratory, Institut d'Investigació Biomèdica de Bellvitge-Institut Català d'Oncologia (IDIBELL-ICO), Barcelona, Spain and [2]Department of Biochemistry and Molecular Biology, Universitat Autònoma de Barcelona, Barcelona, Spain. Correspondence: Dr R Alemany, Translational Research Laboratory, Institut d'Investigació Biomèdica de Bellvitge-Institut Català d'Oncologia (IDIBELL-ICO), Av Gran Via de l'Hospitalet 199-203, L'Hospitalet de Llobregat, 08907 Barcelona, Spain.
E-mail: ralemany@iconcologia.net
Received 29 November 2013; accepted 16 December 2013; published online 17 January 2014

MATERIALS AND METHODS

Cell lines

Human HEK293 and A549 lung adenocarcinoma cell lines were obtained from the American Type Culture Collection (ATCC, Manassas, VA, USA). HP-1 Syrian hamster pancreatic tumor cell line was obtained from M Yamamoto (Minneapolis, MN, USA) with MA Hollingsworth (Nebraska, NE, USA) permission. All were maintained with Dulbecco's modified Eagle's medium (DMEM) supplemented with 10% fetal bovine serum (FBS, Invitrogen Carlsbad, CA, USA) and penicillin-streptomycin (PS, Gibco-BRL, Barcelona, Spain). All cell lines were routinely tested for mycoplasma contamination.

Recombinant Ad

ICOVIR-15 has been previously described by our group.[9] pAdZ-ICOVIR-15i was generated by homologous recombination in bacteria[38] following a positive–negative selection method based on the RpsL-Neo cassette to substitute the wild-type i-leader for the truncated i-leader containing iLG397T mutation (G to T point-mutation in the 397 nucleotide of the i-leader sequence) in the pAdZ-ICOVIR-15 plasmid. The sequence containing the truncated i-leader was amplified by PCR from pAdR1 plasmid[6] with the primers Ad7131F (5′-GCGGTTGAGGACAAACTCT-3′) and Ad8751R (5′-GCCCGTCGTCTTCACGCAG-3′) (Sigma-Aldrich, Spruce St, St Louis, MO, USA). The resulting plasmid was transfected into HEK293 cells generating ICOVIR-15i. After transfection the virus was plaque-purified in A549 cells. All viruses were amplified in A549 cells and purified by cesium chloride gradients following standard protocols. Plasmids and viruses were sequenced to confirm the presence of all genetic modifications. Virus-containing cell extracts were functionally titered in TU ml^{-1} (TU, transducing units) using an anti-hexon staining-based method. Purified viruses were physically titered by optical density at 260 nm in vp ml^{-1} (vp, viral particles) and functionally titered by anti-hexon staining. The ratios between functional and physic titer were similar for the viruses used, 48.3 vp per TU for ICOVIR-15 and 76.87 vp per TU for ICOVIR-15i.

Plaque assay

A549 cells seeded in six-well plates were infected with serial dilutions of the indicated viruses. Four hours after infection, the medium was removed and cells were covered with a 1:1 DMEM 5% FBS: 1% agarose mix. Once the agarose overlay solidified DMEM 5% FBS was added. To study the plaque size, after 7 days for A549 and 15 days for HP-1 cells, the plaque assays were stained by incubation with 0.5 mg ml^{-1} thiazolyl blue tetrazolium bromide (MTT; Sigma-Aldrich, St Louis, MO, USA) at 37 °C and 5% CO_2 for 4 h. To isolate clones by plaque purification, after 7 days, the media was removed and single isolated plaques were picked with a filter tip and resuspended in 500 μl of DMEM 5% FBS.

In vitro cytotoxicity assays

For *in vitro* cytotoxicity, 3×10^4 A549 cells and 1×10^4 HP-1 cells were seeded in 96-well plates and infected in suspension with serial 1/5 dilutions of the indicated viruses starting from 200 TU per cell for A549 and 300 TU per cell for HP-1. At day 4 postinfection (for A549 cells) and at day 8 postinfection (for HP-1 cells), plates were washed with phosphate-buffered saline (PBS) and stained for total protein content with BCA (bicinchoninic acid assay; Pierce Biotechnology, Rockford, IL, USA). Absorbance was quantified at 540 nm after 30 min of incubation. IC_{50} value, equivalent to the virus dose required to produce 50% cell growth inhibition, was calculated from dose-response curves by standard nonlinear regression (GraFit; Erithacus Software, Horley, UK) using an adapted Hill equation. The two-tailed Student's *t*-test was used to study the statistical significance of the IC_{50} differences between both viruses. For gemcitabine experiments, 1×10^4 HP-1 cells were seeded in 96-well plates the day before the infection. Gemcitabine (Lilly S.A; Indianapolis, IN, USA) was added to a final concentration of 5 and 10 nM just after the infection and incubated for 11 days.

Virus release and production assays

A549 and HP-1 cells seeded in 24-well plates were infected in triplicates with 20 TU per cell of the indicated virus to allow 80–100% infection. Four hours after infection, medium was removed, cells were washed three times with PBS, and incubated with fresh medium. At indicated time points samples of supernatant (SN, containing the released virus) and cell extract (CE, containing all media and cells representing the total amount of virus produced) were collected. Virus was quantified by an anti-hexon staining-based method in HEK293 cells. The two-tailed Student's *t*-test was used to evaluate the statistical significance of the difference in virus release and production between different viruses.

Evaluation of antitumor efficacy *in vivo*

In vivo studies were performed at the ICO-IDIBELL facility (Barcelona, Spain) AAALAC unit 1155, and approved by the IDIBELL's Ethical Committee for Animal Experimentation. Human lung carcinoma and Syrian hamster pancreatic tumors were established by subcutaneous injection of 2×10^6 A549 cells or 4×10^6 HP-1 cells, respectively, into the flanks of 8-week-old female BAlb/C nu/nu mice (Harlan, Indianapolis, IN, USA), and 1×10^6 HP-1 cells into the flanks of 6-week-old female Golden Syrian hamsters (Janvier, Le Genest Saint Isle, France). When tumors reached 100–150 mm^3 (for mice) or 200 mm^3 (for Syrian hamsters) animals were randomized ($n =$ 12–14 tumors per group for mice and $n = 9$–10 tumors per group for Syrian hamsters) and treated with a single intratumoral injection of PBS or 2×10^9 vp per tumor for mice or 2.5×10^{10} vp per tumor for Syrian hamster of ICOVIR-15 or ICOVIR-15i in a total volume of 25 μl per tumor. For indicated experiments, 50 mg kg^{-1} of gemcitabine at day 0, 3, 6 and 9 was administrated intraperitoneally. This dose is equivalent in mice to half the standard dose in humans.[39] Tumor size and animal weight were measured twice a week. Tumor volume and growth were calculated as previously.[9] The two-tailed Student's *t*-test was used to study the statistical significance of the differences in the tumor growth of the different treatment groups. For Kaplan–Meier survival curves, end point was established at a tumor volume $\geqslant 500$ mm^3 for mice and $\geqslant 2000$ mm^3 for Syrian hamster. Animals whose tumor size never reached the threshold were included as right-censored information. A log-rank test was used to determine the statistical significance of the differences in time-to-event.

Immunohistofluorescence detection of adenoviral E1A protein in xenograft tumor

OCT-embedded sections of the A549 xenograft tumors at the end of the efficacy experiment were incubated with anti-Ad-2/5 E1A (13S-5) SC-430 rabbit polyclonal IgG (Santa Cruz Biotechnology, Santa Cruz, CA, USA) and Alexa Fluor 488-labeled goat anti-rabbit IgG (Invitrogen Molecular Probes, Eugene, OR, USA) antibodies and counterstained with 4,6-diamino-2-phenylindole. Section images were obtained on an Olympus BX60 fluorescence microscope (Olympus America, Melville, NY, USA).

Lymphocyte proliferation assay

Peripheral blood mononuclear cells (PBMCs) from the hamsters treated with ICOVIR-15 or ICOVIR-15i alone or in combination with gemcitabine and the corresponding PBS controls were isolated by a standard ficoll gradient protocol. All PBMCs samples were diluted at 3×10^6 cells per ml, labeled with carboxyfluorescein succinimidyl ester (CFSE), (Sigma-Aldrich, St Louis, MO, USA) at a final concentration of 10 μM, and exposed to target cells at 10:1 ratio during 5 days. Target cells were infected PBMCs, infected and non-infected HP-1 cells. PBMCs were infected at 200 TU per cell and HP-1 cells at 40 TU per cells with purified ICOVIR-15 for 3 h at 37 °C to ensure antigen presentation just before the exposure to CFSE-labeled PBMCs samples. As a positive control, we treated PBMCs with Concanavalin A at a final concentration of 5 μg ml^{-1}. As a negative control we used non-stimulated PBMCs labeled with CFSE. After 5 days, the proliferation of the PBMCs was analyzed by flow cytometry; results are presented as cell division index. The cell division index was calculated according to the formula: percentage of $CFSE^{diminished}$ cells after antigen stimulation divided by percentage of $CFSE^{diminished}$ cells without stimulation,[40] where the percentage of $CFSE^{diminished}$ cells corresponds to the ratio of proliferating cells over the total number of cells. The Mann–Whitney test was used to evaluate the statistical significance of the difference in lymphocyte proliferation between each treatment.

RESULTS AND DISCUSSION

iLG397T i-leader truncating mutation enhances ICOVIR-15 plaque size, cytotoxicity and virus release *in vitro*

To increase the potency of ICOVIR-15, the iLG397T i-leader truncating mutation[6] was inserted into its genome generating ICOVIR-15i. In A549 cells, a human lung carcinoma cell line highly permissive to Ad replication, ICOVIR-15i displayed large plaque phenotype, representative of an enhanced cell-to-cell spread

(Figure 1a) and enhanced cytotoxicity, leading to a 163.3-fold ($P = 0.006$) decrease in the IC_{50} compared with ICOVIR-15 (Figure 1b). Virus production and release kinetic studies confirmed that ICOVIR-15i was released more efficiently from the infected cells compared with ICOVIR-15, showing a 29.4-fold ($P = 0.046$) and 2.2-fold ($P = 0.005$) increase in the extracellular virus at 24 h post infection (h.p.i) and 40 h.p.i, respectively. Total virus production remained unaffected (Figure 1c). These results demonstrated that controlled expression of E1A-Δ24 by the E2F and Sp-1 boxes does not affect the function of the truncated i-leader in permissive cells.

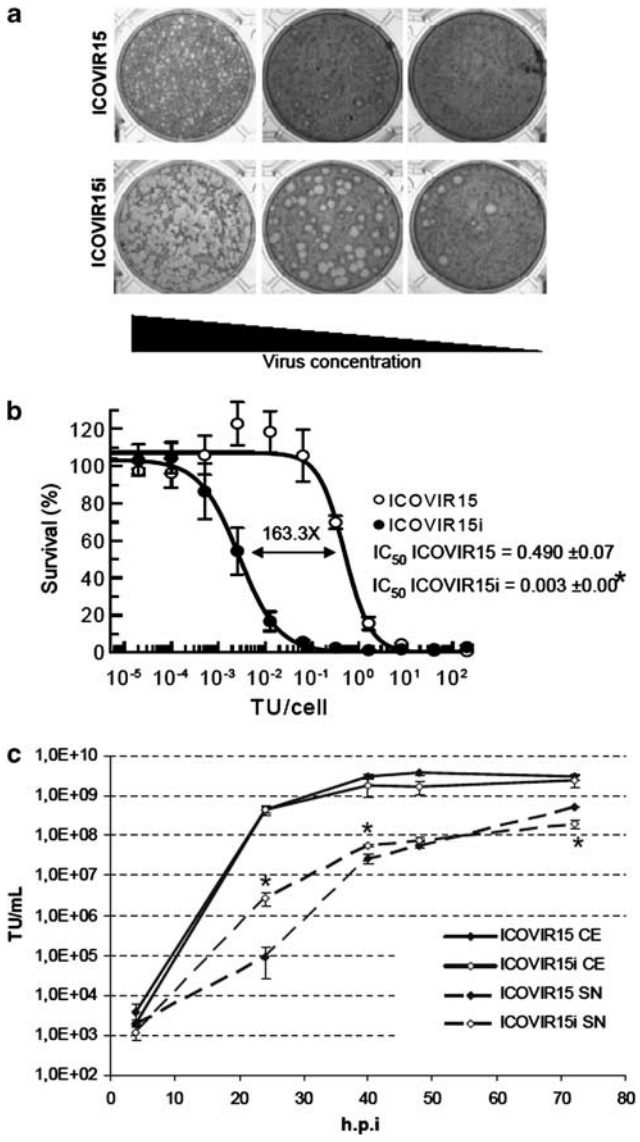

Figure 1. iLG397T mutation enhances ICOVIR-15 plaque size, cytotoxicity, and virus release *in vitro*. (**a**) Comparative plaque size of ICOVIR-15 and ICOVIR-15i in A549 cells at day 7 postinfection. (**b**) Cytotoxicity assay. Comparative dose-response curves of ICOVIR-15 and ICOVIR-15i at day 4 post infection in A549 cells. Mean IC_{50} values ± s.d. in TU per cell for each virus and the cytotoxicity increase are shown in the figure. The two-tailed unpaired Student's *t*-test was used to evaluate the statistical significance of the IC_{50} difference between both viruses. *Significant $P < 0.05$ compared with ICOVIR-15. (**c**) Kinetics of virus production and release of ICOVIR-15 and ICOVIR-15i in A549 cells. Extracellular (SN) and total virus produced (CE) were measured at the indicated time points. Mean values ($n = 3$) ± s.d. are plotted. *Significant $P < 0.05$ by two-tailed unpaired Student's *t*-test compared with ICOVIR-15. TU, transducing units; h.p.i, hour post-infection; CE, cell extract; SN, supernatant.

iLG397T mutation enhances ICOVIR-15 antitumor efficacy in immunocompromised mice

Nude mice bearing subcutaneous A549 lung carcinoma tumors were treated with a single intratumoral administration of PBS or 2.0×10^9 viral particles per tumor (vp per tumor) of ICOVIR-15 or ICOVIR-15i. ICOVIR-15i improved antitumor efficacy compared with ICOVIR-15 in this immunodeficient model, leading to a 3.5-fold decrease in the percentage of tumor growth compared with PBS ($P = 0.006$) and a 2.3-fold decrease compared with ICOVIR-15 ($P = 0.023$) at the end of the experiment (Figure 2a). Tumor growth

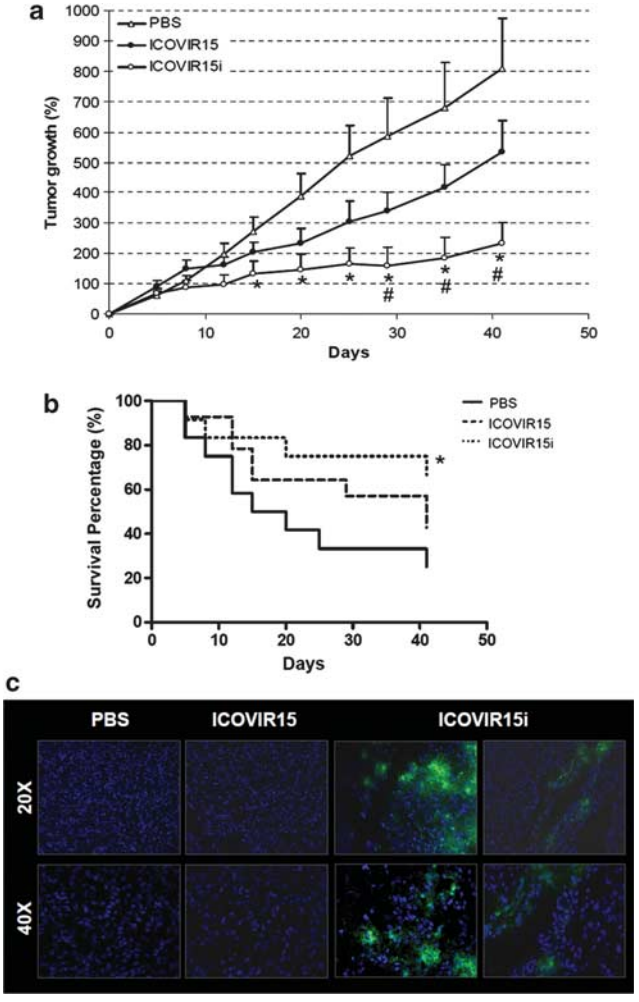

Figure 2. iLG397T mutation enhances ICOVIR-15 antitumor efficacy in immunocompromised mice. (**a**) Nude mice bearing human A549 lung carcinoma xenograft subcutaneous tumors were treated with a single intratumoral dose of PBS, or ICOVIR-15 or ICOVIR-15i at 2.0×10^9 vp per tumor. Mean percentage of tumor growth value ($n = 12$–14 tumors) ± s.e.m. are plotted. *Significant $P < 0.05$ by two-tailed unpaired Student's *t*-test compared with PBS group. #Significant $P < 0.05$ by two-tailed unpaired Student's *t*-test compared with ICOVIR-15 group. (**b**) Kaplan–Meier survival curves after administration of a single intratumoral dose of PBS, or ICOVIR-15 or ICOVIR-15i at 2.0×10^9 vp per tumor. The end point was established at a tumor volume of $\geqslant 500\,mm^3$. *Significant $P < 0.05$ by log-rank test compared with mice treated with PBS. (**c**) Immunofluorescent detection of adenovirus (Ad) E1A protein in the OCT-embedded tumors at the end of the treatment. PBS, phosphate-buffered saline; vp, viral particle.

delay resulted in a statistically significant increase in the mean survival rate from 22.2 days for the PBS to 33.5 days for the animals treated with ICOVIR-15i ($P = 0.043$) (Figure 2b).

The presence of virus in the tumors at the end of treatment was assessed by immunological staining against E1A protein. Virus was detected in all tumor sections analyzed for the ICOVIR-15i-treated group, but could not be detected in ICOVIR-15-treated tumors (Figure 2c), confirming the enhanced intratumoral spread of the i-leader truncated oncolytic Ad.

iLG397T mutation enhances ICOVIR-15 plaque size and cytotoxicity in a Syrian hamster tumor model

To characterize the effect of iLG397T mutation in an immunocompetent model, the phenotype of ICOVIR-15i was assessed in HP-1, a pancreatic carcinoma cell line from Syrian hamster.[21] *In vitro*, ICOVIR-15i generated large plaques compared with ICOVIR-15 (Figure 3a), and enhanced cytotoxicity with a statistically significant 15.7-fold decrease in the IC_{50} ($P = 0.008$) compared with ICOVIR-15 (Figure 3b). Although iLG397T mutation maintains its phenotype in this Syrian hamster cell line, the differences between both viruses were lower compared with the differences in human cells (Figures 1a, b and c). This could be explained by the lower permissiveness of this model compared with human cells (100-fold lower than in human A549 cells, data not shown). However, our results showed that HP-1 are more permissive to Ad replication than other hamster cell lines (such as HaPT-1, H2T or Amel-3; data not shown) and therefore, was selected in our studies. In contrast to the IC_{50} cytotoxicity, experimental conditions that allowed only one replication round, such as the infection at high multiplicity of infection (M.O.I), did not show release or production advantages for ICOVIR-15i compared with ICOVIR-15 (Figure 3c), contrary to the results found in human cells (Figure 1c). This suggests that several rounds of virus replication were needed in less permissive cells to maximize the differences between both viruses.

iLG397T mutation combined with gemcitabine increases ICOVIR-15 antitumor activity in Syrian hamsters

To further enhance the oncolytic potency of ICOVIR-15i in immunocompetent animal models, we combined it with gemcitabine. Gemcitabine has shown synergistic effects with different oncolytic Ad at clinical[22] and pre-clinical levels due to several mechanisms: (i) an E1A-induced sensitization of cancer cells to gemcitabine,[19,23] (ii) increased infectivity due to coxsackievirus-adenovirus receptor and integrin overexpression,[20,23] (iii) activation of promoters that regulate replication of the oncolytic Ad,[19] and (iv) apoptosis activation when combined with E1b/19K-deleted mutants.[17,18] However, depending on the timing before infection, nucleotide analogs such as gemcitabine could hamper viral DNA replication and cell lysis.[20] Another reason that supports the combination of the i-leader-truncated fast-release mutant with chemotherapy is that stroma blocks dissemination of chemotherapy drugs from blood vessels to the tumor cells.[24] Consequently, targeting tumor cells and cancer-associated fibroblast with ICOVIR-15i may not only improve the spread of the oncolytic virus, but also the penetration of the chemotherapeutic drugs. Conversely, chemotherapy can reduce the intratumoral interstitial pressure by killing tumor cells, and enhance the penetration of the virus into the tumor mass.[25]

First, we studied the *in vitro* cytotoxicity of ICOVIR-15i and ICOVIR-15 combined with increasing doses of gemcitabine (always below its IC_{50} value). *In vitro*, gemcitabine did not have a synergistic effect with the virus. On the contrary, ICOVIR-15i was as cytotoxic as ICOVIR-15 when combined with gemcitabine (Figure 4a). However, in hamsters bearing subcutaneous HP-1 tumors and treated with a single intratumoral dose of PBS, ICOVIR-15, or ICOVIR-15i at 2.5×10^{10} vp per tumor alone or in combination with a low dose of gemcitabine (a dose of $50\,mg\,kg^{-1}$ intraperitoneally at days 0, 3, 6 and 9 post virus administration), only the combination of ICOVIR-15i with gemcitabine resulted in antitumor activity (Figure 4b). ICOVIR-15i/gemcitabine combination induced a 2.6-fold statistically significant decrease in the tumor growth compared with PBS, and an improvement in the mean survival time compared with other treatments, which increased from 29.9 days in the PBS group to 36.8 days (Figure 4c). No activity was seen with ICOVIR-15 or ICOVIR-15i alone, gemcitabine alone, or the combination of ICOVIR-15 and gemcitabine. Virus replication in the tumors at the end of the experiment could not be detected in any of the treatment groups by immunofluorescent staining against E1A protein (data not

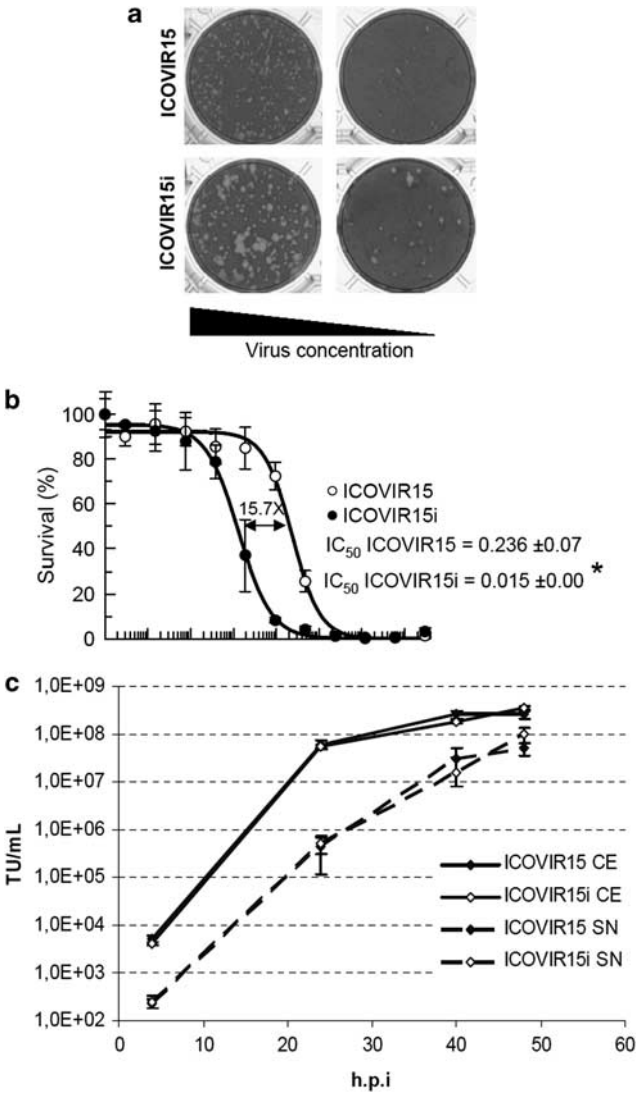

Figure 3. iLG397T mutation enhances ICOVIR-15 plaque size and cytotoxicity in a Syrian hamster tumor model *in vitro*. (**a**) Comparative plaque size of ICOVIR-15 and ICOVIR-15i in HP-1 cells at day 15 postinfection. (**b**) Cytotoxicity assay. Comparative dose-response curves of ICOVIR-15 and ICOVIR-15i at day 8 after infection in HP-1 cells. Mean IC_{50} values ± s.d. in TU per cell for each virus and the cytotoxicity increase are shown in the figure. The two-tailed unpaired Student's *t*-test was used to evaluate the statistical significance of the IC_{50} difference between both viruses. *Significant $P < 0.05$ compared with ICOVIR-15. (**c**) Kinetics of virus production and release of ICOVIR-15 and ICOVIR-15i in HP-1 cells. Extracellular (SN) and total virus produced (CE) was measured at the indicated time points. Mean values ($n = 3$) ± s.d. are plotted. TU, transducing units; h.p.i., hour postinfection; CE, cell extract; SN, supernatant.

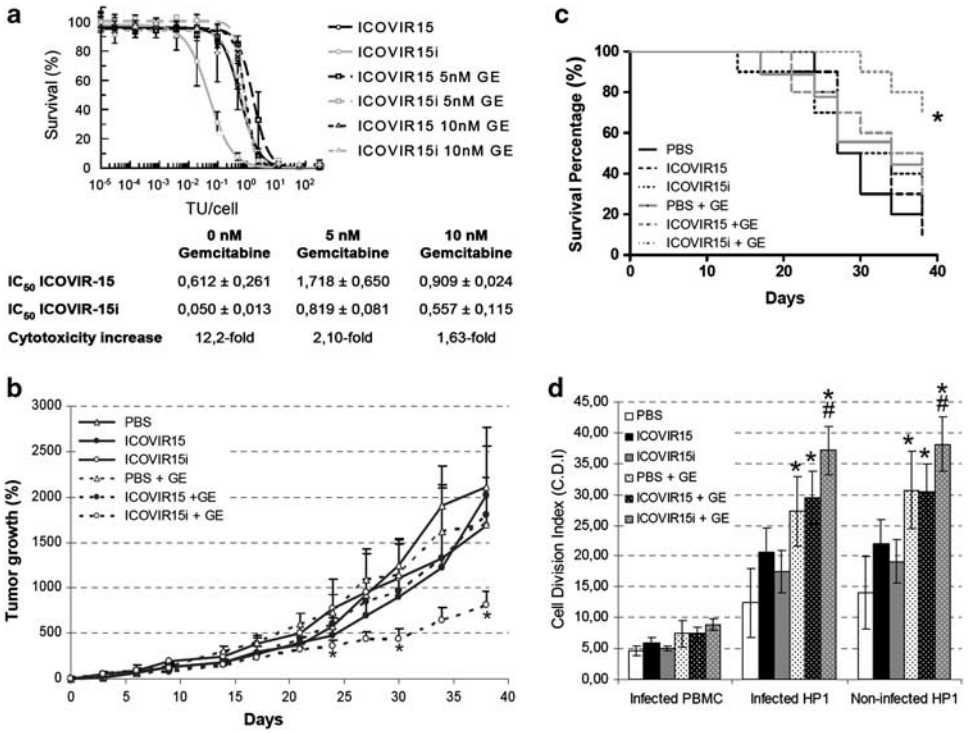

Figure 4. iLG397T mutation combined with gemcitabine increases ICOVIR-15 antitumor activity *in vivo* in Syrian hamsters. (**a**) Cytotoxicity assay. Comparative dose-response curves of ICOVIR-15 and ICOVIR-15i at day 11 postinfection in HP-1 cells, incubated with 0, 5 and 10 nM of gemcitabine. IC_{50} in TU per cell for each virus and the cytotoxicity increase are shown in the figure. (**b**) Syrian hamsters bearing HP-1 pancreatic carcinoma allograft subcutaneous tumors were treated with a single intratumoral dose of PBS, or ICOVIR-15 or ICOVIR-15i at 2.5×10^{10} vp per tumor alone or in combination with gemcitabine (4 intraperitoneal doses of 50 mg kg^{-1} at days 0, 3, 6 and 9 post administration). Mean percentage of tumor growth value ($n = 9$–10 tumors) ± s.e.m. are plotted. *Significant $P < 0.05$ by two-tailed unpaired Student's *t*-test compared with PBS group. (**c**) Kaplan–Meier survival curves after administration of a single intratumoral dose of PBS, or ICOVIR-15 or ICOVIR-15i at 2.5×10^{10} vp per tumor alone or in combination of gemcitabine (4 intraperitoneal doses of 50 mg kg^{-1} at days 0, 3, 6 and 9 post administration). The end point was established at a tumor volume of $\geqslant 2000$ mm^3. *Significant $P < 0.05$ by log-rank test compared with hamsters treated with PBS. (**d**) Lymphocyte proliferation assay. Total hamster PBMCs at the end of treatment were isolated, labeled and exposed to infected PBMCs, and infected and non-infected HP-1 cells for 5 days. Lymphocyte proliferation was assessed and the cell division index representing the percentage of cells that proliferate after antigen stimulation divided by the percentage of cells that proliferate without stimulation was determined. Mean cell division index values ± s.e.m. are represented. *Significant $P < 0.05$ by Mann–Whitney test compared with PBS. #Significant $P < 0.05$ by Mann–Whitney test compared with ICOVIR-15i.

shown). The lower permissiveness of hamster cells compared with human cells tampered the iLG397T mutation phenotype *in vitro* and hindered it *in vivo*. The elimination of the virus by the immune system, independently of the i-leader truncation, may also have contributed to the lack of antitumor activity in hamsters, which precluded the observation of a phenotype related to the i-leader truncation when administered alone.

For a rational combination of gemcitabine and i-leader truncated oncolytic Ad, the mechanism relying on the antitumor activity in immunocompetent animals should be addressed. Emerging clinical and experimental data indicate that immunogenic cell death improves the response to cytotoxic agents recruiting mature, specific immune effector cells to the tumor.[26] Some of these cells have immunosuppressive functions and become dominant as the tumor is cleared by the cytotoxic response. Regulatory cells induce tissue remodeling and angiogenesis, but the incomplete eradication of malignant cells gives rise to tumor regrowth.[26] Moreover, gemcitabine enhances antigen presentation, and inhibits regulatory T cells, and immature myeloid cells.[27–31] Although most immunogenic cytotoxic compounds trigger a protective immune response, they fail to control the disease, therefore several adjuvants to increase immunogenic cell death and Th1 response could synergize with chemotherapies.[32] Oncolytic Ads induce a necrosis-like cell death, a release of HSP70 and HMBG1 (immunogenic cell death markers)[33] together with other immunostimulatory factors and generate a source of tumor-associated antigens available for cross-priming of dendritic cells, ensuring polyclonal T cell activation.[33–35] As a preliminary test of this immunogenic hypothesis we observed upon incubation with HP-1 cells, the highest lymphocyte proliferation in animals treated with the ICOVIR-15i/gemcitabine combination (Figure 4d). Ad infection of HP-1 target cells did not change lymphocyte proliferation, and no significant lymphocyte proliferation was observed upon incubation with infected PBMCs, suggesting a specific immune response against HP-1 cells. In addition, we studied the antitumor efficacy of the ICOVIR-15i/gemcitabine combination in xenografted HP-1 tumors in nude mice and confirmed that in the absence of immunity ICOVIR-15i/gemcitabine had no antitumor activity (Supplementary Figure S1). These results highlight the low permissivity of HP-1 cells to Ad replication, and suggest a role of the immune system behind the antitumor efficacy shown in the treatment with ICOVIR-15i/gemcitabine in immunocompetent animals. Although we could not detect virus replication in the Syrian hamster tumors, we cannot exclude the role of ICOVIR-15i replication in Syrian hamster fibroblasts in the observed antitumor efficacy.

Supporting this immune-mediated hypothesis, Boozari and coworkers described a combination of an oncolytic Ad with a proteasome inhibitor that caused endoplasmic reticulum stress-induced apoptosis responsible for triggering immunogenic cell

death. This immunogenic cell death induced a potent antitumor immune response capable of controlling the primary tumors and also the non-injected metastasis.[36] It is intriguing to speculate whether the iLG397T mutation in particular, or the fast-release mutations in general, in combination with gemcitabine induce a more immunogenic cell death.

Our results highlight the interest of the i-leader truncation in particular, and the fast-release mutants in general, to improve the potency of oncolytic Ads, and support the combination of fast-release mutants with chemotherapeutic drugs for cancer treatment. Studying the combination of i-leader truncated oncolytic mutants with different chemotherapeutic drugs with higher capacity to suppress regulatory cells[37] or induce immunogenic cell death is warranted.

CONFLICT OF INTEREST

The authors declare no conflict of interest.

ACKNOWLEDGEMENTS

We thank Dr Miriam Bazan Peregrino for extensive revision of the manuscript. CPS was supported by a master fellowship from 'La Caixa' and a predoctoral fellowship (PFIS) granted by the 'Instituto de Salud Carlos III' FI08/00163. This work was supported by a BIO2011-30299-C02-01 grant from the 'Ministerio de Educación y Ciencia' of the Government of Spain (RA) and a 2009SGR283 research grant from the 'Generalitat de Catalunya' (RA).

REFERENCES

1 Pesonen S, Kangasniemi L, Hemminki A. Oncolytic adenoviruses for the treatment of human cancer: focus on translational and clinical data. *Mol Pharm* 2011; **8**: 12–28.
2 Alemany R. Design of improved oncolytic adenoviruses. *Adv Cancer Res* 2012; **115**: 93–114.
3 Ganesh S, Gonzalez Edick M, Idamakanti N, Abramova M, Vanroey M, Robinson M *et al.* Relaxin-expressing, fiber chimeric oncolytic adenovirus prolongs survival of tumor-bearing mice. *Cancer Res* 2007; **67**: 4399–4407.
4 Guedan S, Rojas JJ, Gros A, Mercade E, Cascallo M, Alemany R. Hyaluronidase expression by an oncolytic adenovirus enhances its intratumoral spread and suppresses tumor growth. *Mol Ther* 2010; **18**: 1275–1283.
5 Gros A, Guedan S. Adenovirus release from the infected cell as a key factor for adenovirus oncolysis. *Open Gene Ther J* 2010; **3**: 24–30.
6 Puig-Saus C, Gros A, Alemany R, Cascallo M. Adenovirus i-leader truncation bioselected against cancer-associated fibroblasts to overcome tumor stromal barriers. *Mol Ther* 2012; **20**: 54–62.
7 Yan W, Kitzes G, Dormishian F, Hawkins L, Sampson-Johannes A, Watanabe J *et al.* Developing novel oncolytic adenoviruses through bioselection. *J Virol* 2003; **77**: 2640–2650.
8 Subramanian T, Vijayalingam S, Chinnadurai G. Genetic identification of adenovirus type 5 genes that influence viral spread. *J Virol* 2006; **80**: 2000–2012.
9 Rojas JJ, Guedan S, Searle PF, Martinez-Quintanilla J, Gil-Hoyos R, Alcayaga-Miranda F *et al.* Minimal RB-responsive E1A promoter modification to attain potency, selectivity, and transgene-arming capacity in oncolytic adenoviruses. *Mol Ther* 2010; **18**: 1960–1971.
10 Doronin K, Toth K, Kuppuswamy M, Ward P, Tollefson AE, Wold WS. Tumor-specific replication-competent adenovirus vectors overexpressing the adenovirus death protein. *J Virol* 2000; **74**: 6147–6155.
11 Gros A, Martinez-Quintanilla J, Puig C, Guedan S, Mollevi DG, Alemany R *et al.* Bioselection of a gain of function mutation that enhances adenovirus 5 release and improves its antitumoral potency. *Cancer Res* 2008; **68**: 8928–8937.
12 Gros A, Puig C, Guedan S, Rojas JJ, Alemany R, Cascallo M. Verapamil enhances the antitumoral efficacy of oncolytic adenoviruses. *Mol Ther* 2010; **18**: 903–911.
13 Alemany R, Cascallo M. Oncolytic viruses from the perspective of the immune system. *Future Microbiol* 2009; **4**: 527–536.
14 Khoobyarian N, Barone F, Sabet T, El-Domeiri AA, Das Gupta TK. Inhibition of melanoma growth in hamsters by type-2 adenovirus. *J Surg Oncol* 1975; **7**: 421–425.
15 Thomas MA, Spencer JF, La Regina MC, Dhar D, Tollefson AE, Toth K *et al.* Syrian hamster as a permissive immunocompetent animal model for the study of oncolytic adenovirus vectors. *Cancer Res* 2006; **66**: 1270–1276.
16 Thomas MA, Spencer JF, Toth K, Sagartz JE, Phillips NJ, Wold WS. Immunosuppression enhances oncolytic adenovirus replication and antitumor efficacy in the Syrian hamster model. *Mol Ther* 2008; **16**: 1665–1673.
17 Cherubini G, Kallin C, Mozetic A, Hammaren-Busch K, Muller H, Lemoine NR *et al.* The oncolytic adenovirus AdDeltaDelta enhances selective cancer cell killing in combination with DNA-damaging drugs in pancreatic cancer models. *Gene Ther* 2011; **18**: 1157–1165.
18 Leitner S, Sweeney K, Oberg D, Davies D, Miranda E, Lemoine NR *et al.* Oncolytic adenoviral mutants with E1B19K gene deletions enhance gemcitabine-induced apoptosis in pancreatic carcinoma cells and anti-tumor efficacy *in vivo*. *Clin Cancer Res* 2009; **15**: 1730–1740.
19 Onimaru M, Ohuchida K, Nagai E, Mizumoto K, Egami T, Cui L *et al.* Combination with low-dose gemcitabine and hTERT-promoter-dependent conditionally replicative adenovirus enhances cytotoxicity through their crosstalk mechanisms in pancreatic cancer. *Cancer Lett* 2010; **294**: 178–186.
20 Nelson AR, Davydova J, Curiel DT, Yamamoto M. Combination of conditionally replicative adenovirus and standard chemotherapies shows synergistic antitumor effect in pancreatic cancer. *Cancer Sci* 2009; **100**: 2181–2187.
21 Bortolanza S, Bunuales M, Alzuguren P, Lamas O, Aldabe R, Prieto J *et al.* Deletion of the E3-6.7 K/gp19K region reduces the persistence of wild-type adenovirus in a permissive tumor model in Syrian hamsters. *Cancer Gene Ther* 2009; **16**: 703–712.
22 Hecht JR, Bedford R, Abbruzzese JL, Lahoti S, Reid TR, Soetikno RM *et al.* A phase I/II trial of intratumoral endoscopic ultrasound injection of ONYX-015 with intravenous gemcitabine in unresectable pancreatic carcinoma. *Clin Cancer Res* 2003; **9**: 555–561.
23 Bhattacharyya M, Francis J, Eddouadi A, Lemoine NR, Hallden G. An oncolytic adenovirus defective in pRb-binding (dl922-947) can efficiently eliminate pancreatic cancer cells and tumors *in vivo* in combination with 5-FU or gemcitabine. *Cancer Gene Ther* 2011; **18**: 734–743.
24 Neesse A, Michl P, Frese KK, Feig C, Cook N, Jacobetz MA *et al.* Stromal biology and therapy in pancreatic cancer. *Gut* 2010; **60**: 861–868.
25 Russell SJ, Peng KW, Bell JC. Oncolytic virotherapy. *Nat Biotechnol* 2012; **30**: 658–670.
26 Shiao SL, Ganesan AP, Rugo HS, Coussens LM. Immune microenvironments in solid tumors: new targets for therapy. *Genes Dev* 2011; **25**: 2559–2572.
27 Liu WM, Fowler DW, Smith P, Dalgleish AG. Pre-treatment with chemotherapy can enhance the antigenicity and immunogenicity of tumours by promoting adaptive immune responses. *Br J Cancer* 2010; **102**: 115–123.
28 Plate JM, Plate AE, Shott S, Bograd S, Harris JE. Effect of gemcitabine on immune cells in subjects with adenocarcinoma of the pancreas. *Cancer Immunol Immunother* 2005; **54**: 915–925.
29 Rettig L, Seidenberg S, Parvanova I, Samaras P, Curioni A, Knuth A *et al.* Gemcitabine depletes regulatory T-cells in human and mice and enhances triggering of vaccine-specific cytotoxic T-cells. *Int J Cancer* 2011; **129**: 832–838.
30 Le HK, Graham L, Cha E, Morales JK, Manjili MH, Bear HD. Gemcitabine directly inhibits myeloid derived suppressor cells in BALB/c mice bearing 4T1 mammary carcinoma and augments expansion of T cells from tumor-bearing mice. *Int Immunopharmacol* 2009; **9**: 900–909.
31 Ma Y, Kepp O, Ghiringhelli F, Apetoh L, Aymeric L, Locher C *et al.* Chemotherapy and radiotherapy: cryptic anticancer vaccines. *Semin Immunol* 2010; **22**: 113–124.
32 Locher C, Conforti R, Aymeric L, Ma Y, Yamazaki T, Rusakiewicz S *et al.* Desirable cell death during anticancer chemotherapy. *Ann N Y Acad Sci* 2010; **1209**: 99–108.
33 Schierer S, Hesse A, Knippertz I, Kaempgen E, Baur AS, Schuler G *et al.* Human dendritic cells efficiently phagocytose adenoviral oncolysate but require additional stimulation to mature. *Int J Cancer* 2012; **130**: 1682–1694.
34 Chen M, Barnfield C, Naslund TI, Fleeton MN, Liljestrom P. MyD88 expression is required for efficient cross-presentation of viral antigens from infected cells. *J Virol* 2005; **79**: 2964–2972.
35 Schulz O, Diebold SS, Chen M, Naslund TI, Nolte MA, Alexopoulou L *et al.* Toll-like receptor 3 promotes cross-priming to virus-infected cells. *Nature* 2005; **433**: 887–892.
36 Boozari B, Mundt B, Woller N, Struver N, Gurlevik E, Schache P *et al.* Antitumoural immunity by virus-mediated immunogenic apoptosis inhibits metastatic growth of hepatocellular carcinoma. *Gut* 2010; **59**: 1416–1426.
37 Dias JD, Hemminki O, Diaconu I, Hirvinen M, Bonetti A, Guse K *et al.* Targeted cancer immunotherapy with oncolytic adenovirus coding for a fully human monoclonal antibody specific for CTLA-4. *Gene Ther* 2012; **19**: 988–998.
38 Stanton RJ, McSharry BP, Armstrong M, Tomasec P, Wilkinson GW. Re-engineering adenovirus vector systems to enable high-throughput analyses of gene function. *Biotechniques* 2008; **45**: 659–662.
39 Laquente B, Lacasa C, Ginesta MM, Casanovas O, Figueras A, Galan M *et al.* Antiangiogenic effect of gemcitabine following metronomic administration in a pancreas cancer model. *Mol Cancer Ther* 2008; **7**: 638–647.
40 Gujar SA, Michalak TI. Flow cytometric quantification of T cell proliferation and division kinetics in woodchuck model of hepatitis B. *Immunol Invest* 2005; **34**: 215–236.

Supplementary Information accompanies the paper on Cancer Gene Therapy website (http://www.nature.com/cgt)

A pRb-responsive, RGD-modified, and Hyaluronidase-armed Canine Oncolytic Adenovirus for Application in Veterinary Oncology

Eduardo Laborda[1,2], Cristina Puig-Saus[1], Alba Rodriguez-García[1], Rafael Moreno[1], Manel Cascalló[3], Josep Pastor[4] and Ramon Alemany[1]

[1]Translational Research Laboratory, IDIBELL-Institut Català d'Oncologia, Barcelona, Spain; [2]Biochemistry and Molecular Biology Department, Autonomous University of Barcelona, Barcelona, Spain; [3]VCN Biosciences, Barcelona, Spain; [4]Animal Medicine and Surgery Department, Fundació Hospital Clínic Veterinari, Autonomous University of Barcelona, Barcelona, Spain

Human and canine cancer share similarities such as genetic and molecular aspects, biological complexity, tumor epidemiology, and targeted therapeutic treatment. Lack of good animal models for human adenovirotherapy has spurred the use of canine adenovirus 2-based oncolytic viruses. We have constructed a canine oncolytic virus that mimics the characteristics of our previously published human adenovirus ICOVIR17: expression of E1a controlled by E2F sites, deletion of the pRb-binding site of E1a, insertion of an RGD integrin-binding motif at the fiber Knob, and expression of hyaluronidase under the major late promoter/IIIa protein splicing acceptor control. Preclinical studies showed selectivity, increased cytotoxicity, and strong hyaluronidase activity. Intratumoral treatment of canine osteosarcoma and melanoma xenografts in mice resulted in inhibition of tumor growth and prolonged survival. Moreover, we treated six dogs with different tumor types, including one adenoma, two osteosarcomas, one mastocitoma, one fibrosarcoma, and one neuroendocrine hepatic carcinoma. No virus-associated adverse effects were observed, but toxicity associated to tumor lysis, including disseminated intravascular coagulation and systemic failure, was found in one case. Two partial responses and two stable diseases warrant additional clinical testing.

Received 18 April 2013; accepted 14 January 2014; advance online publication 4 March 2014. doi:10.1038/mt.2014.7

INTRODUCTION

In dogs as in humans, cancer is a major cause of mortality.[1,2] More than four million new cancer diagnoses in pet dogs are expected per year.[2] Virotherapy with conditionally replicative viruses in general, adenovirus (Ad) in particular is a promising therapy for cancer.[3] Several animal species have been used as models for cancer therapy with human Ad (hAd).[4] Often, xenograft-implanted nude mice are used to analyze efficacy and immune-competent mice are used for toxicity.[5] However, the mouse is nonpermissive to hAd replication. Syrian Hamster has been suggested as a better model than mouse[6] because it is semipermissive to hAd replication. Despite this advantage, hamster tumors are still engrafted showing a structure and progression different from that of spontaneous tumors. These fundamental differences lead to poor preclinical to clinical correlations in efficacy and, occasionally, to nonexpected toxicity events.[7]

HAd5 replication has been demonstrated in established and primary canine cell lines[8] pointing the dog as a good model to analyze preclinically human conditionally replicative Ads (CRAds). Moreover, an immune-stimulatory human vector (AdCD40L) has been administered in canine melanoma patients with promising results, warranting future application in human patients.[9] In this context, the dog has been suggested as an ideal syngeneic model for virotherapy. Pet dogs develop cancer spontaneously due to an increased life expectancy and an exposure to similar environmental conditions to humans.[10] Canine patients provide an outbred genetic background and they are genetically closer to humans than laboratory rodents.[11] Moreover, cancer therapy occurs in the presence of an immune system and the biologic behavior and clinical presentation of certain canine tumors are similar to their human counterparts.[2] Dogs are routinely vaccinated with canine adenovirus type 2 (CAV2)-based vaccines[12] to elicit a crossreacting protection against CAV1.[13] Thus, dogs have variable titers of specific neutralizing antibodies resembling human population, with implications for the efficacy and safety of the treatment.[14] With the aforementioned, treatment of pet-dog patients with a canine CRAd (cCRAd) based on CAV2 would fulfill the requirements of a good predictive model of human cancer treatment.[15] On the other hand, cCRAds may benefit canine cancer patients as nearly all cancer treatments for dogs are palliative[1] and around 50% of dogs older than 10 years diagnosed with cancer die because of it.[2] Developing new cancer therapies for canine patients may bring veterinary medicine at the forefront of cancer therapy research.

With this aim, an osteocalcin (OC) promoter-controlled cCRAd (OCCAV) has been developed and used to treat canine xenografts.[16,17] OCCAV has proven safe in laboratory Beagles intravenously injected with up to 2×10^{12} viral particles (vp)[18]: only one Grade 4 neutropenia was described, with no other important abnormalities. Necropsies did not show evidence of splenic or

Correspondence: Ramon Alemany, Translational Research Laboratory, IDIBELL-Institut Català d'Oncologia, Av Gran Via de l'Hospitalet 199–203, L'Hospitalet de Llobregat, 08907 Barcelona, Spain. E-mail: ralemany@iconcologia.net

hepatic destruction even when biodistribution pointed out these organs as the main targeted tissues. However, OCCAV efficacy in tumor-suffering dogs remains to be studied and the selective replication in OC-expressing cells will limit the number of patients eligible for treatment.

Our group has previously generated ICOVIR17, an oncolytic Ad based on hAd5, with good results in preclinical studies.[19] In the present study, we developed ICOCAV17, a CAV2-based cCRAd with similar characteristics to ICOVIR17, and two parental viruses, CAV2RGD and ICOCAV15, homologous to their human counterparts AdwtRGD and ICOVIR15, respectively.[20,21] *In vitro* assays showed functional bioactivity of cCRAds and preclinical studies in tumor-harboring nude mice proved intratumoral injection as a safe and effective administration route. However, intravenous toxicity in mice showed marked thrombocytopenia and loss of body weight. Thus, the intratumoral route was chosen for the treatment of six canine patients with ICOCAV17. Results include two partial responses (PR), two stable diseases, and two progressive diseases.

RESULTS

In vitro characterization of cell lines and cCRAds

A schematic representation of the viruses used in this study is shown in **Figure 1a**. All viruses rendered similar yields (9,000 to 10,090

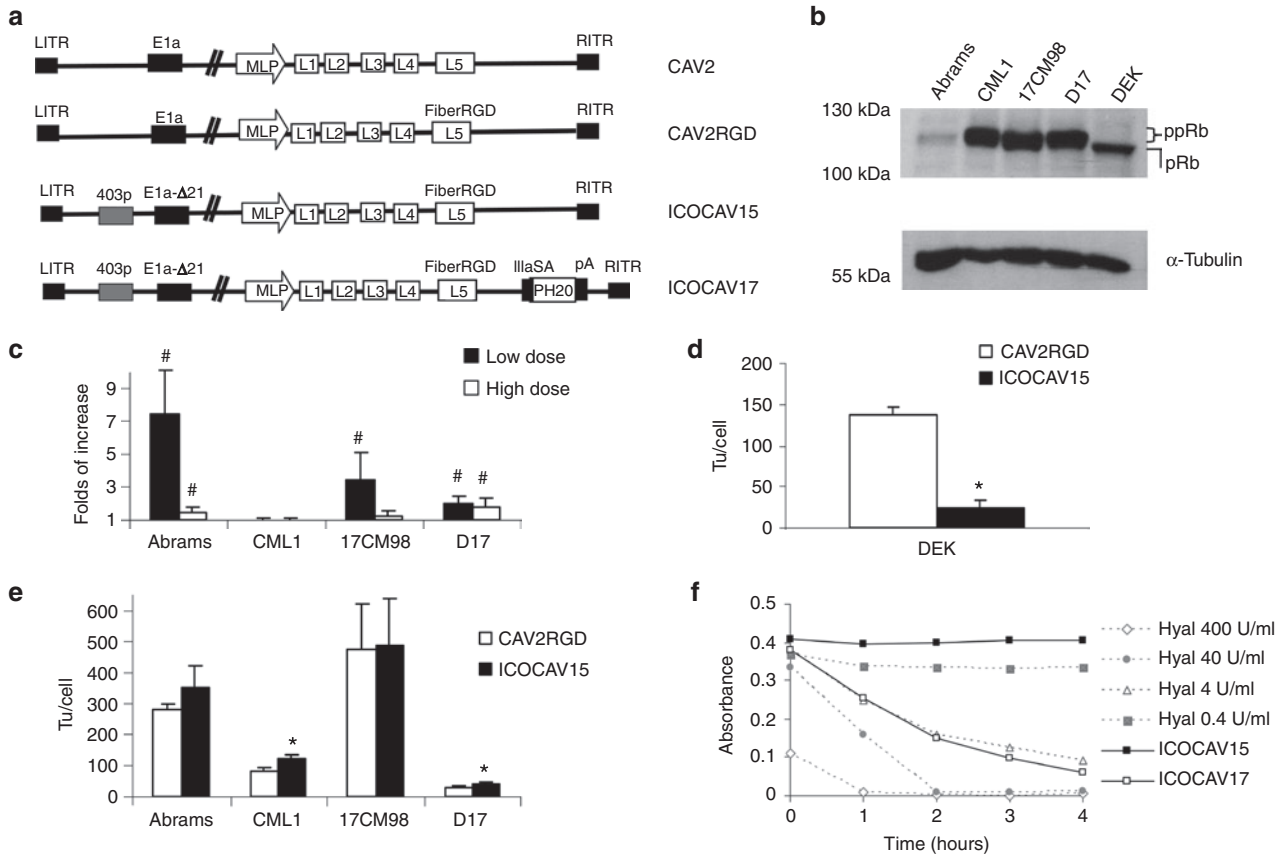

Figure 1 Adenoviruses and cells used in this study and *in vitro* characterization. (**a**) Schematic representation of viruses used in this study. CAV2 is the canine wild-type virus serotype 2. CAV2RGD contains an RGD motif (FiberRGD) in the HI-loop of the CAV2 fiber. ICOCAV15 and ICOCAV17 are canine conditionally replicative adenoviruses, based on CAV2RGD, in which the endogenous E1a promoter have been modified inserting four palindromic E2F-binding sites and one Sp-I-binding site (403p) at the 403 nucleotide position of the virus genome, 21 base pairs of E1a region (E1aΔ21) homologous to Δ24 in human oncolytic adenoviruses have been deleted. ICOCAV17 is armed with the human PH20 hyaluronidase (PH20) under the control of the canine IIIa protein Splicing Acceptor (IIIaSA). MLP, Major late promoter; pA, polyadenylation signal. (**b**) Western blot of pRb in canine tumor cells and dog epidermal keratinocytes (DEK). Both hypophosphorylated (pRb) and hyperphosphorylated (ppRb) forms of the protein were resolved. Abrams cell line expressed low levels of ppRb. α-Tubulin was used as loading control. (**c**) Comparison of infectivity between CAV2 and CAV2RGD in four canine tumor cell lines. Abrams, 17CM98, D17, and CML1 cells were infected with an equal number of viral particles per cell of each virus using two different doses. Immune staining against viral hexon protein was performed 24 hours after infection, and the number of infected cells counted. The ratio between CAV2RGD and CAV2 of three independent assay results ± SD is shown. (**d**) ICOCAV15 total production yields in a cycle-arrested nontumor canine cell line. DEK were seeded in 24-wells plates. After 20 days in confluence, DEK were infected with 8 transducing units (tu)/cell of CAV2RGD or ICOCAV15. Two days postinfection, total virus production was measured. Three independent assay results ± SD are shown. (**e**) Virus production of ICOCAV15 in tumor cells. Different tumor cell lines were infected with a dose of virus that resulted in >80% transduction (20 tu/cell for D17 and CML1 and 30 tu/cell for Abrams and 17CM98). Two days after infection, total virus production was measured in triplicate. Results ± SD are shown. (**f**) Hyaluronidase expression in cells infected with ICOCAV17. DK28Cre cells were infected with ICOCAV15 or ICOCAV17 with 20 tu/cell. After 48 hours, supernatants from infected cells were incubated with a solution of Hyaluronan (HA) for 0, 1, 2, 3, or 4 hours and analyzed. Four samples with known concentration of purified hyaluronidase were used as references. HA degradation was measured by absorbance (600 nm). #Statistical significance between CAV2 and CAV2RGD ($P < 0.05$) by two-tailed unpaired Student's *t*-test; *Statistical significance between CAV2RGD and ICOCAV15 ($P < 0.05$) by two-tailed unpaired Student's *t*-test.

vp/cell) in DK28Cre cells.[22] To test the function of these cCRAds, *in vitro* assays were performed in four canine tumor cell lines. Abrams and D17 (pulmonary metastasis) derive from osteosarcoma (OS),[23] and 17CM98 and CML1 from melanoma.[24] Dog epidermal keratinocytes (DEK) were used as nontumor control cells. Studies point pRb pathway as necessary to cause cancer.[25,26] We characterized pRb status of the cell lines used in this study by western blot (**Figure 1b**). Tumor cells contained hyperphosphorylated pRb (ppRb). In contrast, pRb from DEK was hypophosphorylated (pRb). Additionally, tumor cells were analyzed for expression of Coxsackie virus and adenovirus receptor (CAR) (data not shown). All cells had detectable levels of CAR. CML1 and D17 expressed similar levels to DK28Cre, while 17CM98 expressed lower levels and Abrams expressed even higher levels than DK28Cre. The insertion of RGD at the fiber HI-loop of hAds enhances infectivity and allows the virus to infect cells CAR independently.[20,27] Similarly, CAV2RGD showed enhanced infectivity compared to CAV2 (**Figure 1c**). When we infected cells with a dose of 20 vp/cell for Abrams, 10 vp/cell for 17CM98, 2 vp/cell for D17, and 6 vp/cell for CML1, the infectivity was increased 7.4 times ($P = 0.008$), 3.4 times ($P = 0.04$), and 2 times ($P = 0.03$) in Abrams, 17CM98, and D17 cells, respectively. When infecting with a fivefold higher dose for Abrams, 17CM98, and D17 and a twofold higher dose for CML1, the infectivity was increased 1.4 times ($P = 0.03$), 1.15 times ($P = 0.2$), and 1.7 times ($P = 0.009$) in Abrams, 17CM98, and D17 cells, respectively. No differences were seen in CML1 cells at any dose. To test E2F-driven selectivity, progeny virus production was analyzed in tumor cells and arrested[28] DEK. In DEK, the progeny production of ICOCAV15 showed a decrease of 84% ($P = 0.03$) compared with the parental virus CAV2RGD (**Figure 1d**). Conversely, virus progeny production was increased for ICOCAV15 compared with CAV2RGD in two out of four tumor cell lines (CML1 ($P = 0.008$) and D17 ($P = 0.02$)), and a trend for improved production was observed in the other two cell lines (Abrams and 17CM98; **Figure 1e**). To confirm the activity of the hyaluronidase of ICOCAV17, a hyaluronic acid (HA) degradation assay[29] was performed (**Figure 1f**). Supernatants (SN) from cells infected with ICOCAV17 degraded HA to an equivalent level of 4 units/ml of hyaluronidase, while ICOCAV15 SN did not degrade HA at all. Finally, cytotoxicity was analyzed at days 6–8 comparing all viruses simultaneously (**Figure 2**). Under the conditions of time and transducing units (tu)/cell used, CAV2 was not able to induce cytotoxicity (evidence of cytopathic effect) in Abrams and 17CM98 cells, even at a dose of 2,000 tu/cell. In D17 cells, CAV2RGD decreased the IC_{50} (amount of virus needed to reduce the cell culture viability by 50%) 1.9-fold ($P = 0.032$) compared to CAV2. The E2F-binding sites rendered ICOCAV15 more

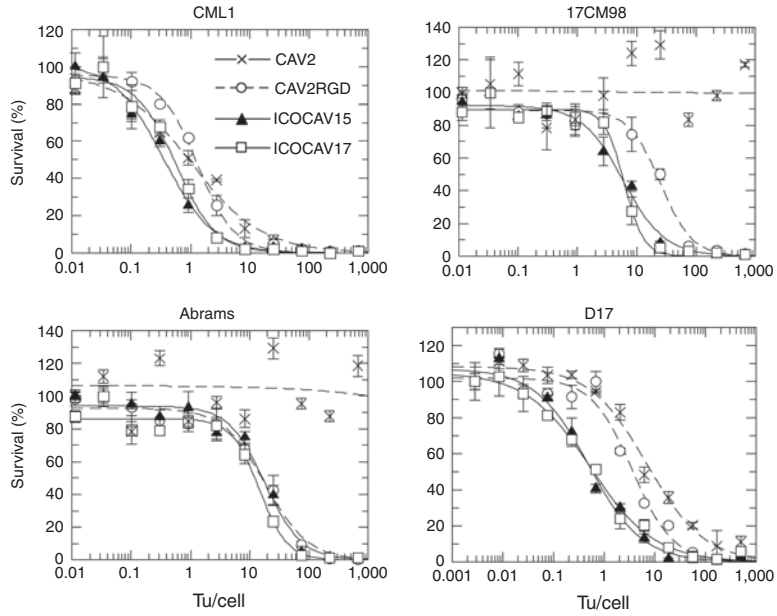

IC50	CAV2	CAV2RGD	ICOCAV15	ICOCAV17
CML1	1.03 ± 0.31	1.30 ± 0.11	0.35 ± 0.04* #	0.57 ± 0.07* #
17CM98	∞	25.01 ± 3.70*	5.9 ± 0.79* #	6.1 ± 0.62* #
Abrams	∞	18.48 ± 2.74*	18.09 ± 2.69*	14.61 ± 2.07*
D17	7.02 ± 1.24	3.59 ± 0.79*	0.49 ± 0.09* #	0.53 ± 0.08* #

Figure 2 Comparative cytotoxicity of canine viruses in four canine tumor cell lines. Infection with the indicated viruses, at doses ranging from 2,000 to 0.01 transducing units (tu)/cell for Abrams, CML1, and 17CM98 or from 500 to 0.001 tu/cell for D17 was performed. The IC50 values (tu/cell needed to reduce by 50% the cell viability) at days 6–8 after infection are shown. Three different replicates were quantified for each cell line. Mean ± SD are plotted. IC50 $\rightarrow\infty$ for CAV2 at 17CM98 and Abrams cells indicates estimated values of IC50 over 10^6 tu/cell. *Significant ($P < 0.05$) compared to CAV2 by two-tailed unpaired Student's *t*-test; #Significant ($P < 0.05$) compared to CAV2RGD by two-tailed unpaired Student's *t*-test.

cytotoxic decreasing the IC_{50} by 3.7 times ($P = 0.013$), 7.2 times ($P = 0.0009$), and 4 times ($P = 0.005$) in CML1, D17, and 17CM98, respectively, compared to CAV2RGD. ICOCAV17 showed similar IC_{50} values to ICOCAV15. No differences between CAV2RGD, ICOCAV15, and ICOCAV17 were seen in Abrams cells.

Toxicity and biodistribution profile of canine adenoviruses after systemic administration in Balb/C immunocompetent mice

We had previously determined a tolerable dose for wild-type viruses (CAV2 and CAV2RGD) and a peak of body weight loss at day 2 after systemic administration (data not shown). Thus, mice were intravenously injected with 1×10^{11} vp of ICOCAV17 or control viruses. Body weight was monitored daily and overall survival, liver enzymes (aspartate aminotransferase and alanine aminotransferase), and hematology were determined at day 3 after viral injection. At that time, animals were sacrificed and organs of groups injected with CAV2 and CAV2RGD were collected and analyzed for presence of virus.

As expected, weight loss showed a peak of toxicity 48 hours postinjection for all viruses (**Figure 3a**). No animal died or lost more than 10% of its body weight. Viruses with the RGD motif in the capsid induced a significant decrease of body weight compared to CAV2. Moreover, animals injected with ICOCAV15 or ICOCAV17 had a slower recovery than those injected with CAV2RGD. Hematology analysis showed a dramatic decrease in platelets for all viruses (**Figure 3b**). Compared to phosphate-buffered saline, all viruses induced a significant lymphopenia and a modest but significant increase of basophils, whereas only CAV2RGD and ICOCAV17 decreased monocytes significantly (**Figure 3c**).

Although a mild increase of liver enzymes was observed, none of the viruses increased significantly alanine aminotransferase or aspartate aminotransferase compared to PBS group (**Figure 3d**), consistent with the biodistribution results, where we did not find a marked liver tropism (**Figure 3e**). Instead, CAV2 and CAV2RGD showed a heterogeneous tropism. The spleen, lungs, liver, and kidney showed the highest concentrations of CAV2 and

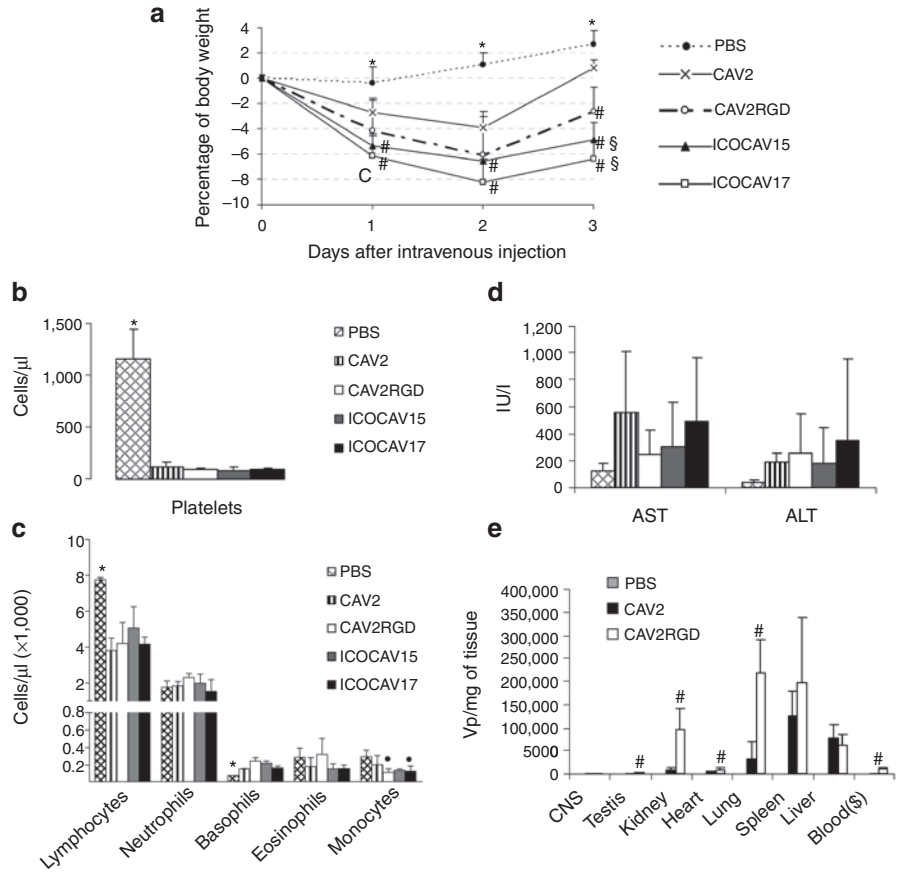

Figure 3 Toxicity and biodistribution profile after systemic administration of canine adenoviruses in immunocompetent mice. Balb/C immunocompetent mice were injected intravenously with PBS or 1×10^{11} viral particles of CAV2, CAV2RGD, ICOCAV15, or ICOCAV17. The average values for (**a**) percentage of body weight variation during all the experiment and (**b**) platelet concentration, (**c**) leukocyte concentration, and (**d**) serum transaminases at day 3 after administration. (**e**) Biodistribution of CAV2 and CAV2RGD in mice tissues. Tissues were harvested 3 days after administration, snap frozen, and quantitatibe polymerase chain reaction assayed for the presence of viruses. Results are reported as viral genomes per milligram of tissue. ($) Blood concentration is reported as viral genomes per milliliter of blood. Mean values ± SD of $n = 5$ mice/group are depicted. *Statistical significance compared with groups injected with viruses ($P < 0.05$) by two-tailed unpaired Student's *t*-test. #Statistical significance compared with CAV2 ($P < 0.05$) by two-tailed unpaired Student's *t*-test. §Statistical significance compared with CAV2RGD ($P < 0.05$) by two-tailed unpaired Student's *t*-test.·Statistical significance compared with PBS ($P < 0.05$) by two-tailed unpaired Student's *t*-test. ALT, alanine aminotransferase; AST, aspartate aminotransferase; CNS, central nervous system; PBS, phosphate-buffered saline.

CAV2RGD (vp/mg of tissue and vp/ng of total DNA), whereas the liver showed the highest absolute amount of viral genomes (**Supplementary Table S1**). The levels of CAV2RGD were higher than those of CAV2 in the testis, heart, lungs, and kidneys. The viremia at day 3 was 100-fold higher for CAV2RGD compared with CAV2.

ICOCAV17 oncolytic potency in two xenograft models

We evaluated ICOCAV17 efficacy in melanoma and OS tumor models (**Figure 4**), two of the most common and devastating cancers in dogs.[30] Nude mice harboring CML1 or Abrams tumors were injected intratumorally three times (on days 0, 7, and 14) with PBS or a dose of 1×10^{10} vp/tumor of each virus. Intratumoral injections did not decrease animal weight. In Abrams, ICOCAV17 decreased tumor volume at the end of the experiment compared to all other groups (1.52-fold ($P = 0.038$) compared to PBS, 1.91-fold ($P = 0.039$) compared to CAV2, 1.87-fold ($P = 0.006$) compared to CAV2RGD, and 1.67-fold ($P = 0.01$) compared to ICOCAV15). In CML1, ICOCAV17 reduced tumor volume fivefold ($P = 0.04$) and 2.7-fold ($P = 0.002$) compared to PBS and CAV2, respectively, at the end of the experiment (day 21 for PBS and day 26 for CAV2). Although differences in tumor volume between ICOCAV15 and PBS groups did not reach statistical significance in CML1, they did when percentage of tumor growth was analyzed at days 7 ($P = 0.02$) and 12 ($P = 0.03$) (data not shown). ICOCAV17 injection increased the survival of Abrams tumor-bearing mice compared to PBS ($P = 0.044$), CAV2 ($P = 0.009$), CAV2RGD ($P = 0.004$), and ICOCAV15 ($P = 0.005$), and compared to PBS ($P = 0.01$) and CAV2 ($P = 0.004$) in CML1 tumor-bearing mice. ICOCAV15 prolonged ($P = 0.058$) the mean survival from 13 and 15 days to 20.5 days, compared to PBS and CAV2 groups, respectively, in the CML1 model. Staining of tumors against late Ad proteins was performed at the end of the experiment (**Supplementary Figure S1 and Supplementary Materials and Methods**). We were able to detect virus in 1 or 2 tumors from each group and a trend for increased dissemination of ICOCAV17 compared with the other groups was observed, primarily in Abrams tumors. After efficacy and toxicity studies in mice, six canine patients were enrolled in an investigational trial with ICOCAV17 (see **Table 1** for a summary of all six cases):

Clinical case I. A 14-year-old entire male Husky that had received surgery 2 years before to remove a sweat gland adenoma, was admitted to the Veterinary Hospital with a mass located at the prepuce skin that caused dysuria. Infiltrative sweat gland adenoma was diagnosed by fine needle aspiration. Due to the poor general condition of the dog and poor benefit of second-line chemotherapy for recurrent sweat gland adenoma,[31] chemotherapy and surgical treatment were declined. The dog was selected for investigational therapy with ICOCAV17.

Treatment and response: physical examination showed a general poor body condition and hind leg weakness. Biochemistry and hematological analysis were within normal limits. ICOCAV17 was injected in four points of the adenoma mass. One day after injection, mild temporal bleeding in one out of four administration points was observed. Fever was detected on day 21 after treatment associated to an anal sac abscess which was controlled with broad spectrum antibiotics. Biochemistry, coagulation, and hematological analysis and physical examination showed no signs of systemic toxicity through all the treatment. Tumor progressively decreased in size and dysuria disappeared within 3 days after virus administration. For at least 6 months, the tumor was in PR with a decrease of 51% in size (**Figure 5**). In the last check-up, 11 months after

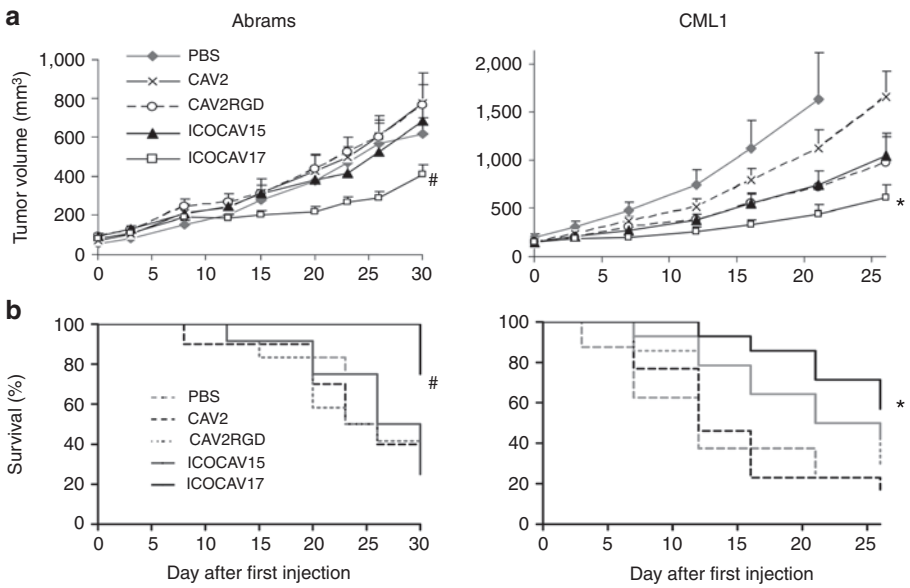

Figure 4 Efficacy and survival after canine adenovirus intratumor injections. Nude mice bearing canine subcutaneous xenografts of osteosarcoma (Abrams) or melanoma (CML1) were treated with three injections (Day 0, 7, and 14) with phosphate-buffered saline (PBS) or 1×10^{10} viral particles per tumor of CAV2, CAV2RGD, ICOCAV15, or ICOCAV17. (**a**) Mean tumor volume values ± SE are plotted ($n = 10$–12). (**b**) Kaplan–Meier survival curves. The end point was established at a volume of ≥500 mm^3. #Statistical significance between ICOCAV17 and PBS, CAV2, CAV2RGD, and ICOCAV15 ($P < 0.05$) by two-tailed unpaired Student's *t*-test. *Statistical significance between ICOCAV17 and PBS and CAV2 ($P < 0.05$) by two-tailed unpaired Student's *t*-test.

Table 1 Summary of patients

Patient ID	Tumor type	Chemotherapy concomitant treatment	Neutralizing antibody titer (days posttreatment)					Virus load in whole blood (vp/ml) (days posttreatment)					Response		
			0	3–5	7–10	11–15	>15	0	1–2	3–4	5–10	>15	RECIST (%)	Other criteria[a] (virus bioactivity)	Survival (days)
Case I	Infiltrative adenoma	No	80	640			32,000	0	1.1×10^5	3.5×10^4		0	PR (−51%)	Improve QoL	>300[c]
Case II	Osteosarcoma	No	2,560	5,120	128,000	256,000		0	1,830	<500	<500		SD	Stable QoL (primary tumor and lung metastasis necrosis)	11
Case III	Mast cell tumor	Toceranib (TKI)[b]	640	1,280	1,280								PR (−70%)	Worse QoL	10
Case IV	Osteosarcoma	Toceranib (TKI)[b]	160		16,000	256,000	512,000	0	1.2×10^5	9.8×10^5		0	PD	Stable QoL (tumor growth stabilization at inoculation site)	70
Case V	Fibrosarcoma	No	80	160	32,000		16,000	0	6.4×10^5	2.6×10^5	1,860	0	SD	Stable QoL (temporally tumor stabilization→ surgical resection)	>200[c]
Case VI	Hepatic endocrine carcinoma	No	ND	20	5,120	21,000	32,000	0	6.3×10^6	2.8×10^6	2.7×10^4	0	SD	Stable QoL (tumor necrosis induction)	22

ND, nondetectable; PR, partial response; PD, progressive disease; SD, stable disease; TKI, tyrosine kinase inhibitor.
A summary of patient tumor type, concomitant chemotherapy treatment, neutralizing antibody titers, viral load in whole blood, treatment responses evaluated by RECIST 1.1 criteria, a health related quality of live questionnaire and virus bioactivity and survival of patients after treatment. [a]Health-related quality of life questionnaire (QoL). [b]2,75 mg/kg/PO/48 hours. [c]Patients still alive at the moment of submission of this manuscript.

virus inoculation (1 month previous to current submission), progressive disease was observed with a tumor volume similar to that at the start of treatment.

Clinical case II. A 7-year-old entire male Ibizan Warren Hound was referred to the Veterinary Hospital with a large humeral mass on the right proximal humerus compatible with OS. Owner reported that lesions started being evident 1 month before, although normal dog activity had not been compromised until 1 week before the visit. Humerus fracture and multiple lung metastases were detected by radiography (**Figure 6a**). Patient presented with normal appetite, alert status, biochemistry, coagulation, and hematologic profiles, except for an increase in alkaline phosphatase. Owner declined euthanasia and conventional treatment protocols. The dog was selected for ICOCAV17 treatment.

Treatment and response: ICOCAV17 was administered using echoguidance within four points aiming at the primary tumor, although swelling hindered accurate echographic differentiation between normal and tumor tissue. Mild temporary swelling with turgor at the injection sites was observed for 48 hours which reverted afterwards. No signs of systemic toxicity were noted throughout the treatment. Appetite and alert status remained unaltered. Tumor size did not show evidence of decrease by echo- or radiographic imaging. On day 10 after administration, patient showed an open and bleeding wound distal to the administration points (**Figure 6a**). Signs of self-trauma on this site were evident. Due to the poor prognosis and the presence of this wound, the dog was euthanized. Histopathology examination showed large necrotic tumor areas (**Figure 6a**) around the points of virus administration, whereas a nontumor area injected accidentally during echoguided administration only showed minimal signs

Figure 5 Treatment response after a single intratumoral administration of ICOCAV17 in an infiltrative adenoma canine patient. Patient I was admitted to the Veterinary Hospital with urinating problems due to a mass in the prepuce skin. Previously excised relapsing adenoma was diagnosed. A dose of 1×10^{12} viral particles of ICOCAV17 was administered intratumorally (Day 0). At that time, the tumor size was $5.6\times5\times3.5$ cm. Six months after treatment, the tumor size had reduced by 51% (RECIST) and was $2.9\times2.8\times2.2$ cm. Tumor size measured by caliper (left) and the depth measured by echographic imaging (right) at days 0 and 180 after treatment, are shown. Right panel: #tumor tissue; *normal tissue. A scale in centimeter is shown in the echographic images.

of bleeding with lack of necrosis. Moreover, necrotic areas in a metastatic nodule of the lung were observed. Virus replication was confirmed by immunohistochemistry for Ad late proteins in both injected tumor and lung metastasis (**Figure 6b**). Healthy adjacent muscular tissue showed no evidence of virus presence (**Figure 6b**).

Clinical case III. A 7-year-old entire male Labrador Retriever was admitted to the Veterinary Hospital with a relapsing cutaneous thoracic mast cell tumor confirmed by fine needle aspiration. Conventional chemotherapy (Vinblastine, Prednisone, and Lomustine) and tyrosine kinase receptor inhibitor (Toceranib) were applied for one and a half month with no response. Tumor started bleeding, ulcerated and progressed, reaching a threefold volume increase since relapse. The dog was selected for investigational therapy with ICOCAV17. As chemotherapy and hyaluronidase synergy has been reported,[32,33] and considering the fast tumor progression and the experience with the two previous cases, Toceranib was used concomitantly to seek chemosensitization with hyaluronidase.

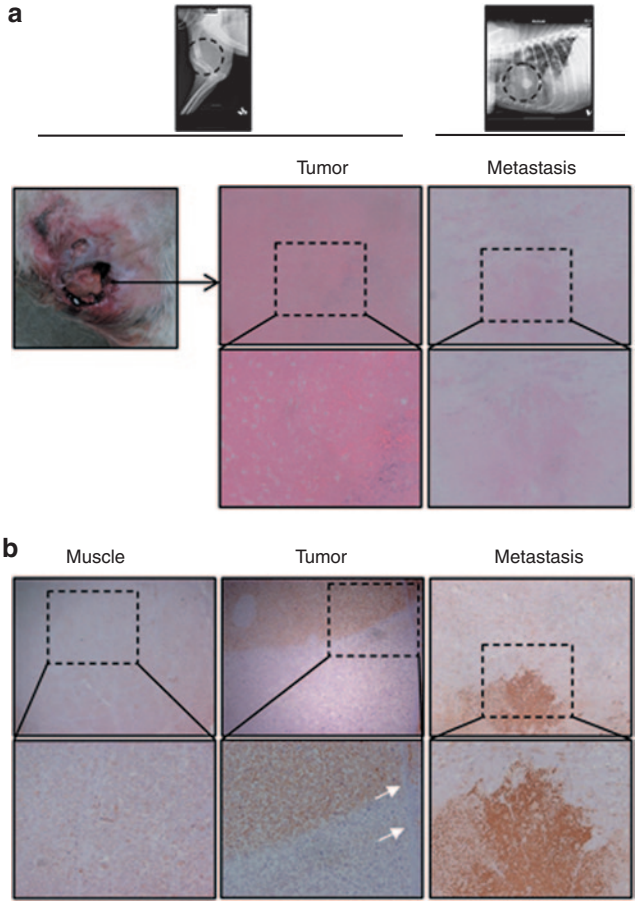

Figure 6 Histopathology and immunohistochemistry staining of healthy tissue, primary tumor, and lung metastasis of an osteosarcoma patient (Case II). Patient II suffered an osteosarcoma in the right front extremity. ICOCAV17 was intratumorally injected in four different sites by echoguidance. (**a**) Euthanasia due to a self-traumatic wound (left panel) was performed 11 days after administration. Broad areas of necrosis were detected in the primary tumor but also in a lung metastatic nodule in the anatomopathological study (central and right panel, respectively). (**b**) Ad detection (brown precipitate) was performed by immune staining using an anti-adenovirus late protein antibody in deparaffinized sections from both, primary and metastatic lesions (central and right panel, respectively). A fibrotic barrier (magnified area; white arrows) is observed in the tumor. Samples from healthy tissue surrounding injected areas were also stained against adenovirus late proteins with no Ad detection (left panel). (**a** and **b**) Upper panel: original magnification ×40. Lower panel: original magnification ×200.

Treatment and response: previrus administration; hematological and biochemical analysis showed mild increase in alanine aminotransferase, alkaline phosphatase, anemia, a hematocrit of 26%, and thrombocytopenia (1.2×10^5 platelets/μl). ICOCAV17 was injected in 10 different points within the thoracic tumor mass. Severe tumor swelling was observed for 48 hours postvirus inoculation. However, tumor necrosis and progressive reduction in tumor volume were evident from day 3 postinoculation until day 10. Hematological and biochemical parameters did not change for the first 7 days after virus inoculation, but later the patient developed progressive renal and hepatic failure. Due to the inflammatory nature of mast cells, the organ failure was attributed to the extensive lysis of mast cell tumor cells and the prolonged unstable general condition (tumor bleeding with low hematocrit and thrombocytopenia). Euthanasia was performed 10 days after virus administration. At that time, tumor size had reduced by 70%. Necropsy showed infarcts in several organs (kidneys, liver, spleen, and heart) with petechiae and general jaundice. Disseminated intravascular coagulation (DIC) was diagnosed. Disseminated intravascular coagulation is a multifactor induced pathology common in dogs. Multiple causes such as viremia, systemic inflammatory response, or direct endothelial damage, lead to coagulation disorders that can evolve in a disseminated intravascular coagulation.

Clinical case IV. A 7-year-old Golden Retriever entire male, was admitted to the Veterinary Hospital with a humeral OS. Limb amputation was declined by the owner. Despite treatment with conventional chemotherapy, nonsteroidal anti-inflammatory drugs, and Toceranib, the disease progressed. Lesions compatible with metastases were observed at the shoulder and spinal bone. The dog was selected for ICOCAV17 investigational treatment. Taking into account the bad prognosis of the patient and the previous results, a combination with Toceranib was considered.

Treatment and response: Before virus administration, the dog presented with hematology and biochemistry profile within normal levels, except for mild elevation of alkaline phosphatase. After intratumoral administration of ICOCAV17 within the primary humeral lesion, swelling of injected areas was observed followed by a control of tumor growth restricted to the injected areas, whereas enlarging of tumor was observed in the surrounding areas. No toxicity-related symptoms were observed through the treatment. No signs of bioactivity or benefit in terms of quality of life were observed and patient was euthanatized 2 months postvirus injection due to progressive disease. Virus replication could not be demonstrated by immunohistochemistry at this time point.

Clinical case V. A 15-year-old Catalan Sheep Dog spayed female was admitted to the Veterinary Hospital with a history of right leg subcutaneous fibrosarcoma at the distal ulna area, previously

treated by surgery and radiotherapy. Limb amputation was declined by the owner. Biochemistry and hematology analysis were within reference limits and physical examination did not show any disorders. Due to the previous case results, in an attempt to avoid tumor relapsing and to study virus replication in a short time period after virus injection, the dog was selected for investigational treatment in a neoadjuvant setting before surgery.

Treatment and response: ICOCAV17 was inoculated at 6 points within the tumor. Initial swelling of the tumor was observed, followed by tumor progression 10 days after virus injection. No adverse events were observed. Fifteen days after administration, tumor was surgically excised. Immunohistochemistry showed areas of virus replication in the subcutaneous tumor tissue (**Figure 7**, left panel), although tumor areas without virus replication were also observed (**Figure 7**, right panel). The dog recovered normally from surgery and after 8 months (last check up, 1 month before current submission) she had no evidence of tumor relapse.

Clinical case VI. A 15-year-old small cross bred entire male was referred to the Veterinary Hospital with a 2-year history of multiple subcutaneous and hepatic nodules. The treatment with steroidal anti-inflammatory drugs had held the disease stable, however tumors were progressing during the last 2 months. Subcutaneous nodules on both flanks, below the jaw, and in the cervical area were observed. Thoracic radiographs and abdominal ultrasound showed nodules on the liver, kidneys, and lungs. A marked alkaline phosphatase increase and normal levels of alanine aminotransferase were observed on biochemistry, and hematology showed a hematocrit of 25.5% and mild nonregenerative anemia.

Treatment and response: Two subcutaneous nodules, one on each flank, were injected with 5×10^{11} vp of ICOCAV17 each. No adverse effects were observed. Neutrophil count increased on day 2, presumably due to mild local reaction. The turgidity of the injected nodules decreased, however, in the last check up, only a 14% reduction in tumor volume was observed in one, with an increase of 7% in the other. The progression of the disease led to death of the patient 22 days after administration due to cardiac arrest. We were not able to detect virus replication in any of the tumors analyzed, however, when the percentage of necrotic area was analyzed, a twofold significant increase within the injected tumors was observed (**Supplementary Figure S2 and Supplementary Materials and Methods**).

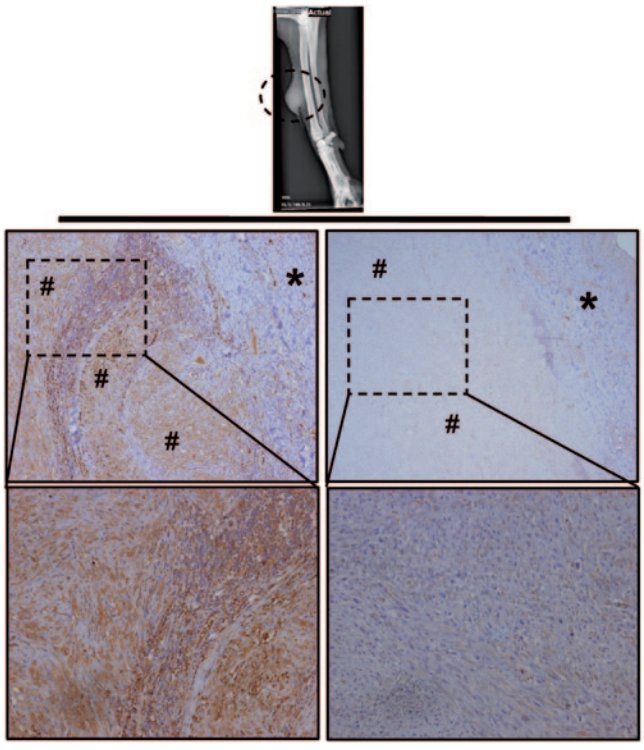

Figure 7 Immunohistochemistry staining of fibrosarcoma tumor from patient V. A Catalan Sheep Dog with a relapsing fibrosarcoma at the distal ulna area of the right leg was admitted to the Hospital. A neoadjuvant setting of virotherapy with ICOCAV17 was performed injecting the virus before surgical resection. Tumor was resected 15 days after injection and embedded in paraffin. Tumor sections were stained with anti-adenovirus late protein antibody. Left panel: virus was detected (brown precipitate) in subcutaneous tumor section. Right panel: tumor section staining did not result in virus detection. (*) skin, (#) tumor tissue. Upper panel: original magnification ×40. Lower panel: original magnification ×200.

Neutralizing antibodies (Nabs) and virus in whole blood and in body secretions

We performed a neutralizing assay using serums from patients and canine Ad vector CAVGFP (wild-type capsid) (**Table 1**). All patients, except patient VI, had detectable Nabs against canine Ad before treatment, which was expected due to vaccination with CAV-2. After treatment, Nabs titer progressively increased until the last follow-up for all patients except Case V. Virus load in whole blood was analyzed by quantitative polymerase chain reaction (PCR) (**Table 1**) (Case III not available). ICOCAV17 was detected early after administration and progressively decreased in time, with the latest positive samples found 7 days after administration (Cases IV and VI). Body secretions (urine, saliva, and feces) were analyzed by anti-hexon staining (daily for the first 4 days postadministration). No canine Ad infectious particles were detected at any time.

DISCUSSION

The increasing incidence of cancer in dogs requires new therapies that overcome resistance against conventional treatments. Herein, we constructed ICOCAV17, a cCRAd based on CAV2 for the treatment of a broad spectrum of canine cancers. ICOCAV17 infected tumor cells more efficiently, showed pRb-mediated selectivity, enhanced cytotoxicity *in vitro* compared with control viruses, and inhibited tumor growth in two canine xenografts *in vivo*. Moreover, six canine patients were treated intratumorally. No adverse side events directly associated to ICOCAV17 administration occurred. Two PR and the observation of virus biological activity in four out of six cases warrant further studies with ICOCAV17. Importantly, the similarities shared by ICOCAV17 with its human counterpart,[19] make it appropriate for extrapolating data from a syngeneic and tumor-spontaneous suffering model to humans.

Preclinical characterization showed that RGD-motif insertion enhanced infectivity and propagation of CAV2 in three out of four cell lines. The effect on infectivity of RGD on CAV2 could not be directly extrapolated from previous data with hAds as CAV2 attaches to and enters cells using a different pathway and lacks

an integrin-interacting motif.[34,35] The CAR and integrins influence CAV2 trafficking, although exact mechanisms are still unknown. We did not find a correlation between CAR-expression levels of the cell lines and CAV2 or CAV2RGD infectivity, suggesting, as mentioned before,[34] the existence of other influencing receptors for CAV2. According to the results obtained, the insertion of the RGD motif does not inhibit CAR interaction as we did not observe a decrease in infectivity in any of the cell lines tested. To achieve pRb-E2F-based selectivity,[21,36,37] four imperfect palindromic E2F-binding sites and one Sp-I-binding site were inserted in the endogenous E1a promoter of CAV2RGD and the pRb-binding site of E1a was deleted. The homology between hAd5 and CAV2 E1 proteins has been previously described.[38] The Δ24 deletion in hAd, homologous to the Δ21 deletion in the canine Ad, hinders the virus to release cellular E2F from pRb-E2F complexes, conferring selectivity for cells with free E2F, which are the majority of tumor cells,[37] while restringing viral replication in nonreplicating cells.[21] In this study, the E1a-modified promoter increased virus burst size and enhanced cytotoxicity in tumor cells, while diminished by more than 80% the total virus production in cell cycle-arrested nontumor cells. The correlation of pRB status and permissiveness to ICOCAV15 supports a pRB-pathway regulation similar to ICOVIR15, although coimmunoprecipitation assays would be required to demonstrate that pRB does not bind to the mutated canine E1a, and that the complex pRB-E2F binds to the inserted E2F boxes.

An extracellular matrix rich in HA limits the efficacy of the CRAds hindering viral intratumor spread.[39] Concentrations of HA are elevated in several human[40] and canine tumors.[41] High levels of HA were detected by immunohistochemistry of sections from CML1 or Abrams xenografts, while 17CM98 tumors showed nondetectable HA levels (**Supplementary Figure S3 and Supplementary Materials and Methods**). Human PH20 hyaluronidase was inserted instead of isogeneic canine hyaluronidase for two reasons: hPH20 is active at a neutral pH whereas canine PH20 exhibits hyaluronidase activity at an acidic pH[42] and CAV2 is already a xenogeneic DNA for the dog. In order to link PH20 expression to CAV replication, we inserted the human PH20 under the control of the canine IIIa protein splicing acceptor which was isolated by sequence alignment with hAd5. Thus, ICOCAV17 represents the first armed canine oncolytic Ad. *In vitro* assays did not show any replication impairment for ICOCAV17 compared with ICOCAV15. A therapeutic advantage for the PH20-armed virus was observed in efficacy studies in two canine xenografts. Detection of virus over paraffin-embedded tumors was performed at the experiment end point, when animals were sacrificed (**Supplementary Figure S1 and Supplementary Materials and Methods**), which may have decreased the possibilities to detect virus. However, a slight increase in the positive area of tumors treated with ICOCAV17 compared to the other viruses was observed, mainly in Abrams tumors, suggesting an enhanced dissemination due to the Hyaluronidase activity.

The toxicity of cCRAds in mice had not been characterized before. Herein, canine viruses induced an important systemic toxicity with marked thrombocytopenia and body weight loss that was aggravated when using RGD-modified viruses. These results suggest that the toxicity could be related to the capsid. The modifications of the E1a promoter were able to reduce by more than 80% the viral production in a cell-cycle arrested cell line, but they were not able to reduce systemic toxicity in Balb/C mice. Thus, reinforcing the hypothesis of a capsid-related toxicity. However, the lack of an antibody against canine E1a hinders the possibility to elucidate the impact of E1a in this toxicity. Further, contrary to the results obtained in dogs by Smith *et al.*,[18] the biodistribution performed in mice showed no specific liver tropism for canine viruses. Moreover, the RGD modified fiber increased the presence of virus in some organs and the persistence in blood, suggesting a change in the virus tropism with a slight liver detargeting. A possible explanation might be that CAV2 remains bound to mouse blood cells without being so efficiently cleared by the liver as are hAds. This could be accentuated for CAV2RGD, thus allowing both viruses to reach multitude of body organs. In whole, these results discouraged us to use the intravenous administration route.

Our main aim was to treat canine patients with a fully-replication competent Ad. Six patients with different tumor types were enrolled in an investigational treatment. The dose of 1×10^{12} vp per animal administered intratumorally was estimated, using a 10 times lower dose than a well-tolerated dose in mice adjusted by weight. We did not reinject canine patients as we had already observed an antitumor response in Case I and III within 3 days postadministration. Moreover, 2×10^{12} vp of OCCAV had been administered intravenously in dogs with no signs of toxicity.[18]

Biochemistry, hematology, and coagulation analysis as well as physical examination were performed daily for at least 4 days after administration. No signs of toxicity associated to ICOCAV17 were observed, even when virus titers reached 10^6 vp per milliliter of blood. The lytic virus activity in tumors caused adverse side events in Case II and III. Case II patient suffered a self-traumatic wound, possibly due to the pain induced by the necrotic tumor tissue. Patient III suffered a disseminated intravascular coagulation as a result of a prolonged bleeding and a massive tumor lysis. To achieve better outcomes, patients with lower tumor loads would be desirable and an accurate selection and control of patients with proinflammatory tumors should be addressed. The immunohistochemistry of nontumor tissue located near injected sites from Case II did not show any evidence of virus replication and no evidence of necrosis in the healthy tissue was detected under macroscopic and microscopic examination. No pathology was found in healthy areas of tissue surrounding the injected sites of any patient. These findings support the E2F/Δ21-conferred selectivity observed *in vitro* and the good tolerance to ICOCAV17 injected intratumorally.

RECIST has been questioned to measure virotherapy efficacy[43] as viruses induce tumor swelling, which can be misinterpreted as progression. Other criteria, based on health-related quality of life,[44] or overall survival have been proposed. Efficacy was seen in Case I and III with a 51% and 70% of reduction in size, respectively. Benefits of the concomitant treatment in Case III should be clarified in future studies. Moreover, a benefit in terms of quality of life was clearly observed in Case I where dysuria disappeared at day 3. The necrosis associated to viral replication suggests virus activity in Case II. While in Case VI, tumor necrosis could not be linked to viral replication. Case IV and V did not show such a marked benefit, although virus replication was found in

the tumor of patient V. Temporary tumor growth stabilization in both patients was observed. The tumor of Patient V was surgically resected 15 days after viral administration. The recovery from the surgical procedure was normal and no tumor relapse was observed at a follow-up 8 months later. This reinforces the safety of the treatment with ICOCAV17 and may suggest a benefit in terms of progression-free survival.

Although tumors use multiple pathways to suppress the immune system, oncolytic viruses could provide intratumoral danger signals that spark an immune response.[45] Our most evident antitumor responses were found in adenoma and mastocitoma patient dogs. Whether the benign characteristics of these tumors are associated with a lower immunosuppression that could facilitate antitumor immunity remains to be studied.

Previous studies suggest that pre-existing immunity against the virus may increase the safety of the treatment, while efficacy by direct administration may not be inhibited.[14,46] Case II had the highest Nabs at the baseline but ICOCAV17 induced necrosis in the primary tumor and in a metastatic lung lesion. This suggests a systemic transport of infective particles even in the presence of Nabs. The higher tumor necrosis and viral systemic dissemination in Case II compared to Case IV, could be associated to higher cell permissiveness to ICOCAV17 replication and the higher accessibility of lung metastasis compared to bone metastases. Recently, Factor X has been described to protect hAd5 from Nabs[47] but, the interaction of CAV2 capsid with canine blood factors remains largely unexplored. Levels of Nabs increased progressively until the last measurement in all patients except for Case V. This exception could be associated to the tumor resection that removed the main virus load. Extended presence of virus in blood has been suggested as a sign of virus replication. Oncolytic effect was evident for at least 6 months (Case I), although we were not able to detect viremia later than 7 days in any case. Virus load in blood decreased progressively in all patients. Therefore, we consider a rapid clearance of circulating cCRAds from blood. We could not find a correlation between virus load in blood, Nabs levels, and antitumor activity or toxicity, pointing at permissiveness to CAV replication as a key factor for efficacy. Accordingly, IC_{50} values (**Figure 2**) suggest a very heterogeneous permissiveness to CAV replication. Even when the tumor cells came from the same tumor type (Abrams and D17 from OS, and CML1 and 17CM98 from melanoma), IC_{50} values were very different. Furthermore, no infectious particles were detected on any of the body fluids analyzed, suggesting a low viral leakage from the tumor and diminishing the shedding risk. However, special care must be undertaken if bleeding or effusions are observed.

In summary, intratumorally treatment of dogs with ICOCAV17 was well tolerated and efficacy was observed in an infiltrative adenoma and a mast cell tumor. ICOCAV17 replicated in tumors and caused tumor necrosis. Enrolling patients with less advanced disease could improve efficacy and reduce adverse events. Finally, dogs with cancer should be considered as a valuable model for human virotherapy.

MATERIALS AND METHODS

Recombinant adenoviruses. **Figure 1a** shows a schematic diagram outlining the structure of the viruses used in this study. pTG5412 containing the wild-type canine adenovirus serotype 2 (CAV2) genome and CAVGFP,[22] a canine vector expressing green fluorescence protein, were a kind gift of Dr Eric Kremer (Institut de Génétique Moléculaire de Montpellier, Montpellier, France). We have generated pCAL-CAV2 using a cut and repair homologous recombination in yeast.[48] pCAL-CAV2 contains the CAV2 genome and the elements needed for selection, amplification, and homologous recombination in yeast (*Saccharomyces cerevisae* YPH857). To this aim, we amplified CAL,[49] a fragment containing the centromere, an autonomously replication sequence "ARS", and a yeast selection gene (Leucine), and we inserted two homologue sequences to pTG5412 in 5′ and 3′. Next, pTG5412 was partially digested with Not I. pCAL-CAV2 was generated by homologous recombination between CAL fragment and the partially digested pTG5412.

CAV2RGD has an RGD motif (CDCRGDCFC) inserted in the Hi-loop (nucleotide position 28110) of the CAV2 fiber. CAV2RGD was generated taking advantage of a unique Sal I site present in pCAL-CAV2. To this aim, two annealing PCRs were performed. First, the RGD motif and a 5′ homologue sequence to pCAL-CAV2 were generated. Then, a second PCR to insert a homologue sequence to pCAL-CAV2 in 3′ was performed using the product from PCR 1 as a template. By homologous recombination, the final product was cloned in Sal I-digested pCAL-CAV2, generating pCAL-CAV2RGD.

To generate ICOCAV15, a fragment of the CAV2-E1a promoter containing four E2F-binding site hairpins (underlined), one Sp-1 binding site (underlined and italics type), and a PmeI restriction site (boldface type) (5′-tcggcggctcgtggctc*tttggc*ggcaaaaagga*tttcgc*gcgtaaaagtggttcgaagtactcg gcggctcgtggctc*tttcgc*ggcaaaaagga*tttggc*gcgtaaaagtggacagtt**gtttaaac**cgacca caaac*cccgccc*agcgtcttgtcattggcgtcga - 3′) following nucleotide 403 of CAV2 genome, and a deletion of 21 base pairs (nucleotide positions 818–838), was designed and cloned in pUC57 flanked by two Xma I restriction sites (GenScript, Piscataway, NJ). A unique Swa I site was used to digest pCAL-CAV2RGD. Homologous recombination was performed between SwaI digested pCAL-CAV2RGD and the fragment obtained from Xma I digestion of pUC57.

To create the PH20 expressing canine adenovirus, a PCR product flanked by two homologue sequences downstream ICOCAV15 fiber protein and containing the CAV2 IIIa protein splicing acceptor (5′-ggccggccctatgaggaagaggagaaccctgatggctccgtctcatttcaacagc - 3′), the human PH20 cDNA, and a polyadenilation signal, was generated by three annealing reactions and inserted by a cut and repair homologue recombination in yeast using the unique Sal I site of pICOCAV15. The viral genomic structures were verified by sequence analysis. All viruses were generated, plaque purified, and amplified in DK28Cre cells. All viruses were purified on CsCl gradients according to standard techniques.

Cell lines. DK28Cre[22] cells were a kind gift of Dr Eric Kremer (Institut de Génétique Moléculaire de Montpellier). Abrams canine OS cell line and 17CM98 and CML1 canine melanoma cells were provided by Dr David Vail (School of Veterinary Medicine, University of Wisconsin-Madison, Wisconsin). D17 canine OS cells were obtained from the American Type Culture Collection (Manassas, VA). DEK are an established primary canine cell line obtained from CELLnTEC (CELLnTEC Advanced Cell Systems AG, Bern, Switzerland). All cells, except DEK, were cultured at 37 °C under 5% CO_2 in Dulbecco's modified Eagle's medium supplemented with antibiotic solution (100 U/ml penicillin G and 100 U/ml streptomycin) and 5% fetal bovine serum. DEKs were cultured at 37 °C under 5% CO_2 in CnT-09 medium from CELLnTEC (CELLnTEC Advanced Cell Systems AG). All cells lines were routinely tested for mycoplasma presence.

Protein expression analysis. Cells were seeded in six-well plates. Whole-cell protein extracts were prepared when tumor-cell cultures reached 80% of confluence or 20 days after confluence for DEKs by incubation in ice-cold radioimmunoprecipitation assay lysis buffer (150 mmol/l NaCl, 1% Nonidet NP-40, 0.5% deoxycholate, 0.1% sodium dodecyl sulfate, 50 mmol/l Tris, pH 8.0), containing phenylmethylsulfonylfluoride (1 mmol/l),

sodium orthovanidate (1 mmol/l), aprotinin (1%), and leupeptin (20 µg/ml) for 1 hour at 4 °C. Clarified samples (25 µg/lane) were separated by a 6.5% sodium dodecyl sulfate–polyacrylamide gel electrophoresis and transferred to a nitrocellulose membrane (GE Healthcare, Arlington Heights, IL). Rb protein detection was performed by immunoblotting membranes using a monoclonal anti-Rb primary antibody (Mouse, Clone G3-245; BD PharMingen, San Jose, CA) and a sheep anti-mouse antibody conjugated with horseradish peroxidase (GE Healthcare, Little Chalfont, UK). A mouse monoclonal anti-α-tubulin antibody (Clone DM1A; Sigma-Aldrich, St Louis, MO) and a sheep peroxidase-conjugated anti-mouse antibody (GE Healthcare) were used for immunoblotting of α-tubulin as a loading control.

Infectivity assay. Abrams or D17 cells (80,000) or 17CM98 or CML1 cells (30,000) were seeded in 96-well plates. After 24 hours, cells were infected in triplicate with serial dilutions of CAV2 or CAV2RGD, starting from 1,000 vp per cell. After 24 hours, medium was removed and immune staining against hexon protein was performed according to an anti-hexon staining-based method.[17] Infected cells expressing hexon protein were counted in the same dilution for both viruses in wells, showing a number of infected cells between 10 and 100, the ratio between CAV2RGD and CAV2 was calculated in triplicate.

Production assays. The selectivity of ICOCAV15 was measured by comparing total production yields in differentiated DEK. DEK become cell-cycle arrested when they are confluent.[28] DEK express cell cycle exit and terminal differentiation markers (p21, p27, Involucrin, Loricrin, and Dsg-1) progressively since they reach confluence.[28] DEK were seeded in 24-well plates and cultured for 20 days at 37 °C and 5%CO_2 with CnT-09. Medium was removed thrice a week and fresh medium was added.

For virus production, differentiated DEK were infected with 8 tu/cell, CML1, D17 cells were infected with 20 tu/cell, and Abrams and 17CM98 with 30 tu/cell of each virus to allow for 80 to 100% infection. After 4 hours, infection medium was removed and cells were washed twice with PBS and incubated with fresh medium. Cells and medium (cell extract) were harvested 48 hours postinfection and subjected to three rounds of freeze-thaw lysis. Viral titers of cell extract were determined in triplicate according to an anti-hexon staining-based method[17] in DK28Cre cells.

Measurement of CAR expression by flow cytometric analysis. Briefly, cell cultures (3×10^5 cells) were incubated with the goat anti-mouse CAR polyclonal antibody CXADR according to the manufacturer's instructions (R&D Systems, Minneapolis, MN) at 4 °C for 1 hour. For the visualization of the anti-CAR antibody, a second incubation with donkey anti-goat Alexa Fluor 488 antibody (diluted 1:300; Invitrogen; Life-technologies, Carlsbad, CA) was conducted at room temperature for 1 hour. Cell samples were analyzed for fluorescence with a Gallios Beckman Coulter flow cytometer (Beckman Coulter, Miami, FL) using a 488-nm laser for excitation. All cytometric data were analyzed with FlowJo software (FlowJo. 7.6.5; Tree Star, Ashland, OR).

Assay for hyaluronidase activity. Hyaluronidase activity assay was performed as described previously.[29] In brief, DK28Cre cells were infected with 20 tu/cell of each virus to allow for 80 to 100% infection. Four hours postinfection, medium was removed and cells incubated with fresh medium. After 48 hours, a volume of hyaluronan solution (3 mg/ml) was added to the cell medium and cells incubated at 37 °C. After this, at 0, 1, 2, 3, and 4 hours, aliquots were removed, boiled for 5 minutes, and centrifuged. Five volumes of sodium acetate buffer (0.1% bovine serum albumin) were added to the supernatant to precipitate hyaluronan. After 10 minutes at room temperature, the turbidity was measured at 600 nm. Samples with a known concentration of purified hyaluronidase (400, 40, 4, and 0.4 UI/ml) were used as hyaluronan degradation standard curve.

In vitro ***cytotoxicity assays.*** Cytotoxity assays were performed by seeding 20,000 D17 cells, 10,000 Abrams, or 5,000 CML1 or 17CM98 cells per well in 96-well plates in Dulbecco's modified Eagle's medium with 5% fetal bovine serum. Cells were infected with serial dilutions starting with 2,000 tu/cell for Abrams, 17CM98 or CML1 cells, or 500 tu/cell for D17 cells. At days 6–8 postinfection, plates were washed with PBS and stained for total protein content (bicinchoninic acid assay, Pierce Biotechnology, Rockford, IL). Absorbance was quantified and the tu per cell required to produce a 50% of inhibition in cell viability (IC_{50} value) was estimated from dose–response curves by standard nonlinear regression (GraFit; Erithacus Software, Horley, UK), using an adapted Hill equation.

In vivo ***toxicity and biodistribution study.*** Mice for toxicology and efficacy studies were maintained at the facility of the ICO-IDIBELL (Barcelona, Spain), AAALAC unit 1155. All animal studies have been approved by the Institut d'Investigació Biomèdica de Bellvitge Ethical Committee for Animal Experimentation. A single dose of 1×10^{11} vp was injected intravenously into the tail vein of 8-week-old immunocompetent Balb/C male mice in a volume of 150 µl in PBS ($n = 5$). Daily observations for body weight and morbidity were performed. At day 3 postinjection, mice were sacrificed, exsanguinated, and samples were collected. Blood samples were collected by intracardiac puncture and clinical biochemical and hematological determinations were performed by the Clinical Biochemistry and Hematological Services of the Veterinary Faculty at the Autonomous University of Barcelona. For biodistribution analysis, organs were frozen until processing and DNA was purified following the QIAamp DNA Mini Kit (QIAGEN, Valencia, CA) protocol for DNA Purification from tissues. DNA from blood was extracted from 200 µl of whole blood using the QIAamp DNA Blood Mini Kit (QIAGEN). Purified DNA samples were quantified in triplicate by real-time PCR LightCycler480 Roche, using the primers (forward primer: 5′-TGTGGGCCTGTGTGATTCCT-3′ and reverse primer: 5′-CCAGAATCAGCCTCAGTGCTC-3′), and a Taqman probe (FAM-CTCGAATCAGTGTCAGGCTCCGCA-TAMRA), which identify E1A region. Virus loads were calculated using LightCycler v4.05 software (Roche, Basel, Switzerland) and a regression standard curve based on serial dilutions of pCAL-CAV (1×10^7 to 1 vp/µl).

Evaluation of **in vivo** ***antitumoral efficacy.*** Subcutaneous Abrams or CML1 canine tumors were established by injection of 2×10^6 cells into the flanks of 6-week-old female Balb/c *nu/nu* mice. Once tumors reached the desired mean tumor volume (100 mm^3 for Abrams tumors and 150 mm^3 for CML1 tumors), mice were randomly distributed into treatment groups (n = 10–12 tumors per group) and treated (experimental day 0) with an intratumoral injection at days 0, 7, and 14 with 25 µl of PBS or 1×10^{10} vp of CAV2, CAV2RGD, ICOCAV15, or ICOCAV17 in a volume of 25 µl in PBS. Mice status was monitored daily during the 3 days after virus administration. Tumor size and mice status were monitored twice a week. Tumor volume was defined by the equation $V\,(mm^3) = \pi/6 \times W^2 \times L$, where W and L are the width and the length of the tumor, respectively. When animals from each group displayed uncontrolled tumor growth, the mice were euthanized.

For Kaplan–Meier survival curves, end point was established at tumor volume of ≥500 mm^3. The survival curves obtained were compared for the different treatments. Animals whose tumor size never achieved the maximum allowed size were included as right censored information.

Patients. Patients with advanced solid tumors (**Table 1**) refractory to conventional treatments or with a bad prognosis under routinely protocols were eligible for oncolytic virotherapy with ICOCAV17. The inclusion criteria were solid, accessible tumors, refractory or with a bad expected response to conventional therapies and no major organ functions deficiencies. Specific exclusion criteria were immune suppressed animals, with liver disease (hyperbilirubinemia, threefold or higher elevated liver enzymes), thrombocytopenia ($<1 \times 10^5$ Plt/µl), hematocrit < 25%, or cardiorespiratory dysfunctions.

Treatment protocol. ICOCAV17 therapy was approved by the Small Animal Internal Medicine Department of the Veterinary Teaching Hospital (Fundació Hospital Clinic Veterinari) of the Autonomous University of Barcelona. Informed consent was obtained from the dog owners.

Once patients were accepted for treatment with oncolytic virus, on the day of treatment, they were isolated in a facility approved for virus administration in the fundació Hospital Clinic Veterinari of the Autonomous University of Barcelona. Animals were isolated until day 4 after virus administration. Tumors were divided in equal in size quadrants and dose was distributed equally. All patients received a single echoguided intratumoral total dose of 1×10^{12} vp of ICOCAV17 diluted in 1 mililiter of sterile PBS. General anesthesia or sedation with local anesthesia was used according to veterinary recommendation. In Case I, II, and VI, no other agents rather than antibiotics or palliative unrelated agents were given. In Case III and IV, concomitant treatment with the same previously administered chemotherapeutic agents was performed (**Table 1**). Patient V was not concomitantly treated with chemotherapy although surgical resection procedure was included on the protocol before starting the treatment.

Monitoring of patients. Patients were monitored daily for the first 4 days. Attitude, appetite, temperature, cardiac and respiratory frequency, and tumor appearance were checked every 8 hours. Biochemical, hematologic, and coagulation (prothrombin time, partial thromboplastin time, and fibrinogen) analysis were performed once a day, as well as blood, urine, saliva, and fecal sampling. After hospitalization, differences in sampling schedule were adapted to practical issues related to owner time availability. In Case III, the patient was held in observation through the whole process due to its hematologic disorders and evident tumor lysis from day 3. Tumor size was assessed by a caliper and echographic imaging. Maximum tumor diameters were calculated according to RECIST v1.1 (ref. [50]): complete response (CR; undetectable tumor after treatment), PR (≥ 30% reduction in the sum of tumor diameters), stable disease (no reduction or increase), and progressive disease (≥ 20% increase in tumor size).

Analysis of viral infective particles from body secretions. Samples from saliva were obtained using the Salivette system (Sarstedt, Numbrecht, Germany). Samples from urine were obtained using a urinary catheter or intravesical injection. Samples of feces were obtained from the rectum. All samples were frozen until processing. The fecal samples were diluted 1/100 W/V in PBS with penicillin and streptomycin and homogenized. Before titering, samples were centrifuged (10,000*g* for 10'). Once centrifuged, viral titers were determined in triplicate according to an anti-hexon staining-based method[17] in DK28Cre cells. Limits of detection were 100 tu/ml of urine or saliva and 10,000 tu/g of feces.

Histopathology and immunohistochemistry. Samples obtained from tumor or healthy tissues (Case II, IV, V, and VI) were fixed in 10% buffered paraformaldehyde for 24 hours and embedded in paraffin. Routine hematoxylin-eosin staining and immunohistochemistry against adenovirus late proteins were performed. Blocks were cut into 4-µm thick sections and were deparaffinized, endogenous peroxidase activity blocked, and antigen retrieval was performed in citrate buffer. After rehydration, sections were blocked for 30 minutes with 20% normal horse serum diluted in PBS 1% bovine serum albumin. Samples were incubated with rabbit anti-late adenovirus proteins polyclonal IgG (Ab6982 Abcam; cross reactivity against CAV2)[17] overnight at 4 °C. Slides were washed thrice in PBS 0.2% Triton X-100 and incubated with EnVision (Dako, Hamburg, Germany) according to the manufacturer's instructions. After washing, sections were developed with diaminobenzidine (Dako Laboratories, Glostrup, Denmark) and counterstained with hematoxylin. Images of sections were captured on a Nikon Eclipse 80i microscope (Nikon Instruments), using the software NIS-Element Basic Research 3.2 (Nikon, Melville, NY).

Neutralizing antibody titer determination. Samples of serum were heated at 56 °C for 30 minutes in order to inactivate complement. Serial dilutions of inactivated samples were performed in free-serum Dulbecco's modified Eagle's medium in 96-well plates in triplicate, starting from 1/10 (limit of detection) for low titer samples to 1/1,000 for high titer samples. A volume of 100 µl containing 1×10^5 tu of CAVGFP, was added to each well and incubated for 1 hour at room temperature. Afterwards, 5×10^4 DK28Cre cells per well were seeded and cultured overnight at 37 °C and 5% CO_2. The neutralizing antibody titer was determined as the lowest degree of dilution that inhibited the cell transduction by more than 50%.

Quantitative real-time PCR for presence of ICOCAV17 in whole blood samples. DNA was extracted from 200 µl of whole blood using the QIAamp DNA Blood Mini Kit (QIAGEN). Purified DNA samples were quantified in triplicate by real-time PCR LightCycler480 Roche, using the primers (forward primer: 5′-TGTGGGCCTGTGTGATTCCT-3′ and reverse primer: 5′-CCAGAATCAGCCTCAGTGCTC-3′), and a Taqman probe (FAM-CTCGAATCAGTGTCAGGCTCCGCA-TAMRA), which identifies E1A region. Virus loads were calculated using LightCycler v4.05 software and a regression standard curve based on serial dilutions of pICOCAV17 (1×10^7 to 1 vp/µl). The limit of quantification for the assay was 500 vp/ml.

Statistical analysis. Statistics were done with SPSS 13.0 software (IBM, Armonk, NY). Two-tailed Student's unpaired *t*-test was used to compare data, except for survival analysis when data was processed with Kaplan–Meyer analysis.

SUPPLEMENTARY MATERIAL

Figure S1. Immunohistochemistry of tumors from *in vivo* efficacy assays in Abrams and CML1 models.
Figure S2. Hematoxilin & Eosin staining of tumors from patient VI.
Figure S3. Hyaluronic acid detection within three canine xenografts tumors.
Table S1. Systemic biodistribution of CAV2 and CAV2RGD in Balb/C mice.
Materials and Methods.

ACKNOWLEDGMENTS

We thank Sergi Trocoli, Mireia Palau, Francesc Gonzalez, Marta Molla, and Carles Prat for valuable clinical advice and the dog owners who willingly participated in our study as well as the volunteers, nursing staff, and clinicians at the Veterinary Hospital, Mercedes Saez for statistical assistance, and Ruth Riches for linguistic assistance. We thank Erik Kremer and Francesc Viñals for providing some reagents. E.L. was supported by a predoctoral fellowship (FPU) granted by the Spanish Ministry of Education and Science. This work was supported by a grant from the Spanish Ministry of Education and Science, BIO2011-30299-C02-01 and PLE2009-0115 from Spanish Ministry of Economy and Competitivity and received partial support from the Generalitat de Catalunya 2009SGR284. No conflict of interest from any of the authors exists.

REFERENCES

1. Patil, SS, Gentschev, I, Nolte, I, Ogilvie, G and Szalay, AA (2012). Oncolytic virotherapy in veterinary medicine: current status and future prospects for canine patients. *J Transl Med* **10**: 3.
2. Hansen, K and Khanna, C (2004). Spontaneous and genetically engineered animal models; use in preclinical cancer drug development. *Eur J Cancer* **40**: 858–880.
3. Russell, SJ, Peng, KW and Bell, JC (2012). Oncolytic virotherapy. *Nat Biotechnol* **30**: 658–670.
4. Jogler, C, Hoffmann, D, Theegarten, D, Grunwald, T, Uberla, K and Wildner, O (2006). Replication properties of human adenovirus *in vivo* and in cultures of primary cells from different animal species. *J Virol* **80**: 3549–3558.
5. Halldén, G, Hill, R, Wang, Y, Anand, A, Liu, TC, Lemoine, NR *et al.* (2003). Novel immunocompetent murine tumor models for the assessment of replication-competent oncolytic adenovirus efficacy. *Mol Ther* **8**: 412–424.
6. Thomas, MA, Spencer, JF, La Regina, MC, Dhar, D, Tollefson, AE, Toth, K *et al.* (2006). Syrian hamster as a permissive immunocompetent animal model for the study of oncolytic adenovirus vectors. *Cancer Res* **66**: 1270–1276.
7. Raper, SE, Chirmule, N, Lee, FS, Wivel, NA, Bagg, A, Gao, GP *et al.* (2003). Fatal systemic inflammatory response syndrome in a ornithine transcarbamylase deficient patient following adenoviral gene transfer. *Mol Genet Metab* **80**: 148–158.
8. Ternovoi, VV, Le, LP, Belousova, N, Smith, BF, Siegal, GP and Curiel, DT (2005). Productive replication of human adenovirus type 5 in canine cells. *J Virol* **79**: 1308–1311.
9. Westberg, S, Sadeghi, A, Svensson, E, Segall, T, Dimopoulou, M, Korsgren, O *et al.* (2013). Treatment efficacy and immune stimulation by AdCD40L gene therapy of spontaneous canine malignant melanoma. *J Immunother* **36**: 350–358.

10. Paoloni, M and Khanna, C (2008). Translation of new cancer treatments from pet dogs to humans. *Nat Rev Cancer* **8**: 147–156.
11. Kirkness, EF, Bafna, V, Halpern, AL, Levy, S, Remington, K, Rusch, DB *et al.* (2003). The dog genome: survey sequencing and comparative analysis. *Science* **301**: 1898–1903.
12. Buonavoglia, C and Martella, V (2007). Canine respiratory viruses. *Vet Res* **38**: 355–373.
13. Decaro, N, Martella, V and Buonavoglia, C (2008). Canine adenoviruses and herpesvirus. *Vet Clin North Am Small Anim Pract* **38**: 799–814, viii.
14. Dhar, D, Spencer, JF, Toth, K and Wold, WS (2009). Effect of preexisting immunity on oncolytic adenovirus vector INGN 007 antitumor efficacy in immunocompetent and immunosuppressed Syrian hamsters. *J Virol* **83**: 2130–2139.
15. Arendt, M, Nasir, L and Morgan, IM (2009). Oncolytic gene therapy for canine cancers: teaching old dog viruses new tricks. *Vet Comp Oncol* **7**: 153–161.
16. Hemminki, A, Kanerva, A, Kremer, EJ, Bauerschmitz, GJ, Smith, BF, Liu, B *et al.* (2003). A canine conditionally replicating adenovirus for evaluating oncolytic virotherapy in a syngeneic animal model. *Mol Ther* **7**: 163–173.
17. Alcayaga-Miranda, F, Cascallo, M, Rojas, JJ, Pastor, J and Alemany, R (2010). Osteosarcoma cells as carriers to allow antitumor activity of canine oncolytic adenovirus in the presence of neutralizing antibodies. *Cancer Gene Ther* **17**: 792–802.
18. Smith, BF, Curiel, DT, Ternovoi, VV, Borovjagin, AV, Baker, HJ, Cox, N *et al.* (2006). Administration of a conditionally replicative oncolytic canine adenovirus in normal dogs. *Cancer Biother Radiopharm* **21**: 601–606.
19. Guedan, S, Rojas, JJ, Gros, A, Mercade, E, Cascallo, M and Alemany, R (2010). Hyaluronidase expression by an oncolytic adenovirus enhances its intratumoral spread and suppresses tumor growth. *Mol Ther* **18**: 1275–1283.
20. Dmitriev, I, Krasnykh, V, Miller, CR, Wang, M, Kashentseva, E, Mikheeva, G *et al.* (1998). An adenovirus vector with genetically modified fibers demonstrates expanded tropism via utilization of a coxsackievirus and adenovirus receptor-independent cell entry mechanism. *J Virol* **72**: 9706–9713.
21. Rojas, JJ, Guedan, S, Searle, PF, Martinez-Quintanilla, J, Gil-Hoyos, R, Alcayaga-Miranda, F *et al.* (2010). Minimal RB-responsive E1A promoter modification to attain potency, selectivity, and transgene-arming capacity in oncolytic adenoviruses. *Mol Ther* **18**: 1960–1971.
22. Kremer, EJ, Boutin, S, Chillon, M and Danos, O (2000). Canine adenovirus vectors: an alternative for adenovirus-mediated gene transfer. *J Virol* **74**: 505–512.
23. MacEwen, EG, Pastor, J, Kutzke, J, Tsan, R, Kurzman, ID, Thamm, DH *et al.* (2004). IGF-1 receptor contributes to the malignant phenotype in human and canine osteosarcoma. *J Cell Biochem* **92**: 77–91.
24. Thamm, DH, Huelsmeyer, MK, Mitzey, AM, Qurollo, B, Rose, BJ and Kurzman, ID (2010). RT-PCR-based tyrosine kinase display profiling of canine melanoma: IGF-1 receptor as a potential therapeutic target. *Melanoma Res* **20**: 35–42.
25. Koenig, A, Bianco, SR, Fosmire, S, Wojcieszyn, J and Modiano, JF (2002). Expression and significance of p53, rb, p21/waf-1, p16/ink-4a, and PTEN tumor suppressors in canine melanoma. *Vet Pathol* **39**: 458–472.
26. Mendoza, S, Konishi, T, Dernell, WS, Withrow, SJ and Miller, CW (1998). Status of the p53, Rb and MDM2 genes in canine osteosarcoma. *Anticancer Res* **18**(6A): 4449–4453.
27. Suzuki, K, Fueyo, J, Krasnykh, V, Reynolds, PN, Curiel, DT and Alemany, R (2001). A conditionally replicative adenovirus with enhanced infectivity shows improved oncolytic potency. *Clin Cancer Res* **7**: 120–126.
28. Kolly, C, Suter, MM and Müller, EJ (2005). Proliferation, cell cycle exit, and onset of terminal differentiation in cultured keratinocytes: pre-programmed pathways in control of C-Myc and Notch1 prevail over extracellular calcium signals. *J Invest Dermatol* **124**: 1014–1025.
29. Gmachl, M, Sagan, S, Ketter, S and Kreil, G (1993). The human sperm protein PH-20 has hyaluronidase activity. *FEBS Lett* **336**: 545–548.
30. Withrow, SJ, Vail, DM and Page, RL (2012). *Withrow & MacEwen's Small Animal Clinical Oncology*, Elsevier/Saunders: St Louis, MO.
31. Simko, E, Wilcock, BP and Yager, JA (2003). A retrospective study of 44 canine apocrine sweat gland adenocarcinomas. *Can Vet J* **44**: 38–42.
32. Bookbinder, LH, Hofer, A, Haller, MF, Zepeda, ML, Keller, GA, Lim, JE *et al.* (2006). A recombinant human enzyme for enhanced interstitial transport of therapeutics. *J Control Release* **114**: 230–241.
33. Baumgartner, G (1998). The impact of extracellular matrix on chemoresistance of solid tumors–experimental and clinical results of hyaluronidase as additive to cytostatic chemotherapy. *Cancer Lett* **131**: 1–2.
34. Soudais, C, Boutin, S, Hong, SS, Chillon, M, Danos, O, Bergelson, JM *et al.* (2000). Canine adenovirus type 2 attachment and internalization: coxsackievirus-adenovirus receptor, alternative receptors, and an RGD-independent pathway. *J Virol* **74**: 10639–10649.
35. Chillon, M and Kremer, EJ (2001). Trafficking and propagation of canine adenovirus vectors lacking a known integrin-interacting motif. *Hum Gene Ther* **12**: 1815–1823.
36. Johnson, L, Shen, A, Boyle, L, Kunich, J, Pandey, K, Lemmon, M *et al.* (2002). Selectively replicating adenoviruses targeting deregulated E2F activity are potent, systemic antitumor agents. *Cancer Cell* **1**: 325–337.
37. Cascallo, M, Alonso, MM, Rojas, JJ, Perez-Gimenez, A, Fueyo, J and Alemany, R (2007). Systemic toxicity-efficacy profile of ICOVIR-5, a potent and selective oncolytic adenovirus based on the pRB pathway. *Mol Ther* **15**: 1607–1615.
38. Shibata, R, Shinagawa, M, Iida, Y and Tsukiyama, T (1989). Nucleotide sequence of E1 region of canine adenovirus type 2. *Virology* **172**: 460–467.
39. Strauss, R and Lieber, A (2009). Anatomical and physical barriers to tumor targeting with oncolytic adenoviruses in vivo. *Curr Opin Mol Ther* **11**: 513–522.
40. Toole, BP (2004). Hyaluronan: from extracellular glue to pericellular cue. *Nat Rev Cancer* **4**: 528–539.
41. Docampo, MJ, Rabanal, RM, Miquel-Serra, L, Hernández, D, Domenzain, C and Bassols, A (2007). Altered expression of versican and hyaluronan in melanocytic tumors of dogs. *Am J Vet Res* **68**: 1376–1385.
42. Sabeur, K, Foristall, K and Ball, BA (2002). Characterization of PH-20 in canine spermatozoa and testis. *Theriogenology* **57**: 977–987.
43. Koski, A, Kangasniemi, L, Escutenaire, S, Pesonen, S, Cerullo, V, Diaconu, I *et al.* (2010). Treatment of cancer patients with a serotype 5/3 chimeric oncolytic adenovirus expressing GMCSF. *Mol Ther* **18**: 1874–1884.
44. Reid, J, Wiseman-Orr, ML, Scott, EM and Nolan, AM (2013). Development, validation and reliability of a web-based questionnaire to measure health-related quality of life in dogs. *J Small Anim Pract* **54**: 227–233.
45. Elsedawy, NB and Russell, SJ (2013). Oncolytic vaccines. *Expert Rev Vaccines* **12**: 1155–1172.
46. Hu, JC, Coffin, RS, Davis, CJ, Graham, NJ, Groves, N, Guest, PJ *et al.* (2006). A phase I study of OncoVEXGM-CSF, a second-generation oncolytic herpes simplex virus expressing granulocyte macrophage colony-stimulating factor. *Clin Cancer Res* **12**: 6737–6747.
47. Xu, Z, Qiu, Q, Tian, J, Smith, JS, Conenello, GM, Morita, T *et al.* (2013). Coagulation factor X shields adenovirus type 5 from attack by natural antibodies and complement. *Nat Med* **19**: 452–457.
48. Giménez-Alejandre, M, Gros, A and Alemany, R (2012). Construction of capsid-modified adenoviruses by recombination in yeast and purification by iodixanol-gradient. *Methods Mol Biol* **797**: 21–34.
49. Sikorski, RS and Hieter, P (1989). A system of shuttle vectors and yeast host strains designed for efficient manipulation of DNA in Saccharomyces cerevisiae. *Genetics* **122**: 19–27.
50. Eisenhauer, EA, Therasse, P, Bogaerts, J, Schwartz, LH, Sargent, D, Ford, R *et al.* (2009). New response evaluation criteria in solid tumours: revised RECIST guideline (version 1.1). *Eur J Cancer* **45**: 228–247.

Cancer Therapy: Preclinical

Clinical Cancer Research

Safety and Efficacy of VCN-01, an Oncolytic Adenovirus Combining Fiber HSG-Binding Domain Replacement with RGD and Hyaluronidase Expression

Alba Rodríguez-García[1], Marta Giménez-Alejandre[2], Juan Jose Rojas[3], Rafael Moreno[1], Miriam Bazan-Peregrino[2], Manel Cascalló[2], and Ramon Alemany[1]

Abstract

Purpose: Tumor targeting upon intravenous administration and subsequent intratumoral virus dissemination are key features to improve oncolytic adenovirus therapy. VCN-01 is a novel oncolytic adenovirus that combines selective replication conditional to pRB pathway deregulation, replacement of the heparan sulfate glycosaminoglycan putative-binding site KKTK of the fiber shaft with an integrin-binding motif RGDK for tumor targeting, and expression of hyaluronidase to degrade the extracellular matrix. In this study, we evaluate the safety and efficacy profile of this novel oncolytic adenovirus.

Experimental Design: VCN-01 replication and potency were assessed in a panel of tumor cell lines. VCN-01 tumor-selective replication was evaluated in human fibroblasts and pancreatic islets. Preclinical toxicity, biodistribution, and efficacy studies were conducted in mice and Syrian hamsters.

Results: Toxicity and biodistribution preclinical studies support the selectivity and safety of VCN-01. Antitumor activity after intravenous or intratumoral administration of the virus was observed in all tumor models tested, including melanoma and pancreatic adenocarcinoma, both in immunodeficient mice and immunocompetent hamsters.

Conclusion: Oncolytic adenovirus VCN-01 characterized by the expression of hyaluronidase and the RGD shaft retargeting ligand shows an efficacy–toxicity prolife in mice and hamsters by intravenous and intratumoral administration that warrants clinical testing. *Clin Cancer Res; 1–13. ©2014 AACR.*

Introduction

The use of viruses to treat cancer is an old concept that has been revisited during the last two decades with viruses genetically modified to acquire selectivity and potency. Currently, genetically modified herpes simplex virus, vaccinia viruses, and adenoviruses are in phase III clinical trials. GM-CSF expression by these viruses seeks to elicit antitumor immunotherapy (1, 2). Despite that this immune mechanism of action is expected to be systemic, the strong local immunosuppressive tumor environment may require that the virus reaches and replicates in all tumor nodules for effectiveness (3). Accordingly, it would be beneficial to improve systemic tumor targeting and intratumoral dissemination of oncolytic viruses.

Poor adenovirus tumor targeting upon intravenous administration has been associated with multiple neutralizing interactions in blood, tropism for liver and spleen, and clearance by macrophages (4). Different capsid modifications are being explored to avoid liver transduction and to expose specific ligands for tumor cells (5). The mutation of the putative heparan sulfate-glycosaminoglycans (HSG) binding domain KKTK, located in the fiber shaft, abrogates liver transduction in mice, rats, and non-human primates (6–8). However, the insertion of targeting peptides in the HI loop of these shaft-modified fibers does not rescue viral infection of tumor cells (9, 10). Our group previously described that the replacement of the KKTK domain with an RGD motif significantly increased tumor cell transduction and improved the tumor-to-liver ratio *in vivo* in the context of a nonreplicative adenovirus (11). Moreover, when incorporated in an oncolytic adenovirus background, the RGDK modification resulted in increased bioavailability after systemic administration and, consequently, in better antitumor efficacy when compared with a virus containing the RGD motif in the HI loop of the fiber (12).

Regarding intratumoral dissemination, the extracellular matrix (ECM) has a prominent role at inhibiting viral spread, acting as a physical barrier and raising the interstitial fluid pressure (IFP) in tumors (13–15). To tackle this problem, oncolytic viruses have been armed with ECM-degrading enzymes such as relaxin, decorin, metalloprotease-9, chondroitinase ABC (16–20), or PH20 hyaluronidase as we have previously reported (21). In addition, recombinant hyaluronidase enhances the penetration and efficacy of several chemotherapeutic agents including docetaxel,

[1]Translational Research Laboratory, IDIBELL-Institut Català d'Oncologia, L'Hospitalet de Llobregat, Barcelona, Spain. [2]VCN Biosciences, Sant Cugat del Vallès, Barcelona, Spain. [3]Department of Surgery, University of Pittsburgh Cancer Institute, University of Pittsburgh, Pittsburgh, Pennsylvania.

Note: Supplementary data for this article are available at Clinical Cancer Research Online (http://clincancerres.aacrjournals.org/).

Corresponding Author: Ramon Alemany, IDIBELL-Institut Català d'Oncologia, Av Gran Via de l'Hospitalet 199-203, L'Hospitalet de Llobregat, 08907 Barcelona, Spain. Phone: 34-9326-074-62; Fax: 34-9326-074-66; E-mail: ralemany@iconcologia.net

doi: 10.1158/1078-0432.CCR-14-2213

Translational Relevance

Oncolytic adenoviruses are promising agents for cancer therapy. However, clinical experience points the need to increase antitumor efficacy. Inefficient tumor targeting after systemic administration and poor intratumor dissemination of the oncolytic adenovirus are key factors to improve. In this work, we address both of these limitations by combining a tumor targeting capsid modification and the expression of the extracellular matrix–degrading enzyme hyaluronidase in a single oncolytic adenovirus named VCN-01. We report a good safety and efficacy profile of this virus in two different animal models, mice and hamster. We think that this novel oncolytic adenovirus could contribute to improve clinical outcome of patients with cancer in which standard treatments have failed. The results presented here have supported the recent initiation of two phase I clinical trials in patients with pancreatic cancer or other tumor types.

doxorubicin, or gemcitabine, presumably due to a reduction of the IFP in tumors (22–24).

Here, we present the combination of the retargeting RGDK modification of the fiber and the expression of hyaluronidase in a novel oncolytic adenovirus, named VCN-01. This virus shows selective and potent replication in tumor cells *in vitro*, similar to that of the oncolytic adenoviruses containing the same modifications separately. *In vivo*, the increased blood persistence associated to the RGDK mutation combined with the hyaluronic acid (HA) degradation driven by hyaluronidase resulted in an improved antitumor efficacy of VCN-01 without increasing the toxicity of the parental virus. Overall, the observed results support the ongoing clinical development of the oncolytic adenovirus VCN-01.

Materials and Methods

Cell lines

Human embryonic kidney 293, A549 lung carcinoma, Skmel-28 melanoma, BxPC3, Rwp1 and MiaPaCa-2 pancreatic carcinomas and SCC-25 and SCC-29 head and neck tumor cell lines were obtained from the American Type Culture Collection (ATCC). NP-9, NP-18, NP-31, and NP-29 pancreatic tumor cell lines were established in our laboratory (25, 26). HP-1 Syrian hamster pancreatic tumor cell line was obtained from M. Yamamoto (Minneapolis, MN) with MA Hollingsworth (Nebraska, NE) permission. All were maintained with DMEM supplemented with 5% FBS (Invitrogen) and penicillin–streptomycin (PS; Gibco-BRL) at 37°C and 5% CO_2. All cell lines were routinely tested for mycoplasma contamination by PCR, microbial presence by microscopic observation, and antibiotic deprivation and morphology by microscopic observation. Pancreatic islets were kindly provided by Dr. Montanya of the Endocrinology Service of the Hospital de Bellvitge, Barcelona, Spain.

Recombinant adenoviruses

Human adenovirus serotype 5 (Adwt) was obtained from the ATCC, and AdwtRGDK, AdTLRGDK, ICOVIR-15K, and ICOVIR-17 have been previously described (11, 21, 27). All viruses were propagated in A549 cells. VCN-01 was created by replacing the fiber containing the RGD motif in the HI loop for the RGDK fiber in the ICOVIR-17 genome. To achieve this, an *Eco*RI digestion fragment of the pBSattKKT plasmid15 (11) containing the RGDK fiber was recombined in *Saccharomyces cerevisiae* YPH857 with the pICOVIR17CAL plasmid (CAU sequence, which includes the yeast autonomous replication elements and a selectable marker for uracil, was replaced by CAL, analogous to CAU but with a selectable marker for leucine instead of uracil in pICOVIR17CAU plasmid; ref. 21) partially digested with *Nde*I. VCN-01 was obtained by transfection into HEK293 cells of the large *Pac*I fragment of pICOVIR17RGDKCAL, amplified in A549 cells, and purified on CsCl gradient according to standard techniques.

Assay for hyaluronidase activity

A549 cells were infected with 20 transduction units (TU)/cell. Four hours after infection, cells were washed with PBS and fresh media were added. Seventy-two hours after infection, the supernatant was collected and concentrated with Amicon Ultra centrifugal filters (Millipore). Supernatant samples were mixed with an HA (Sigma) solution in phosphate buffer (pH 5.35) and were incubated overnight at 37°C. Samples were precipitated with 5 volumes of a solution containing 24 mmol/L sodium acetate, 79 mmol/L acetic acid, and 0.1% of bovine albumin (pH 3.75), and the absorbance at 600 nm was read. Units of activity were determined according to a standard curve of hyaluronidase activity, generated from a solution of bovine testicular hyaluronidase (Sigma; ref. 28).

Viral production assays

Cells were infected with 30 TU/cell (Skmel-28 and NP-18) or 20 TU/cell (NP-9 and HP-1) of each virus to allow 80% to 100% infectivity. Four hours after infection, cells were washed 3 times with PBS and incubated with fresh medium. At indicated time points, cells and medium (CE) were harvested and subjected to 3 rounds of freeze-thaw lysis. Viral titers of CE were determined in triplicate according to an anti–hexon staining-based method in HEK293 cells (29).

In vitro cytotoxicity assays

Of note, 40,000 Skmel-28, NP-18 or NP-31, 20,000 NP-29 or BxPC-3, 15,000 NP-9, Rwp-1, MiaPaCa-2, SCC-29 or SCC-25 or 10,000 HP-1 cells/well were seeded in 96-well plates in DMEM 5% FBS. Cells were infected per triplicate with serial dilutions starting with 400 TU/cell for SCC-25, 300 TU/cell for Rwp-1, MiaPaCa-2, and SCC-29, or 200 TU/cell for Skmel-28, NP-18, NP-9, NP-29, NP-31, BxPC-3, and HP-1. Quiescent primary human fibroblast cultures maintained in conditions of overconfluence and serum deprivation were infected per triplicate with serial 1/3 dilutions of VCN-01 or Adwt-RGDK starting at 0.1 TU/cell. At days 5 to 6 after infection for tumor cells and day 10 for fibroblasts, plates were washed with PBS and stained for total protein content (bicinchoninic acid assay; Pierce Biotechnology). Absorbance was quantified and the TU/cell required to produce 50% inhibition (IC_{50} value) was estimated from dose–response curves by standard nonlinear regression (GraFit; Erithacus Software), using an adapted Hill equation.

Replication selectivity in pancreatic islets

Isolated islets in 100 μL of CMRL1066 media supplemented with 0.5% of albumin were infected in triplicate with AdTL-RGDK (nonreplicative vector), Adwt-RGDK (capsid-modified wild-type

virus), or VCN-01 at 200 TU/cell (assuming 1,000 cells/islet). Infection was performed in suspension and with constant agitation during 2 hours at 37°C. Islets were washed 3 times with PBS and seeded in 96-well plates with fresh medium. After washing, a small fraction of the supernatant was collected, and the input virus was titrated by anti–hexon staining (background level). At day 6 after infection, islets and medium were harvested and freeze-thawed 3 times to obtain the cell extract and the viral titer of each sample was determined.

In vivo studies

Most of the animal studies were performed at the IDIBELL facility (AAALAC unit 1155) and approved by the IDIBELL's Ethical Committee for Animal Experimentation. Toxicity and biodistribution studies in Syrian hamsters were performed in TNO Triskelion facilities under Good Laboratory Practice (GLP) conditions.

In vivo toxicity study in mice

Vehicle (PBS) or 5×10^{10} viral particles (vp) of ICOVIR-17 or VCN-01 were injected intravenously into the tail vein in 6-week-old immunocompetent Balb/C male mice in a finale volume of 200 μL ($n = 1$–6). Animals were examined daily for clinical signs of toxicity. At different time points after the administration of the virus, blood aliquots were collected via tail vein and platelets were counted. At days 7, 12, or 28 after injection, mice were killed and blood and serum samples were collected by intracardiac puncture. Clinical biochemical and hematologic determinations were performed by the Clinical Biochemistry and Hematological Services of the Veterinary Faculty at the Autonomous University of Barcelona. Concentration of several cytokines in sera samples was evaluated at different time points using the Luminex xMAP technology platform.

In vivo biodistribution study in mice

NP-18 tumors were established by the subcutaneous injection of 1×10^7 cells into the flanks of 6-week-old female Balb/C *nu/nu* mice. When tumors reached an average volume of 300 to 400 mm^3, animals were randomized into different treatment groups and treated with a single intravenous injection of vehicle (PBS) or 5×10^{10} vp of VCN-01 in a total volume of 150 μL via tail vein. At days 2, 7, and 28 after administration, mice were sacrificed and organs were harvested and frozen. Samples were mechanically homogenized and total DNA was extracted according to the QIAamp DNA Mini Kit (QIAGEN). Genome copy levels were quantified by real-time PCR–based method using VCN-01–specific oligonucleotides (forward primer: 5′-ACATTGCCCAAGAATAAAGAAT CG-3′, reverse primer: 5′-TGGAATCAGAAGGAAGGTGAA-3′).

GLP toxicity and biodistribution *in vivo* studies in hamster

Five-week-old female Syrian golden hamsters (*Mesocricetus auratus*) were injected systemically with 2.5×10^{11} vp or 4×10^{11} vp of VCN-01 or vehicle (Tris Buffer) via cannulation of the jugular vein in a total volume of 270 μL ($n = 6$). Animals were examined daily for clinical signs of toxicity, and at days 2, 8, and 28 after administration, subgroups of hamsters were killed and whole blood and serum samples were collected. Clinical biochemistry of transaminase levels and hematologic determinations were performed. For biodistribution analysis, organs from animals treated with the higher dose of VCN-01, 4×10^{11} vp ($n = 5$), were collected and frozen. Samples were processed and analyzed as reported in the previous section.

Antitumor activity in mice and hamsters *in vivo*

To assess systemic efficacy, subcutaneous Skmel-28 or NP-18 tumors were established by the injection of 9×10^6 or 5×10^6 cells respectively into the flanks of 6-week-old male Balb/C *nu/nu* mice. Once tumors reached the desired mean volume (100 mm^3 for Skmel-28 and 180 mm^3 for NP-18), mice were randomized ($n =$ 10–16 tumors/group) and treated with a single intravenous injection of vehicle (PBS) or 4.5×10^{10} vp of ICOVIR-17 or VCN-01 in a total volume of 200 μL via tail vein.

To evaluate efficacy after intratumoral administration, Skmel-28, NP-18, or NP-9 tumors were established by the injection of 9×10^6, 2×10^6, or 5×10^6 cells respectively into the flanks of 6-week-old male Balb/C *nu/nu* mice. When the tumors reached an appropriate mean volume (150 mm^3 for Skmel-28 and NP-18 and 80 mm^3 for NP-9), they received a single intratumoral injection of PBS or 2×10^9 vp of VCN-01 in the case of Skmel-28 and NP-9 and 4×10^9 vp in NP-18 tumors in a final volume of 25 μL. HP-1 tumors were established by injection of 5×10^5 cells into the flanks of 6-week-old female immunocompetent Syrian hamsters. Once tumors reached the desired mean volume (220 mm^3), they were injected with vehicle or 2.5×10^{10} vp of VCN-01 ($n = 10$ tumors/group) . In all animal experiments, tumor progression and morbidity status were monitored three times weekly. Tumor volume was defined by the equation $V(mm^3) = \pi/6 \times W^2 \times L$, where W and L are width and length of the tumor, respectively. The percentage of growth was calculated as $((V–V_0)/V_0 \times 100)$, where V_0 is the tumor volume on day 0.

Tumor histochemistry

HA and adenovirus staining with anti-E1A antibody staining was performed as previously described (21, 30). Masson trichromic staining was performed using the Accustain Trichrome Stain Kit (Sigma Aldrich) according to the manufacturer's indications.

Statistical analysis

The two-tailed Student *t* test was used to evaluate the statistical significance between groups except for hamster toxicity analysis, in which the Kruskal–Wallis test was used, and for the Kaplan–Meier survival curves, where log-rank test was performed.

Results

In vitro characterization of VCN-01

Parental viruses ICOVIR-15K, which has the KKTK to RGDK fiber shaft replacement, and ICOVIR-17, which expresses hyaluronidase, have been described before and were used as controls for the *in vitro* characterization assays (12, 21). As VCN-01, they are based in ICOVIR-15, a virus with E1a mutated in the pRB-binding site and under the control of minimal E2F binding sites to allow for selective replication in a broad range of tumor cells with pRB pathway alterations (31). Note that we apply the "ICOVIR" nomenclature to our viruses with these E1a modifications to achieve tumor-selective replication.

An enzymatic activity assay performed using supernatants of infected cells confirmed hyaluronidase expression by VCN-01 at similar levels than ICOVIR-17 (Fig. 1A). To measure the effect of RGDK and hyaluronidase combination on virus fitness, the yield of VCN-01 was compared with ICOVIR-15K and ICOVIR-17 in

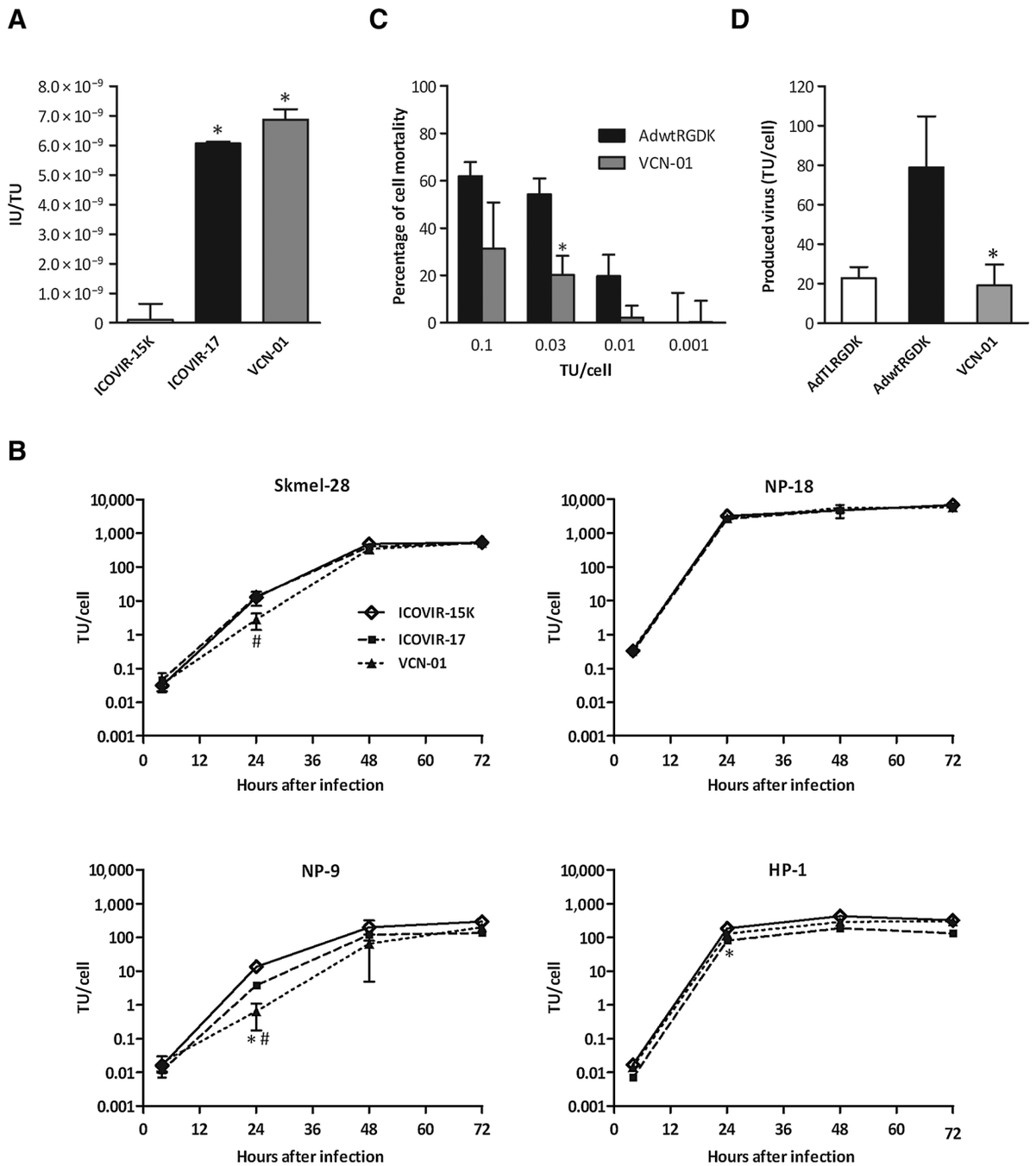

Figure 1.

In vitro characterization of VCN-01. A, hyaluronidase expression levels of VCN-01. Hyaluronidase activity was evaluated in concentrated supernatants of A549 cells 72 hours after the infection with ICOVIR-15K, ICOVIR-17, or VCN-01 by digesting HA samples with these supernatants. Mean values +SD are plotted. *, significant ($P < 0.05$) by two-tailed unpaired Student *t* test compared with ICOVIR-15K group. B, viral production of VCN-01 in tumor cells. Different tumor cell lines were infected at high multiplicity of infection with ICOVIR-15K, ICOVIR-17, or VCN-01. At indicated time points, cell extracts were harvested and titrated by an anti–hexon staining-based method. Mean values +SD are shown. *, VCN-01 significant ($P < 0.05$) by two-tailed unpaired Student *t* test compared with ICOVIR-15K group; #, VCN-01 significant ($P < 0.05$) by two-tailed unpaired Student *t* test compared with ICOVIR-17 group. C, replication selectivity of VCN-01 *in vitro*. Human fibroblasts were infected with serial dilutions of VCN-01 and AdwtRGDK (wild-type nonselective adenovirus) and cell viability was determined at day 10 after infection. Mean values of percentage of cell mortality +SD are plotted (left). D, human primary pancreatic islets were infected with AdTLRGDK (nonreplicative virus), AdwtRGDK, and VCN-01. Six days after infection, islets and culture supernatant were collected and total virus content was determined according to an anti–hexon staining-based method. Mean + SD are plotted (right). *, VCN-01 significant ($P < 0.05$) by two-tailed unpaired Student *t* test compared with AdwtRGDK. IU, international units.

different tumor cell lines. Despite a minor delay on replication in two cell lines at 24 hours after infection, VCN-01 production was similar to control viruses at later time points (Fig. 1B). Cytotoxicity in a panel of tumor cell lines was also evaluated as an index of virus replication potency. All viruses induced a similar cytotoxic profile with relative VCN-01 IC_{50} values ranging from half to 3-fold compared with the parental viruses (Table 1).

VCN-01 replication was studied in two human primary normal cell models to check if replication was tumor selective. Primary human fibroblasts were made quiescent by overconfluence and serum deprivation, and the ability of VCN-01 and RGDK wild-type adenovirus (AdwtRGDK) to kill them was assessed by infecting the cells with serial viral dilutions to determine the viability percentage at day 10 after infection. VCN-01 demonstrated to be less cytotoxic in this model than the nonselective AdwtRGDK (Fig. 1C). Selectivity was also evaluated in human pancreatic islets *in vitro*, as patients with pancreatic cancer are candidates for treatment. Same viral progeny levels were detected at day 6 after infection in the samples infected with VCN-01 and the nonreplicative negative control (AdTLRGDK), whereas wild-type adenovirus (AdwtRGDK) replicated in normal human pancreatic islets (Fig. 1D).

In vivo toxicity upon VCN-01 systemic administration in immunocompetent mice

Balb/C immunocompetent mice were injected with vehicle or 5×10^{10} vp of ICOVIR-17 (selected for comparative studies as it is the most efficacious parental virus) or VCN-01 via tail vein to assess toxicity after intravenous administration. Weight loss, liver enzymes (aspartate aminotransferase, AST, and alanine aminotransferase, ALT), hematologic parameters, and viremia were determined at different time points. Wild-type adenovirus 5 (Adwt) was included as a control, but given the high toxicity associated with its administration, animals were sacrificed at day 3. VCN-01 caused a similar and reversible body weight loss profile to that of ICOVIR-17, reaching the maximum loss (9%) at day 7 after administration (Fig. 2A). Other toxicologic events observed at day 7 were moderate nonsignificant increases in AST (2.9-fold for ICOVIR-17 and 2.4-fold for VCN-01) and ALT levels (12-fold for ICOVIR-17 and 9-fold for VCN-01; Fig. 2B), thrombocytopenia (Fig. 2C), and increased monocytes and neutrophils counts (Fig. 2D), but at days 12 and 28 these parameters were normal.

A higher viremia was detected in VCN-01–treated animals compared with ICOVIR-17 (17.5-, 8.7-, and 4.1-fold at 5, 15, and 60 minutes, respectively). Moreover, half-life of VCN-01 was significantly higher (3.15 vs. 2.11 minutes for ICOVIR-17; Supplementary Fig. S1). To evaluate the innate immune response elicited by the systemic exposure to VCN-01, eight cytokines were measured at different time points. Virus administration induced a rapid statistically significant rise in blood levels of IFNγ, IP-10, IL6, and TNF-α that were normalized by day 10 except for IP-10, which remained significantly elevated (Fig. 2E).

In vivo toxicity upon VCN-01 systemic administration in Syrian hamster

A GLP toxicity study was performed in Syrian hamsters (*Mesocricetus auratus*), considered more permissive to human adenovirus replication than mice (32). Hamsters were injected intravenously with vehicle, 2.5×10^{11} (low dose) or 4×10^{11} (high dose) vp of VCN-01. At days 2, 8, and 28 after administration, subgroups of animals were sacrificed, and body weight loss, clinical chemistry of the blood, and hematology were studied. Several parameters were altered at day 2 in the animals treated with the high dose of VCN-01. Most notable were the 7% body weight loss (Fig. 3A), elevation in transaminase levels (65.1-fold for AST and 23.8-fold for ALT; Fig. 3B), alkaline phosphatase levels (Supplementary Fig. S2A), thrombocytopenia (Fig. 3C) accompanied with an increased prothrombin time (Supplementary Fig. S2D), and higher monocyte and neutrophil counts (Fig. 3D), although at days 8 and 28 these parameters were normalized. These changes were dose-dependent and associated to histopathologic changes in the liver, characterized by necrosis, nuclear inclusion bodies, and hemorrhages, findings that had subsided in animals sacrificed 8 or 28 days after injection (data not shown). Any alterations were detected in creatinine or urea levels, indicating no renal toxicity (Supplementary Fig. S2B and S2C).

Biodistribution of VCN-01 upon intravenous administration *in vivo*

Mice carrying NP-18 human xenografts were treated with a single intravenous dose of 5×10^{10} vp. At days 2, 7, and 28 after administration, animals were sacrificed and viral genomes were quantified by quantitative real-time PCR analysis in target tissue

Q11 **Table 1.** Comparative cytotoxicity *in vitro* of VCN-01, ICOVIR-15K, and ICOVIR-17 in different tumor cell lines

Tumor type	Cell line	IC_{50} (TU/cell)			Cytotoxicity increase vs. ICOVIR-15K	Cytotoxicity increase vs. ICOVIR-17
		ICOVIR-15K	ICOVIR-17	VCN-01		
Human melanoma	Skmel-28	0.36 ± 0.05	0.25 ± 0.02	0.54 ± 0.05	0.67	0.46
	NP-18	0.12 ± 0.01	0.15 ± 0.02	0.15 ± 0.01	0.80	1
	NP-9	2.94 ± 0.74	1.34 ± 0.22	2.44 ± 0.27	1.20	0.55
	NP-29	3.31 ± 0.63	1.90 ± 0.22	3.57 ± 0.50	0.93	0.53
Human pancreatic adenocarcinoma	NP-31	5.58 ± 1.13	2.11 ± 0.61	3.47 ± 0.83	1.61	0.61
	BxPC-3	1.31 ± 0.36	1.61 ± 0.19	1.43 ± 0.19	0.92	1.13
	Rwp-1	0.07 ± 0.003	0.076 ± 0.007	0.053 ± 0.002	1.32	1.43
	MiaPaca2	0.091 ± 0.007	0.076 ± 0.003	0.074 ± 0.007	1.23	1.03
Hamster pancreatic adenocarcinoma	HP-1	1.03 ± 0.12	1.28 ± 0.12	0.70 ± 0.06	1.47	1.83
Human head and neck adenocarcinoma	SCC-29	2.47 ± 0.18	1.64 ± 0.24	0.78 ± 0.14	3.17	2.10
	SCC-25	27.23 ± 4.13	35.44 ± 3.20	29.10 ± 7.28	0.94	1.22

NOTE: Cells were infected with the indicated viruses at doses ranging from 400 to 0.0002 TU per cell. IC_{50} values (TU per cell required to cause a reduction of 50% in cell culture viability, $n = 3$) ± SD at days 5 to 10 after infection and VCN-01 cytotoxicity increase are shown.

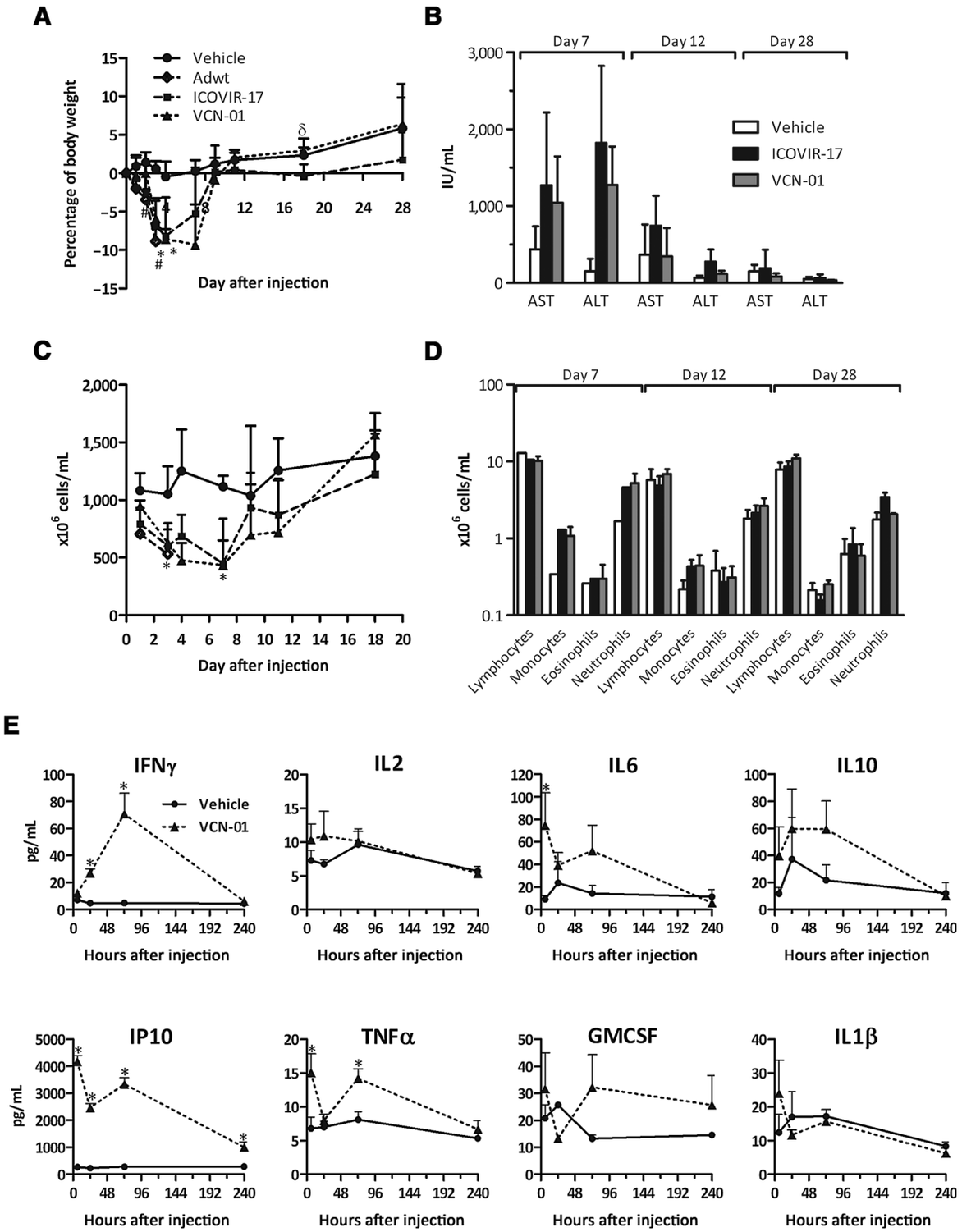

Figure 2.

Toxicity profile after systemic administration of VCN-01 in immunocompetent mice. The average values for (A) body weight variation, (B) serum transaminase levels, (C) platelets concentration, and (D) blood cell counts in Balb/C peripheral blood at indicated time points after intravenous administration of 5×10^{10} viral particles per mouse of Adwt (wild-type Ad5), ICOVIR-17, or VCN-01 are shown. Adwt-injected mice were sacrificed at day 3 due to lethal toxicity. Mean values +SD are depicted. E, average concentration values of IFNγ, IL2, IL6, IL10, IP-10, TNFα, GM-CSF, and IL1β cytokines at indicated time points assessed by Luminex xMAP technology platform. Mean +SEM are plotted ($n = 3$–6). *, VCN-01 significant ($P < 0.05$) by two-tailed unpaired Student t test, compared with vehicle group. #, VCN-01 significant ($P < 0.05$) compared with Adwt. δ, VCN-01 significant ($P < 0.05$) compared with ICOVIR-17 group. Normal AST and ALT values in male Balb/C mice are 135 IU/L (95% interval, 55–352) and 60 IU/L (95% interval, 41–131), respectively. IU, international units.

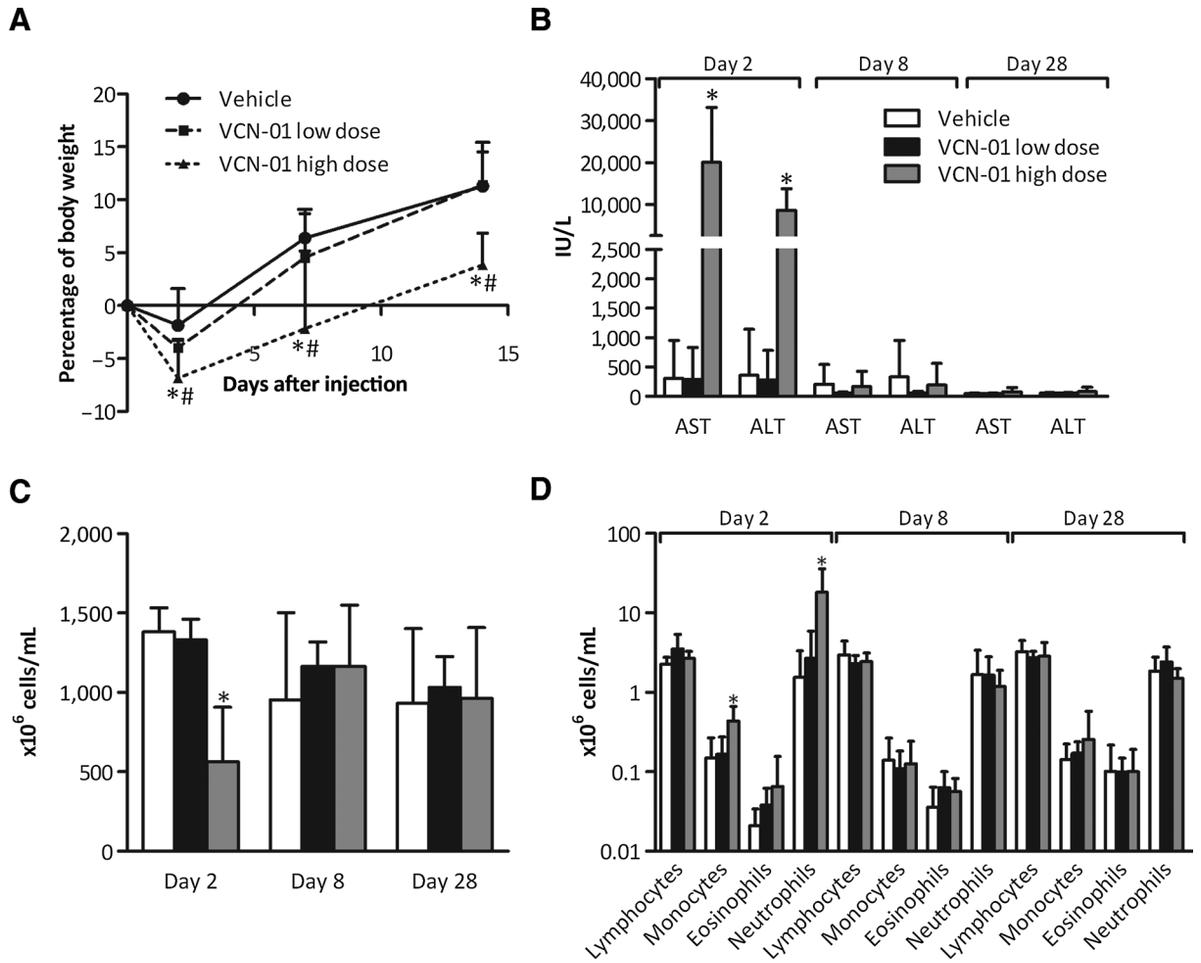

Figure 3.
Toxicity profile after systemic administration of VCN-01 in immunocompetent Syrian hamster. The average values for (A) body weight variation, (B) serum transaminase levels, (C) platelets concentration, and (D) blood cell counts in hamsters peripheral blood at indicated time points after intravenous administration of 2.5×10^{11} or 4×10^{11} viral particles of VCN-01 are shown. Mean values +SD are depicted. *, VCN-01 high dose significant ($P < 0.05$) by Kruskal–Wallis test, compared with vehicle group. #, VCN-01 high dose significant ($P < 0.05$) compared with VCN-01 low dose. Normal AST and ALT values in female Syrian hamster are 32 ± 13.2 IU/L and 29 ± 10.4 IU/L, respectively. IU, international units.

(tumors) and in other relevant nontarget organs (liver and spleen). Viral genomes were detected in the three tissues at the earliest time point (day 2), with most of the virus present in the liver (Fig. 4A). Importantly, at days 7 and 28, this organ was negative for VCN-01 genomes. The clearance of a lower amount of virus found in the spleen seemed delayed compared with the liver. In contrast, VCN-01 genomes increased over time in tumors, indicating replication.

Because hamster cells are semipermissive to adenovirus replication, a GLP biodistribution study was carried out in individuals without tumors as complementary to safety study presented above, in animals receiving the high intravenous dose of 4×10^{11} vp/hamster. Viral genomes presence was analyzed in different organs at days 2, 8, and 28. At day 2, viral DNA was found in all tissues tested, with highest levels in liver (Fig. 4B, different panels), although only residual amounts were detected at days 8 and 28. As mentioned above, the presence of virus at this late time points was not associated to morphology changes. Specific evaluation of ovaries by FISH revealed no presence of virus DNA in germinal cells (data not shown).

Antitumor activity of VCN-01 upon systemic administration

VCN-01 efficacy after systemic administration was compared with that of its non-RGDK counterpart, ICOVIR-17, to assess if RGDK modification provides an improvement in this context, as previously reported with ICOVIR-15 (12). Mice carrying Skmel-28 or NP-18 tumors were injected intravenously with vehicle or 4.5×10^{10} vp of ICOVIR-17 or VCN-01 and tumor growth was monitored. In Skmel-28–bearing mice, antitumor efficacy was maintained throughout the study (for up to 83 days) in VCN-01–treated animals, whereas after a similar curve of initial antitumor activity, a relapse was observed by day 53 after treatment in ICOVIR-17 group (Fig. 5A, left). Statistical differences in the percentage of tumor growth between both groups were observed from day 53 after treatment until the end of the study ($P = 0.00027$), when tumor size was 2.4-fold larger in the ICOVIR-17–treated animals than in the VCN-01–injected ones. Moreover,

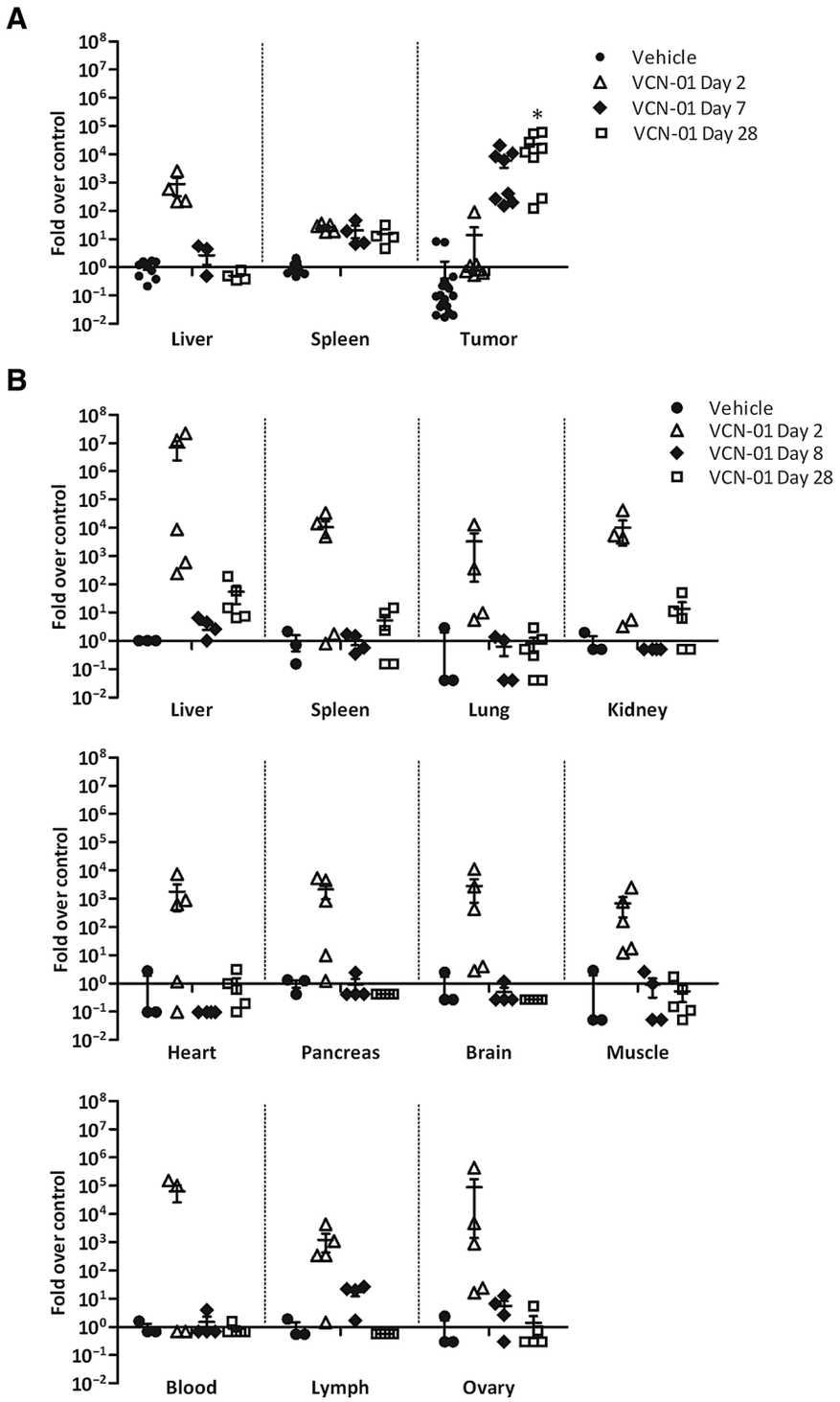

Figure 4.
Biodistribution profile of VCN-01 after intravenous administration. A, Balb/C nude mice carrying NP-18 (pancreatic adenocarcinoma) human xenograft tumors or (B) immunocompetent Syrian hamsters were treated intravenously with VCN-01 at a dose level of 5×10^{10} and 4×10^{11} viral particles, respectively. Animals were sacrificed at indicated time points and different organs were harvested in each case. Samples were mechanically homogenized, total DNA was extracted, and VCN-01 genome copy levels were quantified by real-time PCR–based method. VCN-01 genome copies in 100 nanograms of total DNA for vehicle group was set as 1 (control) and data are expressed as number of VCN-01 genome copies fold over control ± SEM ($n = 4$–18 samples/group). *, VCN-01 significant ($P < 0.05$) by two-tailed unpaired Student *t* test, compared with vehicle group.

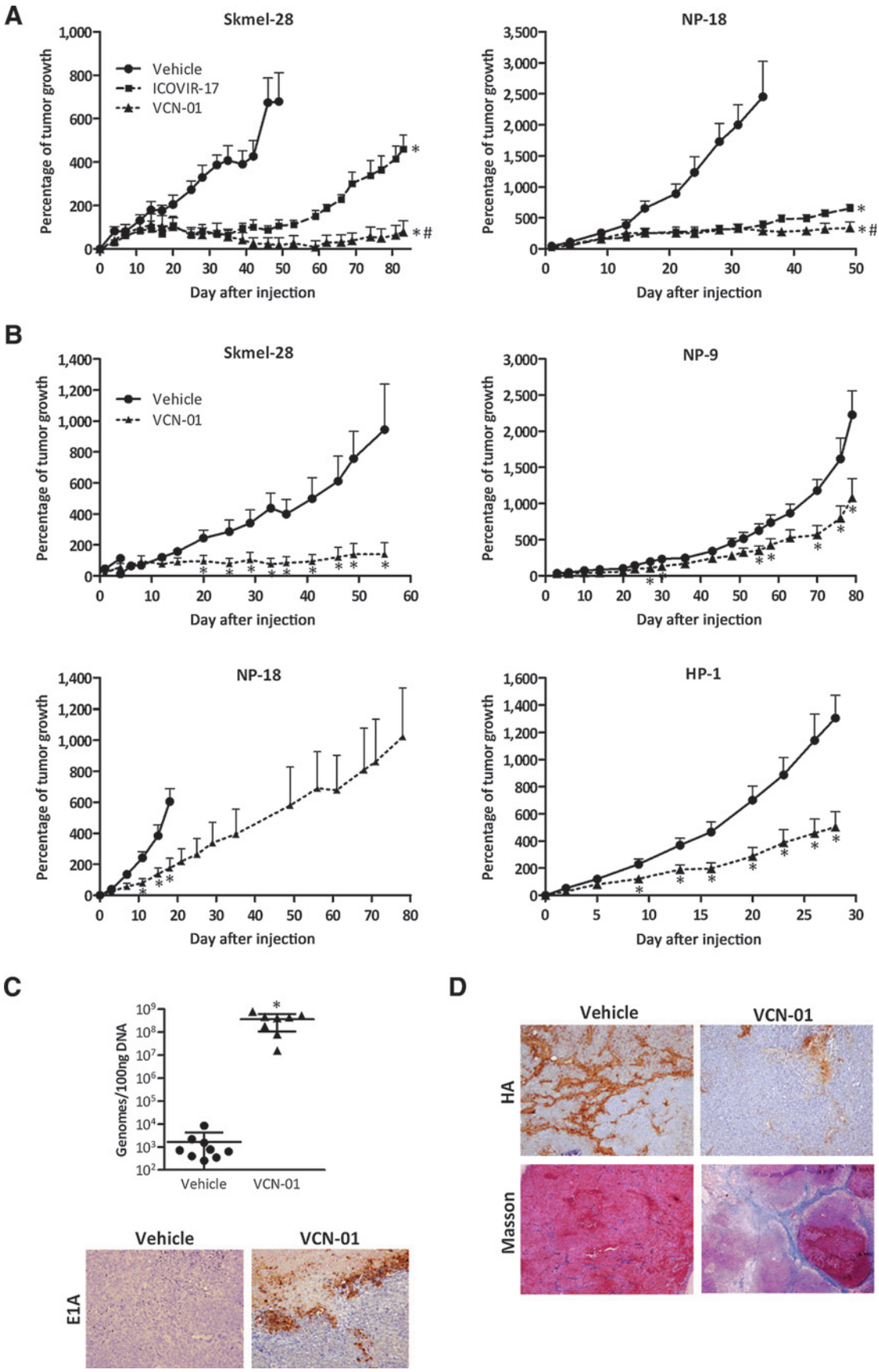
A
Skmel-28
Vehicle
ICOVIR-17
VCN-01
Percentage of tumor growth
Day after injection
NP-18
B
Skmel-28
Vehicle
VCN-01
NP-9
NP-18
HP-1
C
Genomes/100ng DNA
Vehicle
VCN-01
E1A
D
Vehicle
VCN-01
HA
Masson

50% of VCN-01–treated tumors were regressing at this final time point. A similar result was observed in mice bearing NP-18 tumors, in which a greater control of the tumor growth was observed in the animals treated with VCN-01 than with ICOVIR-17 (Fig. 5A, right). These differences were significant from day 30 to day 49 after administration ($P = 0.0132$), when the study ended.

Antitumor activity of VCN-01 upon intratumoral administration

VCN-01 efficacy after intratumoral administration was also studied given the intended clinical application of this administration route. Mice carrying Skmel-28, NP-9, or NP-18 human xenografts were treated with a single intratumoral injection of vehicle or 2×10^9 vp of VCN-01 for Skmel-28 and NP-9. For NP-18, 4×10^9 vp were injected as it is a faster-growing model compared with the other two. To reduce animal number, no further comparison with ICOVIR-17 was considered. Significant reduction in tumor growth could be seen in all three models and, at the end of the studies, the mean tumor size of VCN-01–treated groups was 4.2- and 1.6-fold smaller compared with nontreated tumors in Skmel-28 and NP-9 models, respectively. In the case of NP-18, mock-treated animals had to be killed at day 18 after administration due to large tumors, when mean tumor size of VCN-01–treated tumors was 3.6-fold smaller compared with the control (Fig. 5B, different panels).

Because mice are not permissive to Ad5 replication, a hamster model was included to evaluate the antitumor efficacy in the presence of immune system. HP-1 tumors were treated with a single intratumoral injection of vehicle or 2.5×10^{10} vp of VCN-01. Virus treatment significantly reduced tumor growth from day 9 after administration until the end of the study by day 28, when tumor volume was 2.1-fold smaller in VCN-01–treated animals (Fig. 5B). VCN-01 was able to significantly increase the survival of the animals in all tumor models tested in mice and hamsters (Supplementary Fig. S3).

Changes induced by VCN-01 in the ECM of tumors

To characterize the activity of VCN-01 and the histologic changes produced in the ECM of the tumors at late time points, we performed studies in NP-18 tumors on day 78 after VCN-01 intratumoral treatment. The intratumoral replication of VCN-01 was demonstrated by quantification of viral genomes by real-time PCR (Fig. 5C, top) and E1A immunohistochemistry in tumor sections (Fig. 5C, bottom). Histochemical analysis of HA showed that, whereas in vehicle-treated tumors HA was extensively and homogenously distributed among tumor mass, tumors treated with VCN-01 showed a dramatic decrease in the intratumoral HA content (Fig. 5D, top). In addition, Masson trichromic staining was used to detect connective tissue and collagen fibers. Similar to HA, collagen was homogeneously distributed in vehicle-injected tumors. In contrast, those treated with VCN-01 displayed collagen structures forming bundles that surrounded infected zones (Fig. 5D, bottom).

Discussion

Oncolytic viruses can potentially eliminate tumor cells directly by lysis or indirectly by immune responses. Antitumor immunity is so appealing that most viruses in clinical trials are armed with immunostimulatory genes (1, 2). Nevertheless, improving oncolytic traits should not be underestimated because large tumors may need extensive tumor debulking by viral infection and replication in order to be rejected by cytotoxic T lymphocytes (CTL). Therefore, the arrival of the virus to the tumors and intratumoral spread are important factors to be improved (3).

In the present work, we have combined two different modifications previously described by our group addressing both of these issues in a single oncolytic adenovirus, VCN-01: the KKTK to RGDK replacement to improve the half-life in blood of the virus after systemic administration (11, 12), and the expression of hyaluronidase to enhance the intratumoral spread (21). We hypothesized that this combination in a highly active oncolytic adenovirus of broad applicability as our previously described ICOVIR-15 (31) would generate an interesting candidate for clinical development. In this context, it is worthy to highlight that DNX-2401 (formerly Ad-D24RGD), a parental virus to ICOVIR-15, has received fast-track designation from the FDA after promising results in a phase I trial in glioblastoma (33).

For safety in clinical development, impaired VCN-01 replication was demonstrated in two different nontumor models *in vitro*, and different safety studies were conducted in two rodent species *in vivo*: mouse and hamster. Mice are poorly permissive to Ad5 replication (34); nevertheless, this animal model allows the study of toxicity associated to the viral capsid, the expression of early adenoviral genes such as E1A, and the innate immune

Figure 5.
Antitumor activity of VCN-01. A, antitumor efficacy after intravenous administration. Nude mice bearing subcutaneous xenografts of Skmel-28 (melanoma) or NP-18 (pancreatic adenocarcinoma) tumors were injected intravenously with vehicle or 4.5×10^{10} viral particles per mouse of ICOVIR-17 or VCN-01. Mean percentage of tumor growth value + SEM is plotted ($n = 10$ tumors/group). *, VCN-01 significant ($P < 0.05$) by two-tailed unpaired Student *t* test compared with mice injected with vehicle. #, VCN-01 significant ($P < 0.05$) by two-tailed unpaired Student *t* test compared with mice injected with ICOVIR-17 (from day 53 to day 83 in Skmel-28 model and from day 30 to day 49 in NP-18 model). B, antitumor efficacy after intratumoral administration. Skmel-28 (melanoma), NP-18, or NP-9 (pancreatic carcinoma) xenograft tumors in nude mice were treated intratumorally with a single injection of vehicle or VCN-01 at a dose of 2×10^9 (Skmel-28 and NP-9) or 4×10^9 (NP-18) viral particles per tumor. Syrian hamster bearing HP-1 (hamster pancreatic carcinoma) subcutaneous tumors were treated with one intratumoral injection of vehicle or 2×10^{11} viral particles per tumor of VCN-01. Mean percentage of tumor growth + SEM is plotted ($n = 8$–14 tumors/group). *, significant ($P < 0.05$) by two-tailed unpaired Student *t* test compared with control group. Presence of VCN-01 in NP-18 (pancreatic adenocarcinoma) tumors 78 days after treatment with a single intratumoral injection of 4×10^9 viral particles was assessed by viral genomes quantification by real-time PCR method in DNA extracted from homogenized tumors (C, top, mean + SD is plotted) and by immunohistochemical staining of the early viral protein E1A (C, bottom; original magnification, ×400). HA (D, top; original magnification, ×100) and Masson trichromic staining (D, bottom; original magnification, ×100) were also performed in deparaffinized tumor sections. Black dots marks nuclei, red areas reveal keratin and acidic fibers, pink marks cytoplasm, and blue stain collagen fibers. *, significant ($P < 0.05$) by two-tailed unpaired Student *t* test compared with mice injected with vehicle.

responses mainly triggered by the capsid (35) because the cytokine pattern induced by systemic administration of adenoviruses in mice is similar to humans (36, 37). Syrian hamsters are considered semipermissive to human adenovirus replication and have been used to evaluate the toxicologic events related to the expression of late adenoviral genes (32). Despite the differential permissiveness, similar toxicity profile was observed in both species, suggesting its independency on viral replication. Toxicity was dose-dependent and mainly due to direct infection of liver cells and the consequent expression of early viral proteins. The acute inflammatory cytokine–mediated immunity induced within the first 72 hours after VCN-01 administration also contributed to liver pathology. Although this initial cytokine induction could have some implications in antitumor activity, this seems unlikely as nonreplicative vectors, that induce cytokines (38), do not show antitumor activity (39). Importantly, because VCN-01 replication is impaired in normal tissues, toxicity was transient and disappeared once the levels of viral proteins decreased in initially infected cells (40). Accordingly, adverse events observed in hamsters were normalized by day 8. In summary, VCN-01 toxicology data obtained in the preclinical studies are similar to the previously described for ICOVIR-15, ICOVIR-15K, and ICOVIR-17 (12, 21) and detected alterations match with the most common toxicity events reported after systemic administration of adenoviruses in clinical trials (35–37, 41). Biodistribution studies were consistent with the toxicology pattern, with highest levels of viral genomes in the liver at early time points, in agreement with previous reports (32, 42–45). However, at later time points only residual traces of viral DNA were observed in liver as well as in other nontarget organs. These results are especially relevant in hamster model, in which replication of the virus occurs at a certain level. In contrast, the increase over time in viral genome levels in tumor samples of the human xenograft model in mice indicated active and selective replication of VCN-01.

We observed that compared with a virus which has the RGD motif inserted in the HI loop, the RGDK fiber shaft mutation does not increase toxicity upon intravenous administration. Nevertheless, this mutation significantly improved the antitumor activity of ICOVIR-17 after a single intravenous administration in two different tumor models *in vivo* (Skmel-28 and NP-18). This fact is very relevant because ICOVIR-17 was already the result of a series of steps to optimize oncolytic potency (21). Efficacy via intratumoral administration was also evaluated as this route has been commonly used to treat tumor types such as pancreatic adenocarcinoma, glioblastoma, and head and neck adenocarcinoma. A single intratumoral injection of VCN-01 significantly reduced tumor growth and increased survival when compared with control group in all tumor models tested. HP-1 model was of particular interest as hamsters have been proposed as a good model to study oncolytic adenoviruses in an immunocompetent environment. However, in our hands, the replication permissiveness is much lower than in human cells. In addition, hamsters develop an antiadenoviral immune response which causes viral clearance and prevents subsequent infection of tumor cells even after intratumoral administration. Thomas and colleagues (46) suggested to immunosuppress hamsters with drugs like cyclophosphamide as a way to increase antitumor efficacy, allowing sustained viral replication and oncolysis. Certainly, efficacy studies in Ad5 seropositive models or upon repeated administration in immunocompetent animals and in combination with immunomodulation or chemotherapy will be needed to better understand the potential and limitations of VCN-01.

Arming oncolytic viruses with ECM-degrading enzymes is a commonly exploited strategy to enhance viral penetration of solid tumors (14). Different modulators of ECM such as decorin, relaxin, metalloprotease 9, or chondroitinase ABC have been used to increase viral spread and antitumor efficacy in different tumor types taking into account specific ECM compositions (16–20). High levels of HA are present in almost 87% of pancreatic adenocarcinomas (22, 47), and hyaluronidase expression by VCN-01 can provide a particular advantage to treat this tumor type. As it is shown in Fig. 5D, hyaluronidase activity causes a dramatic decrease in HA content of treated tumors that may facilitate intratumoral virus spread. Furthermore, early clinical trials have demonstrated that hyaluronidase enhances chemotherapy efficacy in patients with cancer (48). Preclinical studies by Jacobetz and colleagues have attributed the beneficial effect of hyaluronidase to a lower interstitial pressure in HA-depleted tumors, leading to blood vessel decompression and increasing the vascular permeability, thereby favoring the penetration of drugs to the tumor core (23). These studies strongly suggest the possibility of combining VCN-01 with chemotherapies such as gemcitabine, which is the current standard-of-care treatment in pancreatic ductal adenocarcinoma. In addition, hyaluronidase administration expressed from an oncolytic virus provides some advantages compared with recombinant enzymes. VCN-01 restricts transgene expression to tumor sites and, consequently, may limit systemic side effects. In fact, a recent phase II clinical trial testing PEGPH20 in combination with chemotherapy (NCT01839487) was transiently halted because of associated toxicity. Moreover, in contrast to recombinant enzymes which have a relatively short half-life and may require readministrations, sustained delivery of hyaluronidase could be achieved with a replicating virus.

Despite the notable improvement of antitumor activity obtained with VCN-01, complete tumor regressions were rare. Masson staining of tumors suggests that collagen bundles surround the infected areas of the tumors, impairing the spread of the virus. Besides ECM and malignant cells, solid tumors contain stromal cells such as cancer-associated fibroblasts (CAF), endothelial, and inflammatory cells which physically limit viral spread. In this sense, it would be interesting to combine the enzymatic degradation of the ECM by hyaluronidase with a strategy directed to eliminate stromal cells. Our group recently described that the truncation of the i-leader adenoviral protein enhanced the release and cytotoxicity of the virus in CAFs *in vitro* and increased its antitumor activity *in vivo* (49, 50).

In conclusion, VCN-01 addresses two of the main limitations in the treatment of cancer with oncolytic adenoviruses: tumor targeting and spread across the ECM barrier. Altogether, the present study supports VCN-01 as a potential candidate for clinical development. Currently, two phase I clinical trials are ongoing: one in pancreatic cancer by endoscopic ultrasound-guided intratumoral injection and another one targeting different tumor types by intravenous administration (NCT02045602 and NCT02045589).

Disclosure of Potential Conflicts of Interest

M. Cascalló has ownership interest (including patents) in VCN Biosciences. R. Alemany reports receiving a commercial research grant and is a consultant/

advisory board member for VCN Biosciences. No potential conflicts of interest were disclosed by the other authors.

Authors' Contributions

Conception and design: A. Rodríguez-García, J.J. Rojas, M. Cascalló, R. Alemany

Development of methodology: A. Rodríguez-García, M. Giménez-Alejandre, J.J. Rojas, R. Moreno, M. Bazan-Peregrino, R. Alemany

Acquisition of data (provided animals, acquired and managed patients, provided facilities, etc.): A. Rodríguez-García, M. Giménez-Alejandre, J.J. Rojas, M. Bazan-Peregrino

Analysis and interpretation of data (e.g., statistical analysis, biostatistics, computational analysis): A. Rodríguez-García, M. Giménez-Alejandre, M. Bazan-Peregrino, M. Cascalló, R. Alemany

Writing, review, and/or revision of the manuscript: A. Rodríguez-García, M. Bazan-Peregrino, M. Cascalló, R. Alemany

Administrative, technical, or material support (i.e., reporting or organizing data, constructing databases): R. Moreno, M. Cascalló, R. Alemany

Study supervision: M. Cascalló, R. Alemany

Acknowledgments

The authors thank the technical support of Marga Nadal (Institut Català d'Oncologia-IDIBELL) and histopathologic examination by Enric Condom i Mundó (Hospital Universitari de Bellvitge) in FISH study.

Grant Support

A. Rodríguez-García was supported by a pre-doctoral fellowship (PFIS) granted by the "Instituto de Salud Carlos III." This work was supported by a BIO2011-30299-C02-01 grant from the `Ministerio de Educación y Ciencia' of the Government of Spain, VALTEC 09-02-105 from the Generalitat de Catalunya, ACCIO10, and a 2009SGR283 research grant from the "Generalitat de Catalunya."

The costs of publication of this article were defrayed in part by the payment of page charges. This article must therefore be hereby marked *advertisement* in accordance with 18 U.S.C. Section 1734 solely to indicate this fact.

Received August 29, 2014; revised November 5, 2014; accepted November 5, 2014; published OnlineFirst xx xx, xxxx.

References

1. Bartlett DL, Liu Z, Sathaiah M, Ravindranathan R, Guo Z, He Y, et al. Oncolytic viruses as therapeutic cancer vaccines. Mol Cancer 2013;12:103.
2. Elsedawy NB, Russell SJ. Oncolytic vaccines. Expert Rev Vaccines 2013;12: 1155–72.
3. Russell SJ, Peng KW, Bell JC. Oncolytic virotherapy. Nat Biotechnol 2012;30:658–70.
4. Alemany R. Chapter four–Design of improved oncolytic adenoviruses. Adv Cancer Res 2012;115:93–114.
5. Coughlan L, Alba R, Parker AL, Bradshaw AC, McNeish IA, Nicklin SA, et al. Tropism-modification strategies for targeted gene delivery using adenoviral vectors. Viruses 2010;2:2290–355.
6. Nicol CG, Graham D, Miller WH, White SJ, Smith TA, Nicklin SA, et al. Effect of adenovirus serotype 5 fiber and penton modifications on in vivo tropism in rats. Mol Ther 2004;10:344–54.
7. Smith TA, Idamakanti N, Marshall-Neff J, Rollence ML, Wright P, Kaloss M, et al. Receptor interactions involved in adenoviral-mediated gene delivery after systemic administration in non-human primates. Hum Gene Ther 2003;14:1595–604.
8. Smith TA, Idamakanti N, Rollence ML, Marshall-Neff J, Kim J, Mulgrew K, et al. Adenovirus serotype 5 fiber shaft influences in vivo gene transfer in mice. Hum Gene Ther 2003;14:777–87.
9. Bayo-Puxan N, Cascallo M, Gros A, Huch M, Fillat C, Alemany R. Role of the putative heparan sulfate glycosaminoglycan-binding site of the adenovirus type 5 fiber shaft on liver detargeting and knob-mediated retargeting. J Gen Virol 2006;87:2487–95.
10. Kritz AB, Nicol CG, Dishart KL, Nelson R, Holbeck S, Von Seggern DJ, et al. Adenovirus 5 fibers mutated at the putative HSPG-binding site show restricted retargeting with targeting peptides in the HI loop. Mol Ther 2007;15:741–9.
11. Bayo-Puxan N, Gimenez-Alejandre M, Lavilla-Alonso S, Gros A, Cascallo M, Hemminki A, et al. Replacement of adenovirus type 5 fiber shaft heparan sulfate proteoglycan-binding domain with RGD for improved tumor infectivity and targeting. Hum Gene Ther 2009; 20:1214–21.
12. Rojas JJ, Gimenez-Alejandre M, Gil-Hoyos R, Cascallo M, Alemany R. Improved systemic antitumor therapy with oncolytic adenoviruses by replacing the fiber shaft HSG-binding domain with RGD. Gene Ther 2011;19:453–7.
13. Parato KA, Senger D, Forsyth PA, Bell JC. Recent progress in the battle between oncolytic viruses and tumours. Nat Rev 2005;5:965–76.
14. Smith E, Breznik J, Lichty BD. Strategies to enhance viral penetration of solid tumors. Hum Gene Ther 2011;22:1053–60.
15. Strauss R, Lieber A. Anatomical and physical barriers to tumor targeting with oncolytic adenoviruses in vivo. Curr Opin Mol Ther 2009;11: 513–22.
16. Choi IK, Lee YS, Yoo JY, Yoon AR, Kim H, Kim DS, et al. Effect of decorin on overcoming the extracellular matrix barrier for oncolytic virotherapy. Gene Ther 2010;17:190–201.
17. Dmitrieva N, Yu L, Viapiano M, Cripe TP, Chiocca EA, Glorioso JC, et al. Chondroitinase ABC I-mediated enhancement of oncolytic virus spread and antitumor efficacy. Clin Cancer Res 2011;17:1362–72.
18. Ganesh S, Gonzalez Edick M, Idamakanti N, Abramova M, Vanroey M, Robinson M, et al. Relaxin-expressing, fiber chimeric oncolytic adenovirus prolongs survival of tumor-bearing mice. Cancer Res 2007;67:4399–407.
19. Kim JH, Lee YS, Kim H, Huang JH, Yoon AR, Yun CO. Relaxin expression from tumor-targeting adenoviruses and its intratumoral spread, apoptosis induction, and efficacy. J Natl Cancer Inst 2006;98:1482–93.
20. Schafer S, Weibel S, Donat U, Zhang Q, Aguilar RJ, Chen NG, et al. Vaccinia virus-mediated intra-tumoral expression of matrix metalloproteinase 9 enhances oncolysis of PC-3 xenograft tumors. BMC Cancer 2012;12:366.
21. Guedan S, Rojas JJ, Gros A, Mercade E, Cascallo M, Alemany R. Hyaluronidase expression by an oncolytic adenovirus enhances its intratumoral spread and suppresses tumor growth. Mol Ther 2010;18:1275–83.
22. Jacobetz MA, Chan DS, Neesse A, Bapiro TE, Cook N, Frese KK, et al. Hyaluronan impairs vascular function and drug delivery in a mouse model of pancreatic cancer. Gut 2013;62:112–20.
23. Provenzano PP, Cuevas C, Chang AE, Goel VK, Von Hoff DD, Hingorani SR. Enzymatic targeting of the stroma ablates physical barriers to treatment of pancreatic ductal adenocarcinoma. Cancer Cell 2012;21:418–29.
24. Thompson CB, Shepard HM, O'Connor PM, Kadhim S, Jiang P, Osgood RJ, et al. Enzymatic depletion of tumor hyaluronan induces antitumor responses in preclinical animal models. Mol Cancer Ther 2010;9:3052–64.
25. Batra SK, Metzgar RS, Worlock AJ, Hollingsworth MA. Expression of the human MUC1 mucin cDNA in a hamster pancreatic tumor cell line HP-1. Int J Pancreatol 1992;12:271–83.
26. Villanueva A, Garcia C, Paules AB, Vicente M, Megias M, Reyes G, et al. Disruption of the antiproliferative TGF-beta signaling pathways in human pancreatic cancer cells. Oncogene 1998;17:1969–78.
27. Rojas JJ, Cascallo M, Guedan S, Gros A, Martinez-Quintanilla J, Hemminki A, et al. A modified E2F-1 promoter improves the efficacy to toxicity ratio of oncolytic adenoviruses. Gene therapy 2009;16:1441–51.
28. Dorfman A, Ott ML. A turbidimetric method for the assay of hyaluronidase. J Biol Chem 1948;172:367–75.
29. Cascallo M, Alonso MM, Rojas JJ, Perez-Gimenez A, Fueyo J, Alemany R. Systemic toxicity-efficacy profile of ICOVIR-5, a potent and selective oncolytic adenovirus based on the pRB pathway. Mol Ther 2007;15: 1607–15.
30. Guedan S, Grases D, Rojas JJ, Gros A, Vilardell F, Vile R, et al. GALV expression enhances the therapeutic efficacy of an oncolytic adenovirus by inducing cell fusion and enhancing virus distribution. Gene Ther 2012;19:1048–57.
31. Rojas JJ, Guedan S, Searle PF, Martinez-Quintanilla J, Gil-Hoyos R, Alcayaga-Miranda F, et al. Minimal RB-responsive E1A promoter modification to attain potency, selectivity, and transgene-arming capacity in oncolytic adenoviruses. Mol Ther 2010;18:1960–71.

32. Thomas MA, Spencer JF, La Regina MC, Dhar D, Tollefson AE, Toth K, et al. Syrian hamster as a permissive immunocompetent animal model for the study of oncolytic adenovirus vectors. Cancer Res 2006;66:1270–6.
33. Suzuki K, Fueyo J, Krasnykh V, Reynolds PN, Curiel DT, Alemany R. A conditionally replicative adenovirus with enhanced infectivity shows improved oncolytic potency. Clin Cancer Res 2001;7:120–6.
34. Jogler C, Hoffmann D, Theegarten D, Grunwald T, Uberla K, Wildner O. Replication properties of human adenovirus in vivo and in cultures of primary cells from different animal species. J Virol 2006;80:3549–58.
35. Muruve DA. The innate immune response to adenovirus vectors. Hum Gene Ther 2004;15:1157–66.
36. Nemunaitis J, Cunningham C, Buchanan A, Blackburn A, Edelman G, Maples P, et al. Intravenous infusion of a replication-selective adenovirus (ONYX-015) in cancer patients: safety, feasibility and biological activity. Gene Ther 2001;8:746–59.
37. Zhang Y, Chirmule N, Gao GP, Qian R, Croyle M, Joshi B, et al. Acute cytokine response to systemic adenoviral vectors in mice is mediated by dendritic cells and macrophages. Mol Ther 2001;3:697–707.
38. Gregory SM, Nazir SA, Metcalf JP. Implications of the innate immune response to adenovirus and adenoviral vectors. Future Virol 2011;6:357–74.
39. He D, Sun L, Li C, Hu N, Sheng Y, Chen Z, et al. Anti-tumor effects of an oncolytic adenovirus expressing hemagglutinin-neuraminidase of Newcastle disease virus in vitro and in vivo. Viruses 2014;6:856–74.
40. Lichtenstein DL, Spencer JF, Doronin K, Patra D, Meyer JM, Shashkova EV, et al. An acute toxicology study with INGN 007, an oncolytic adenovirus vector, in mice and permissive Syrian hamsters; comparisons with wild-type Ad5 and a replication-defective adenovirus vector. Cancer Gene Ther 2009;16:644–54.
41. Small EJ, Carducci MA, Burke JM, Rodriguez R, Fong L, van Ummersen L, et al. A phase I trial of intravenous CG7870, a replication-selective, prostate-specific antigen-targeted oncolytic adenovirus, for the treatment of hormone-refractory, metastatic prostate cancer. Mol Ther 2006;14:107–17.
42. Ying B, Toth K, Spencer JF, Meyer J, Tollefson AE, Patra D, et al. INGN 007, an oncolytic adenovirus vector, replicates in Syrian hamsters but not mice: comparison of biodistribution studies. Cancer Gene Ther 2009;16:625–37.
43. Bernt KM, Ni S, Gaggar A, Li ZY, Shayakhmetov DM, Lieber A. The effect of sequestration by nontarget tissues on anti-tumor efficacy of systemically applied, conditionally replicating adenovirus vectors. Mol Ther 2003;8:746–55.
44. Page JG, Tian B, Schweikart K, Tomaszewski J, Harris R, Broadt T, et al. Identifying the safety profile of a novel infectivity-enhanced conditionally replicative adenovirus, Ad5-delta24-RGD, in anticipation of a phase I trial for recurrent ovarian cancer. Am J Obstet Gynecol 2007;196:389 e1–9; discussion e9–10.
45. Shayakhmetov DM, Li ZY, Ni S, Lieber A. Analysis of adenovirus sequestration in the liver, transduction of hepatic cells, and innate toxicity after injection of fiber-modified vectors. J Virol 2004;78:5368–81.
46. Thomas MA, Spencer JF, Toth K, Sagartz JE, Phillips NJ, Wold WSM. Immunosuppression enhances oncolytic adenovirus replication and antitumor efficacy in the syrian hamster model. Mol Ther 2008;16:1665–73.
47. Kultti A, Li X, Jiang P, Thompson CB, Frost GI, Shepard HM. Therapeutic targeting of hyaluronan in the tumor stroma. Cancers 2012;4:873–903.
48. Baumgartner G, Gomar-Hoss C, Sakr L, Ulsperger E, Wogritsch C. The impact of extracellular matrix on the chemoresistance of solid tumors–experimental and clinical results of hyaluronidase as additive to cytostatic chemotherapy. Cancer Lett 1998;131:85–99.
49. Puig-Saus C, Gros A, Alemany R, Cascallo M. Adenovirus i-leader truncation bioselected against cancer-associated fibroblasts to overcome tumor stromal barriers. Mol Ther 2012;20:54–62.
50. Puig-Saus C, Laborda E, Rodriguez-Garcia A, Cascallo M, Moreno R, Alemany R. The combination of i-leader truncation and gemcitabine improves oncolytic adenovirus efficacy in an immunocompetent model. Cancer Gene Ther 2014;21:68–73.

Article under review in Gene Therapy

Insertion of exogenous epitopes in the E3-19K of oncolytic adenoviruses to enhance TAP-independent presentation and immunogenicity

Alba Rodríguez-García, Raúl Gil-Hoyos, Carlos Alberto Fajardo, Luis Alfonso Rojas, Marcel Arias-Badia, Ramon Alemany

Translational Research Laboratory, IDIBELL-Institut Català d'Oncologia, L'Hospitalet de Llobregat, Barcelona, Spain.

* Correspondence should be addressed to:

Ramon Alemany PhD. (ralemany@iconcologia.net)

IDIBELL-Institut Català d'Oncologia

Av Gran Via de l'Hospitalet, 199-203

L'Hospitalet de Llobregat

08907 – Barcelona, SPAIN

Tel: + 34 93 2607462

Fax: + 34 93 2607466

E-mail: ralemany@iconcologia.net

RUNNING TITLE: TAP-independent epitopes in oncolytic adenoviruses

WORD COUNT: 2909

ABSTRACT

Oncolytic adenoviruses can promote immune responses against tumors by expressing and/or displaying tumor-associated antigens. However, the strong immunodominance of viral antigens mask responses against tumor epitopes. In addition, defects in MHC class I antigen presentation pathway such as the downregulation of the transporter associated with antigen processing (TAP) are frequently associated with immune evasion of tumor cells. To promote the immunogenicity of exogenous epitopes in the context of an oncolytic adenovirus, we have taken advantage of the ER localization of the viral protein E3-19K. We have inserted tumor-associated epitopes after the ER-targeting signal sequence of this protein and flanked them with linkers cleavable by the protease furin to facilitate their TAP-independent presentation. This strategy allowed an enhanced presentation of the exogenous epitopes in TAP-deficient tumor cells *in vitro* and the generation of higher specific immune responses *in vivo* that were able to significantly control tumor growth in immunized mice.

KEYWORDS: Oncolytic adenovirus; exogenous epitopes; immune responses; TAP-independent; immunodominance; antitumor efficacy.